

## BIO-MINERAL PROCESSING OF DOUBLE REFRACTORY GOLD ORES USING LACCASE-MEDIATOR SYSTEM

ディエゴ モイセス メンドーサ フローレス

<https://hdl.handle.net/2324/6787585>

---

出版情報 : Kyushu University, 2022, 博士 (工学) , 課程博士  
バージョン :  
権利関係 :





# **BIO-MINERAL PROCESSING OF DOUBLE REFRACTORY GOLD ORES USING LACCASE-MEDIATOR SYSTEM**

By

DIEGO MOIZES MENDOZA FLORES

A thesis submitted to Kyushu University

For a degree of Doctor of Engineering

Department of Earth Resources Engineering

Graduate School of Engineering

Kyushu University

Fukuoka, Japan

March 2023

# CONTENTS

Abstract.....	x
List of Tables .....	xiv
List of Figures.....	xix
 <b>Chapter 1: Introduction .....</b>	<b>1</b>
1.1. Gold ore classification.....	2
1.1.1. Free-milling gold ores.....	3
1.1.2. Refractory gold ores.....	5
1.1.2.1. Sulfidic gold ores.....	5
1.1.2.2. Carbonaceous gold ores.....	7
1.2. Mineral processing of refractory gold ores .....	13
1.2.1. Sulfide pre-treatment .....	13
1.2.2. Carbonaceous matter pre-treatment .....	15
1.2.3. Sequential biological pre-treatment .....	17
1.3. Lignin-degrading enzymes.....	19

1.3.1. Peroxidases .....	19
1.3.2. Laccase.....	20
1.3.2.1. Laccase-mediator system.....	23
1.4. Objective of the thesis .....	24
References.....	26
 <b>Chapter 2: Methodology .....</b>	<b>48</b>
2.1. Enzyme studies.....	49
2.1.1. Laccase activity.....	49
2.1.2. Temperature effect on laccase activity .....	51
2.1.3. Michaelis-Menten kinetics.....	52
2.1.4. Protein assay .....	52
2.2. Solution analysis .....	54
2.2.1. Inductively coupled plasma-optical emission spectrometry (ICP-OES) and mass spectrometry (ICP-MS) .....	54
2.2.2. Dissolved total organic carbon (TOC).....	55
2.2.3. Three-dimensional fluorescence spectrometry .....	55

2.2.4. Gas-chromatography mass spectrometry (GC-MS) .....	56
2.2.5. High-performance liquid chromatography (HPLC) .....	57
2.3. Solid characterization .....	58
2.3.1. X-ray diffraction (XRD) .....	58
2.3.2. X-ray fluorescence spectrometry (XRF) .....	58
2.3.3. CHN elemental analysis .....	58
2.3.4. Thermogravimetric-differential thermal analysis (TG-DTA) ..	59
2.3.5. Fourier transforms infrared spectroscopy (FT-IR) .....	59
2.3.6. Raman spectroscopy .....	59
2.3.7. Scanning electron microscopy (SEM) .....	60
2.3.8. Specific surface area (BET) .....	60
2.3.9. Mineral liberation analysis (MLA) .....	60
References .....	61

### **Chapter 3: Trace analysis of gold in double refractory gold ores by induced coupled plasma spectrometry .....64**

3.1. Introduction .....	65
3.2. Experimental .....	67

3.2.1. Materials .....	67
3.2.2. Reagents, instrumentation, and standard .....	68
3.2.3. Sample digestion .....	70
3.3. Results and Discussion .....	73
3.3.1. Gold ores characterization .....	73
3.3.2. Interferences in gold analysis by ICP-OES .....	77
3.3.3. Effect of different acid ratios on gold determination and memory effect elimination in ICP-MS .....	79
3.3.4. Effect of different acid ratios on gold determination by ICP-OES .....	82
3.3.5. Comparing the effects of different acid ratios on gold determination by ICP-OES and ICP-MS .....	86
3.4. Conclusions .....	87
References .....	87

<b>Chapter 4: Enzymatic degradation of powder activated carbon with laccase against cell-free spent medium from <i>Phanerochaete chrysosporium</i> .....</b>	<b>91</b>
--	-----------

4.1. Introduction .....	92
4.2. Experimental .....	94
4.2.1. Materials .....	94
4.2.2. CFSM harvesting .....	95
4.2.3. Laccase from <i>Trametes versicolor</i> treatment .....	95
4.2.4. CFSM treatment.....	96
4.2.5. Characterization of untreated and bio-treated carbonaceous matter surrogate.....	97
4.2.6. $\text{Au}(\text{CN})_2^-$ adsorption test.....	98
4.3. Results and Discussion.....	98
4.3.1. Physical changes on the surface of PAC .....	98
4.3.2. Chemical changes in PAC as a surrogate of carbonaceous matter in DRGO .....	101
4.3.3. $\text{Au}(\text{CN})_2^-$ uptake.....	104
4.4. Conclusions .....	105
References.....	106

<b>Chapter 5: Degradation of powder activated carbon by laccase-mediator system.....</b>	<b>112</b>
5.1.Introduction .....	113
5.2.Experimental .....	116
5.2.1. Materials .....	116
5.2.2. Laccase activity assay .....	116
5.2.3. Laccase-mediator system using HBT for treating PAC .....	117
5.2.4. Sequential organic solvent extraction of LMS-degraded products for characterization by GC-MS .....	117
5.2.5. Characterization of untreated and LMS-treated PAC.....	118
5.2.6. Adsorption of $\text{Au}(\text{CN})_2^-$ on PAC before and after enzyme treatment.....	118
5.3.Results and Discussion.....	119
5.3.1. Laccase activity in the system .....	119
5.3.2. Changes in surface morphologies of PAC by LMS treatment .....	121
5.3.3. Chemical alterations of PAC by LMS treatment.....	124
5.4.Conclusions .....	143



References.....	146
-----------------	-----

**Chapter 6: Characterization of organic compounds in  
carbonaceous gold ores before and after laccase-mediator  
system treatment..... 155**

6.1.Introduction .....	156
6.2.Experimental .....	158
6.2.1. Materials and CM characterization.....	158
6.2.2. Soxhlet extraction and GC-MS characterization .....	158
6.2.3. Sequential bio-treatment and carbonaceous matter degradation by lignin-degrading enzymes .....	161
6.2.3.1. Solid residue characterization.....	162
6.2.4. Gold extraction.....	163
6.3.Results and discussion.....	165
6.3.1. Carbon content, Raman spectra and preg-robbing test.....	165
6.3.2. TG-DTA.....	167
6.3.3. GC-MS characterization of PXX, BOG, and SYM.....	169

6.3.4. EPS interference on Au recovery in laccase treatment of BOG...	195
6.3.4.1. Pre-washing optimization and characterization of BOG after BIOX treatment .....	195
6.3.4.2. Gold recovery and EPS interference on Lcc/LMS treatment....	200
6.3.4.3. Preg-robbing test and Raman spectroscopy .....	207
6.3.4.4. Interpretation of EPS interference and LMS treatment.....	210
6.3.5. GC-MS characterization after LMS treatment on SYM.....	211
6.4. Conclusions .....	221
References.....	223

## **Chapter 7: Conclusions..... 231**

### **Supplemental Information**

<b>Chapter 6S: Carbonaceous matter degradation by fungal enzyme treatment to improve Ag recovery from Au-Ag bearing concentrate, PXX.....</b>	<b>236</b>
---	------------

6S.1. Introduction .....	237
6S.2. Experimental.....	238
6S.2.1. Sample preparation and characterization.....	238
6S.2.2. Sequential bio-treatment of carbonaceous silver concentrate (CSC) .....	240
6S.2.2.1. Biooxidation of sulfides in CSC by mixed thermophilic archaea .....	240
6S.2.2.2. Degradation of carbonaceous matter by cell-free spent medium (CFSM) from <i>Phanerochaete chrysosporium</i> .....	241
6S.2.3. Characterization of the bio-treated residues .....	243
6S.3. Results and discussion.....	243
6S.4. Conclusions .....	258
References.....	259
Acknowledgments .....	264

## Abstract

Gold ores in which gold particles are trapped within sulfide minerals are called "refractory gold ores," and the ores associated with carbonaceous shale are classified as "double refractory gold ores (DRGO)." Since  $\text{Au}(\text{CN})_2^-$  complexes are adsorbed on the carbonaceous matter (CM) in cyanidation, the conventional extraction makes gold recovery loss of 30 to 70% (preg-robbing effect). In addition, DRGO is not suitable for general flotation beneficiation due to the poor separation of carbonaceous and sulfide minerals, despite its higher gold grade than ordinary gold ores, making it unsuitable for economic exploitation. However, DRGOs are distributed over five continents, and the gold resources are estimated to be equivalent to a fraction of the world's total gold production. It is no exaggeration to say that there is now a global demand for hydrometallurgy to recover gold from DRGOs without causing environmental impacts.

The present work reports on a (bio)hydrometallurgy for graphitic gold ores that avoids roasting, which releases toxic gases, and achieves the necessary mineral degradation at ambient temperature and pressure with a low environmental impact and proposes a new direction that uses the laccase (Lcc) reaction among ligninolytic enzymes, which has never been attempted before, to recover gold from DRGO with different degrees of graphitization. This provides a new guideline for the sequential DRGO treatment process for each ore, through a molecular-level study of degraded products by laccase reaction.

First, **Chapter 1** reviews the occurrence of DRGO, the troubles encountered in DRGO, and the importance of overcoming their pre-treatment to improve gold beneficiation. The overview of conventional and novel pre-treatments is listed, focusing on DRGO sequential bio-treatment as a continuous effort to decrease air pollution from

conventional processes. Next, Lcc was compared with lignin-degrading enzymes like lignin peroxidase (LiP) and manganese peroxidase (MnP), pointing out the advantages of laccase over the peroxidases. Finally, the objectives of this thesis were proposed.

The methodology to approach the above objectives was summarized in **Chapter 2**, where biochemical approaches (enzyme assay), elemental and mineralogical characterization (X-ray fluorescence spectroscopy and X-ray diffraction), solution analysis (inductive coupled plasma-optical emission spectroscopy, ICP-OES and inductive coupled plasma-mass spectroscopy, ICP-MS), and several unique characterizations for carbonaceous matter (Raman spectroscopy, thermogravimetric analysis, three-dimensional fluorescence spectrometry) are included. In particular, gas chromatography-mass spectrometry (GC-MS) played an essential role in the molecular-level characterization of CM and its by-products derived from enzyme reactions.

First of all, the analytical and preparation problems behind the trace analysis of Au in DRGO were pointed out and overcome in **Chapter 3**. In determining Au by ICP-OES, the coexisting Fe strongly interfered with the 1st dominant Au optical emission peak at 242 nm. After the matrix normalization by adding the same Fe concentrations as in unknown samples to the Au standard solutions, the accuracy of Au determination was improved. In acid digestion of gold ore samples, the acid ratio from normal aqua regia (HCl: HNO<sub>3</sub> =3:1) was modified to highly reverse aqua regia (HCl: HNO<sub>3</sub> =1:5) to increase the oxidizing ability. The optimized conditions were applied to three different DRGOs, where the detection limit was 20 ppb in ICP-OES. As for ICP-MS, the memory effect derived from the reduction of Au(III) to Au(0), and the consequent deposition was overcome by adding 1% L-cysteine as a sacrificing oxidant and ligand.

**Chapter 4** elucidated the superiority of Lcc over LiP and MnP in the degradation of powder activated carbon (PAC) as a carbon surrogate. Lcc treatment largely decreased the gold robbing index than the mixture of LiP and MnP under the same enzymatic activity. As such, in **Chapter 5**, the supplemented electron mediator of 1-hydroxybenzotriazole (HBT) improved the degradation efficiency with some direct evidence of bio-degraded products by GC-MS. Laccase-mediator system (LMS) treatment for 7 days physically and chemically altered the surface of PAC with the reduction of specific surface area and pore volume. The disruption of aromatic moieties into aliphatic compounds and the formation of oxygen-containing functional groups, mainly carbonyl groups, were revealed by GC-MS. Subsequently, the adsorption density of  $\text{Au}(\text{CN})_2^-$  on the surface-degraded PAC was dramatically decreased from 46.0 to 7.36  $\mu\text{mol/g}$ . These experimental conditions were applied to natural DRGO.

In **Chapter 6**, the organic carbon from three carbonaceous gold ores: PXX and SYM (flotation concentrates), and BOG (after bio-oxidation of flotation concentrate), were characterized. There was an extreme contrast between PXX and SYM as poorly and highly preg-robbing ores. As for BOG (moderately), the surface property was influenced by the presence of extracellular polymeric substances (EPS) formed during intensive bio-oxidation of sulfides. LMS pre-treatment was applied to the above three ores to decompose CM. Almost 100% of Au was recovered from PXX by cyanidation without any pretreatments. Meanwhile, its Ag recovery reached only 33.7%, and it improved to almost 100% after LMS treatment. Au recovery in BOG yielded 77% after sulfide decomposition and further improved to >90% after removing jarosite by oxalic acid washing. However, the presence of EPS layers on CM interfered with laccase reaction by enzyme activity consumption, resulting in a slight increase to 92%.

Therefore, for SYM,  $\text{FeCl}_3$  leaching was applied for the decomposition of sulfides avoiding the formation of jarosite and EPS. GC-MS results for the LMS-treated SYM confirmed the presence and increment of fatty acids and aliphatic hydrocarbon, indicating LMS degradation went through the disturbance of the benzene rings from the defective sites of CM and made the CM surface became more hydrophilic. Finally, sequential treatment of SYM improved Au recovery in cyanidation as shown in 44% (original)  $\rightarrow$  77% ( $\text{FeCl}_3$  leaching)  $\rightarrow$  86% (LMS), which is the most refractory gold ore in the present work.

In **Chapter 7**, the main conclusions of the present thesis were summarized, including a general direction for the pretreatment of DRGO and the applicability of LMS treatment.

## List of Tables

Table 1.1. List of carbonaceous gold ores, their elemental and mineralogical characteristics .....	10
Table 1.2. Biochemical characterization of purified laccases from different fungal species .....	22
Table 1.3. Comparison of the properties and advantages/disadvantages of using different enzymes for CM degradation .....	23
Table 2.1. Characteristics of laccases used in this study .....	49
Table 2.2. Standard solutions for laccase Y-120 modified protein assay ....	53
Table 3.1. Instrumental setting for ICP-OES Optima 8300 .....	68
Table 3.2. Instrumental setting for ICP-MS Agilent 7900 .....	70
Table 3.3. Elemental characterization of different refractory gold ores (wt%) .....	75
Table 3.4. Fe and Si interference on gold determination by ICP-OES ....	79
Table 3.5. Effect of L-cysteine concentration on gold content (g/t) from BOG ore after different acid digestion ratios (n=4) .....	81



Table 3.6. Effect of acid digestion conditions on gold content (g/t) in BOG ore (n = 4).....	82
Table 3.7. Effect of acid digestion conditions on gold content (g/t) in SYM ore (n = 4).....	83
Table 3.8 Au content (g/t) of BOG, PXX, and SYM gold ore, under three different digestion conditions, determined by ICP-OES and ICP-MS ..	85
Table 4.1. Physical properties obtained from N <sub>2</sub> adsorption at 77K of untreated PAC, CFSM-treated PAC after 3, 5 and 7 days of enzyme production, and laccase-treated PAC at 20, 50 and 100 U/L of enzyme activity. Enzyme treatment was for 3 days in all the treated samples ...	99
Table 5.1. Changes in specific surface area and pore volume of untreated and LMS-treated PAC.....	124
Table 5.2. Intermediates detected by GC-MS, peak No. 1~8 in Fig. 5.6 for extracted compounds in ethyl acetate on the LMS-treated PAC using HBT after 2 and 5 days .....	130

Table 5.3. Intermediates detected by GC-MS, peak No. 1~12 in Fig. 5.7 for extracted compounds in hexane on the untreated and LMS-treated PAC using HBT after 7 days .....	132
Table 6.1. Experimental conditions of LMS treatment for BOG .....	164
Table 6.2. Carbon and preg-robbing characterization of three carbonaceous gold ores .....	165
Table 6.3. Mass loss (%) separated in temperature combustion ranges.	168
Table 6.4. Organic moieties detected by GC-MS in Fig. 6.6(a) for extracted compounds in hexane phase from PXX .....	171
Table 6.5. Organic moieties detected by GC-MS in Fig. 6.6(b) for extracted compounds in ethyl acetate phase from PXX .....	174
Table 6.6. Organic moieties detected by GC-MS in Fig. 6.6(c) for extracted compounds in acetone phase from PXX .....	176
Table 6.7. Organic moieties detected by GC-MS in Fig. 6.7(a) for extracted compounds in hexane phase from BOG .....	180
Table 6.8. Organic moieties detected by GC-MS in Fig. 6.7(b) for extracted compounds in ethyl acetate phase from BOG .....	181

Table 6.9. Organic moieties detected by GC-MS in Fig. 6.7(c) for extracted compounds in acetone phase from BOG.....	183
Table 6.10. Organic moieties detected by GC-MS in Fig. 6.8(a) for extracted compounds in hexane phase from SYM .....	188
Table 6.11. Organic moieties detected by GC-MS in Fig. 6.8(b) for extracted compounds in ethyl acetate phase from SYM.....	190
Table 6.12. Organic moieties detected by GC-MS in Fig. 6.8(c) for extracted compounds in acetone phase from SYM.....	193
Table 6.13. Elemental compositions for DA before and after different washing conditions.....	198
Table 6.14. Summary of DAOY series gold recovery, C (wt%) and TOC (mg/L).....	206
Table 6.15. Intermediates detected by GC-MS in Fig. 6.22(b) for extracted compounds in ethyl acetate on the LMS-treated SYM.....	214
Table 6.16. Intermediates detected by GC-MS in Fig. 6.22(c) for extracted compounds in acetone on the LMS-treated SYM.....	217
Table 6S.1. Mineral compositions (wt%) of CSC and DA determined by MLA .....	245

Table 6S.2. Elemental compositions of CSC and DA.....	247
Table 6S.3. XRD peak intensity ratio of sulfides against quartz in as- received sample (CSC), after biooxidation (DA), DA treated by CFSM (DAC) and CSC treated by CFSM (DC) .....	254

## List of Figures

Fig. 1.1. Classification of gold ore types.....	3
Fig. 1.2. Photomicrographs taken under reflected light and uncrossed nicols. A) and B) gold ore sample consists of a smoky and white quartz (qtz)-carbonate matrix with mostly pyrite (py) and minor pyrrhotite (po), chalcopyrite (cpy), sphalerite (sph) and galena (ga). Gold size distribution is heterogeneous and is mainly located at sulfide grain boundaries or as free particles in the matrix . ....	4
Fig. 1.3. Photomicrographs taken under reflected light and uncrossed nicols. C) gold ore sample consists of a smoky and white quartz (qtz)- carbonate matrix with mostly pyrite (py) and minor pyrrhotite (po) and sphalerite (sph). Gold size distribution is heterogeneous and is mainly enclosed in pyrite. ....	6
Fig. 1.4. Model of graphitic structure transformation from carbon under different temperatures .....	8
Fig. 1.5. Contact and non-contact leaching mechanism involved in bio- oxidation.....	15

Fig. 1.6 Schematic illustration of sequential biomineral processing of double refractory gold ore (DRGO). DC: treated DRGO by cell-free spent medium (CFSM) of white-rot fungus <i>Phanerochaete chrysosporium</i> ; DA: treated DRGO by iron-oxidizing archaeon, <i>Acidianus brierleyi</i> ; DCA: treated DC by <i>Acidianus brierleyi</i> ; DAC: treated DA by CFSM. ....	18
Fig. 1.7. Copper centers of laccase: Type 1, Type 2, and Type 3 .....	21
Fig. 1.8. Catalytic cycle of laccase and mechanism of laccase-mediated biodegradation of lignin. ....	24
Fig. 2.1. Location of excitation-emission matrix (EEM) peaks (symbols) based on literature reports and operationally defined excitation and emission wavelength boundaries (dashed lines) for live EEM regions . ....	56
Fig. 3.1. Schematic illustration of processes and problems involved in gold determination in DRGO. ....	69
Fig. 3.2. Schematic illustration that explains the steps in the acid digestion process applied for double refractory gold ores.....	72

Fig. 3.3. XRD patterns of gold ores. Symbols: py (pyrite, PDF 01–042–1340); asp (arsenopyrite, PDF 00–060-0322); jt (jarosite, PDF 01-075-9732); mus (muscovite, PDF 01-080-0743); qtz (quartz, PDF 01–075-8322); chl (chlorite, PDF 00-060-0322); gypsum (gyp, PDF 00-033-0311).....74

Fig. 3.4. ICP-OES spectra in a region of Au (242 nm) for acid-digested samples of BOG, PXX, and SYM gold ore under aqua regia digestion including the standard spectra. ....78

Fig. 3.5. ICP-OES spectra in a region of Au (208 nm) for acid-digested samples of BOG, PXX, and SYM gold ore under aqua regia digestion including the standard spectra. ....78

Fig. 3.6. Wash-out profile for 60 ppb Au showing memory effect in ICP-MS. ....80

Fig. 3.7. ICP-OES spectra in a region of Au (242 nm) for acid-digested samples of BOG sample under three different digestion conditions with the standard spectra. The standard solutions include (a) 0 ppm Fe, (b) 20 ppm Fe, and (c) 0 ppm Fe including a prewashing before the digestion to remove Fe from the sample. ....84

Fig. 4. 1. Schematic illustration of the experimental conditions in Chapter 4.....	97
Fig. 4.2. SEM images of (a) the untreated and Lcc-treated PAC using (b) 20, (c) 50 and (d) 100 U/L of enzyme activity. (e) N <sub>2</sub> adsorption/desorption isotherms of the untreated and laccase-treated PAC samples as detailed. Enzyme treatment was conducted for 3 days. ....	100
Fig. 4.3. SEM images of (a) the untreated and treated PAC using (b) 3 days harvested, (c) 5 days harvested (d) 7 days harvested CFSM. (e) Comparison of the N <sub>2</sub> adsorption/desorption isotherms of the untreated and CFSM-treated PAC samples as detailed. CFSM treatment was conducted for 3 days. ....	101
Fig. 4.4. FTIR spectra of (a) untreated and treated PAC using (b) Lcc 20, (c) Lcc 50, and (d) Lcc 100.....	102
Fig. 4.5. FTIR spectra of (a) untreated and treated PAC using (b) 3 days, (c) 5 days, and (d) 7 days of CFSM harvesting. ....	103
Fig. 4.6. Au(CN) <sub>2</sub> <sup>-</sup> uptake on untreated PAC, CFSM-treated PAC, and Lcc-treated PAC after 24 hours. Initial [Au(CN) <sub>2</sub> <sup>-</sup> ] is 0.23 mM. ....	104



Fig. 5.1. Catalytic cycle of laccase and mechanism of laccase mediated biodegradation of carbon.....	115
Fig. 5.2. Relative enzyme activity of free laccase (Lcc), immobilized Lcc and planktonic Lcc against time at 37°C, pH 4.5. Free (■) refers to the incubation of laccase without PAC. Immobilized (●) refers to the laccase relative activity detected after enzyme adsorption on the surface of PAC. Planktonic (▲) refers to the laccase relative activity in the supernatant over the contact time with PAC.....	120
Fig. 5.3. SEM images of PAC (a) untreated, (b) mediator controlled in the absence of laccase after 2 days, and (c) LMS-HBT treated after 1 day, (d) 2 days, (e) 5 days and (f) 7 days.....	122
Fig. 5.4. Adsorption isotherms of N <sub>2</sub> (a) and (b) NLDFT pore volume distribution of PAC before and after 1, 2 and 7 days of LMS treatment. ....	123
Fig. 5.5. FTIR spectra of PAC (a) untreated, (b) mediator controlled in the absence of laccase after 2 days, and (c) LMS treated after 1 day, (d) 2 days, (e) 5 days and (f) 7 days.....	125

Fig. 5.6. GC-MS total ion chromatograms of extractants in ethyl acetate from the untreated and LMS-treated PAC using HBT for 1~7 days in (a). GC-MS spectra for 2 and 5 days in 12-20 min of retention time we expanded in (b). Peak assignments should be referred in Table 5.2.....	127
Fig. 5.7. GC-MS total ion chromatograms of extractants in hexane from the untreated and LMS-treated PAC using HBT for 1~7 days. Peak assignments should be referred in Table 5.3.....	129
Fig. 5.8. Thermal decomposition characteristics of the untreated PAC and LMS treated PAC after 2 and 7 days, showing (a) mass loss, (b) differential thermal analysis (DTA), and (c) differential thermogravimetry (DTG).....	137
Fig. 5.9. Raman spectra for untreated and LMS treated PAC after 1-7 days. Relative intensity of D-band to G-band are included. ....	139
Fig. 5.10. Changes in HBT concentrations in the LMS over time.....	140
Fig. 5.11. $\text{Au}(\text{CN})_2^-$ uptake on untreated and LMS-treated PAC using HBT for 0~7 days, before and after washing. LMS treatment was performed at 37°C and pH 4.5. ....	142

Fig. 5.12. Schematic illustration of changes in $\text{Au}(\text{CN})_2^-$ uptake (%) on PAC after LMS treatment, showing biodegradation and washing effects. ....	144
Fig. 6.1. Steps of sequential extraction and GC-MS characterization on carbonaceous gold ores. ....	159
Fig. 6.2. Soxhlet apparatus parts and sample thimble location. ....	160
Fig. 6.3. Raman spectra for PXX, BOG, and SYM in a region from 1800 $\text{cm}^{-1}$ to 1200 $\text{cm}^{-1}$ with relative intensities of $I_D/I_G$ . ....	166
Fig. 6.4. Relation between Raman relative intensities ( $I_D/I_G$ ) and $\text{Au}(\text{CN})_2^-$ adsorption abilities on PXX, BOG, and SYM. ....	167
Fig. 6.5. Thermogravimetric analysis (TG-DTA) for PXX, BOG, and SYM, (a) mass loss (%), (b) DTA ( $\mu\text{V}$ ), (c) DTG ( $\text{mg}/\text{min}$ ). ....	169
Fig. 6.6. GC-MS total ion chromatograms of (a) hexane, (b) ethyl acetate, and (c) acetone extracts from PXX after sequential extraction. ....	170
Fig. 6.7. GC-MS total ion chromatograms of (a) hexane, (b) ethyl acetate, and (c) acetone extracts from BOG after sequential extraction. ....	179
Fig. 6.8. GC-MS total ion chromatograms of (a) hexane, (b) ethyl acetate, and (c) acetone extracts from SYM after sequential extraction. ....	187

Fig. 6.9. Particle size distribution of untreated DA, DA after 0.1M HCl washing (DAW), and DA after 0.4 M oxalic acid washing (DAO). ....	195
Fig. 6.10. Changes in XRD patterns of as-received BOG (DA), after 0.1M HCl washing (DAW), and after 0.4 M oxalic acid washing (DAO). ....	197
Fig. 6.11. Differential thermogravimetry (DTG) of as-received BOG (DA), after 0.1M HCl washing (DAW), and after 0.4 M oxalic acid washing (DAO).....	199
Fig. 6.12. Remining Fe concentrations (wt%) on DA during 0.2 M oxalic acid washing.....	199
Fig. 6.13. Gold recovery depending on the multiple additions of Lcc with and without mediator.....	201
Fig. 6.14. Three-dimensional fluorescence spectrum for the supernatant after 0.2 M NaOH at 60°C washing of (a) DA and (b) DAO. ....	202
Fig. 6.15. Total organic carbon (TOC) after 7 days of Lcc/LMS reaction on DAO. 25mg/100 mL and 50 mg/100 mL indicates the final concentration of Lcc in the reaction.....	203

Fig. 6.16. Three-dimensional fluorescence spectrum for the supernatant after 0.2 M NaOH at 60°C washing of DAOY series .....	205
Fig. 6.17. Gold recovery on DAO and DAOY-12 under strong cyanide concentration. ....	207
Fig. 6.18. Uptake of $\text{Au}(\text{CN})_2^-$ on DA, DAO and Lcc/LMS treated DAO (n=2). ....	208
Fig. 6.19. Changes in Raman spectra for solid residues before and after LMS treatment for CM degradation in a region from 1200 $\text{cm}^{-1}$ to 1700 $\text{cm}^{-1}$ with relative intensities of $I_D/I_G$ . ....	209
Fig. 6.20. Graphical interpretation of extracellular polymeric substances (EPS) formation during bio-oxidation and its interference on LMS reaction on BOG. ....	211
Fig. 6.21. Sequential pre-treatment of SYM including laccase-mediator system. ....	212
Fig. 6.22. GC-MS total ion chromatograms of (a) hexane, (b) ethyl acetate, and (c) acetone extracts from SYM after sequential extraction. ....	213
Fig. 6.23. Gold recoveries from the solid residues in SYM sequential pre-treatment, including laccase-mediator system (LMS). ....	221

Fig. 7.1. Flowchart of carbonaceous gold ore treatment to maximize gold recovery.....	235
Fig. 6S.1. Changes in XRD patterns of solid residues after sequential bio-treatment. (a) DA: CSC after bio-oxidation of mixed culture; DAC: treated DA by cell-free spent medium of <i>P. chrysosporium</i> and (b) DC: treated CSC by cell-free spent medium of <i>P. chrysosporium</i> . Symbols: py (pyrite, PDF 01–042–1340); ars (arsenopyrite, PDF 00–060-0322); sco (scorodite, PDF 00-018-0654); mus (muscovite, PDF 01-076-0929); qtz (quartz, PDF 00–014-0218); chl (chlorite, PDF 00-060-0322).....	244
Fig. 6S.2. Thermal decomposition characteristics of the as-received sample (CSC) and the bio-treated residues (DA, DAC and DC), showing (a) mass loss, differential thermal analysis (b) DTA, and (c) differential thermogravimetry DTG. CM means carbonaceous matter. ....	246
Fig. 6S.3. MLA classified images showing (a) electrum, (b) hessite particles, and (c) silver-containing other minerals in CSC. ....	248
Fig. 6S.4. Gold and silver distribution in accordance with the particle size in carbonaceous silver ore concentrate before and after bio-oxidation of mixed culture. Lib: liberated, Exp: exposed and Enc: enclosed.....	249

Fig. 6S.5. Changes in (a) pH, (b) cell density, (c) total Fe, (d) As concentrations, and (e) Eh vs SHE, (f) total Cd and total Ag concentrations with time of biooxidation by mix culture (n=3). ....	251
Fig. 6S.6. MLA classified images showing (a) electrum, (b) silver-containing other minerals in carbonaceous silver ore concentrate after bio-oxidation using mixed culture of <i>Acidianus brierleyi</i> , <i>Acidianus manzaensis</i> and <i>Metallosphaera sedula</i> (DA). ....	252
Fig. 6S.7. Particle size distribution of the as-received sample (CSC) and the bio-treated solid residues (DA, DAC and DC). ....	255
Fig. 6S.8. Schematic illustration of Ag recovery in sequential biomineral processing of carbonaceous silver concentrate (CSC). DA: treated CSC by iron- and sulfur-oxidizing mixed archaea culture, <i>Acidianus brierleyi</i> , <i>Acidianus manzaensis</i> and <i>Metallosphaera sedula</i> ; DAC: treated DA by CFSM of <i>Phanerochaete chrysosporium</i> ; DC: treated CSC by CFSM of <i>P. chrysosporium</i> .....	257

# **Chapter 1:**

## **Introduction**



## **1.1. Gold ore classification**

Gold has been a synonym for wealth, power, and prosperity in humankind since ancient times, making it valuable and desirable for accumulation. Even now, its demand is still rising worldwide regardless of its limited and finite amount (Neesse, 2014). Gold has unique properties like malleability, ductility, conductivity, and high corrosion resistance, making it suitable for numerous utilizations (Liu et al., 2022). In the past, gold was known to be used for jewelry (De Marchi et al., 2014; Fening, 2015; Kaspin et al., 2021; Nithisathian et al., 2012), decoration (Hunt, 1979; Stevenson, 2017), and monetary exchange (Burkhalter & Murphy, 1989; Bursche et al., 2010; Oddy & La Niece, 1986; Watson, 1967). However, nowadays, we can see broad applications in electronics (Bishop et al., 2010; Christie & Cameron, 1994; Kato & Okinaka, 2004), dentistry (Bapat et al., 2020; Donaldson, 2013; Knosp et al., 2003), medicine (Demann et al., 2005; Giljohann et al., 2010; Hegde et al., 2022; Higby, 1982; Panyala et al., 2009), material development (Coetzee et al., 2011; Corti & Holliday, 2004), economy (Dooley et al., 2006; Salisu et al., 2022; Sui et al., 2021; Verbrugge & Geenen, 2019), and aerospace industry (Basheer, 2020; Miyakawa, 1980; Sloboda, 1971). Global estimation of gold reserves is calculated to be 54,000 tons, and due to the high gold demand, the extraction of this noble metal seems to continue unstoppably for a while (Sousa et al., 2022). Until now, gold is industrially mainly obtained from primary resources (gold ore deposits) and seldom amounts from secondary resources (waste) (Costa et al., 2022). Nevertheless, the first ones are becoming scarce, and low-grade ores remain for extraction (Zammit et al., 2012). The problem with low-grade ores is that pre-treatments are required to extract gold efficiently, and this is because gold is strongly associated with other minerals due to its natural occurrence (Costa et al., 2022).

Therefore, a better understanding of the gold location and association improve its processing and beneficiation. Since the discovery of cyanidation in the late 19<sup>th</sup> century (Marsden & House, 2006), this leaching reagent has dominated the preference in gold hydrometallurgy, and about 90% of gold ores are treated by this method (Tu et al., 2019). In this context, gold is classified into two major categories: free-milling and refractory (Adams, 2016) based on their mineralogical characteristics and processing. Although several authors classify gold ores in different ways (Sousa et al., 2022), as observed in Fig. 1.1, for the scope of the present work, further details of the two categories mentioned above are given, especially the refractory gold ores.



Fig. 1.1. Classification of gold ore types (Zhou & Gu, 2016)

#### 1.1.1. Free-milling gold ores

These gold ore types are generally defined based on the recovery obtained by the standard cyanidation process, yielding equal or more than 95% of gold recovery without difficult pre-treatments (Afenya, 1991). Unlike placers, which can be recovered directly

without any treatment, free-milling ores typically need crushing and grinding for processing (Prasad et al., 1991). In these ores, gold grains are principally liberated from their mineral matrix, generally silicates, oxides, and/or sulfides (Fig. 1.2). Depending on the gold association with these minerals, care should be taken during cyanidation because of interferences and cyanide and oxygen consumption (La Brooy et al., 1994). Although there are still some gold mines in operation in Canada, Uzbekistan, the United States of America, Peru, Australia, and South Africa (Marsden & House, 2006), the rapid depletion of free-milling ores globally is causing gold mines change their attention to the refractory gold ores.

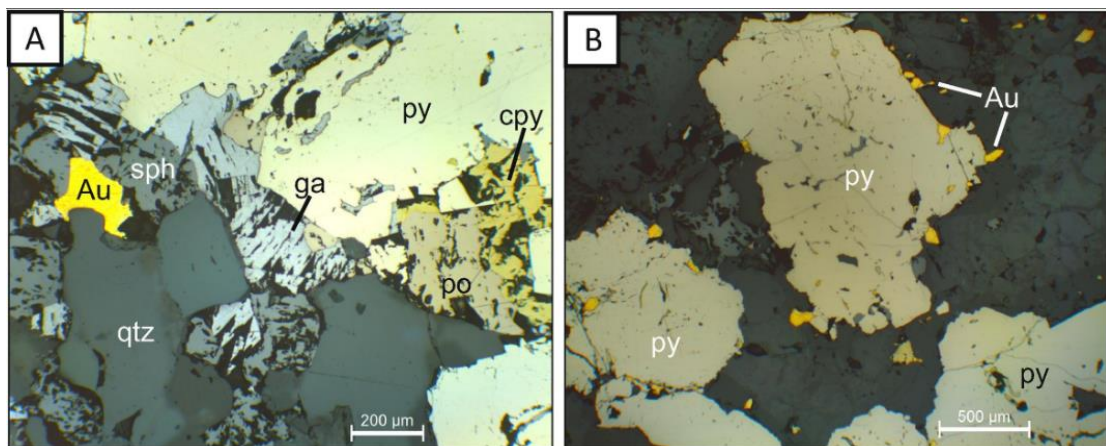


Fig. 1.2. Photomicrographs taken under reflected light and uncrossed nicols. A) and B) gold ore sample consists of a smoky and white quartz (qtz)-carbonate matrix with mostly pyrite (py) and minor pyrrhotite (po), chalcopyrite (cpy), sphalerite (sph) and galena (ga). Gold size distribution is heterogeneous and is mainly located at sulfide grain boundaries or as free particles in the matrix (Ferraz da Costa et al., 2022).

### 1.1.2. Refractory gold ores

Unlike free-milling gold ores, the refractory ones cannot be extracted successfully by cyanidation; they require additional pre-treatments beforehand to achieve acceptable recoveries for economic feasibility. Vaughan (2004) classified them into three categories: a) mildly refractory: 80-95%, b) moderately refractory: 50-80%, and c) highly refractory: <50% gold recovery. The degree of refractoriness depends on several mineralogical occurrences like the physical encapsulation of gold, passivation of gold caused by associated minerals, reagent consumption by host minerals, and the presence of carbonaceous matter or insoluble gold alloys (Goodall & Scales, 2007). The most common and studied cases of refractoriness include sulfides and/or carbonaceous matter ores, which will be discussed following.

#### 1.1.2.1. Sulfidic gold ores

Gold deposits are often associated with quartz-carbonate veins containing a variety of sulfides, which generally host gold in their matrix due to natural transportation and deposition in hydrothermal systems (Bancroft & Jean, 1982; Tivey et al., 1995; Zhu et al., 2011). Among sulfides, pyrite ( $\text{FeS}_2$ ) and arsenopyrite are the most encountered hosts for gold (Ariffin & Hewson, 2007; La Brooy et al., 1994; Morey et al., 2008). However, gold can also be aggregated in pyrrhotite ( $\text{Fe}_{1-x}\text{S}$ ), sphalerite ( $\text{ZnS}$ ), galena ( $\text{PbS}$ ), chalcopyrite ( $\text{CuFeS}_2$ ), bornite ( $\text{Cu}_5\text{FeS}_4$ ), covellite ( $\text{CuS}$ ), and/or chalcocite ( $\text{Cu}_2\text{S}$ ) (Ahn et al., 2019; Deschênes & Ghali, 1988; Hurley & Crocket, 1985; Kesler et al., 2002; Liu et al., 2017; Lorenzen & van Deventer, 1992; Ubaldini et al., 2000; Wang et al., 2019; Wu et al., 2021).

The meager leaching characteristics of sulfidic ores rely on the fact that gold occurs like sub-micrometer particles ( $<1\ \mu\text{m}$ ) encapsulated in the sulfide matrix (Fig. 1.3), limiting the access of cyanide (Morey et al., 2008). Despite this, the surrounding sulfide minerals can also produce deleterious effects through the excessive consumption of cyanide and/or oxygen (La Brooy et al., 1994; Vaughan, 2004). This effect was observed primarily in pyrrhotite, which has side reactions with cyanide, forming thiocyanate and ferrocyanide, thus causing the rapid expending of both cyanide and oxygen (Lorenzen & van Deventer, 1992).

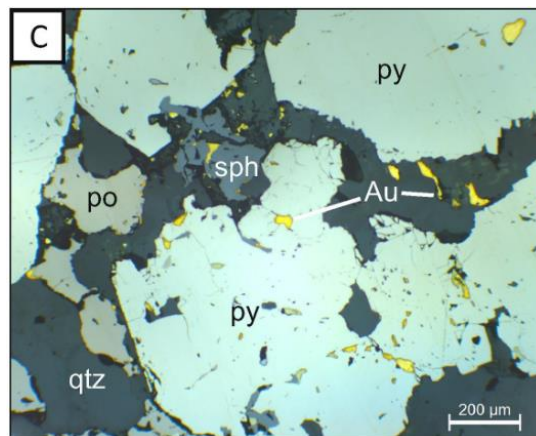


Fig. 1.3. Photomicrographs taken under reflected light and uncrossed nicols. C) gold ore sample consists of a smoky and white quartz (qtz)-carbonate matrix with mostly pyrite (py) and minor pyrrhotite (po) and sphalerite (sph). Gold size distribution is heterogeneous and is mainly enclosed in pyrite (Ferraz da Costa et al., 2022).

Although exclusive gold association with copper minerals is uncommon, it can be found mainly in chalcopyrite and less in proportion in bornite (Adams et al., 2008). However, copper minerals are also described as cyanide consumers because they can form various

copper cyanide complexes leading to the addition of large amounts of cyanide and increasing operational costs (Adams et al., 2008; La Brooy et al., 1994). These expenses are also reflected in the insertion of remediation stages to treat excess cyanide.

#### 1.1.2.2. Carbonaceous gold ores

The term preg-robbing has been used since the late 1980s by metallurgists. It refers to the adsorption of  $\text{Au(CN)}_2^-$  by naturally occurring CM during cyanidation, causing gold losses (Miller et al., 2016). In sedimentary rocks, the carbonaceous matter (CM) is commonly associated with sulfides and is directly involved in Au metallogenesis (Mirasol-Robert et al., 2017; Wu et al., 2020). CM originated from organic matter precursors that were in contact with rocks and transformed over time (Greenwood et al., 2013). Similar to the coal formation, organic matter can be graphitized through burial pressure under high temperatures (Miki, 1983), and in the process of diagenesis, the graphitic degree of CM increased (Konadu et al., 2020), as illustrated in Fig. 1.4. Previous works by Abotsi & Osseo-Asare (1986); Ibrado & Fuerstenau (1992); Schmitz et al. (2001); and Yang et al. (2013) have described that CM is composed of three main components: (i) hydrocarbons, that appear to not interact with  $\text{Au(CN)}_2^-$ , but they could coat the surface of CM; (ii) humic acids, that possess a variety of functional groups that chelates Au; and (iii) graphitic/amorphous elemental carbon, that is the responsible for  $\text{Au(CN)}_2^-$  adsorption during cyanidation. The following postulates regarding the adsorption mechanism by CM are well-accepted: (i) Ion-pair adsorption between  $\text{Au(CN)}_2^-$  and CM helped by coexisting cations presented in the alkaline solution (Adams & Fleming, 1989); (ii) unpaired  $\text{Au(CN)}_2^-$  adsorption by  $\pi$  electron donation from aromatic carbon in the CM to Au from  $\text{Au(CN)}_2^-$  (Ibrado & Fuerstenau, 1995),

and (iii) by electrostatic interaction at CM active sites, mainly at the edge of the graphitic structure (Sibrell & Miller, 1992; Lagerge et al., 1999). Although the chemical characteristics of CM define its preg-robbing ability, the carbon content in the ore (wt%) and the specific surface area should also be considered because the adsorption capacity of CM could increase drastically if these factors are high enough (Miller et al., 2016). Hence, a comprehensive characterization of CM from a physic-chemical aspect is necessary to examine the preg-robbing degree. One way to indirectly estimate the preg-robbing ability of CM is by Raman spectroscopy, which appears to show a good correlation to the preg-robbing capacities of CM (Konadu et al., 2020; Ng et al., 2022).

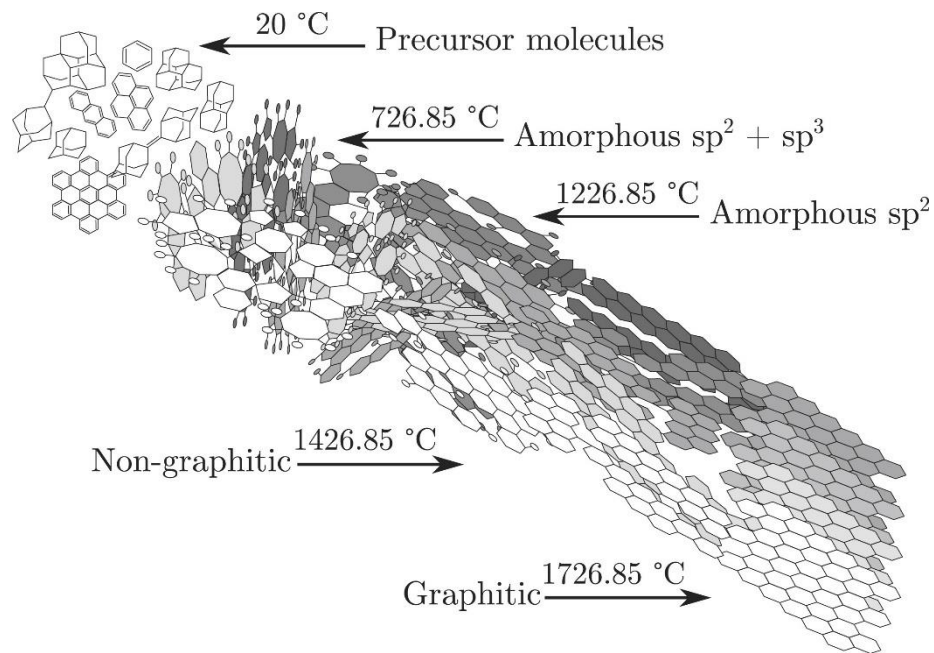


Fig. 1.4. Model of graphitic structure transformation from carbon under different temperatures (Schuepfer et al., 2020)

Although carbonaceous gold ores carry several challenges for their beneficiation, the rapid depletion of free-milling gold ores is causing mining companies to look for new gold sources like carbonaceous gold ores. Table 1.1 shows some examples of carbonaceous gold ores used for different approaches. These have been found dispersed worldwide with different carbon contents (wt%), gold contents (g/t), and gold recoveries (<75%). As described previously, a quartz matrix having a sulfide and CM association is generally observed in gold deposits. However, occasionally, there are cases where gold grains are trapped in sulfides and CM is present in the ore, causing  $\text{Au}(\text{CN})_2^-$  adsorption if Au is somehow liberated. Such gold ores are classified as double refractory gold ores (DRGO), and special pre-treatments are necessary before cyanidation to achieve acceptable gold recoveries. The following section discusses and summarizes some of the pre-treatments in previous studies.



Table 1.1. List of carbonaceous gold ores, their elemental and mineralogical characteristics

Location	Sample type	Organic carbon content (wt%)	Gold content (g/t)	Gold recovery (%)	Associated minerals	Reference
Qinling Mountains, Shaanxi Province, China	Raw ore	1.79	4.00	4.55	Quartz, dolomite, barite, calcite, muscovite, and pyrite	Xiao et al. (2022)
Shaanxi, China	Raw ore	11.00*	21.11	-	Quartz, pyrite, muscovite, and wurtzite	Wu et al. (2022)
Qinling Mountains, Shaanxi Province, China	Raw ore	5.05	2.90	-	Quartz, dolomite, barite, muscovite, pyrite, and limonite	Zhang et al. (2022)
Zijin Shuiyindong gold mine, China	Raw ore	0.92	7.85	-	Quartz, ankerite, dolomite, pyrite, arsenopyrite, marcasite, and trace amounts of pyrrhotite	Ng et al. (2022)
Syama mine, Mali	Flotation concentrate	4.16	24.00	41.50	Quartz, magnesite, chlorite, pyrite, muscovite, albite, and dolomite	Sakai et al. (2022)
Ghana	Raw ore	0.95	17.20	6.40	Quartz, muscovite, ephesite, biotite, gypsum, and pyrite	Owusu et al. (2021)
United States of America	Flotation concentrate	5.10	30.60	67.00	Quartz, muscovite, chlorite, arsenopyrite, pyrite	Mendoza et al. (2021)

Location	Sample type	Organic carbon content (wt%)	Gold content (g/t)	Gold recovery (%)	Associated minerals	Reference
Ghana	Flotation concentrate	4.40	28.60	-	Quartz, muscovite, arsenopyrite, and pyrite	Amankwah & Ofori-Sarpong (2020)
Gansu, China	Raw ore	3.44	21.13	13.15	Quartz and pyrite	Wu et al. (2020)
Prestea Bogoso mining region, Ghana	Flotation concentrate	5.86*	40.40	25.00	Quartz, illite, pyrite, feldspar, iron oxyhydroxide, rutile	Konadu et al. (2020)
Shandong Gold Co., China	Flotation concentrate	0.90	21.90	67.0	Quartz, calcite, and dolomite	Wang et al. (2020)
Yunnan province, China	Flotation concentrate	6.95*	18.05	28.70	Quartz, carbonates, arsenopyrite, and pyrite	Xu et al. (2020)
Paracatu, Minas Gerais, Brazil	Flotation concentrate	0.28 organic 1.06 elemental	12.66	-	Quartz, muscovite, pyrite, and arsenopyrite	Santiago and Ladeira (2019)
Yunnan Gold & Mining Group Co., Ltd., China	Flotation concentrate	8.29*	29.40	5.90	Quartz, mica, arsenopyrite, and pyrite	Wang et al. (2019)
Agnico Eagle Mines Kittilä mine, Finland	Flotation concentrate	3.3	73.60	2.10	Quartz, arsenopyrite, and arsenic-bearing pyrite	Ahtiainen et al. (2018)
Sumatra and Sulawesi, Indonesia	Flotation concentrate	1.85*	2.48	47.80	Quartz, mica, feldspar, gypsum, calcite, dolomite, and pyrite	Mubarok et al. (2017)

Location	Sample type	Organic carbon content (wt%)	Gold content (g/t)	Gold recovery (%)	Associated minerals	Reference
Ghana	Flotation concentrate	3.60	30.00	41.00	Pyrite, arsenopyrite, chalcopyrite, and pyrrhotite	Ofori-Sarpong et al. (2013)
Goldstrike mining area, Nevada, USA	Raw ore	5.95*	1.52	0	Quartz, dolomite, pyrite, and muscovite	Nanthakumar et al. (2007)
-	Flotation concentrate	6.10*	65.30	-	Pyrite and arsenopyrite	Amankwah et al. (2005)
Stawell gold mine, Australia	Raw ore	0.25	3.65	-	Quartz, muscovite, chlorite, dolomite, calcite, chalcopyrite, pyrrhotite, biotite, arsenopyrite, and pyrite	Tan et al. (2005)
Western district of Victoria, Australia	Raw ore	-	1.54	15.60	Quartz, clinochlore, pigeonite, and pyrite	Goodall et al. (2005)
Goldstrike mining area, Nevada, USA	Raw ore	0.8 - 3.8	2.50 - 9.25	0 - 92.50	Quartz, pyrite, other sulfide minerals, and carbonates	Schmitz et al. (2001)
Carlin Trend, Nevada, USA	Raw ore	0.79	5.13	<10%	Quartz, montmorillonite, kaolinite, illite, sericite, marcasite, and pyrite	Fernández et al. (2000)

\*Total carbon (wt%).

## **1.2. Mineral processing of refractory gold ores**

### **1.2.1. Sulfide pre-treatment**

The main objective of pre-treat sulfides in refractory gold ores is to liberate gold from the sulfidic matrix (Fig. 1.3), usually pyrite and arsenopyrite. However, pre-treating sulfides help to remove gold-leaching reagent consumers, which is also valuable before the cyanidation process. Several pre-treatments, including pyrometallurgical and hydrometallurgical, were developed and applied in previous reports. The pyrometallurgical techniques include standard roasting (Nazari et al., 2017; Prasad et al., 1991; Komnitsas & Pooley, 1989), microwave-assisted roasting (Amankwah & Ofori-Sarpong, 2020; Amankwah & Pickles, 2009; Nanthakumar et al., 2007), additive assisted roasting (He et al., 2020; Liu et al., 2019), acid leaching (Wang et al., 2018; Zhang et al., 2018), and alkaline leaching (Anderson, 2016; Celep & Serbest, 2015; Alp et al., 2014; Celep et al., 2011). Roasting was the pre-treatment par excellence in the past due to its effectiveness in oxidizing sulfides and liberating gold. Despite the ease of this method, large quantities of energy are necessary for continuous operations. Recently, microwave-assisted roasting obtained further improvements for sulfide thermal pre-treatments. The advantage relies on selectively transferring heat to the minerals and decreasing energy consumption (Nanthakumar et al., 2007). Although roasting and its variations for improving gold recovery show benefits and profits at mining scales, sulfur dioxide, and other toxic gases are generated in the process, causing severe air environmental pollution. These ecological concerns also relapse in the acid and alkaline leaching due to the large reagent consumptions and secondary-formed residues through the chemical reactions.

Oppositely to conventional pre-treatments, the use of microorganisms in hydrometallurgy is gaining more attention due to the success of their industrial applications worldwide (Arrascue & van Niekerk, 2006; Chandraprabha et al., 2002; Olson, 1994; Mubarak et al., 2017; Wu, 2018). Bio-oxidation of sulfides is a cost-effective, energy-efficient, and environment-friendly technology that can achieve high gold recoveries competing in effectivity to roasting (Natarajan, 2018). Bio-oxidation has been applied in the major gold-hosts like pyrite (Blight et al., 2000; Canales et al., 2002; Rojas-Chapana et al., 1996) and arsenopyrite (Olson, 1994; Jiang et al., 2008), but other gold-containing sulfides like marcasite and pyrrhotite (Uboldini et al., 2000; Yadollahi et al., 2021) has been a target for research as well. The iron-oxidizing bacteria *Acidithiobacillus ferrooxidans* has been the most used and studied mesophile to understand the oxidation mechanisms involved in sulfide oxidation. According to Natarajan (2018), there are two mechanisms: non-contact and contact. The first involves planktonic bacterial oxidation of  $\text{Fe}^{2+}$  to  $\text{Fe}^{3+}$  in solution, which then enters in contact with the sulfides for further oxidation, liberating  $\text{Fe}^{2+}$  in the process and thus repeating the cycle. On the other hand, the contact leaching mechanism includes the use of extracellular polymeric substances (EPS) as support for cellular attachment on the sulfides. EPS has a pivotal role in the interaction of bacteria and the mineral for further oxidation of  $\text{Fe}^{2+}$  to  $\text{Fe}^{3+}$  on the surface (Gehrke et al., 1998). The above-described mechanisms are summarized in Fig. 1.5.

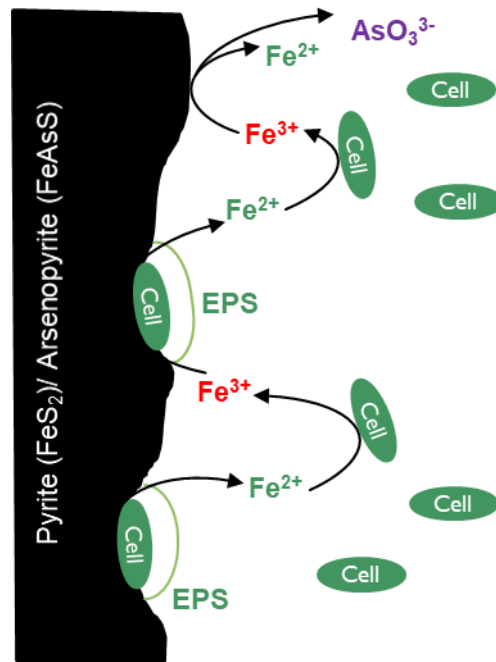


Fig. 1.5. Contact and non-contact leaching mechanism involved in bio-oxidation. Adapted from Natarajan (2018).

#### 1.2.2. Carbonaceous matter pre-treatment

Yang et al. (2013) classify the CM pre-treatment techniques into two (i) removing or decomposing methods and (ii) partial or complete passivating methods. CM can be completely removed by roasting and other thermal techniques like sulfides. However, in the same manner as sulfide roasting, the high energy consumption and emission of greenhouse gases like CO<sub>2</sub> due to the combustion of carbon decreases their feasibility due to the current environmental restrictions for safeguarding the Sustainable Development Goals (SDGs) (Liu et al., 2022). Other decomposing techniques include pressure oxidation, chlorination, nitric acid treatment, and bio-oxidation (Miller et al., 2016; Yang et al., 2013; Afenya, 1991). As for passivation, this can be chemically achieved by using blanking agents like kerosene, diesel, and aromatic hydrocarbons.

These organic surfactants can modify the CM surface and thus cause electrostatic repulsion between CM and  $\text{Au}(\text{CN})_2^-$ , reducing its preg-robbing ability (Afenya, 1991). Recently, the CM surface coating was also studied by Owusu et al. (2021) on carbonaceous gold ores, suggesting that naphthalene sulphonate could be a good candidate for decreasing the  $\text{Au}(\text{CN})_2^-$  adsorption behavior of CM. Among the described pre-treatments, bio-oxidation is a new process that has gained promising applicability in natural carbonaceous gold ores (Amankwah et al., 2005). The beneficial effects include not only the disruption of the aromatic structure but also passivation might be encountered (Brierley & Kulpa, 1992; Amankwah et al., 2005; Yang et al., 2013; Konadu et al., 2019a). Passivation by bacteria is strongly related to the secretion of EPS on the ore surface because of its composition, mainly including sugars, lipids, and organic acids (Gehrke et al., 1998).

The findings of Portier (1991) and Brierley & Kulpa (1992) introduced the concept of using microorganisms like heterotrophic bacteria and fungi to degrade CM. Years later, Amankwah et al. (2005) used actinomycete *Streptomyces setonii* to enhance the gold recovery by 13.6% in carbonaceous gold ore. The following studies by Ofori-Sarpong et al. (2010, 2013a) expanded the application of living organisms in a myco-hydrometallurgical approach using *Phanerochaete chrysosporium*. In these studies, the lignin-degrading enzymes like lignin peroxidase (LiP) and manganese peroxidase (MnP) secreted by *P. chrysosporium* started to gain relevance in the understanding of CM degradation by using coal surrogates and DRGO. Finally, the fungal approach to treat CM was optimized by Konadu et al. (2017) through the use of cell-free spent medium (CFSM) from *P. chrysosporium* on activated carbon (CM surrogate) degradation. Enzymatic characterization of the CFSM revealed the presence of LiP and

MnP in the extracted cocktail (Harada et al., 2016; Kudo et al., 2017). Moreover, solid characterization by  $^{13}\text{C}$  NMR and FTIR revealed the transformation of poly-aromatic carbon into aliphatic carbons over the process. These findings and the direct intervention of peroxidases in the degradation of CM surrogate were not shown in previous reports. Then, the application of CFSM on a DRGO helped by direct observation demonstrated that the peroxidases predominantly decomposed the defect-bearing graphitic carbon into humic-like substances, forming C-Si-Al agglomerates in the process (Konadu et al., 2019b).

Within the CM treatments described above, the use of lignin-degrading enzymes as an alternative to degrade CM keeps advancing and developing new applications in the mineral processing of gold. Consequently, the current work will explore the application of another lignin-degrading enzyme that was not detected in CFSM and, therefore, not reported previously.

### 1.2.3. Sequential biological pre-treatment

The mineral processing of sulfides and CM in DRGO through biological pre-treatments in one single step is a challenging task, especially because the microorganisms used in bio-oxidation processes cannot decompose CM in the same way as sulfides (Yang et al., 2013). Thus, improvements in gold recovery rely on the sulfide decomposition grade and possible passivation caused by secreted metabolites without assuring CM degradation. In such understanding, the use of other living organisms with the capacity to oxidize CM was introduced and evaluated. However, the differences in growth solution media and optimal environmental conditions like pH and temperature differ



among the species. As a result, separating the bio-treatments into two stages was applied by several authors to improve the total efficiency of gold recovery (Konadu 2019a; Ofori-Sarpong et al., 2013b; Yen et al., 2009; Brierley & Kulpa, 1992). Furthermore, starting the sequential bio-treatment with the sulfide decomposition result in protecting the following CM oxidation process by dissolving hazardous elements like arsenic, silver, and cadmium which causes inhibitory effects on microorganisms and secreted enzymes (Bailey & Hansford, 1993; Mendoza et al., 2021). This observation was specially appointed by Konadu et al. (2019a), who demonstrated that gold recoveries in DRGO yielded 92% after the sequential pre-treatment and alkaline washing (Fig. 1.6).

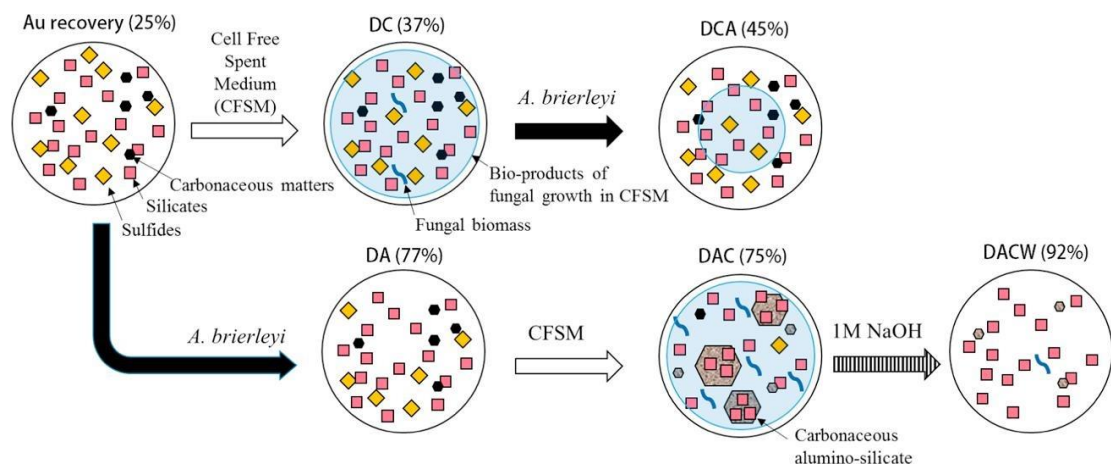


Fig. 1.6 Schematic illustration of sequential biomineral processing of double refractory gold ore (DRGO). DC: treated DRGO by cell-free spent medium (CFSM) of white-rot fungus *Phanerochaete chrysosporium*; DA: treated DRGO by iron-oxidizing archaeon, *Acidianus brierleyi*; DCA: treated DC by *Acidianus brierleyi*; DAC: treated DA by CFSM (Konadu et al., 2019a).

### 1.3. Lignin-degrading enzymes

The importance of lignin-degrading enzymes, especially the peroxidases secreted by *Phanerochaete chrysosporium*, in CM degradation was pointed out in previous sections and applied to several studies (Cindy et al., 2021; Mendoza et al., 2021; Konadu et al., 2019; Konadu et al., 2017; Liu et al., 2016, 2014; Ofori-Sarpong et al., 2010). The necessity to scale up the enzymatic pre-treatment of CM for industrial approaches involves the search for conditions where enzyme applications can be adapted to mining operations. As such, peroxidases have some drawbacks compared to other extracellular enzymes such as laccase, which are also known to be responsible for natural lignin degradation. In the following sub-sections, further discussions of their differences are detailed.

#### 1.3.1. Peroxidases

The most studied peroxidases are lignin peroxidase (LiP, EC 1.11.1.14) and manganese peroxidase (MnP, EC 1.11.1.13), which were initially reported in *Phanerochaete chrysosporium* (Kuwahara et al., 1984; Tien & Kirk, 1984). Both enzymes are heme-containing glycoproteins and require H<sub>2</sub>O<sub>2</sub> for catalytic oxidation (Fakoussa & Hofrichter, 1999). LiP possesses a high redox potential (1.2-1.5 V) that allows it to degrade various organic substrates, including phenolic and non-phenolic compounds (Peralta et al., 2017). Despite its oxidation strength, LiP is a susceptible enzyme with several disadvantages for biotechnological applications: (i) unstable at high temperatures, (ii) vulnerable to solvent and excess presence of H<sub>2</sub>O<sub>2</sub>, and (iii) scarce production for commercial approaches (Biko et al., 2020). As for MnP, the catalytic

cycle resembles LiP but with the difference that MnP oxidizes  $\text{Mn}^{2+}$  to  $\text{Mn}^{3+}$ , which acts as an electron shuttle when it is stabilized by organic acids (Fakoussa & Hofrichter, 1999). Still, some disadvantages rely on its limited production to certain basidiomycetous and its sensitive to high  $\text{H}_2\text{O}_2$  concentrations like LiP (Hofrichter, 2002). Therefore, the utilization of peroxidases seems complicated when looking at broad biotechnological approaches like in mineral processing. Besides the fungal peroxidases, a series of white-rot basidiomycetes produce laccase (Lcc), a multi-copper oxidase, which is also responsible for lignin degradation in nature and it was discovered several years before the peroxidases (Peralta et al., 2017).

### 1.3.2. Laccase

Laccase (Lcc, EC 1.10.3.2) is widely produced by several organisms, including the majority of ligninolytic fungi (Agrawal et al., 2018), some bacteria (Claus, 2004) and plants (Bai et al., 2023). Fungal laccases possess a more comprehensive range of adaptability (pH and temperature) and specificity during substrate oxidation. Although, like any other enzyme, laccase activity can be inhibited by some inorganic and organic substances, as listed in Table 1.3. Therefore, when applying to the mineral processing of gold ores, care should be taken to avoid inhibition. Laccase is a so-called green biocatalyst because it only requires molecular oxygen ( $\text{O}_2$ ) as a co-substrate, avoiding toxic  $\text{H}_2\text{O}_2$  for its catalytic activation (Rivera-Hoyos et al., 2013). Lcc constitutes four copper atoms divided into Type 1, 2, and 3 (Fig. 1.7). Type I gives the characteristic blue color to the protein and is the site where substrate oxidation occurs. Type 2 and 3 copper are strategically positioned close to each other to form the trinuclear cluster where  $\text{O}_2$  is reduced to subsequently release  $\text{H}_2\text{O}$  (Agrawal et al., 2018; Claus, 2004).

As a result, the oxidation of substrates generates the release of active radicals (Chen et al., 2017) that further accompany non-enzymatic reactions like (i) cross-linking, (ii) polymer degradation, and (iii) bond cleavage. However, unlike LiP, the low standard redox potential of Lcc ( $< 1.0$  V) appears to be a disadvantage because non-phenolic compounds ( $> 1.5$  V) are not targeted for Lcc oxidation (Munk et al., 2015). Therefore, some reports suggest that adding small organic molecules, called mediators, is necessary to achieve broad oxidation of substrates with higher standard redox potentials (Christopher et al., 2014; Galli & Gentili, 2004). Considering the addition of a mediator and the feasibility of expanding the use of Lcc in various substrates, a comparing table that includes LiP, MnP, and Lcc is presented (Table 1.4).

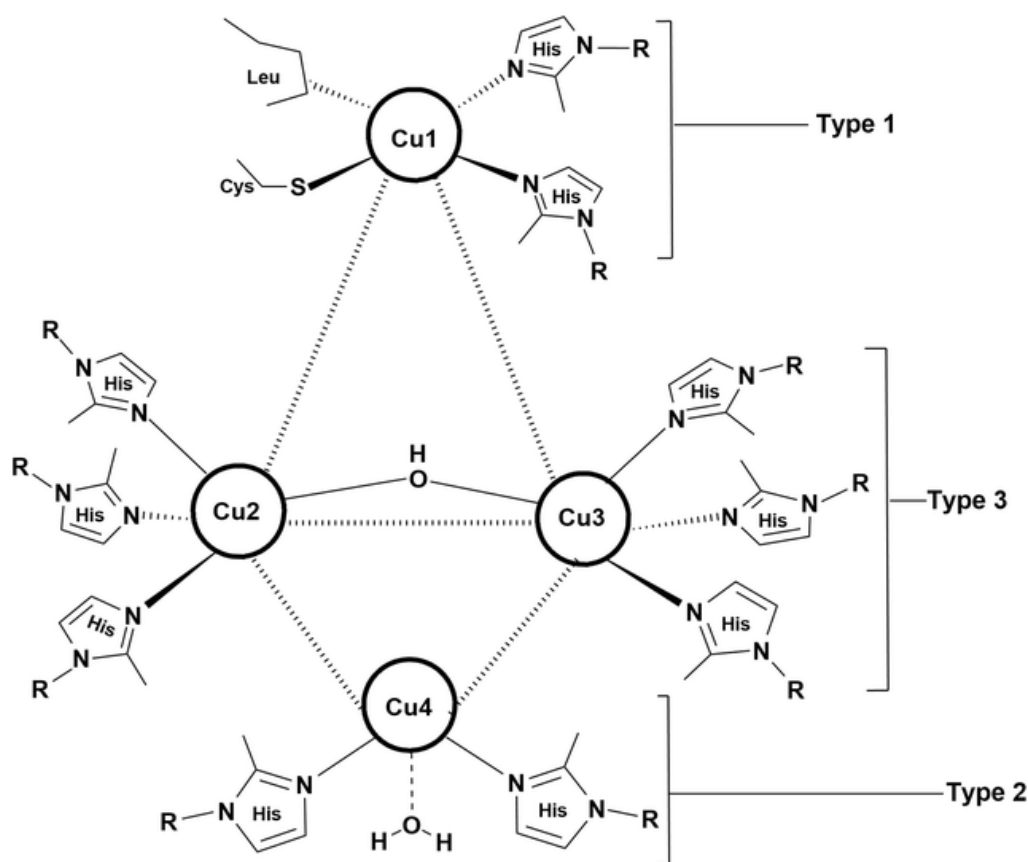


Fig. 1.7. Copper centers of laccase: Type 1, Type 2, and Type 3 (Agrawal et al., 2018).

Table 1.2. Biochemical characterization of purified laccases from different fungal species

Host name	Type	Molecular weight (kDa)	pH		Temperature		Inhibitors		Reference
			Range of activity	Optimal	Range of activity	Optimal	Inorganic	Organic	
<i>Aureobasidium pullulans</i> NAC8	Yeast-like fungus	68.4	3.0–6.0	4.5	45°C–55°C	45°C	Ni <sup>2+</sup> , Co <sup>2+</sup> , and NaN <sub>3</sub>	thioglycolic acid, 2-mercaptoethanol	Ademakinwa & Agboola (2016)
<i>Marasmius</i> Sp. BBKAV79	White-rot fungus	75.0	5.0–7.2	5.5	37°C–55°C	40°C	Hg <sup>2+</sup> and Ag <sup>+</sup> (strong inhibitors) H <sub>2</sub> O <sub>2</sub> , NaCl	phenylmethanesulfonyl fluoride (PMSF), sodium dodecyl sulfate (SDS)	Vantamuri & Kaliwal (2016)
<i>Trametes versicolor</i>	White-rot fungus	100.0	-	3.0	25°C–70°C	50°C	-  Fe <sup>2+</sup> (strong inhibitor)	-	Bertrand et al. (2015)
<i>Echinodontium taxodii</i> 2538	White-rot fungus	56.0	2.2–6.0	3.0	30°C–60°C	60°C	Cu <sup>2+</sup> , Ni <sup>2+</sup> , Zn <sup>2+</sup> , Co <sup>2+</sup> , Ca <sup>2+</sup> , Ba <sup>2+</sup> , Hg <sup>2+</sup> , K <sup>+</sup> , and NaN <sub>3</sub> (partial inhibitors)	dithiothreitol and 1,4-dioxane (strong inhibitors)	Shi et al. (2014)
<i>Cyathus bulleri</i>	Bird's nest fungus	60.0	2.0–6.0	5.2	25°C–70°C	45°C	NaN <sub>3</sub> . KCN, Hg <sup>2+</sup> (strong inhibitors)	SDS and β-mercaptoethanol, cetyltrimethyl ammonium bromide	Vasdev et al. (2005)

Table 1.3. Comparison of the properties and advantages/disadvantages of using different enzymes for CM degradation. Adapted from (Fakoussa & Hofrichter, 1999)

Characteristic	Lignin-peroxidase (LiP)	Mn-peroxidase (MnP)	Laccase (Lcc)
Redox potential	1200 – 1500 mV	1100 mV	(400) – 960 mV
Activation	H <sub>2</sub> O <sub>2</sub>	H <sub>2</sub> O <sub>2</sub>	O <sub>2</sub>
Substrate	Aromatic compounds (phenolic and non-phenolic)	Specific to Mn(II)	Aromatic compounds (phenolic)
Stability	Very low	Very low	Very high
pH range / opt.	2 – 5 / 2.5 – 3	2 – 6 / 4 – 4.5	2 – 8.5 / 3.5 – 7
Temp. range	30 – 55°C	30 – 55°C	20 – 60°C
Mediator	Veratryl alcohol	Mn <sup>2+/3+</sup>	HBT, ABTS
Catalytic center	Fe-protoporphyrin	Fe-protoporphyrin	Four copper-atoms
Availability	Limited	Limited	Wider
Industrial application	Difficult	Difficult	Promising

#### 1.3.2.1.Laccase-mediator system

Adding an electron carrier between Lcc and substrate, called mediator, increases the reach of Lcc application (Munk et al., 2015). Mediators are characterized as small aromatic molecules that, after being oxidized by Lcc, diffuse as radicals and access the target due to their small sizes (Fig. 1.8), generating reactions that Lcc alone cannot accomplish (Galli & Gentili, 2004). Until now, natural mediators for Lcc are still under investigation. Therefore, synthetic mediators and their application on lignin models have helped to understand the mechanism involved in them.

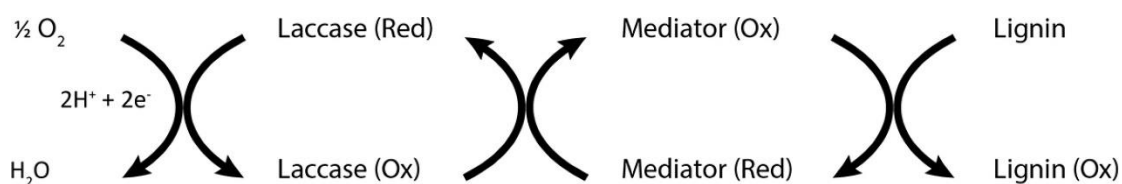


Fig. 1.8. Catalytic cycle of laccase and mechanism of laccase-mediated biodegradation of lignin (Longe et al., 2018).

Among the synthetic mediators, 1-hydroxybenzotriazole (HBT) and 2,2'-azinobis(3-ethylbenzthiazoline-6-sulfonate) (ABTS) are the most reported due to their high performances on degrading countless substrates (Andreu & Vidal, 2011; Jeon & Park, 2020; Longe et al., 2018; Naghdi et al., 2018; Nguyen et al., 2014). Fabbrini et al. (2002a, 2002b) reported their oxidation mechanism, which includes hydrogen transfer (HAT) and electron transfer (ET), respectively. The impact of the laccase-mediator system (LMS) has been studied widely in lignin and its models, responding to their application in several businesses, including pulp and paper, forestall, and the food industry (Minussi et al., 2002; Singh & Arya, 2019; Widsten & Kandelbauer, 2008). Considering that CM is a lignin precursor, as detailed in section 1.1.2.2., LMS application on CM is a profit of investigation for industrial applications.

#### 1.4. Objective of the thesis

Previous studies have optimized the fungal enzymatic treatment of carbonaceous matter (CM) in DRGO by peroxidases and demonstrated its efficiency in degrading CM. However, industrial approaches to peroxidase usage, especially in extracted spent medium, seem nonprofitable due to drawbacks in enzyme production, low activities,

enzyme stabilities, hydrogen peroxide consumption, and upgrade handling caused by complicated procedures. Moreover, the application of purified peroxidases on CM degradation was not possible due to their high cost of purification. Thus, seeking new enzymatic alternatives to resolve these bottlenecks to ensure industrial applicability in operating gold mines is imperative. Laccase is another lignin-degrading enzyme associated with lignin degradation, and its application relies on numerous industries, expecting the mining business. When laccase is applied in the presence of a mediator, its oxidation capabilities are expanded to substrates with high standard redox potentials, equaling the advantages of peroxidases.

Moreover, when using fungal enzymes to degrade organic substrates, the identification of by-products and reaction intermediates is generally observed through analytical methods like gas chromatography-mass spectrometry (GC-MS). As for the author's knowledge, GC-MS was not previously used for such commitment. Based on the above statements, this study selected purified laccase in the presence and absence HBT as a mediator for the degradation of carbonaceous matter in DRGO. The specific objectives of this work are detailed as follows:

- 1) Compare the degradation abilities of purified laccase from *Trametes versicolor* in the absence of a mediator with CFSM from *Phanerochaete chrysosporium* in preliminary experiments using powder-activated carbon (PAC) as a surrogate.
- 2) Apply LMS using HBT on PAC degradation and characterize its physical and chemical changes through several techniques, including  $\text{Au}(\text{CN})_2^-$  adsorption and GC-MS.
- 3) Investigate the degradation of carbonaceous matter in gold ores using laccase at a molecular level.



- 4) Investigate the relationship of graphiticity in carbonaceous matter with gold recovery in cyanidation.
- 5) Study the graphiticity as an index to express the refractoriness in enzymatic degradation of carbonaceous matter in gold ores.

Finally, an additional chapter evaluates the effect of different acid ratios (HCl: HNO<sub>3</sub>) on gold extraction from DRGO. Additionally, investigations of the impact of matrix matching for Fe concentrations in the Au standard solutions for ICP-OES and L-cysteine as a scarifying oxidant to prevent the reduction of [AuCl<sub>2</sub>]<sup>-</sup> into Au(0), which causes “memory effect” in ICP-MS.

## References

- Abotsi, G. M. K., & Osseo-Asare, K. (1986) Surface chemistry of carbonaceous gold ores I. Characterization of the carbonaceous matter and adsorption behavior in aurocyanide solution. *International Journal of Mineral Processing*, 18(3–4), 217–236.
- Adams, M. D. (2016) Gold Ore Processing. In M. D. Adams (Ed.), *Developments in Mineral Processing* (2nd ed.).
- Adams, M. D., & Fleming, C. A. (1989) The mechanism of adsorption of aurocyanide onto activated carbon. *Metallurgical and Materials Transactions B* 1989 20:3, 20(3), 315–325.
- Adams, M., Lawrence, R., & Bratty, M. (2008) Biogenic sulphide for cyanide recycle and copper recovery in gold–copper ore processing. *Minerals Engineering*, 21(6), 509–517.

- Ademakinwa, A. N., & Agboola, F. K. (2016) Biochemical characterization and kinetic studies on a purified yellow laccase from newly isolated *Aureobasidium pullulans* NAC8 obtained from soil containing decayed plant matter. *Journal of Genetic Engineering and Biotechnology*, 14(1), 143–151.
- Afenya, P. M. (1991) Treatment of carbonaceous refractory gold ores. *Minerals Engineering*, 4(7–11), 1043–1055.
- Agrawal, K., Chaturvedi, V., & Verma, P. (2018) Fungal laccase discovered but yet undiscovered. *Bioresources and Bioprocessing*, 5(1).
- Ahn, J., Wu, J., Ahn, J., & Lee, J. (2019) Comparative investigations on sulfidic gold ore processing: A novel biooxidation process option. *Minerals Engineering*, 140(April), 105864.
- Ahtiainen, R., Lundström, M., & Liipo, J. (2018) Preg-robbing verification and prevention in gold chloride-bromide leaching. *Minerals Engineering*, 128, 153–159.
- Alp, I., Celep, O., Paktunç, D., & Thibault, Y. (2014) Influence of potassium hydroxide pretreatment on the extraction of gold and silver from a refractory ore. *Hydrometallurgy*, 146, 64–71.
- Amankwah, R. K., & Ofori-Sarpong, G. (2020) Microwave roasting of flash flotation concentrate containing pyrite, arsenopyrite and carbonaceous matter. *Minerals Engineering*, 151, 106312.
- Amankwah, R. K., & Pickles, C. A. (2009) Microwave roasting of a carbonaceous sulphidic gold concentrate. *Minerals Engineering*, 22(13), 1095–1101.

- Amankwah, R. K., Yen, W.-T., & Ramsay, J. A. (2005) A two-stage bacterial pretreatment process for double refractory gold ores. *Minerals Engineering*, 18(1), 103–108.
- Anderson, C. G. (2016) Alkaline sulfide gold leaching kinetics. *Minerals Engineering*, 92, 248–256.
- Andreu, G., & Vidal, T. (2011) Effects of laccase-natural mediator systems on kenaf pulp. *Bioresource Technology*, 102(10), 5932–5937.
- Ariffin, K. S., & Hewson, N. J. (2007) Gold-Related Sulfide Mineralization and Ore Genesis of the Penjom Gold Deposit, Pahang, Malaysia. *Resource Geology*, 57(2), 149–169.
- Arrascue, M. E. L., & van Niekerk, J. (2006) Biooxidation of arsenopyrite concentrate using BIOX® process: Industrial experience in Tamboraque, Peru. *Hydrometallurgy*, 83(1–4), 90–96.
- Bai, Y., Ali, S., Liu, S., Zhou, J., & Tang, Y. (2023) Characterization of plant laccase genes and their functions. *Gene*, 852, 147060.
- Bailey, A. D., & Hansford, G. S. (1993) Factors affecting bio-oxidation of sulfide minerals at high concentrations of solids: A review. *Biotechnology and Bioengineering*, 42(10), 1164–1174.
- Bancroft, G. M., & Jean, G. (1982) Gold deposition at low temperature on sulphide minerals. *Nature* 1982 298:5876, 730–731.

Bapat, R. A., Chaubal, T. V., Dharmadhikari, S., Abdulla, A. M., Bapat, P., Alexander, A., Dubey, S. K., & Kesharwani, P (2020). Recent advances of gold nanoparticles as biomaterial in dentistry. *International Journal of Pharmaceutics*, 586, 119596.

Basheer, A. A. (2020) Advances in the smart materials applications in the aerospace industries. *Aircraft Engineering and Aerospace Technology*, 92(7), 1027–1035.

Bertrand, B., Martínez-Morales, F., Tinoco-Valencia, R., Rojas, S., Acosta-Urdapilleta, L., & Trejo-Hernández, M. R. (2015) Biochemical and molecular characterization of laccase isoforms produced by the white-rot fungus *Trametes versicolor* under submerged culture conditions. *Journal of Molecular Catalysis B: Enzymatic*, 122, 339–347.

Biko, O. D. V., Viljoen-Bloom, M., & van Zyl, W. H. (2020) Microbial lignin peroxidases: Applications, production challenges and future perspectives. *Enzyme and Microbial Technology*, 141(September), 109669.

Bishop, P. T., Ashfield, L. J., Berzins, A., Boardman, A., Buche, V., Cookson, J., Gordon, R. J., Salcianu, C., & Sutton, P. A. (2010) Printed gold for electronic applications. *Gold Bulletin* 2010 43:3, 43(3), 181–188.

Blight, K., Ralph, D. E., & Thurgate, S. (2000) Pyrite surfaces after bio-leaching: a mechanism for bio-oxidation. *Hydrometallurgy*, 58(3), 227–237.

Brierleyi, J. A., & Kulpa, C. F. (1992) Microbial consortium treatment of refractory precious metal ores - Patent No. US5127942A.

Burkhalter, S. B., & Murphy, R. F. (1989) Tappers and sappers: rubber, gold and money among the Mundurucú. *American Ethnologist*, 16(1), 100–116.

- Bursche, A., Więcek, T., Bursche, A., & Więcek, T. (2010) Roman gold coins and medallions, pierced or looped, from the collections of the National Museum of Ukrainian History in Kyiv. *Wiadomości Numizmatyczne*, 2.
- Canales, C., Acevedo, F., & Gentina, J. C. (2002) Laboratory-scale continuous bio-oxidation of a gold concentrate of high pyrite and enargite content. *Process Biochemistry*, 37(10), 1051–1055.
- Celep, O., Alp, I., & Deveci, H. (2011) Improved gold and silver extraction from a refractory antimony ore by pretreatment with alkaline sulphide leach. *Hydrometallurgy*, 105(3–4), 234–239.
- Celep, O., & Serbest, V. (2015) Characterization of an iron oxy/hydroxide (gossan type) bearing refractory gold and silver ore by diagnostic leaching. *Transactions of Nonferrous Metals Society of China*, 25(4), 1286–1297.
- Chandraprabha, M. N., Modak, J. M., Natarajan, K. A., & Raichur, A. M. (2002) Strategies for efficient start-up of continuous biooxidation process for refractory gold ores. *Minerals Engineering*, 15(10), 751–753.
- Chen, M., Wang, L., Tan, T., Luo, X. C., Zheng, Z., Yin, R. C., Su, J. H., & Du, J. F. (2017) Radical mechanism of laccase-catalyzed catechol ring-opening. *Wuli Huaxue Xuebao/ Acta Physico - Chimica Sinica*, 33(3), 620–626.
- Christie, I. R., & Cameron, B. P. (1994) Gold electrodeposition within the electronics industry. *Gold Bulletin* 1994 27:1, 27(1), 12–20.
- Christopher, L. P., Yao, B., & Ji, Y. (2014) Lignin biodegradation with laccase-mediator systems. *Frontiers in Energy Research*, 2, 1-13.

- Cindy, Sakai, R., Mendoza, D. M., Konadu, K. T., & Sasaki, K. (2021) Significance of acid washing after biooxidation of sulfides in sequential biotreatment of double refractory gold ore from the syama mine, Mali. *Minerals*, 11(12), 1316.
- Claus, H. (2004) Laccases: Structure, reactions, distribution. *Micron*, 35(1–2), 93–96.
- Coetzee, L. L., Theron, S. J., Martin, G. J., Merwe, J. D. Van Der, & Stanek, T. A. (2011) Modern gold deportments and its application to industry. *Minerals Engineering*, 24(6), 565–575.
- Corti, C. W., & Holliday, R. J. (2004) Commercial aspects of gold applications: From materials science to chemical science. *Gold Bulletin* 2004 37:1, 37(1), 20–26.
- Costa, F. R., Nery, G. P., Carneiro, C. D. C., Kahn, H., & Ulsen, C. (2022) Mineral characterization of low-grade gold ore to support geometallurgy. *Journal of Materials Research and Technology*, 21, 2841–2852.
- De Marchi, V., Lee, J., & Gereffi, G. (2014) Globalization, recession and the internationalization of industrial districts: Experiences from the Italian Gold Jewellery Industry, 22(4), 866–884.
- Demann, E. T. K., Stein, P. S., & Haubenreich, J. E. (2005) Gold as an implant in medicine and dentistry. *Journal of Long-Term Effects of Medical Implants*, 15(6), 687–698.
- Deschênes, G., & Ghali, E. (1988) Leaching of gold from a chalcopyrite concentrate by thiourea. *Hydrometallurgy*, 20(2), 179–202.
- Donaldson, J. A. (2013) The use of gold in dentistry. *Gold Bulletin* 1980 13:3, 13(3), 117–124.

- Dooley, M. P., Isard, P., & Taylor, M. P. (2006) Exchange rates, country-specific shocks, and gold, 5(3), 121–129.
- Fabbrini, M., Galli, C., & Gentili, P. (2002a) Comparing the catalytic efficiency of some mediators of laccase. *Journal of Molecular Catalysis - B Enzymatic*, 16(5–6), 231–240.
- Fabbrini, M., Galli, C., & Gentili, P. (2002b) Radical or electron-transfer mechanism of oxidation with some laccase/mediator systems. *Journal of Molecular Catalysis B: Enzymatic*, 18(1–3), 169–171.
- Fakoussa, R. M., & Hofrichter, M. (1999) Biotechnology and microbiology of coal degradation. In *Applied Microbiology and Biotechnology* (Vol. 52, Issue 1, pp. 25–40).
- Fening, P. A. (2015) Design Trends in Gold Jewellery Making in Ghana and global cultural influence. *Journal of Arts and Humanities*, 4(4), 57–62.
- Fernández, R. R., Sohn, H. Y., & LeVier, K. M. (2000) Process for treating refractory gold ores by roasting under oxidizing conditions. *Mining, Metallurgy & Exploration* 2000 17:1, 17(1), 1–6.
- Ferraz da Costa, M., Kyle, J. R., Lobato, L. M., Ketcham, R. A., Figueiredo e Silva, R. C., & Fernandes, R. C. (2022) Orogenic gold ores in three-dimensions: A case study of distinct mineralization styles at the world-class Cuiabá deposit, Brazil, using high-resolution X-ray computed tomography on gold particles. *Ore Geology Reviews*, 140, 104584.
- Galli, C., & Gentili, P. (2004) Chemical messengers: Mediated oxidations with the enzyme laccase. *Journal of Physical Organic Chemistry*, 17(11), 973–977.

- Gehrke, T., Telegdi, J., Thierry, D., & Sand, W. (1998) Importance of extracellular polymeric substances from *Thiobacillus ferrooxidans* for bioleaching. *Applied and Environmental Microbiology*, 64(7), 2743–2747.
- Giljohann, D. A., Seferos, D. S., Daniel, W. L., Massich, M. D., Patel, P. C., & Mirkin, C. A. (2010) Gold nanoparticles for biology and medicine. *Angewandte Chemie*, 49(19), 3280–3294.
- Goodall, W. R., Leatham, J. D., & Scales, P. J. (2005) A new method for determination of preg-robbing in gold ores. *Minerals Engineering*, 18(12), 1135–1141.
- Goodall, W. R., & Scales, P. J. (2007) An overview of the advantages and disadvantages of the determination of gold mineralogy by automated mineralogy. *Minerals Engineering*, 20(5), 506–517.
- Greenwood, P. F., Brocks, J. J., Grice, K., Schwark, L., Jaraula, C. M. B., Dick, J. M., & Evans, K. A. (2013) Organic geochemistry and mineralogy. I. Characterisation of organic matter associated with metal deposits. *Ore Geology Reviews*, 50, 1–27.
- Gregory J. Olson. (1994) Microbial oxidation of gold ores and gold bioleaching. *FEMS Microbiology Letters*, 119, 1–6.
- Harada, A., Sasaki, K., & Kaneta, T. (2016) Direct determination of lignin peroxidase released from *Phanerochaete chrysosporium* by in-capillary enzyme assay using micellar electrokinetic chromatography. *Journal of Chromatography A*, 1440, 145–149.
- He, Y., Hu, X., Zi, F., Yang, B., & Cheng, H. (2020) Solidification of sulfur and arsenic in gold concentrate and leaching of the gold by thiosulfate. *Asia-Pacific Journal of Chemical Engineering*, 15(1), e2396.



- Hegde, M., Pai, P., Gangadhar, M., & Sundara, K. (2022) Environmental Nanotechnology , Monitoring & Management Gold nanoparticle based biosensors for rapid pathogen detection : A review. Environmental Nanotechnology, Monitoring & Management, 18, 100756.
- Higby, G. J. (1982) Gold in medicine. Gold Bulletin 1982 15:4, 15(4), 130–140.
- Hofrichter, M. (2002) Review: Lignin conversion by manganese peroxidase (MnP). In Enzyme and Microbial Technology 30(4), 454–466.
- Hunt, L. B. (1979) Gold in the pottery industry. Gold Bulletin 1979 12:3, 12(3), 116–127.
- Hurley, T. D., & Crocket, J. H. (1985) A gold-sphalerite association in a volcanogenic base-metal- sulfide deposit near Tilt Cove, Newfoundland. Canadian Mineralogist, 23(3), 423–430.
- Ibrado, A. S., & Fuerstenau, D. W. (1992) Effect of the structure of carbon adsorbents on the adsorption of gold cyanide. Hydrometallurgy, 30(1–3), 243–256.
- Ibrado, A. S., & Fuerstenau, D. W. (1995) Infrared and X-ray photoelectron spectroscopy studies on the adsorption of gold cyanide on activated carbon. Minerals Engineering, 8(4–5), 441–458.
- Jeon, S. J., & Park, J. H. (2020) Refolding, characterization, and dye decolorization ability of a highly thermostable laccase from *Geobacillus sp.* JS12. Protein Expression and Purification, 173, 105646.
- Jiang, T., Li, Q., Yang, Y. Bin, Li, G. Hui, & Qiu, G. Zhou. (2008) Bio-oxidation of arsenopyrite. Transactions of Nonferrous Metals Society of China, 18(6), 1433–1438.

John O. Marsden, C. I. H. (2006) *The Chemistry of Gold Extraction* (2nd ed.). Society for Mining, Metallurgy, and Exploration, Inc. (SME).

Kaspin, S., Khairi, H., Hassan, O. H., Mohamad, N., & Norazmi Bin Nordin, M. (2021) Identifying factors leading to gold losses during the fabrication process and assessing its impact on the Smes Jewellery Industry. *Turkish Journal of Computer and Mathematics Education*, 12(7), 975–985.

Kato, M., & Okinaka, Y. (2004) Some recent developments in non-cyanide gold plating for electronics applications. *Gold Bulletin* 2004, 37(1), 37–44.

Kesler, S. E., Chryssoulis, S. L., & Simon, G. (2002) Gold in porphyry copper deposits: its abundance and fate. *Ore Geology Reviews*, 21(1–2), 103–124.

Knosp, H., Holliday, R. J., & Corti, C. W. (2003) Gold in dentistry: Alloys, uses and performance. *Gold Bulletin* 2003, 36(3), 93–102.

Komnitsas, C., & Pooley, F. D. (1989). Mineralogical characteristics and treatment of refractory gold ores. *Minerals Engineering*, 2(4), 449–457.

Konadu, K. T., Sasaki, K., Kaneta, T., Ofori-Sarpong, G., & Osseo-Asare, K. (2017) Bio-modification of carbonaceous matter in gold ores: Model experiments using powdered activated carbon and cell-free spent medium of *Phanerochaete chrysosporium*. *Hydrometallurgy*, 168, 76–83.

Konadu, K. T., Harrison, S. T. L., Osseo-Asare, K., & Sasaki, K. (2019a) Transformation of the carbonaceous matter in double refractory gold ore by crude lignin peroxidase released from the white-rot fungus. *International Biodeterioration and Biodegradation*, 143

- Konadu, K. T., Huddy, R. J., Harrison, S. T. L., Osseo-Asare, K., & Sasaki, K. (2019b) Sequential pretreatment of double refractory gold ore (DRGO) with a thermophilic iron oxidizing archaeon and fungal crude enzymes. *Minerals Engineering*, 138, 86–94.
- Konadu, K. T., Mendoza, D. M., Huddy, R. J., Harrison, S. T. L., Kaneta, T., & Sasaki, K. (2020) Biological pretreatment of carbonaceous matter in double refractory gold ores: A review and some future considerations. *Hydrometallurgy*, 196, 105434.
- Kudo, S., Harada, A., Kubota, H., Sasaki, K., & Kaneta, T. (2017) Simultaneous Determination of Manganese Peroxidase and Lignin Peroxidase by Capillary Electrophoresis Enzyme Assays. *ACS Omega*, 2(10), 7329–7333.
- Kuwahara, M., Glenn, J. K., Morgan, M. A., & Gold, M. H. (1984). Separation and characterization of two extracellular H<sub>2</sub>O<sub>2</sub>-dependent oxidases from ligninolytic cultures of *Phanerochaete chrysosporium*. *FEBS Letters*, 169(2), 247–250.
- La Brooy, S. R., Linge, H. G., & Walker, G. S. (1994). Review of gold extraction from ores. *Minerals Engineering*, 7(10), 1213–1241.
- Lagerge, S., Zajac, J., Partyka, S., & Groszek, A. J. (1999). Comparative study on the adsorption of cyanide gold complexes onto different carbonaceous samples: Measurement of the reversibility of the process and assessment of the active surface inferred by flow microcalorimetry. *Langmuir*, 15(14), 4803–4811.
- Liu, L., Liu, Q., Zhang, S., Li, Y., & Yang, L. (2022). The thermal transformation behavior and products of pyrite during coal gangue combustion. *Fuel*, 324, 124803.
- Liu, Q., Yang, H., Tong, L., Jin, Z., & Sand, W. (2016). Fungal degradation of elemental carbon in Carbonaceous gold ore. *Hydrometallurgy*, 160, 90–97.

- Liu, Q., Yang, H. Y., & Tong, L. L. (2014). Influence of *Phanerochaete chrysosporium* on degradation and preg-robbing capacity of activated carbon. Transactions of Nonferrous Metals Society of China, 24(6), 1905–1911.
- Liu, W., Fu, X., Rao, S., Yang, T., Zhang, D., & Chen, L. (2017) Selection on the Process for Removing and Recovering Antimony from Antimonial Refractory Gold Ores. Minerals, Metals and Materials Series, Part F7, 489–498.
- Liu, X., Li, Q., Zhang, Y., Jiang, T., Yang, Y., Xu, B., & He, Y. (2019) Improving gold recovery from a refractory ore via Na<sub>2</sub>SO<sub>4</sub> assisted roasting and alkaline Na<sub>2</sub>S leaching. Hydrometallurgy, 185, 133–141.
- Liu, Z. wei, Guo, X. Yi, Tian, Q. hua, & Zhang, L. (2022) A systematic review of gold extraction: Fundamentals, advancements, and challenges toward alternative lixivants. Journal of Hazardous Materials, 440, 129778.
- Longe, L. F., Couvreur, J., Leriche Grandchamp, M., Garnier, G., Allais, F., & Saito, K. (2018) Importance of Mediators for Lignin Degradation by Fungal Laccase. ACS Sustainable Chemistry and Engineering, 6(8), 10097–10107.
- Lorenzen, L., & van Deventer, J. S. J. (1992) Electrochemical interactions between gold and its associated minerals during cyanidation. Hydrometallurgy, 30(1–3), 177–193.
- Mendoza, D. M., Konadu, K. T., Aoki, Y., Kameya, M., & Sasaki, K. (2021) Carbonaceous matter degradation by fungal enzyme treatment to improve Ag recovery from an Au-Ag-bearing concentrate. Minerals Engineering, 163, 106768.
- Miki, T. (1983) Graphitization of carbonaceous matter in sedimentary rocks. Journal of the Sedimentological Society of Japan, 111–120.

- Miller, J. D., Wan, R-Y., & Díaz, X. (2016) Preg-Robbing Gold Ores. *Gold Ore Processing*, 885–907.
- Minussi, R. C., Pastore, G. M., & Durán, N. (2002) Potential applications of laccase in the food industry. *Trends in Food Science & Technology*, 13(6–7), 205–216.
- Mirasol-Robert, A., Grotheer, H., Bourdet, J., Suvorova, A., Grice, K., McCuaig, T. C., & Greenwood, P. F. (2017) Evidence and origin of different types of sedimentary organic matter from a Paleoproterozoic orogenic Au deposit. *Precambrian Research*, 299, 319–338.
- Miyakawa, Y. (1980) Friction and wear performance of gold and gold alloy films. *Gold Bulletin* 1980, 13(1), 21–30.
- Morey, A. A., Tomkins, A. G., Bierlein, F. P., Weinberg, R. F., & Davidson, G. J. (2008) Bimodal Distribution of Gold in Pyrite and Arsenopyrite: Examples from the Archean Boorara and Bardoc Shear Systems, Yilgarn Craton, Western Australia. *Economic Geology*, 103(3), 599–614.
- Mubarok, M. Z., Winarko, R., Chaerun, S. K., Rizki, I. N., & Ichlas, Z. T. (2017) Improving gold recovery from refractory gold ores through biooxidation using iron-sulfur-oxidizing/sulfur-oxidizing mixotrophic bacteria. *Hydrometallurgy*, 168, 69–75.
- Munk, L., Sitarz, A. K., Kalyani, D. C., Mikkelsen, J. D., & Meyer, A. S. (2015) Can laccases catalyze bond cleavage in lignin? *Biotechnology Advances*, 33(1), 13–24.
- Naghdi, M., Taheran, M., Brar, S. K., Kermanshahi-pour, A., Verma, M., & Surampalli, R. Y. (2018) Biotransformation of carbamazepine by laccase-mediator system: Kinetics, by-products and toxicity assessment. *Process Biochemistry*, 67, 147–154.

- Nanthakumar, B., Pickles, C. A., & Kelebek, S. (2007) Microwave pretreatment of a double refractory gold ore. *Minerals Engineering*, 20(11), 1109–1119.
- Natarajan, K. A. (2018) Biotechnology for Gold Mining, Extraction, and Waste Control. In *Biotechnology of Metals* (pp. 179–210).
- Nazari, A. M., Ghahreman, A., & Bell, S. (2017) A comparative study of gold refractoriness by the application of QEMSCAN and diagnostic leach process. *International Journal of Mineral Processing*, 169, 35–46.
- Neesse, T. (2014) Selective attachment processes in ancient gold ore beneficiation. *Minerals Engineering*, 58, 52–63.
- Ng, W. S., Yang, Y., Su, X., Zhong, S., & Chen, M. (2022) Characterization of Preg-Robbing Carbonaceous Minerals from the Shuiyindong Carlin-Type Gold Deposit Via Spectroscopic Techniques. *Mining, Metallurgy and Exploration*, 39(1), 169–188.
- Nguyen, L. N., Hai, F. I., Kang, J., Leusch, F. D. L., Roddick, F., Magram, S. F., Price, W. E., & Nghiem, L. D. (2014) Enhancement of trace organic contaminant degradation by crude enzyme extract from *Trametes versicolor* culture: Effect of mediator type and concentration. *Journal of the Taiwan Institute of Chemical Engineers*, 45(4), 1855–1862.
- Nithisathian, K., Takala, J., Rattanakomut, S., Walsh, J., Wu, Q., Liu, Y., & University, S. (2012) Operational competitiveness development in turbulent business environment: a case study in Thailand fine gold jewelry export industry. *Management and Production Engineering Review*, 3, 53–62.

Oddy, A., & La Niece, S. (1986) Byzantine gold coins and jewellery. *Gold Bulletin* 1986, 19(1), 19–27.

Ofori-Sarpong, G., Tien, M., & Osseo-Asare, K. (2010) Myco-hydrometallurgy: Coal model for potential reduction of preg-robbing capacity of carbonaceous gold ores using the fungus, *Phanerochaete chrysosporium*. *Hydrometallurgy*, 102(1–4), 66–72.

Ofori-Sarpong, G., Osseo-Asare, K., & Tien, M. (2013a) Mycohydrometallurgy: Biotransformation of double refractory gold ores by the fungus, *Phanerochaete chrysosporium*. *Hydrometallurgy*, 137, 38–44.

Ofori-Sarpong, G., Osseo-Asare, K., & Tien, M. (2013b) Pretreatment of Refractory Gold Ores Using Cell-Free Extracts of *P. chrysosporium*: A Preliminary Study. *Advanced Materials Research*, 825, 427–430.

Ofori-Sarpong, G., Amankwah, R. K., & Osseo-Asare, K. (2013c) Reduction of preg-robbing by biomodified carbonaceous matter-A proposed mechanism. *Minerals Engineering*, 42, 29–35.

Owusu, C., Mensah, S., Ackah, K., & Amankwah, R. K. (2021) Reducing preg-robbing in carbonaceous gold ores using passivative or blanking agents. *Minerals Engineering*, 170, 106990.

Panyala, N. R., Peña-Méndez, E. M., & Havel, J. (2009) Gold and nano-gold in medicine: Overview, toxicology and perspectives. In *Journal of Applied Biomedicine*, 7(2), 75–91.

Peralta, R. M., da Silva, B. P., Gomes Côrrea, R. C., Kato, C. G., Vicente Seixas, F. A., & Bracht, A. (2017) Enzymes from Basidiomycetes—Peculiar and Efficient Tools for

Biotechnology. *Biotechnology of Microbial Enzymes: Production, Biocatalysis and Industrial Applications*, 119–149.

Portier, R. J. (1991) Biohydrometallurgical processing of ores, and microorganisms therefor (Patent No. US5021088A).

Prasad, M. S., Mensah-Biney, R., & Pizarro, R. S. (1991) Modern trends in gold processing — overview. *Minerals Engineering*, 4(12), 1257–1277.

Rivera-Hoyos, C. M., Morales-Álvarez, E. D., Poutou-Piñales, R. A., Pedroza-Rodríguez, A. M., Rodríguez-Vázquez, R., & Delgado-Boada, J. M. (2013) Fungal laccases. *Fungal Biology Reviews*, 27(3–4), 67–82.

Rojas-Chapana, J. A., Giersig, M., & Tributsch, H. (1996) The path of sulfur during the bio-oxidation of pyrite by *Thiobacillus ferrooxidans*. *Fuel*, 75(8), 923–930.

Sakai, R., Mendoza, D. M., Konadu, K. T., Cindy, Aoki, Y., Hirajima, T., Ichinose, H., & Sasaki, K. (2022) Laccase-mediator system for enzymatic degradation of carbonaceous matter in the sequential pretreatment of double refractory gold ore from Syama mine, Mali. *Hydrometallurgy*, 212, 105894.

Salisu, A. A., Pierdzioch, C., Gupta, R., & Gabauer, D. (2022) Forecasting stock-market tail risk and connectedness in advanced economies over a century: The role of gold-to-silver and gold-to-platinum price ratios. *International Review of Financial Analysis*, 83, 102300.

Santiago, R. C. C., & Ladeira, A. C. Q. (2019) Reduction of preg-robbing activity of carbonaceous gold ores with the utilization of surface blinding additives. *Minerals Engineering*, 131, 313–320.



- Schmitz, P. A., Duyvesteyn, S., Johnson, W. P., Enloe, L., & McMullen, J. (2001) Adsorption of aurocyanide complexes onto carbonaceous matter from preg-robbing Goldstrike ore. *Hydrometallurgy*, 61(2), 121–135.
- Schuepfer, D. B., Badaczewski, F., Guerra-Castro, J. M., Hofmann, D. M., Heiliger, C., Smarsly, B., & Klar, P. J. (2020) Assessing the structural properties of graphitic and non-graphitic carbons by Raman spectroscopy. *Carbon*, 161, 359–372.
- Shi, L., Yu, H., Dong, T., Kong, W., Ke, M., Ma, F., & Zhang, X. (2014) Biochemical and molecular characterization of a novel laccase from selective lignin-degrading white-rot fungus *Echinodontium taxodii* 2538. *Process Biochemistry*, 49(7), 1097–1106.
- Sibrell, P. L., & Miller, J. D. (1992) Significance of graphitic structural features in gold adsorption by carbon. *Mining, Metallurgy & Exploration*, 9(4), 189–195.
- Singh, G., & Arya, S. K. (2019) Utility of laccase in pulp and paper industry: A progressive step towards the green technology. *International Journal of Biological Macromolecules*, 134, 1070–1084.
- Sloboda, M. H. (1971) Industrial gold brazing alloys. *Gold Bulletin*, 4(1), 2–8.
- Sousa, R., Regufe, M. J., Fiúza, A., Leite, M. M., & Futuro, A. (2022) A systematic review of sustainable gold extraction from raw ores using alternative leaching reagents. *Extractive Industries and Society*, 9.
- Stevenson, J. S. (2017) Alternatives to Gold Plating in the Electronics and Decorative Industries, 59 (part 4), 113–117.

- Sui, M., Rengifo, E. W., & Court, E. (2021) Gold, inflation and exchange rate in dollarized economies – A comparative study of Turkey, Peru and the United States. *International Review of Economics & Finance*, 71, 82–99.
- Tan, H., Feng, D., Lukey, G. C., & van Deventer, J. S. J. (2005) The behaviour of carbonaceous matter in cyanide leaching of gold. *Hydrometallurgy*, 78(3–4), 226–235.
- Tien, M., & Kirk, T. K. (1984) Lignin-degrading enzyme from *Phanerochaete chrysosporium*: Purification, characterization, and catalytic properties of a unique H<sub>2</sub>O<sub>2</sub>-requiring oxygenase. *Proceedings of the National Academy of Sciences of the United States of America*, 81(8), 2280.
- Tivey, M., Larocq, A. C. L., & Petersen, S. (1995) The occurrence of gold in sulfide deposits of the tag hydrothermal field, Mid. Atlantic Ridge\*Markd. Hannington Geological Survey of Canada 601 Booth Street, Ottawa" Ontario K1A 1E8. 33, 1285–1310.
- Tu, Y., Han, P., Wei, L., Zhang, X., Yu, B., Qian, P., & Ye, S. (2019) Removal of cyanide adsorbed on pyrite by H<sub>2</sub>O<sub>2</sub> oxidation under alkaline conditions. *Journal of Environmental Sciences*, 78, 287–292.
- Uboldini, S., Vegliò, F., Beolchini, F., Toro, L., & Abbruzzese, C. (2000) Gold recovery from a refractory pyrrhotite ore by biooxidation. *International Journal of Mineral Processing*, 60(3–4), 247–262.
- Vantamuri, A. B., & Kaliwal, B. B. (2016) Purification and characterization of laccase from *Marasmius sp.* BBKAV79 and effective decolorization of selected textile dyes. *3 Biotech*, 6 (2), 189.

Vasdev, K., Dhawan, S., Kapoor, R. K., & Kuhad, R. C. (2005) Biochemical characterization and molecular evidence of a laccase from the bird's nest fungus *Cyathus bulleri*. *Fungal Genetics and Biology*, 42(8), 684–693.

Vaughan, J. (2004). The Process Mineralogy of Gold: The Classification of Ore Types. *JOM*, 56, 46–48.

Verbrugge, B., & Geenen, S. (2019) The gold commodity frontier: A fresh perspective on change and diversity in the global gold mining economy. *The Extractive Industries and Society*, 6(2), 413–423.

Wang, J., Xie, F., Wang, W., Bai, Y., Fu, Y., & Dreisinger, D. (2020) Eco-friendly leaching of gold from a carbonaceous gold concentrate in copper-citrate-thiosulfate solutions. *Hydrometallurgy*, 191, 105204.

Wang, Q., Hu, X., Zi, F., Qin, X., Nie, Y., & Zhang, Y. (2019) Extraction of gold from refractory gold ore using bromate and ferric chloride solution. *Minerals Engineering*, 136, 89–98.

Wang, Q., Hu, X., Zi, F., Yang, P., Chen, Y., & Chen, S. (2019) Environmentally friendly extraction of gold from refractory concentrate using a copper – ethylenediamine – thiosulfate solution. *Journal of Cleaner Production*, 214, 860–872.

Wang, Y., Xiao, L., Liu, H., Qian, P., Ye, S., & Chen, Y. (2018) Acid leaching pretreatment on two-stage roasting pyrite cinder for gold extraction and co-precipitation of arsenic with iron. *Hydrometallurgy*, 179, 192–197.

Watson, A. M. (1967) Back to Gold-and Silver. *The Economic History Review*, 20(1), 1.

- Widsten, P., & Kandelbauer, A. (2008) Laccase applications in the forest products industry: A review. *Enzyme and Microbial Technology*, 42(4), 293–307.
- Wu, H., Feng, Y., Li, H., Wang, H., & Ju, J. (2020) Co-recovery of manganese from pyrolusite and gold from carbonaceous gold ore using fluidized roasting coupling technology. *Chemical Engineering and Processing - Process Intensification*, 147, 107742.
- Wu, H., Wang, H., Duan, S., Li, H., & He, Q. (2022) Full-process analysis on volatilizing gold, zinc by chlorination roasting and synchronous recovery vanadium by water leaching of carbonaceous gold ore. *Minerals Engineering*, 185, 107682.
- Wu, J., Ahn, J., & Lee, J. (2021) Gold deportment and leaching study from a pressure oxidation residue of chalcopyrite concentrate. *Hydrometallurgy*, 201, 105583.
- Wu, Y. F., Evans, K., Fisher, L. A., Zhou, M. F., Hu, S. Y., Fougereuse, D., Large, R. R., & Li, J. W. (2020) Distribution of trace elements between carbonaceous matter and sulfides in a sediment-hosted orogenic gold system. *Geochimica et Cosmochimica Acta*, 276, 345–362.
- Wu, Z. L. (2018) Sulfide Minerals Bio-Oxidation of a Low-Grade Refractory Gold Ore. *Materials Science Forum*, 921(Ii), 157–167.
- Xiao, H., Jin, J., He, F., Han, Y., Sun, Y., Tang, Z., & Dong, Z. (2022) Accelerating the decarbonization of carbonaceous gold ore by suspension oxidation roasting towards the improvement of gold leaching efficiency. *Advanced Powder Technology*, 33(11), 103833.

- Xu, R., Li, Q., Meng, F., Yang, Y., Xu, B., Yin, H., & Jiang, T. (2020) Bio-oxidation of a double refractory gold ore and investigation of preg-robbing of gold from thiourea solution. *Metals*, 10(9), 1–16.
- Yadollahi, A., Abdollahi, H., Ardejani, F. D., Mirmohammadi, M., & Magdouli, S. (2021) Bio-oxidation behavior of pyrite, marcasite, pyrrhotite, and arsenopyrite by sulfur- and iron-oxidizing acidophiles. *Bioresource Technology Reports*, 15, 100699.
- Yang, H. Y., Liu, Q., Song, X. L., & Dong, J. K. (2013) Research status of carbonaceous matter in carbonaceous gold ores and bio-oxidation pretreatment. *Transactions of Nonferrous Metals Society of China*, 23(11), 3405–3411.
- Yen, W.-T., Amankwah, R. K., & Choi, Y. (2009) Microbial pre-treatment of double refractory gold ores (Patent No. US20090158893A1).
- Zammit, C. M., Cook, N., Brugger, J., Ciobanu, C. L., & Reith, F. (2012) The future of biotechnology for gold exploration and processing. *Minerals Engineering*, 32, 45–53.
- Zhang, S-H., Zheng, Y-J., Cao, P., Li, C-H., Lai, S-Z., & Wang, X-J. (2018) Process mineralogy characteristics of acid leaching residue produced in low-temperature roasting-acid leaching pretreatment process of refractory gold concentrates. *International Journal of Minerals, Metallurgy, and Materials*, 25(10), 1132–1139.
- Zhang, X., Song, Y., Wu, L., Yin, N., Bao, J., & Li, Y. (2022) Unraveling the dissociation mechanism of gold in carbonaceous gold ore during vacuum roasting pretreatment: Effect of pyrite. *Minerals Engineering*, 184, 107658.
- Zhou, J., & Gu, Y. (2016) Geometallurgical Characterization and Automated Mineralogy of Gold Ores. *Gold Ore Processing*, 95–111.

Zhu, Y., An, F., & Tan, J. (2011) Geochemistry of hydrothermal gold deposits: A review. *Geoscience Frontiers*, 2(3), 367–374.

# **Chapter 2:**

# **Methodology**

## 2.1. Enzyme studies

Coarsely purified laccase derived from the fungi *Trametes sp.* was kindly provided by Amano Enzyme Inc. (Nagoya, Japan). The laccase named Y-120 was stocked at -20°C before using it for experimental work. In the early stage of this study, the strength of Y-120 was compared with commercially available laccase from *Trametes versicolor* supplied by Sigma-Aldrich.

Table 2.1. Characteristics of laccases used in this study

Characteristics	Laccase	
Company	Amano enzyme	Sigma- Aldrich
Specimen	<i>Trametes sp.</i>	<i>Trametes versicolor</i>
Color	light green	light brown
Lot. Number	LCR0850709K	BCBZ9936
Lot. Activity	not provided	0.99 µg/mg
Storage temperature	-20°C	2 - 9°C

### 2.1.1. Laccase activity

In preliminary studies, the enzymatic activity was measured by spectrophotometry using three well-known substrates: 2,2'-azino-bis (3-ethylbenzothiazoline-6-sulfonic acid) (ABTS), 2,6-dimethoxyphenol (DMP), and guaiacol. The changes in absorbance due to the oxidation of the substrate were monitored using a microplate reader (Multiskan GO, Thermo, USA) at 420 nm ( $\epsilon_{420} = 36,000 \text{ M}^{-1} \text{ cm}^{-1}$ ) (Qiu et al., 2021; Santana et al., 2018), 468 nm ( $\epsilon_{468} = 49,600 \text{ M}^{-1} \text{ cm}^{-1}$ ) (Csarman et al., 2021; Jeon and Park, 2020), and 470 nm ( $\epsilon_{470} = 26,600 \text{ M}^{-1} \text{ cm}^{-1}$ ) (Unuofin et al., 2022), respectively.



The extinction coefficient is represented as  $\epsilon$ . For this experiment, 5 mg/10 mL of laccase Y-120 was diluted ten times using 0.1 M acetate buffer (pH 4.5) and then used for all the tests. For the assay: 50, 150, and 20  $\mu$ L aliquot of appropriately diluted laccase Y-120 was reacted with 150  $\mu$ L of 1 mM DMP, guaiacol, and ABTS, respectively. Then, the total volume was up to 300  $\mu$ L with 100 mM sodium acetate buffer (pH 4.5). The reaction was conducted at room temperature and terminated after 10 min.

The enzyme activity was calculated according to the following equation (Baltierra-Trejo et al., 2015):

$$U = \frac{\Delta A \times V_t \times D_f \times 10^6}{t \times \epsilon \times d \times V_s}$$

(Eq. 2.1)

where,

U      Enzyme activity ( $\mu\text{mol} \times \text{min}^{-1} \times \text{L}^{-1}$ ).

$\Delta A$     Final absorbance – initial absorbance.

$V_t$       Total volume of the reaction (mL).

t        Reaction time (min).

$\epsilon$         Molar extinction coefficient ( $\text{M}^{-1} \times \text{cm}^{-1}$  or  $\text{L} \times \text{mol}^{-1} \times \text{cm}^{-1}$ ).

d        Optical path (1 cm).

$V_s$       Sample volume including enzyme (mL).

$D_f$       Dilution factor.

As for the experimental work using powder-activated carbon (PAC) as a carbonaceous matter surrogate, the enzyme activity was measured using only ABTS. The reaction mixture (3 mL) for this test consisted of 0.2 mg of laccase and 0.2 mM ABTS in 100 mM acetate buffer (pH 4.5). The addition of laccase initiated the reaction, and the reaction velocity was determined by time-course data of ABTS oxidation between 0 and 5 min; the absorbance change was linear under the experimental conditions. The kinetic data were observed using an IMPLEN P300 spectrophotometer (Germany). One unit (U) was defined as the necessary amount of enzyme capable of oxidizing 1  $\mu$ mol of ABTS per minute. The enzyme activity was also calculated using equation 2.1.

#### 2.1.2. Temperature effect on laccase activity

The effect of the temperature on laccase Y-120 was assessed by measuring the activity under the following temperatures: 25°C, 30°C, 37°C, 40°C, 45°C, 50°C, 60°C, and 70°C. The kinetic data were observed between 0 and 5 min using a JASCO V-750 UV-visible spectrophotometer (Tokyo, Japan) coupled with a programmable temperature controller. On the other hand, the thermal stability was assessed by incubating Y-120 for 0.2, 1, 2, 24, and 48 hours at 4°C, 25°C, 37°C, 45°C, 60°C, and 70°C before measuring the enzyme activity. As for this test, the IMPLEN P300 spectrophotometer (Germany) was selected. ABTS was utilized as the substrate in all the reactions.

### 2.1.3. Michaelis-Menten kinetics

In order to know the relation between the substrate concentration and Y-120 catalysis, Michaelis-Menten kinetics (Navada and Kulal, 2020) was performed using different concentrations of 2,6-dimethoxyphenol (5, 10, 20, 40, 60, 100, 500  $\mu$ M).

$$V_0 = \frac{V_{max} \times [S]}{K_m + [S]} \quad (\text{Eq. 2.2})$$

where,

$V_0$  Initial rate of the reaction

$K_m$  Michaelis-Menten constant

$[S]$  Substrate concentration

$V_{max}$  Maximum rate of the reaction

### 2.1.4. Protein assay

The protein assay was conducted using Takara Bicinchoninic Acid (BCA) protein assay kit, which includes BCA reagent A, BCA reagent B, and bovine serum albumin (BSA) standard solution (2 mg/mL). However, the Takara BCA protocol was modified for laccase Y-120 protein assay because of an overestimation found after using the BSA standard.

Modified protocol (protein range: 50-2000 µg/ml) (0.3 ml reaction)

Before analysis, a working solution was prepared by mixing BCA reagent A and BCA reagent B at a 100:1 ratio. This working solution was stable for 3 days at 4°C after preparation. As for the standard curve preparation, dilutions from the laccase Y-120 standard solution were prepared as detailed in Table 2.1. Then, 100 µL of each dilution was dispensed into a microplate well by adding 200 µL of the working solution. The mixture was incubated for 30 minutes at 37°C, and the absorbance was measured at 562 nm using the microplate reader Multiskan GO, Thermo (Tokyo, Japan).

Table 2.2. Standard solutions for laccase Y-120 modified protein assay

Standard	2 mg/mL laccase Y-120 standard (µL)	Diluent (µL)	Final concentration of laccase Y-120 (µg/mL)
Blank	0	1200	0
Standard 1	100	1500	125
Standard 2	150	1050	250
Standard 3	300	900	500
Standard 4	450	750	750
Standard 5	600	600	1000
Standard 6	900	300	1500
Standard 7	1200	0	2000

## 2.2.Solution analysis

### 2.2.1. Inductively coupled plasma-optical emission spectrometry (ICP-OES) and mass spectrometry (ICP-MS)

Acid digestion was carried out to obtain the elemental composition of carbonaceous gold ore. The digested solutions were filtered and diluted 10-50 times using 0.1 M HNO<sub>3</sub> before supplying them to inductively coupled plasma-optical emission spectrometry (ICP-OES) Perkin Elmer Optima 8300 (Tokyo, Japan). For all the analyses using this equipment, the matrix solution was 0.1 M HNO<sub>3</sub>. The method considered three wavelengths for each analyte. The wavelength with the highest intensity and a correlation coefficient of 0.9995 or more was selected. The wavelengths for each analyte are described as follows, underlining the desired wavelength for concentration calculation:

- Fe: 238.204, 239.562, 259.939 nm
- As: 188.979, 193.696, 197.197 nm
- Al: 396.153, 308.215, 394.401 nm
- K: 766.455, 769.897 nm
- Mg: 286.213, 279.077, 280.271 nm
- Ca: 317.933, 315.887, 393.366 nm
- Mn: 257.604, 260.600 nm

For gold determination, ICP-OES was used when the expected gold concentration was higher than 100 ppb, like in Au(CN)<sub>2</sub><sup>-</sup> adsorption test on the carbonaceous matter surrogate. The conditions were the same as described above. The wavelengths

measured for Au were 267.595 nm, 242.795 nm, and 208.209 nm. The criteria described above were considered to select 242.795 nm wavelength for Au concentration calculations.

Regarding sample solutions containing gold concentration lower than 100 ppb, inductively coupled plasma mass spectrometry (ICP-MS) was selected because it has higher sensitivity for trace concentrations. In this case, the solutions were filtered and diluted 100 times using 1% HCl and 1% L-cysteine (Wang and Brindle, 2014) before supplying them to Agilent 7900 ICP-MS (Tokyo, Japan).

#### 2.2.2. Dissolved total organic carbon (TOC)

The total dissolved organic carbon (TOC) was determined using a Shimadzu VCSH analyzer (Kyoto, Japan). The analysis was conducted in triplicate.

#### 2.2.3. Three-dimensional fluorescence spectrometry

3D fluorescence spectrometry characterizes the residues after LMS treatment of the carbonaceous gold ore to find the humic-like substances' fingerprints (Gao et al., 2017; Zhu et al., 2012). All the liquid samples were filtered (0.20  $\mu\text{m}\phi$ ) and placed in a transparent quartz cuvette. The excitation (Ex) and emission wavelength (Em) used for the measurements were 200 nm – 500 nm and 300 nm to 600 nm, respectively. The analysis was conducted on a JASCO FP-6600 fluorescence spectrometer (Tokyo, Japan), which displayed a maximum emission intensity of 1000 arbitrary units (AU).

The general interpretation of the fingerprints coming from the analysis was compared with the following graph obtained by Chen et al. (2003).

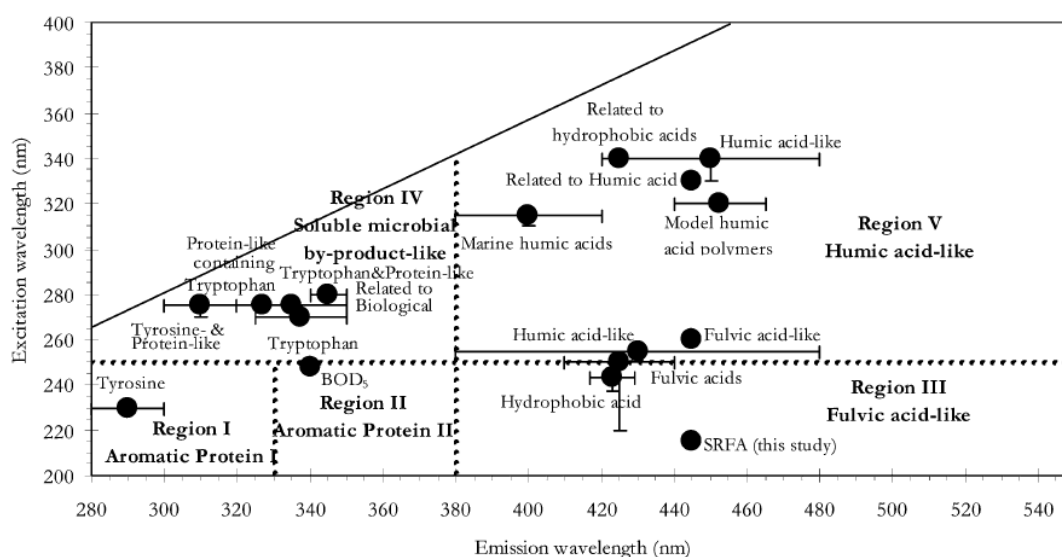


Fig. 2.1. Location of excitation-emission matrix (EEM) peaks (symbols) based on literature reports and operationally defined excitation and emission wavelength boundaries (dashed lines) for live EEM regions (Chen et al., 2003).

#### 2.2.4. Gas-chromatography mass spectrometry (GC-MS)

The degraded products were characterized by gas chromatography-mass spectrometry (GC-MS) measuring for the extractants after a sequential organic extraction on the surface of treated carbonaceous matter residues by LMS. GC-MS analysis was conducted on a Shimadzu QP2010 SE system (Kyoto, Japan). The degraded products were separated using a 30 m fused silica capillary column (SLB-5 ms, Supelco, Bellefonte, PA, USA) with an injection port temperature of 250°C and He as the carrier gas (constant pressure mode: 100 kPa). Mass spectra were observed by electron impact ionization at 70 eV. In the case of powder-activated carbon degraded products, these

were dissolved in (i) ethylene glycol, (ii) methanol, (iii) ethyl acetate, and (iv) hexane and injected in the splitless mode. On the other hand, when carbonaceous matter degraded products were analyzed, the by-products were dissolved using acetone only. The oven temperature was programmed from 120°C (with an initial hold for 2 min) to 320°C (with a final hold for 10 min) using a thermal gradient of 10°C/min.

#### 2.2.5. High-performance liquid chromatography (HPLC)

For HBT and ABTS concentration determination, the supernatant was subjected to high-performance liquid chromatography (HPLC) and quantified using calibration curves of standards. The concentration for the standards is detailed as follows: HBT (0.05, 0.10, 0.25, 0.50, and 1.00 mM) and ABTS (0.01, 0.02, 0.05, 0.10, and 0.20 mM). HPLC analysis was carried out using a Prominence UFLC system (Shimadzu, Kyoto, Japan) consisting of two pumps (LC-20 CE), an auto-injector (SIL-20AC HT) UV-detector (SPD-20A), and a column oven (CTO-20A). Chromatographic separation was performed using an InertSustain AQ-C18 HP column (GL Sciences, Tokyo, Japan; 3.0 mm I. D. × 75 mm) with a column temperature of 40 °C. The mobile phases for HPLC were (A) water with 0.05% phosphoric acid and (B) methanol. The mobile phase gradient was as follows: 0–1.0 min, 10% B; 1.0–4.0 min, 10–100% B; 4.0–6.0 min, 100% B using 1.0 mL/min as a flow rate. A UV monitor was utilized at 310 nm for HBT and 225 nm for ABTS. All the analyses were conducted in duplicate.



## **2.3.Solid characterization**

### **2.3.1. X-ray diffraction (XRD)**

The main mineral phases of carbonaceous gold ore samples were collected by X-ray diffraction (XRD) Rigaku Ultima IV (Akishima, Japan) using Cu K $\alpha$  with 40 kV acceleration voltage and 40 mA applied current. The scanning speed was 2°/min, and the step size was 0.02°. The identification of the XRD patterns was obtained by diffraction analysis software PDXL (Rigaku) based on International Centre for Diffraction Data (ICDD). In the current study, the following PDF cards were used in the mineral identification: py (pyrite, PDF 01–042–1340); ars (arsenopyrite, PDF 00–060–0322); ja (jarosite, PDF 01-075-9732); mus (muscovite, PDF 01–076-0929); qtz (quartz, PDF 00–014–0218); chl (chlorite, PDF 00–060–0322); dol (dolomite, PDF 00-036-0426).

### **2.3.2. X-ray fluorescence spectrometry (XRF)**

The elemental composition of carbonaceous gold ore was determined by X-ray fluorescence (XRF) spectroscopy Rigaku, ZSX Primus II (Akishima, Japan).

### **2.3.3. CHN elemental analysis**

Total carbon content was obtained by CHN elemental analysis Yanaco CHN MT-5 (Kyoto, Japan). All the measurements were conducted in triplicates.

#### 2.3.4. Thermogravimetric-differential thermal analysis (TG-DTA)

The carbon composition changes of the carbonaceous matter surrogate over the laccase-mediator treatment time were followed by thermogravimetric-differential thermal analysis using Bruker TG-DTA 2000SA (Massachusetts, USA). Around 10 mg of the sample was heated from room temperature until 1000°C at 5°C /min in an ambient atmosphere using 100 mL/min of gas flow rate. The reference material  $\alpha$ -Al<sub>2</sub>O<sub>3</sub> was used in all the measurements. As for the carbonaceous gold ore before and after laccase-mediator treatment, Hitachi TG-DTA 7300 (Tokyo, Japan) was utilized. The analytical conditions and sample mass were the same as those used in the previous equipment.

#### 2.3.5. Fourier transforms infrared spectroscopy (FT-IR)

The functional groups present in the carbonaceous matter surrogates were obtained by Fourier transform infrared spectra (FTIR) using FTIR-670 JASCO Plus spectrometer (Tokyo, Japan) in the transmission mode (0.5 wt% dilutions in IR grade KBr crystal). All the spectra were collected in the range of 4000–400 cm<sup>-1</sup> with a triglycine sulfate (TGS) detector.

#### 2.3.6. Raman spectroscopy

The alterations in the sp<sup>2</sup> orbital of the C-C bond were evaluated by Thermo Fisher Scientific DXR Smart Raman spectroscopy (Madison, WI, USA) using a Universal Platform Sampling accessory. In the case of sample dilution, it proceeded by adding a 0.5 wt% sample in IR grade potassium bromide (KBr) crystal (Wako, Osaka, Japan).

The laser excitation wavelength was 532 nm at 10 mW. All the spectra were collected in the range of 1200–1800  $\text{cm}^{-1}$ . The index of the graphitic degree of the carbonaceous matter was evaluated using the relative intensities of defective carbon (D) with graphitic carbon (G),  $I_D/I_G$ .

#### 2.3.7. Scanning electron microscopy (SEM)

The surface morphologies were observed by scanning electron microscopy (SEM) Hitachi SU1000 FlexSEM 1000II (Tokyo, Japan) at an accelerated voltage between 5kV to 20 kV.

#### 2.3.8. Specific surface area (BET)

The BET (Brunauer–Emmett–Teller) specific surface area and pore size distribution of the samples before and after LMS treatment were determined by JAPAN BELL BELSORP-max porosimeter (Osaka, Japan) through  $\text{N}_2$  (99.99%) adsorption. Then, the sample treatment was conducted in two steps: vacuum degassing for 90 min at 150°C and a final vacuum pre-treatment for 15 h at 150°C. Lastly, the data processing was conducted by BEL master software in version 6.3.0.0 (Osaka, Japan) using NLDFT (non-local density functional theory) models.

#### 2.3.9. Mineral liberation analysis (MLA)

FEI Mineral Liberation Analysis (MLA) 650 FEG determined the gold distribution of the original carbonaceous concentrate at Niihama Research Laboratories, Sumitomo

Metal Mining Co., Ltd. The MLA was equipped with two energy dispersive X-ray spectroscopy (EDX) detectors, Brucker Quantax X-Flash5030. The sample briquettes were prepared by mounting powder ore representatives into resin, followed by surface polishing. The measurement procedure was as follows: MLA utilizes a stable back-scattered electron (BSE) to generate a high-resolution image of mineral grains in the polished sections. BSE brightness corresponds with a unique average atomic number of each mineral type. Therefore, it can identify the outer boundary of mineral particles and the inner boundary of mineral phases in locked particles by image processing. Afterward, the EDX of each grain is collected to identify the mineral type. BSE scanning and collecting EDX have been performed automatically. Finally, the collected EDX spectrum was compared with the equipped software's mineral library to identify each grain's mineral type. For this measurement, Extended BSE liberation analysis (XBSE) mode was used to measure their bulk mineralogy at 25 kV of accelerating voltage using 400 times magnification and 1  $\mu\text{m}$ /pixel of resolution. XBSE mode collected BSE images and EDX spectrum of all mineral grains (Fandrich et al., 2007; Goodall and Scales, 2007; Aoki, 2016). In the MLA analysis, 162 fields of the unit section of 750  $\mu\text{m}$   $\times$  750  $\mu\text{m}$  on two briquettes for one sample are targets to observe, corresponding to 15000 ~ 20000 particles for one briquet sample in the present series of observations. The final image processing generates the quantification of mineralogical compositions and gold distribution.

## References

Aoki, Y. (2016) Application of mineralogical analysis with MLA in metallurgical testing for copper-molybdenum ore. *Copper*, 298–309.

- Baltierra-Trejo, E., Márquez-Benavides, L., & Sánchez-Yáñez, J. M. (2015) Inconsistencies and ambiguities in calculating enzyme activity: The case of laccase. *Journal of Microbiological Methods*, 119, 126–131.
- Chen, W., Westerhoff, P., Leenheer, J. A., & Booksh, K. (2003) Fluorescence Excitation-Emission Matrix Regional Integration to Quantify Spectra for Dissolved Organic Matter. *Environmental Science and Technology*, 37(24), 5701–5710.
- Csarman, F., Obermann, T., Zanjko, M. C., Man, P., Halada, P., Seiboth, B., & Ludwig, R. (2021) Functional expression and characterization of two laccases from the brown rot *Fomitopsis pinicola*. *Enzyme and Microbial Technology*, 148, 109801.
- Fandrich, R., Gu, Y., Burrows, D., & Moeller, K. (2007) Modern SEM-based mineral liberation analysis. *International Journal of Mineral Processing*, 84(1–4), 310–320.
- Gao, J., Liang, C., Shen, G., Lv, J., & Wu, H. (2017) Spectral characteristics of dissolved organic matter in various agricultural soils throughout China. *Chemosphere*, 176, 108–116.
- Goodall, W. R., & Scales, P. J. (2007) An overview of the advantages and disadvantages of the determination of gold mineralogy by automated mineralogy. *Minerals Engineering*, 20(5), 506–517.
- Jeon, S. J., & Park, J. H. (2020) Refolding, characterization, and dye decolorization ability of a highly thermostable laccase from *Geobacillus sp.* JS12. *Protein Expression and Purification*, 173, 105646.

- Navada, K. K., & Kulal, A. (2020) Enhanced production of laccase from gamma irradiated endophytic fungus: A study on biotransformation kinetics of aniline blue and textile effluent decolourisation. *Journal of Environmental Chemical Engineering*, 8(2), 103550.
- Qiu, X., Wang, S., Miao, S., Suo, H., Xu, H., & Hu, Y. (2021) Co-immobilization of laccase and ABTS onto amino-functionalized ionic liquid-modified magnetic chitosan nanoparticles for pollutants removal. *Journal of Hazardous Materials*, 401, 123353.
- Santana, T. T., Linde, G. A., Colauto, N. B., & do Valle, J. S. (2018) Metallic-aromatic compounds synergistically induce *Lentinus crinitus* laccase production. *Biocatalysis and Agricultural Biotechnology*, 16, 625–630.
- Unuofin, J. O., Moloantoa, K. M., & Khetsha, Z. P. (2022) The biobleaching potential of laccase produced from mandarin peelings: Impetus for a circular bio-based economy in textile biofinishing. *Arabian Journal of Chemistry*, 15(12), 104305.
- Wang, Y., Baker, L. A., & Brindle, I. D. (2016) Determination of gold and silver in geological samples by focused infrared digestion: A re-investigation of aqua regia digestion. *Talanta*, 148, 419–426.
- Zhu, L., Qi, H. ying, Lv, M. Le, Kong, Y., Yu, Y. W., & Xu, X. Y. (2012) Component analysis of extracellular polymeric substances (EPS) during aerobic sludge granulation using FTIR and 3D-EEM technologies. *Bioresource Technology*, 124, 455–459.

## **Chapter 3:**

# **Trace analysis of gold in double refractory gold ores by induced coupled plasma spectrometry**

### 3.1. Introduction

Gold quantification in low-grade gold ores is one of the essential aspects of mineral processing. On an industrial scale, fire assay is a well-employed dry technique that provides more reliable gold content regardless of the gold mineral matrix and gold type than hydrometallurgical techniques. Despite this, from a laboratory point of view, the employment of this technique requires a large ore mass (30-50 g) and time-consuming operational costs, making it not feasible for routine use (Helmeczi et al., 2018). Therefore, wet chemistry techniques such as acid digestion are typically performed on a laboratory scale (Celep et al., 2011; Ofori-Sarpong et al., 2013; Nazari et al., 2017; Konadu et al., 2019; Mendoza et al., 2021). In this case, sample preparation, instrumental determination, and data evaluation are necessary steps that should be considered to prevent analytical errors in gold contents. Sample preparation includes physical treatments like crushing, grinding, sieving, and homogenization, which helps to reduce the "nugget effect" and thus acquires representative samples before gold analysis. For samples like double refractory gold ores (DRGO) provided for research purposes, these have passed generally through the above-described treatments and a flotation process for gold concentration. Hence, the present chapter will not discuss details about physical treatments.

Sample preparation also includes chemical treatments like dissolution (acid digestion), analyte extraction, and pre-concentration (Wang & Brindle, 2014). As for this study, the focus will be on the dissolution step, which is preferentially accomplished by aqua regia. This acid mixture consists of the molar ratio of  $\text{HCl}:\text{HNO}_3 = 3:1$ , where a stable  $\text{AuCl}_4^-$  complex is formed (Tao et al., 2017). Although this procedure is simple and



extensively used in mineral processing, it was suggested that it could generate erroneous results in gold content (Wang & Brindle, 2014). Recently, Wang et al. (2016) investigated the effect of the acid ratios from aqua regia on gold dissolution, finding that reverse aqua regia (1 HCl: 3 HNO<sub>3</sub>) gave more precise gold content results like the certified values from reference materials. In this case, it was found that the excess of HNO<sub>3</sub> in the acid mixture achieves a complete dissolution of pyrite and other iron-containing minerals that usually locks the gold grains, liberating gold completely for its following oxidative dissolution.

Moreover, Helmeczi et al. (2018) suggest that increasing the HCl: HNO<sub>3</sub> ratio to 1:5 could improve the accuracy of the gold content from geological samples. However, despite these findings, a clear consensus on the acid mixture that can be used, especially in DRGO, might depend on the specific sample type. Another controversial procedure is the addition of HF in the digestion process. Wang & Brindle (2014) have reported that it did not show benefits for gold recoveries even in geological samples containing a silicate matrix. However, this assertion could not be specific to DRGO samples because it has been found that gold grains could also be sequestered or associated in the siliceous matrix (Sakai et al., 2022); therefore, HF is required to dissolve these minerals. In practical terms, the complex mineralogy where gold grains are located in DRGO makes it challenging to establish a standard acid digestion method for gold determination.

Another critical bottleneck in gold determination is selecting the appropriate analytical technique. Among the existing ones, the most used in laboratories are inductively coupled plasma-optical emission spectrometry (ICP-OES) and inductively coupled plasma mass spectrometry (ICP-MS). Nevertheless, it appears that when measuring

gold in these instruments, interferences from other dissolved elements (Rahman et al., 2013) and the "memory effect" (Chen et al., 2000), respectively, could be encountered. Although these findings were studied in other gold-containing samples, the above-described difficulties (Fig. 3.1) still need to be reported or described in DRGO studies. Then, the present chapter attempts to evaluate the effect of different acid ratios (HCl: HNO<sub>3</sub>) on gold extraction from DRGO. Additionally, we investigate the effect of matrix matching for Fe concentrations in the Au standard solutions for ICP-OES and L-cysteine as a scarifying oxidant and complexing reagent to prevent the reduction of [AuCl<sub>2</sub>]<sup>-</sup> into Au(0) and stabilize Au complex, which causes a "memory effect" in ICP-MS.

## **3.2. Experimental**

### **3.2.1. Materials**

The gold ores were flotation concentrate provided by anonymous mines from Mali, Ghana, and the USA. The samples are named as follows: SYM (Mali), BOG (Ghana), and PXX (USA). SYM is a double refractory gold ore (DRGO), PXX is a carbonaceous refractory Au-Ag ore, and BOG is a pre-treated ore that went through an unrevealed bio-oxidation process. Mineral and elemental characterization of the ores was determined by MLA, XRD, XRF, and CHN analysis. Finally, the certified gold content was obtained by fire assay.

### 3.2.2. Reagents, instrumentation, and standard

Concentrated HCl (36(w/v)%), HNO<sub>3</sub> (60(w/v)%), and HF (48(w/v)%) were in an analytical reagent grade and used in all the digestions. Ultra-pure water produced by Millipore synergy unit (18.2 MΩ cm) was used for sample dilutions and experiments. Gold standard solutions (999 mg/L) for inductively coupled plasma (ICP) analysis were purchased from Wako Chemicals (Osaka, Japan). The calibration standards for ICP-OES analysis were prepared using a similar acid matrix obtained after sample dilution. Additionally, the same Fe concentration as in the digested samples was added to all the standard solutions and blank. As a result, the gold calibration standards were prepared at 20, 50, 100, and 150 µg/L. Gold determination was carried out by Optima 8300 inductively coupled plasma optical emission spectrometer, and the instrumental settings are described in Table 3.1.

Table 3.1. Instrumental setting for ICP-OES Optima 8300

Instrument	Optima 8300 ICP-OES
Nebulizer	MEINHARD concentric glass nebulizer, Type A3
Spray chamber	Cyclonic standard glass
Torch	1-slot demountable quartz
Plasma RF power (W)	1300
Plasma gas flow rate (L/min)	10 (Ar)
Auxiliary gas flow rate (L/min)	0.2
Nebulizer gas flow rate (L/min)	0.55 (Ar)
Plasma view	Axial
Replicates	5

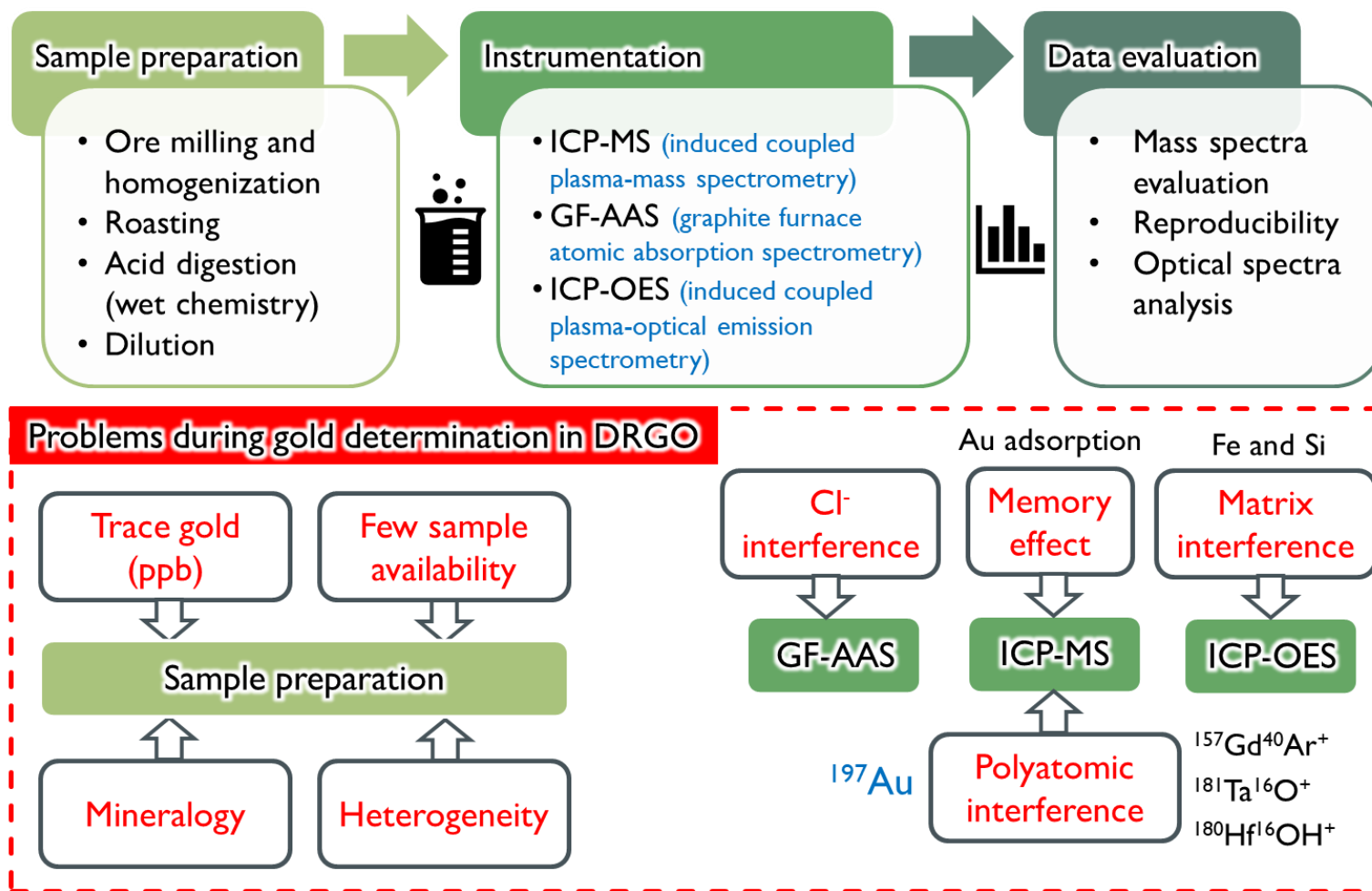


Fig. 3.1. Schematic illustration of processes and problems involved in gold determination in DRGO.

For ICP-MS analysis, the calibration standards were prepared using a solution containing 1% L-cysteine in 1% HCl at 0.1, 0.5, 1, and 2 µg/L. This dilution matrix was also used for the blank and samples. Gold determination was carried out by Agilent 7900 inductively coupled plasma mass spectrometer, and the instrumental settings are described in Table 3.2.

Table 3.2. Instrumental setting for ICP-MS Agilent 7900

Instrument	Agilent 7900 ICP-MS
Plasma mode	General purpose
RF power, W	1500
Plasma gas flow, L/min	15 (Ar)
Nebulizer gas flow, L/min	1.05 (Ar)
Dilution gas flow, L/min	0.9
Sampling depth, mm	10
Sampling time (s)	30
Dwell time, ms	40
Readings	1
Replicates	3

### 3.2.3. Sample digestion

200 mg of each ore was roasted at 800°C for 4 h using a muffle furnace to remove carbonaceous matter and oxidize the sulfides for easy access to the gold-hosted matrix. The roasted samples were placed in a polytetrafluoroethylene (PTFE) container, and 6 mL of concentrated HF were added to decompose the silicates. Afterward, the PTFE container was inserted in a double jacket sealed container for high-pressure reaction decomposition at 150°C for 2 h. The digested solution was then evaporated at 120°C for 12 h to remove the excess before ICP-MS and ICP-OES analysis. The evaporation

left behind a remaining solid, which was then used to dissolve gold. Different acid ratios of HCl: HNO<sub>3</sub> to produce aqua regia (3:1) and two ratios of reverse aqua regia (1:3) and (1:5) were used for the liberation and dissolution of gold from the ores. Similarly, to HF digestion, a double jacket sealed container was used under the same conditions described above. After the acid digestion, the liquid was collected, filtered, and filled up to 50 mL using ultra-pure water. The summary of the acid digestion procedure is illustrated in Fig. 3.2.

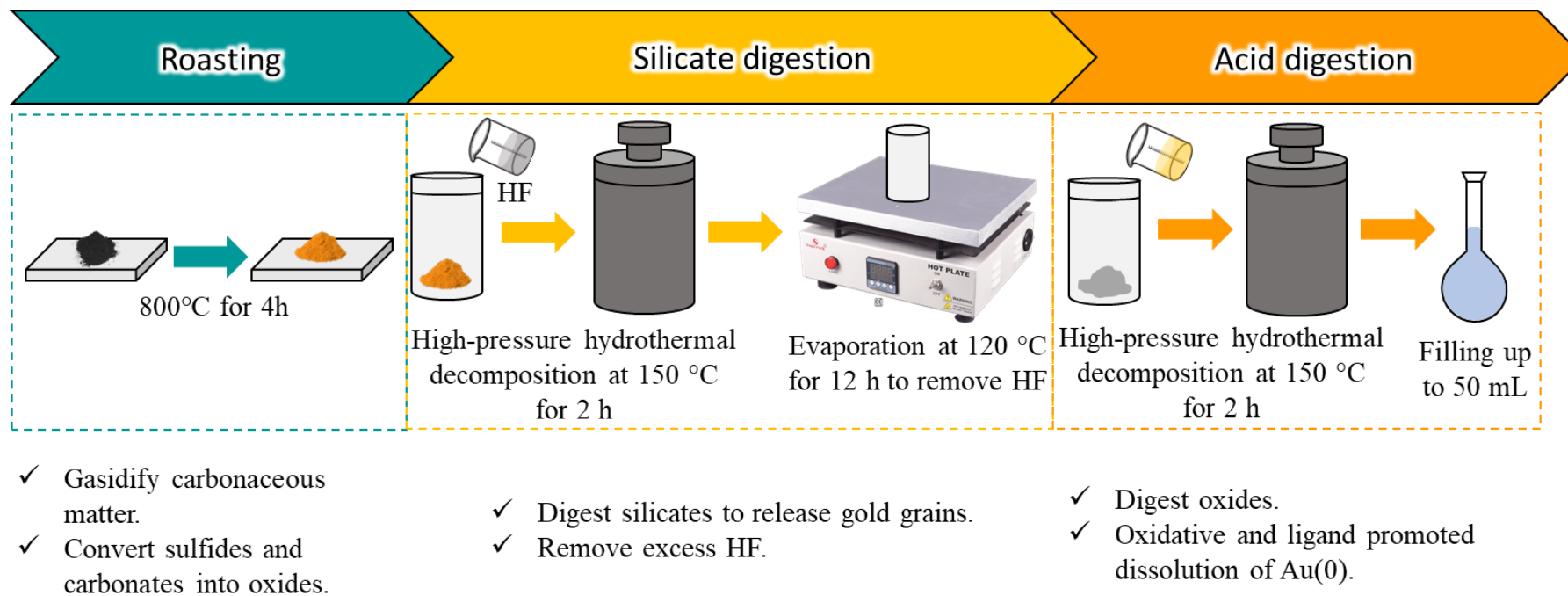


Fig. 3.2. Schematic illustration that explains the steps in the acid digestion process applied for double refractory gold ores.

### 3.3. Results and Discussion

#### 3.3.1. Gold ores characterization

The XRD patterns for BOG, PXX, and SYM (Fig. 3.3) show some similarities in the mineral characterization. SYM and PXX show peaks assigned for silicates like quartz ( $\text{SiO}_2$ ), muscovite ( $\text{KAl}_2(\text{AlSi}_3\text{O}_{10})(\text{OH})_2$ ), and chlorite ( $(\text{Mg}, \text{Al})_6(\text{Si}, \text{Al})_4\text{O}_{10}(\text{OH})_8$ ). Excepting chlorite, quartz and muscovite were also found in Bogoso. XRD also suggests the sulfidic mineral host of gold for the untreated ores is mainly pyrite; however, MLA for PXX revealed gold is also enclosed in arsenopyrite (Mendoza et al., 2021). As for BOG, despite gold being expected to be liberated after sulfide decomposition by bio-oxidation, the presence of secondary formed minerals like jarosite and gypsum could cause re-encapsulation of the small gold grains, as reported by Asamoah (2021). More information on the gold associations between PXX and SYM was previously reported by Mendoza et al. (2021) and Sakai et al. (2022), respectively. Using MLA, it was found that 5.48% and 5.86% of gold were enclosed in silicates in PXX and SYM, respectively. At the same time, unpublished MLA results for BOG indicate 7.58% of gold encapsulation in silicates. These observations suggest that removing HF from the acid digestion process would lead to underestimating the gold contents by not considering the enclosed gold in the siliceous matrix.

The attempt to change the acid ratio of aqua regia is understandable from the point of view of elemental distribution since, as shown in Table 3.3, the weight percentages of analyzed elements are different between the three ores. XRF results were compared with the ones obtained after acid digestion.



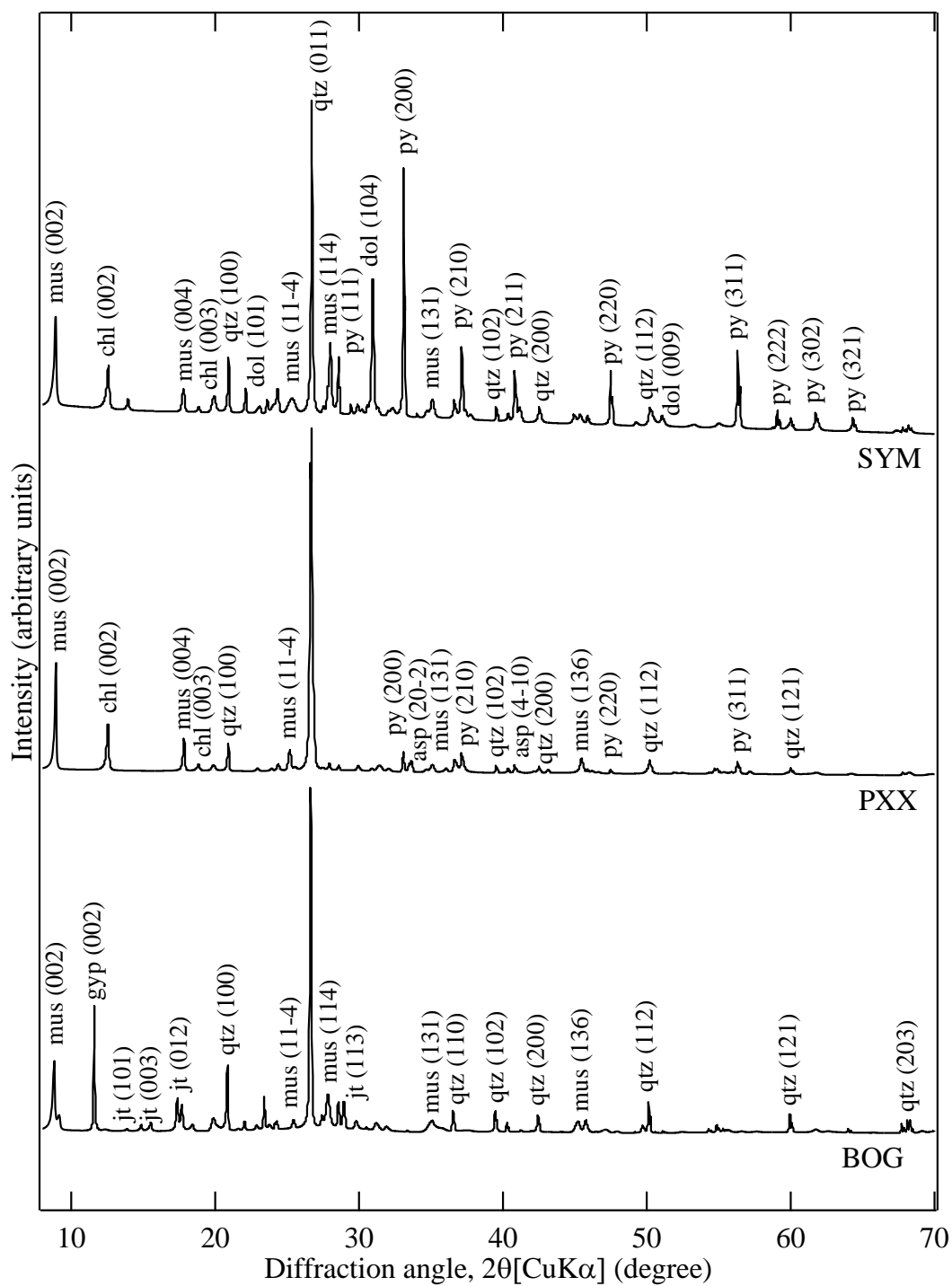


Fig. 3.3. XRD patterns of gold ores. Symbols: py (pyrite, PDF 01-042-1340); asp (arsenopyrite, PDF 00-060-0322); jt (jarosite, PDF 01-075-9732); mus (muscovite, PDF 01-080-0743); qtz (quartz, PDF 01-075-8322); chl (chlorite, PDF 00-060-0322); gypsum (gyp, PDF 00-033-0311).

Table 3.3. Elemental characterization of different refractory gold ores (wt%)

Element	BOG (wt%)					PXX (wt%)					SYM (wt%)				
	XRF CHN		HCl : HNO <sub>3</sub> ratio for digestion			XRF CHN		HCl : HNO <sub>3</sub> ratio for digestion			XRF CHN		HCl : HNO <sub>3</sub> ratio for digestion		
			3:1 (AR)	1:3 (RA)	1:5 (HRA)			3:1 (AR)	1:3 (RA)	1:5 (HRA)			3:1 (AR)	1:3 (RA)	1:5 (HRA)
C	5.3	3.9			N.D.	20.0	5.8			N.D.	6.8	5.3			N.D.
Fe	5.0	N.D.	5.3 ± 0.0	5.3 ± 0.0	5.4 ± 0.0	6.0	N.D.	15.4 ± 0.4	15.2 ± 0.3	16.1 ± 0.4	13.4	N.D.	21.9 ± 0.0	22.9 ± 0.0	23.3 ± 0.0
As	0.4	N.D.	0.4 ± 0.1	0.4 ± 0.1	0.4 ± 0.1	0.1	N.D.	2.3 ± 0.2	2.0 ± 0.2	1.9 ± 0.1	0.1	N.D.	1.2 ± 0.5	1.6 ± 0.2	1.2 ± 0.3
S	4.0	N.D.	1.8 ± 0.0	1.7 ± 0.0	1.8 ± 0.0	2.3	N.D.	0.1 ± 0.0	0.1 ± 0.0	0.2 ± 0.0	6.1	N.D.	1.9 ± 0.0	1.9 ± 0.3	2.0 ± 0.4
K	2.2	N.D.	1.3 ± 0.1	1.3 ± 0.0	1.3 ± 0.1	2.0	N.D.	1.9 ± 0.1	1.7 ± 0.1	1.7 ± 0.0	2.0	N.D.	0.9 ± 0.0	1.0 ± 0.0	0.9 ± 0.0
Si	20.1	N.D.	3.7 ± 0.4	4.3 ± 1.2	3.8 ± 0.7	14.0	N.D.	4.8 ± 1.3	4.0 ± 0.6	4.8 ± 0.8	15.7	N.D.	1.2 ± 0.3	1.3 ± 0.4	2.5 ± 1.0
Al	8.9	N.D.	8.4 ± 0.2	8.4 ± 0.2	8.5 ± 0.2	7.6	N.D.	7.7 ± 0.3	6.2 ± 1.0	3.1 ± 0.3	7.5	N.D.	4.9 ± 0.1	4.8 ± 0.4	1.9 ± 0.4
Mg	0.4	N.D.	0.4 ± 0.0	0.4 ± 0.0	0.4 ± 0.0	0.9	N.D.	1.3 ± 0.0	0.9 ± 0.3	0.2 ± 0.0	1.7	N.D.	1.5 ± 0.0	1.5 ± 0.2	0.3 ± 0.3
Ca	1.6	N.D.	2.4 ± 0.1	2.3 ± 0.1	2.4 ± 0.2	3.1	N.D.	0.7 ± 0.0	0.6 ± 0.0	0.5 ± 0.0	3.1	N.D.	2.5 ± 0.1	2.6 ± 0.1	2.1 ± 0.4
Others	53.5	N.D.			N.D.	58.2	N.D.			N.D.	45.1	N.D.			N.D.

*n* = 4 for acid digestions; N.D.: not determined.

Although there are discrepancies in the obtained results in XRF and acid digestion, it is clear that SYM ore has the highest Fe (wt%) composition, followed by PXX and BOG. This premise was also confirmed by the prominent pyrite peaks observed in XRD (Fig. 3.3). The changes in the acid ratio showed a slight increment in the dissolved Fe when HNO<sub>3</sub> concentration was increased against HCl (Table 3.3). This effect was mainly observed in the untreated ores, unlike BOG, in which negligible wt% increments were detected. The other major elements associated with gold are As, S, and Si. Arsenic contents (wt%) might be affected by the detection limit in XRF; therefore, for the samples containing lower than 1 wt% of As, the determination by XRF was not possible. On the other hand, the contents of sulfur were much underestimated in ICP-OES because the emission wavelength for S (180.731 nm) overlapped with Ca and Al (Ackerman et al., 2012). Furthermore, silicon content was reduced to below 5 wt% due to the evaporation of H<sub>2</sub>SiF<sub>6</sub> (U.S. Coast Guard, 1999) during HF removal at 120°C. Table 3.3 also shows the total carbon provided by CHN analysis. The carbon content in PXX and SYM includes inorganic and organic carbon, while carbon in BOG consists of organic carbon. The inorganic carbon in these samples is attributed to dolomite, as shown in Fig. 3.3. In the case of PXX, the dolomite content was under the detection limit. Still, its existence was elucidated by MLA, as reported by Mendoza et al. (2021). Lastly, BOG did not show any presence of inorganic carbonates, likely due to their dissolution in the bio-oxidation step under strongly acidic conditions. Therefore, the organic carbon in the three samples corresponds to the presence of carbonaceous matter. For such, the roasting procedure prior to acid digestion is essential to avoid incomplete digestion and undesirable gold adsorption. The significant discrepancies in the carbon detection by XRF and CHN are caused by the high carbon detection limit in XRF since carbon is a light element.

### 3.3.2. Interferences in gold analysis by ICP-OES

Initially, BOG (5.3 wt% Fe) and SYM (21.9 wt% Fe) were digested by aqua regia, and the gold concentration was determined by ICP-OES. Au possesses three optical emission wavelengths: 242.795 nm, 208.209 nm, and 267.595 nm in descending order of intensity. Among them, the most sensitive emission wavelength is generally selected for gold determination. As described in section 3.3.1, DRGO includes sulfide minerals associated with Au(0), which are placed after roasting in contact with aqua regia at high pressure and temperature conditions. Their decomposition allows the dissolution of various elements, including Fe. This particular coexisting element (Fe) possesses a wavelength (242.836 nm) close to Au (242.795 nm), as shown in Fig. 3.4. The interference of Fe to the determination of Au was noticed during spectral observation and confirmed by the inaccuracy of the gold content report for BOG and SYM (Table 3.4). The effect of Fe interference on the gold content depends on the Fe concentration, which is clearly manifest in Table 3.4. For samples with low Fe content like BOG (5.3 wt%), the gold content is overestimated, caused by the small shoulder peak from Fe near to Au wavelength. In this case, the peak tail is likely to be counted by the Au signal, resulting in overestimation. Oppositely, overestimation is not observed in samples with high Fe contents like SYM (21.9 wt%). In this case, the influence of the Fe peak leads to underestimation. Fe did not disturb the second wavelength of Au at 208.209 nm, but interference and overlapping were observed by the emission peak derived from Si at 208.201 nm. Although Si was much reduced during HF removal, the remaining concentration of Si was still observable, and interference was stronger than the one observed in the first wavelength (Fig. 3.5), making it difficult to use for analysis, as seen in table 3.4.

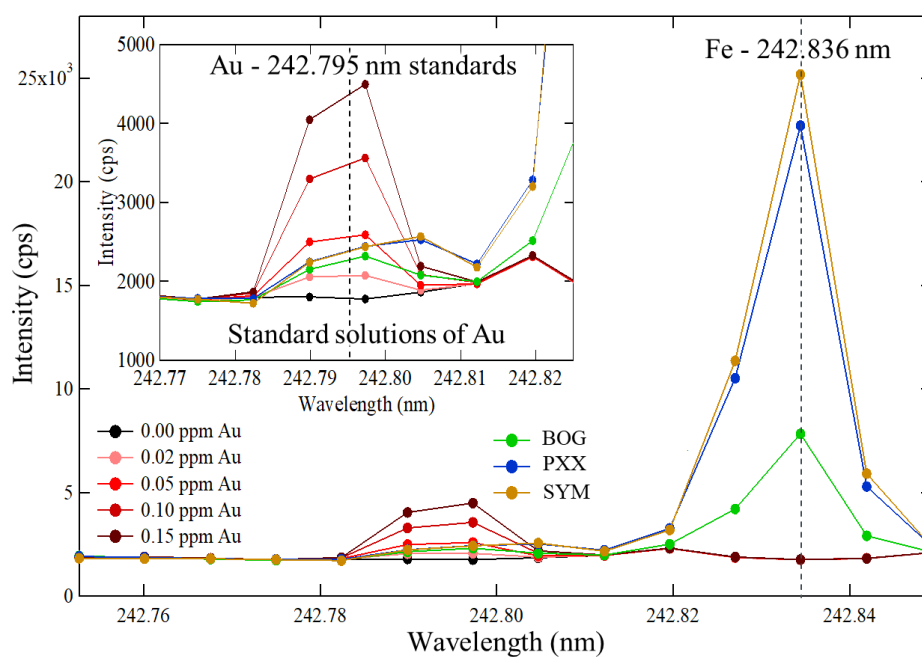


Fig. 3.4. ICP-OES spectra in a region of Au (242 nm) for acid-digested samples of BOG, PXX, and SYM gold ore under aqua regia digestion including the standard spectra.

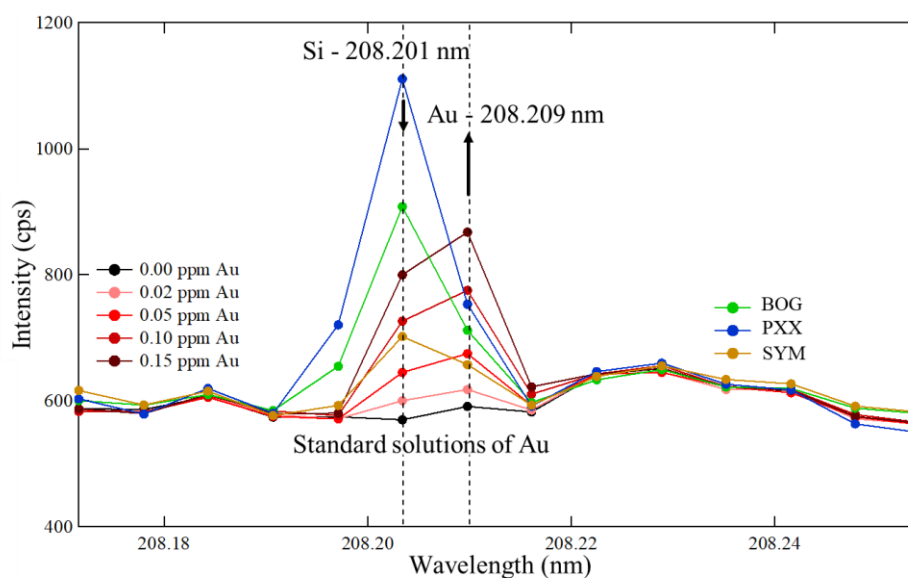


Fig. 3.5. ICP-OES spectra in a region of Au (208 nm) for acid-digested samples of BOG, PXX, and SYM gold ore under aqua regia digestion including the standard spectra.

Consequently, for DRGO samples, quantifying the trace concentrations of Au by ICP-OES is challenging because Fe and Si are ubiquitous main constituents.

Table 3.4. Fe and Si interference on gold determination by ICP-OES

Wavelength (nm)	BOG (5.3 wt% Fe)		SYM (21.9 wt% Fe)	
	Fire assay (g/t)	Aqua regia digestion	Fire assay (g/t)	Aqua regia digestion
208.201		291.2 ± 5.2		70.6 ± 10.2
242.836	28.5	63.1 ± 3.6	24.2	3.5 ± 7.4
267.595		70.6 ± 3.2		-93.0 ± 7.2

### 3.3.3. Effect of different acid ratios on gold determination and memory effect

#### elimination in ICP-MS

When performing ICP-MS analysis, a severe memory effect was detected when ultra-pure water or 0.1 M HNO<sub>3</sub> was employed as the matrix dilution. The memory effect is caused by the adsorption and desorption of Au on the glass-made spray chambers and nebulizers between sample analyses (Chen et al., 2000). Generally, ultra-pure water is used to wash-out the analyte from the injection system for continuous analysis. However, for analytes like Au, the washing-out time could take around 40 minutes when using ultra-pure water, HNO<sub>3</sub>, or HCl as a washing reagent as applied in previous reports (Hall & Pelchat, 1994; Todand et al., 1995; Strnad et al., 2016). Although the washing time depends on the Au concentration, the previous asseveration was confirmed by routine measurements (Fig. 3.6).

Knowing that the memory effect leads to an unfavorable consumption of time and the delivery of overestimated results, L-cysteine was used to look for a simple solution for this deleterious phenomenon. Chen et al. (2000) first reported the effect of this amino acid, and subsequent studies (Wang & Brindle, 2014; Wang et al., 2016; Helmeczi et al., 2018) evaluated its ability on geological samples after acid digestion. Because L-cysteine includes -SH groups, it acts as a sacrificing reagent to prevent the reduction of  $\text{AuCl}_2^+$  into  $\text{Au}(0)$ . In the present work with refractory gold ores, three different concentrations of L-cysteine (0.2%, 0.5%, and 1%) were dissolved in 1% HCl and evaluated as a dilution matrix to avoid the memory effect.

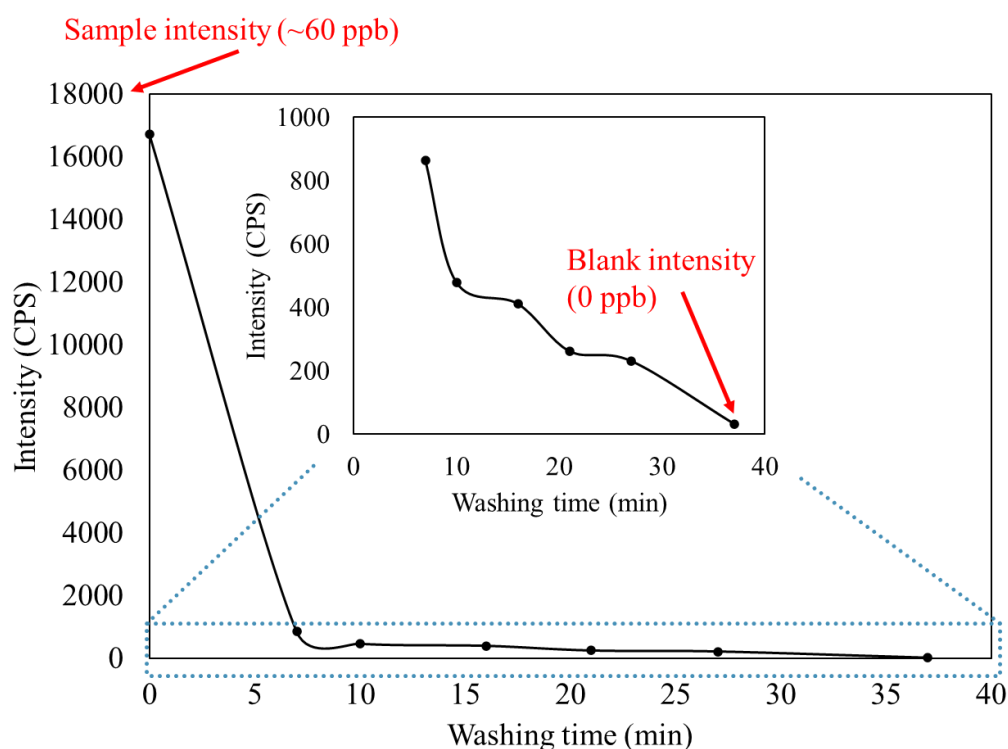


Fig. 3.6. Wash-out profile for 60 ppb Au showing memory effect in ICP-MS.

Memory effect was not reduced when using 0.2% and 0.5% L-cysteine. On the contrary, a strong reduction in the gold content, especially for digestions using a higher molar ratio of HNO<sub>3</sub> than HCl, was observed (Table 3.5). The explanation for this could be due to the consequence of three effects: (a) L-cysteine concentration is too low to stabilize gold and permit the analyte washing out from the introduction system; (b) L-cysteine consumption carried out by free Fe(III) from the digested solution (Jameson & Linert, 1991; Bhattacharyya et al., 2013) or (c) L-cysteine oxidation catalyzed by excess Fe(III) coming from a major dissolution from the reverse aqua regia (Taylor et al., 1966). The increment of L-cysteine concentration to 1% decreased the side effects and completely removed the memory effect. In this case, the washing out time was reduced to 30 seconds compared to the initial 40 minutes shown in Fig. 3.6. Then, for POG and SYM digestion, 1% L-cysteine dissolved in 1% HCl was selected as a dilution matrix.

Table 3.5. Effect of L-cysteine concentration on gold content (g/t) from BOG ore after different acid digestion ratios ( $n=4$ )

Concentrations of L-cysteine in 1% HCl	Fire assay	HCl : HNO <sub>3</sub> ratio for digestion		
		3:1	1:3	1:5
0.2% L-cysteine	24.2	15.7 ± 1.4	10.2 ± 0.3	13.1 ± 1.1
0.5% L-cysteine		17.1 ± 0.1	15.4 ± 2.3	15.9 ± 1.4
1% L-cysteine		22.6 ± 0.5	21.5 ± 0.8	21.3 ± 0.7



### 3.3.4. Effect of different acid ratios on gold determination by ICP-OES

Based on the above observations, modifications in the in-house digestion process regarding the acid ratio and the selection for the dilution matrix were made. One alternative was the addition of a pre-washing of the iron-containing minerals using concentrated  $\text{HNO}_3$  for 24 h under  $150^\circ\text{C}$ . Although the peak interference from Fe was removed (Fig. 3.7). Still, this extra process much decreases gold content no matter the acid ratio of digestion (Table 3.6). Subsequently, the pre-washing step was removed from the digestion process. Another path to resolve Fe interference is the standard addition method, where the detectable amount of Fe (20 ppm) was added into the Au standard solutions matrix to attenuate the effect of the Fe tail on Au spectra.

Table 3.6. Effect of acid digestion conditions on gold content (g/t) in BOG ore ( $n = 4$ )

Acid digestion condition	Acid molar ratio (HCl : $\text{HNO}_3$ )	Fire assay (g/t)	by ICP-OES (242.795 nm)		
			Without Fe in standards	With Fe in standards	After Fe removal
AR	3:1		$63.1 \pm 3.6$	$40.2 \pm 4.6$	$7.2 \pm 2.7$
RA	1:3	28.5	$34.1 \pm 2.5$	$31.7 \pm 2.4$	$1.5 \pm 1.1$
HRA	1:5		$32.8 \pm 2.1$	$29.1 \pm 1.1$	$2.1 \pm 1.6$

First, using ICP-OES, it was found that gold content obtained by reverse aqua regia (1 HCl: 3  $\text{HNO}_3$ ) digestion was closer to the fire assay values than standard aqua regia (3 HCl: 1  $\text{HNO}_3$ ), but it was still overestimated. As a result, after adding Fe into the Au standard solutions, the obtained gold content was close to that of the fire assay (Table 3.7). The condition that gave the most comparable value to the fire assay result was the

acid digestion with highly reverse aqua regia (1 HCl: 5 HNO<sub>3</sub>).

Therefore, the optimized conditions were applied to SYM ore since this sample has the highest iron content. The added Fe was around 90 ppm, whereas the earlier BOG solution contained 20 ppm Fe. As a result, SYM gold content digested by highly reverse aqua regia also showed the closest value to the fire assay. When Fe was not added to the standard solution, the quantitative results of Au were overestimated for BOG and underestimated for SYM, showing the opposite trend as explained previously. The addition of detected Fe into the Au standard solutions shows that this method's detection limit for gold was 20 ppb.

Finally, under the optimized conditions where Fe content determination is necessary for spiking it into the Au standards, it is recommended to use this method for untreated ores after flotation because the Fe content does not change dramatically if several pre-treatment conditions are applied.

Table 3.7. Effect of acid digestion conditions on gold content (g/t) in SYM ore ( $n = 4$ )

Acid digestion condition	Acid molar ratio (HCl : HNO <sub>3</sub> )	Fire assay (g/t)	by ICP-OES (242.795 nm)	
			Without Fe in standards	With Fe in standards
AR	3:1		3.5 ± 7.4	34.2 ± 5.3
RA	1:3	24.2	-0.3 ± 2.8	31.6 ± 2.1
HRA	1:5		-4.2 ± 1.7	26.1 ± 1.3

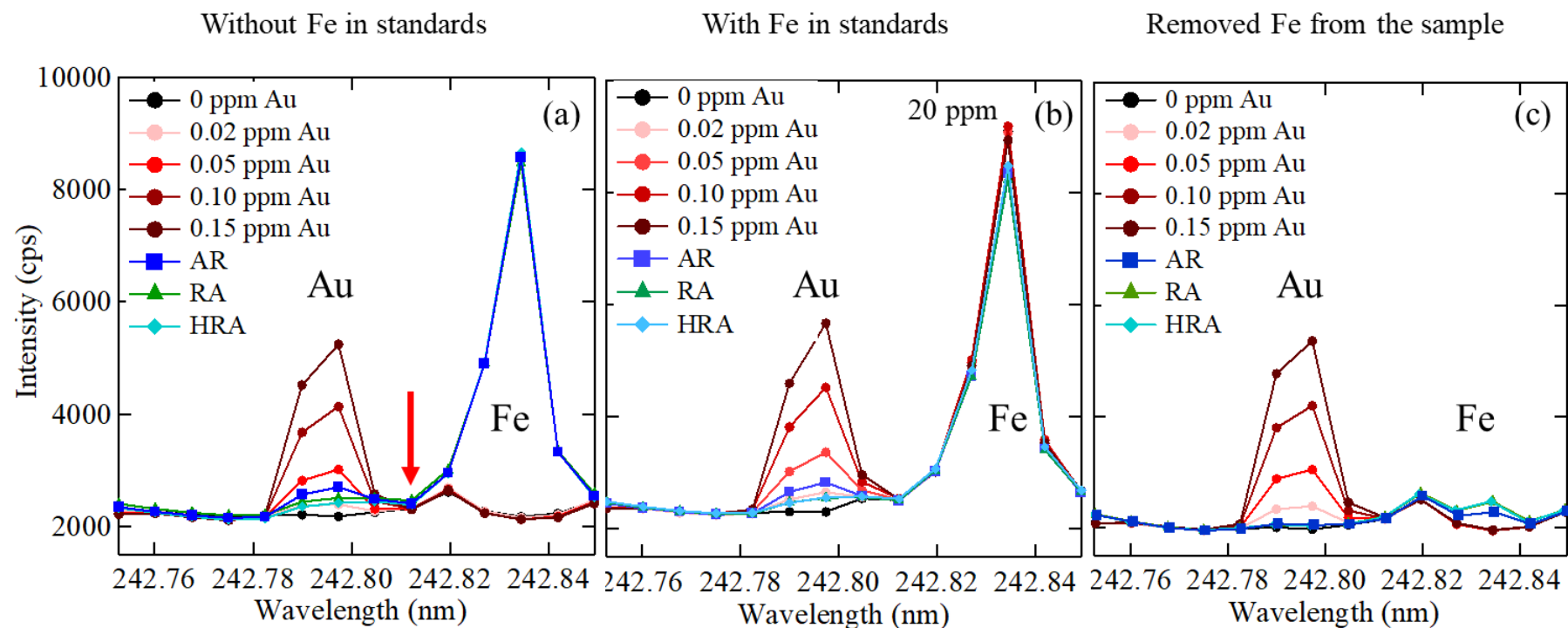


Fig. 3.7. ICP-OES spectra in a region of Au (242 nm) for acid-digested samples of BOG sample under three different digestion conditions with the standard spectra. The standard solutions include (a) 0 ppm Fe, (b) 20 ppm Fe, and (c) 0 ppm Fe including a prewashing before the digestion to remove Fe from the sample.

Table 3.8 Au content (g/t) of BOG, PXX, and SYM gold ore, under three different digestion conditions, determined by ICP-OES and ICP-MS

Sample	Fire assay	ICP-OES ( $n = 4$ )			ICP-MS ( $n = 4$ )		
		HCl : HNO <sub>3</sub> ratio for digestion			HCl : HNO <sub>3</sub> ratio for digestion		
		3:1	1:3	1:5	3:1	1:3	1:5
BOG	28.5	40.2 ± 4.6	31.7 ± 2.4	29.1 ± 1.1	22.6 ± 0.5	21.5 ± 0.8	21.3 ± 0.7
PXX	30.6	24.7 ± 3.0	34.3 ± 5.1	34.1 ± 3.0	24.2 ± 2.1	19.4 ± 1.7	12.7 ± 2.5
SYM	24.2	34.2 ± 5.3	31.6 ± 2.1	26.1 ± 1.3	17.1 ± 0.9	20.9 ± 0.9	16.2 ± 0.7

### 3.3.5. Comparing the effects of different acid ratios on gold determination by ICP-OES and ICP-MS

The adjusted methods for ICP-OES and ICP-MS determination were applied for PXX ore in addition to BOG and SYM. The summary of the results is shown in table 3.8. As can be seen, two effects are observed by changing the acid ratio in the acid digestion. For ICP-OES, highly reverse aqua regia,  $\text{NO}_3^-$  becomes an oxidizing agent for  $\text{Au}(0)$ , and  $\text{Au}(\text{NO}_3)_4^-$  is easily formed, increasing the luminescence intensity of  $\text{AuCl}_4^-$ . Hence, it is thought that it prevents the overestimation of the value and brings it closer to the fire assay results considering the standard error. In the case of ICP-MS, the advantage of using reverse aqua regia was reflected when the Fe wt% in the ore was higher than 6%, and the gold type was not presented as an alloy (electrum) like in PXX. The reduction of HCl in the acid ratio promotes the co-precipitation of gold when silver is precipitated as AgCl (Wang et al., 2016). This is unlikely in HCl excess as in aqua regia digestion. Therefore, for samples like PXX that contain electrum, re-dissolution of these precipitates might be necessary if reverse aqua regia is applied, as Wang et al. (2016) suggested. For samples with high Fe contents like SYM, when reverse aqua regia was used, the beneficial effect of further Fe dissolution and liberation of gold was expected in the gold content. However, the same results were not observed for highly reverse aqua regia. A possible interpretation of this could be the differences in the digestion mechanism used in this study and the ones reported by Helmeczi et al. (2018) using Cold-Block digestion. Nevertheless, further studies might be necessary to understand this controversial result fully.

### 3.4. Conclusions

Three refractory gold ores from different locations were digested by different acid ratios of HCl: HNO<sub>3</sub>. In the determination of Au by ICP-OES, Fe and Si had a strong interference on the two highest Au wavelengths (242 and 208 nm), where the overlapping of Si is stronger without the chance to improve this condition. However, Au measurement by ICP-OES at 242 nm can be overcome after matrix normalization by including the same Fe concentrations as in unknown samples in the Au standard solutions. As a result, the obtained Au contents were in good agreement with the fire assay results, especially in the acid matrix with the molar ratio of HCl: HNO<sub>3</sub> = 1:5 (highly reverse aqua regia). Under the condition, the detection limit of Au was 20 ppb. ICP-MS's memory effect is completely solved when 1% HCl, including 1% L-cysteine, is used to prepare the dilution matrix. For refractory gold ores containing less than 6 wt% Fe, the effect of the excess HNO<sub>3</sub> in acid digestion is negligible. However, excess HNO<sub>3</sub> is recommended for high Fe-containing samples like SYM because of the complete dissolution of Fe. The current results could help establish a standard method for determining Au in DRGO samples.

### References

Ackerman, L., Rohovec, J., & Šebek, O. (2012) Determination of Total Sulfur in Fifteen Geological Materials Using Inductively Coupled Plasma-Optical Emission Spectrometry (ICP-OES) and Combustion/Infrared Spectrometry. *Geostandards and Geoanalytical Research*, 36(4), 407–414.

- Asamoah, R. K. (2021) Specific refractory gold flotation and bio-oxidation products: Research overview. *Minerals*, 11(1), 1–14.
- Bhattacharyya, A., Stavitski, E., Dvorak, J., & Martínez, C. E. (2013) Redox interactions between Fe and cysteine: Spectroscopic studies and multiplet calculations. *Geochimica et Cosmochimica Acta*, 122, 89–100.
- Celep, O., Alp, İ., & Deveci, H. (2011) Improved gold and silver extraction from a refractory antimony ore by pretreatment with alkaline sulphide leach. *Hydrometallurgy*, 105(3–4), 234–239.
- Chen, W., Wee, P., & Brindle, I. D. (2000) Elimination of the memory effects of gold, mercury and silver in inductively coupled plasma atomic emission spectroscopy. *Journal of Analytical Atomic Spectrometry*, 15(4), 409–413.
- Hall, G. E. M., & Pelchat, J. C. (1994) Analysis of geological materials for gold, platinum and palladium at low ppb levels by fire assay-ICP mass spectrometry. *Chemical Geology*, 115(1–2), 61–72.
- Helmeczi, W., Helmeczi, E., Baker, L. A., Wang, Y., & Brindle, I. D. (2018) Development of a general acid method for the digestion of gold ore samples together with a comparison of extraction solvents for gold and determination by microwave-induced plasma-atomic emission spectrometry (MIP-AES). *Journal of Analytical Atomic Spectrometry*, 33(8), 1336–1344.
- Jameson, R. F., & Linert, W. (1991) Complex formation followed by internal electron transfer: The reaction between cysteine and iron(III). *Monatshefte Für Chemie Chemical Monthly*, 122(11), 887–906.

- Konadu, K. T., Huddy, R. J., Harrison, S. T. L., Osseo-Asare, K., & Sasaki, K. (2019) Sequential pretreatment of double refractory gold ore (DRGO) with a thermophilic iron oxidizing archaeon and fungal crude enzymes. *Minerals Engineering*, 138, 86–94.
- Mendoza, D. M., Konadu, K. T., Aoki, Y., Kameya, M., & Sasaki, K. (2021) Carbonaceous matter degradation by fungal enzyme treatment to improve Ag recovery from an Au-Ag-bearing concentrate. *Minerals Engineering*, 163, 106768.
- Nazari, A. M., Ghahreman, A., & Bell, S. (2017) A comparative study of gold refractoriness by the application of QEMSCAN and diagnostic leach process. *International Journal of Mineral Processing*, 169, 35–46.
- Ofori-Sarpong, G., Osseo-Asare, K., & Tien, M. (2013) Mycohydrometallurgy: Biotransformation of double refractory gold ores by the fungus, *Phanerochaete chrysosporium*. *Hydrometallurgy*, 137, 38–44.
- Rahman, M. M., Khan, S. B., Marwani, H. M., Asiri, A. M., Alamry, K. A., & Al-Youbi, A. O. (2013) Selective determination of gold(III) ion using CuO microsheets as a solid phase adsorbent prior by ICP-OES measurement. *Talanta*, 104, 75–82.
- Sakai, R., Mendoza, D. M., Konadu, K. T., Cindy, Aoki, Y., Hirajima, T., Ichinose, H., & Sasaki, K. (2022) Laccase-mediator system for enzymatic degradation of carbonaceous matter in the sequential pretreatment of double refractory gold ore from Syama mine, Mali. *Hydrometallurgy*, 212, 105894.
- Strnad, L., Šebek, O., Fayadová, M., & Vrba, J. (2016) Determination of Gold in e-Waste Dust Samples and Geological Matrices by ICP-MS after Extraction by an HClO<sub>4</sub>-HBr-HI-Aqua Regia Mixture. *Geostandards and Geoanalytical Research*, 40(2), 257–266.



Tao, D., Guo, W., Xie, W., Jin, L., Guo, Q., & Hu, S. (2017) Rapid and accurate determination of gold in geological materials by an improved ICP-MS method. *Microchemical Journal*, 135, 221–225.

Taylor, J. E., Yan, J. F., & Wang, J. L. (1966) The Iron (III)-Catalyzed Oxidation of Cysteine by Molecular Oxygen in the Aqueous Phase. An Example of a Two-Thirds-Order Reaction. *Journal of the American Chemical Society*, 88(8), 1663–1667.

Todand, M. M., JarviS, I., & Jarvis, K. E. (1995) Microwave digestion and alkali fusion procedures for the determination of the platinum-group elements and gold in geological materials by ICP-MS. *Chemical Geology*, 124(1–2), 21–36.

Wang, Y., Baker, L. A., & Brindle, I. D. (2016) Determination of gold and silver in geological samples by focused infrared digestion: A re-investigation of aqua regia digestion. *Talanta*, 148, 419–426.

Wang, Y., & Brindle, I. D. (2014) Rapid high-performance sample digestion for ICP determination by ColdBlock™ digestion: Part 2: Gold determination in geological samples with memory effect elimination. *Journal of Analytical Atomic Spectrometry*, 29(10), 1904–1911.

## **Chapter 4:**

# **Enzymatic degradation of powder activated carbon with laccase against cell-free spent medium from *Phanerochaete chrysosporium***

#### 4.1.Introduction

The application of a sequential biotreatment using the archaea *Acidianus brierleyi* and the cell free-spent medium (CFSM) from the basidiomycetes fungus *Phanerochaete chrysosporium* on a carbonaceous gold ore concentrate was first reported by Konadu et al. (2019). In that report, gold recovery achieved 92% after alkaline washing compared to the initial 24% recovery from the untreated ore. This improvement was accomplished by the action of sulfide decomposition by the archaea, followed by the degradation of carbonaceous matter (CM) by the lignin-degrading enzymes present in CFSM. Quantitative analysis by capillary electrophoresis enzyme assay confirmed that CFSM contains lignin peroxidase (LiP) and manganese peroxidase (MnP) (Kudo et al., 2017). Furthermore, these lignin-degrading enzymes possess high standard redox potentials (LiP: 1.2 – 1.5 V and MnP: 1.1. V) (Fakoussa & Hofrichter, 1999) and, therefore, are believed to be responsible for breaking the C-C bond from aromatic compounds in the CM (Ofori-Sarpong et al., 2013). Although several environmental advantages were found compared to roasting or chemical treatments, the described system seems complicated for a broad biotechnological application due to the peroxidase enzyme activation dependence on H<sub>2</sub>O<sub>2</sub> and low enzyme stability over time (Fakoussa and Hofrichter, 1999). Another drawback is that few fungal species can produce LiP and MnP at considerable concentrations for a large amount of ore treatment (Singh & Chen, 2008). The stabilities of LiP and MnP are relatively low. For those reasons, it was necessary to look for an alternative to overcome these bottlenecks for industrial approaches.

Laccase (Lcc), another lignin-degrading enzyme secreted by several organisms and responsible for the degradation of various aromatic and non-aromatic compounds (Claus, 2004), could be utilized as an alternative to CFSM. This oxidase, contrary to Lip and MnP, does not require toxic  $H_2O_2$  to activate its catalytic capacity for oxidation; instead, it uses  $O_2$  as an electron donor (Shleev et al., 2006). Additionally, the production of this extracellular enzyme is broad compared to the peroxidases (Debnath & Saha, 2020; Zofair et al., 2022), and Lcc presence was not confirmed in the CFSM (Konadu et al., 2019); therefore, its contribution to CM degradation has not been reported.

CM formation, coalification, is a geochemical process that converts buried ligninolytic biomass in various ranks of coal, and it is accomplished under high pressure and heat for long periods. Depending on these variables, the graphitic structure and maturity of CM could be changed from lignite to anthracite (Miki, 1983). High CM maturity is associated with a high graphitic degree and preg-robbing ability, where anthracitic type CM shows the highest gold adsorption capacity due to the abundance of aromatic  $sp^2$  C=C bonding, low O/C atomic ratios and presence of amorphous carbon (Ibrado & Fuerstenau, 1992; Ofori-Sarpong et al., 2010; Konadu et al., 2020). CM composition is divided into three main components: hydrocarbons, humic substances, and elemental carbon (Yang et al., 2013; Miller et al., 2016). Within them, the last one is a mixture of graphitic and amorphous carbon, essentially adsorbs aurocyanide, similar to activated carbon during the carbon-in-pulp process (Ibrado & Fuerstenau, 1995; Tan et al., 2005; Yang et al., 2013). As detailed by Miller et al. (2016), this naturally activated carbon from CM was present in most of the studied carbonaceous gold ores, and its maturity and structure were likely comparable to anthracite (Van Vuuren et al., 2000). However,

regarding the graphiticity, the extraction of this component from carbonaceous gold ores is tedious because of its fineness, low mass percent (< 6%), and coexistence with minerals presented in the matrix ore (Yang et al., 2013; Liu et al., 2016). Therefore, due to its remarkable equivalence in chemical structure, activated carbon has been used as the major surrogate for understanding the gold adsorption mechanisms into CM (Abotsi & Osseo-Asare, 1986; McDougall et al., 1987; Adams, 1990; Miller et al., 2016). Similarly, for the assessment and comprehension of a new biological CM pre-treatment, a carbon substitute is necessary before applying the optimized conditions in the natural carbonaceous gold ore (Ofori-Sarpong et al., 2010; Ofori-Sarpong et al., 2013; Liu et al., 2014; Liu et al., 2016; Konadu et al., 2017). Consequently, the current chapter aims to evaluate the capacity of Lcc to degrade powder-activated carbon (PAC) and compare it with CFSM from *Phanerochaete chrysosporium* through the reduction of  $\text{Au}(\text{CN})_2^-$  adsorption. In these preliminary experiments, a commercially available laccase from *Trametes versicolor* was used for the first time.

## **4.2.Experimental**

### **4.2.1. Materials**

Powder-activated carbon (PAC) in a special grade (Lot No. CAQ3035) supplied by Wako Chemicals (Osaka, Japan) was used in this chapter. As for the enzymes, laccase from *Trametes versicolor* (Lot No. BCBZ9936) provided by Sigma-Aldrich and laboratory-harvested CFSM containing MnP and LiP were used.

#### 4.2.2. CFSM harvesting

For this work, the spent medium harvesting conditions, where the enzymes are constantly active, followed the procedure described in Konadu et al. (2019a; 2019b). *P. chrysosporium* was cultured in a sterile 2 L Erlenmeyer flask containing 500 mL liquid medium at pH 4 adjusted with 1 M NaOH, composed of 10 g glucose, 1.18 g succinic acid, 0.2 g ammonium tartrate, 10 mg thiamine hydrochloride, 25.6 mg 2,6-dimethoxyphenol, 2 g KH<sub>2</sub>PO<sub>4</sub>, 0.5 g MgSO<sub>4</sub>·7H<sub>2</sub>O and 0.1 g CaCl<sub>2</sub>·2H<sub>2</sub>O per liter in addition to 70 mL trace element solution (3 g MgSO<sub>4</sub>·7H<sub>2</sub>O, 1 g NaCl, 0.5 g MnSO<sub>4</sub>·5H<sub>2</sub>O, 0.1 g FeSO<sub>4</sub>·7H<sub>2</sub>O and 0.1 g CuSO<sub>4</sub>·5H<sub>2</sub>O, 10 mg H<sub>3</sub>BO<sub>3</sub> per liter). The flasks were shaken at 37°C and 60 rpm using a Bio-shaker BR-40LF; a silicone porous plug type C was used to cover the flasks to permit constant aeration.

After three, five, and seven day-growth, the fungal tissue was harvested using a sterilized 0.22 µm stericup® filter to separate the CFSM and transfer it into the flasks for PAC treatment. LiP and MnP activity on CFSM after 3 days of harvesting were confirmed to be  $1.1 \pm 0.2$  U/L and  $20.6 \pm 1.2$  U/L, respectively (Konadu et al., 2019). Activities after 7 days harvesting of CFSM were  $3.4 \pm 0.3$  U/L and  $62.2 \pm 0.2$  U/L (Harada et al., 2016; Kudo et al., 2017)

#### 4.2.3. Laccase from *Trametes versicolor* treatment

Around 100 mg of PAC was added to 200 mL 100 mM sodium-acetate buffer (pH 4) in a sterile 500 mL Erlenmeyer flask. Experiments were carried out in triplicate using 19.5 U/L, 49.5 U/L, and 99 U/L of Lcc. Mediators are not included. The treatment was 3 days, and flasks were covered with a porous plug type C to allow aeration and shaken at 30°C and 128 rpm (Fig. 4.1). Then, the solid was collected by filtration and dried

under vacuum with silica gel overnight. The solid residue after this process was further characterized and applied for gold uptake. In this series, the samples are named Lcc 20, Lcc 50, and Lcc 100 for simplicity.

#### 4.2.4. CFSM treatment

In the same way as Lcc treatment, around 100 mg of PAC was added to 200 mL of freshly harvested CFSM in a sterile 500 mL Erlenmeyer flask. Experiments were carried out in triplicate, suspending 3, 5, and 7 days of harvested CFSM on PAC. The treatment was 3 days, and the pH was kept at 4 using a succinic acid buffer. The flasks were shaken at 30°C and 128 rpm and covered with a porous plug type C to allow aeration (Fig. 4.1). Then, the solid was collected by filtration and dried under vacuum with silica gel overnight. The solid residue after this process was further characterized and applied for gold uptake. As in this series, the samples are named CFSM-D3, CFSM-D5, and CFSM-D7.

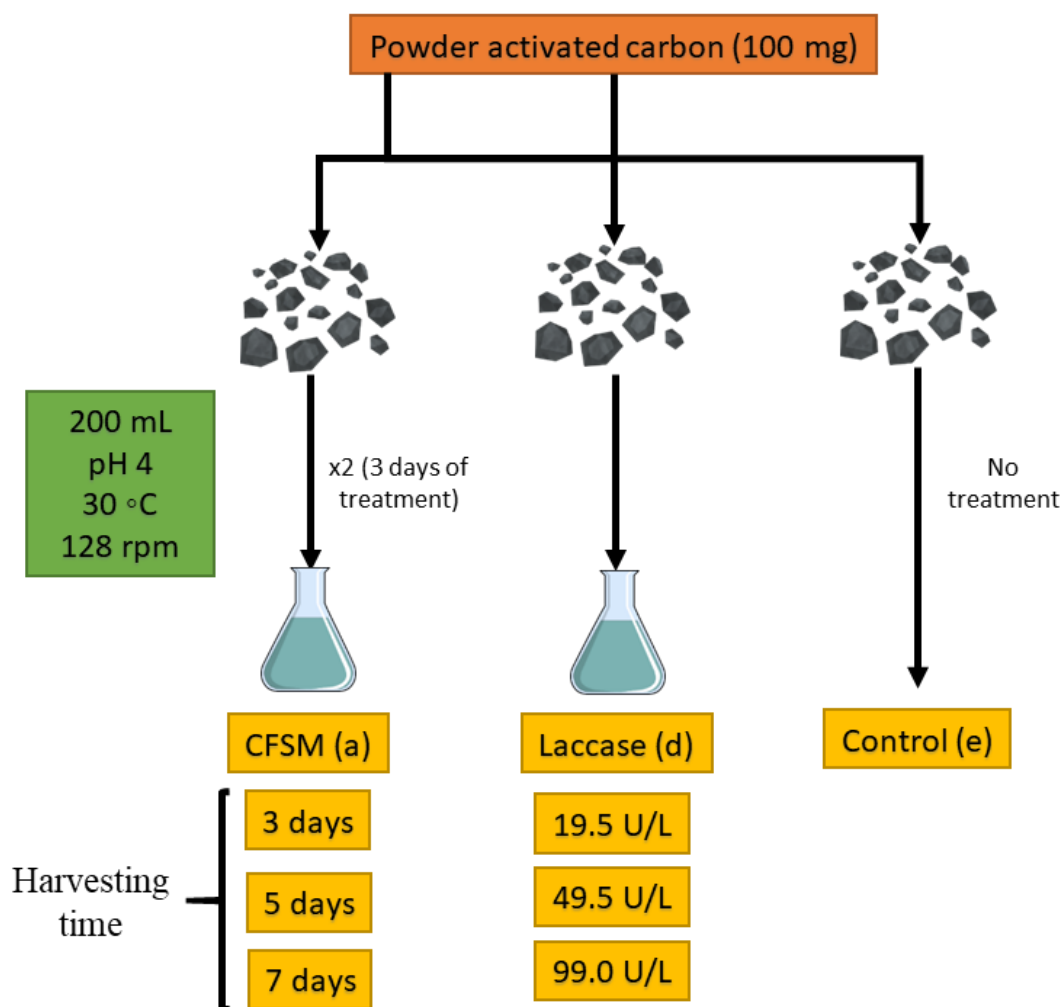


Fig. 4. 1. Schematic illustration of the experimental conditions in Chapter 4.

#### 4.2.5. Characterization of untreated and bio-treated carbonaceous matter surrogate

The chemical alterations in the enzymatic treated PAC were examined using Fourier-transformed infrared spectroscopy (FTIR), and the physical changes were determined by Brunauer, Emmett and Teller (BET)-specific surface area and scanning electron microscope (SEM). Detailed information about these analytical techniques can be found in section 2.3.



#### 4.2.6. $\text{Au}(\text{CN})_2^-$ adsorption test

Potassium dicyanoaurate ( $\text{KAu}(\text{CN})_2$ ) from KANTO CHEMICAL CO., INC. was used to prepare a stock solution of  $\text{Au}(\text{CN})_2^-$ . 36.6 mg of  $\text{KAu}(\text{CN})_2$  was completely dissolved in 500 mL of alkaline water at pH 11.5. The pH of alkaline water was adjusted using 1M KOH. For  $\text{Au}(\text{CN})_2^-$  adsorption experiments, the PAC samples before and after enzymatic treatment were provided as adsorbents. 10 mg of PAC powder samples were suspended in 4.0 mL of 0.23 mM  $\text{Au}(\text{CN})_2^-$ , at pH 11.5, and then the mixture was shaken at 120 rpm and 25°C using Bio-shaker BR-40LF. This experiment was completed in 24 h, and the remaining liquids were subsequently separated by filtration and supplied for determination of the residual  $\text{Au}(\text{CN})_2^-$  concentrations by ICP-OES. The experiments were conducted in duplicate.

### 4.3. Results and Discussion

#### 4.3.1. Physical changes on the surface of PAC

Both enzymatic conditions show a gradual decrease in specific surface area and pore volumes (Table 4.1), except CFMS-D5. The untreated PAC shows a very high surface area of 2342  $\text{m}^2/\text{g}$ , and this value was 1.6 times higher than previously reported by Konadu et al. (2017) using a similar PAC but from another lot. The results show that CFMS had a faster impact on a pore volume reduction than the crude Lcc at 19.5 U/L; however, this effect is comparable when increasing laccase activity to 99.0 U/L. In addition, CFMS contains not only LiP and MnP but also bio-chemicals and metabolites produced by *P. chrysosporium* during harvesting (Ofori-Sarpong, Osseo-Asare, et al., 2013a). Because of this, the reduction of specific surface area could also be influenced

by the adsorption of these organic substances. Table 4.1 also suggests that CFSM harvesting time between 3 and 7 days is a minor factor to consider because the impact on the surface area is minimum. As for Lcc, the reduction of the surface area and pore volume seems to be proportional to the enzyme activity, inferring that not only bio-oxidation is involved but also physical adsorption since PAC could work as a supporting material (Fernández-Fernández et al., 2013). The physical changes for Lcc-treated PAC and CFSM-treated PAC were also observed by SEM, whereby increasing the Lcc activity, the surface of PAC looked much more eroded (Fig. 4.2(d)) as compared to the smooth surface from untreated PAC (Fig. 4.2(a)).

Table 4.1. Physical properties obtained from N<sub>2</sub> adsorption at 77K of untreated PAC, CFSM-treated PAC after 3, 5 and 7 days of enzyme production, and laccase-treated PAC at 20, 50 and 100 U/L of enzyme activity. Enzyme treatment was for 3 days in all the treated samples

Samples	$S_{\text{BET}}$ (m <sup>2</sup> /g)	$S_v$ (cm <sup>3</sup> /g)
PAC	2342	2.12
CFSM-D3	779	0.77
CFSM-D5	844	0.84
CFSM-D7	723	0.72
Lcc 20	1264	1.16
Lcc 50	1069	0.98
Lcc 100	853	0.80

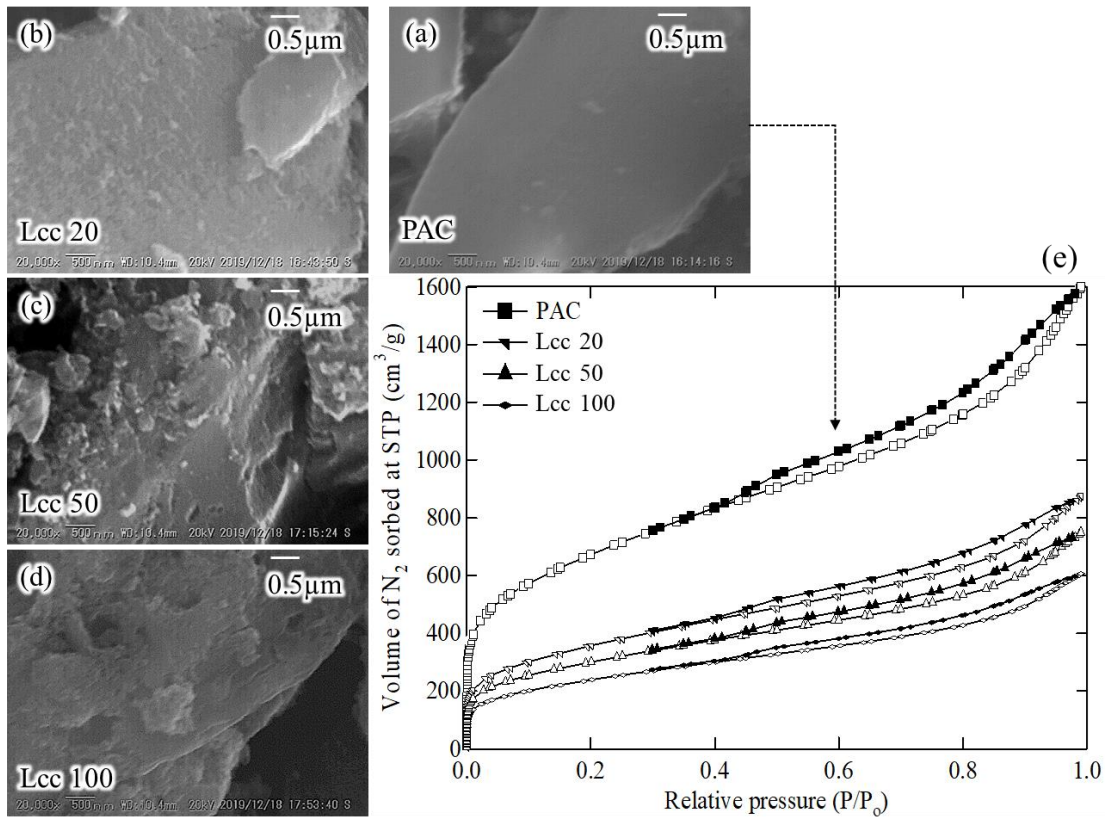


Fig. 4.2. SEM images of (a) the untreated and Lcc-treated PAC using (b) 20, (c) 50 and (d) 100 U/L of enzyme activity. (e) N<sub>2</sub> adsorption/desorption isotherms of the untreated and laccase-treated PAC samples as detailed. Enzyme treatment was conducted for 3 days.

For CFMSM-treated PAC, despite the harvesting time, the erosion occasioned by the CFMSM is not significantly differentiable among the samples (Fig. 4.3(a)-4.3(d)). A possible explanation for this might be that the appearance of micrometer-sized porous is visible within 7-14 days of CFMSM treatment, as shown by Konadu et al. (2017). Nevertheless, under the 3 days of treatment, Lcc and CFMSM treatment seems to similarly alter the physical changes on PAC.

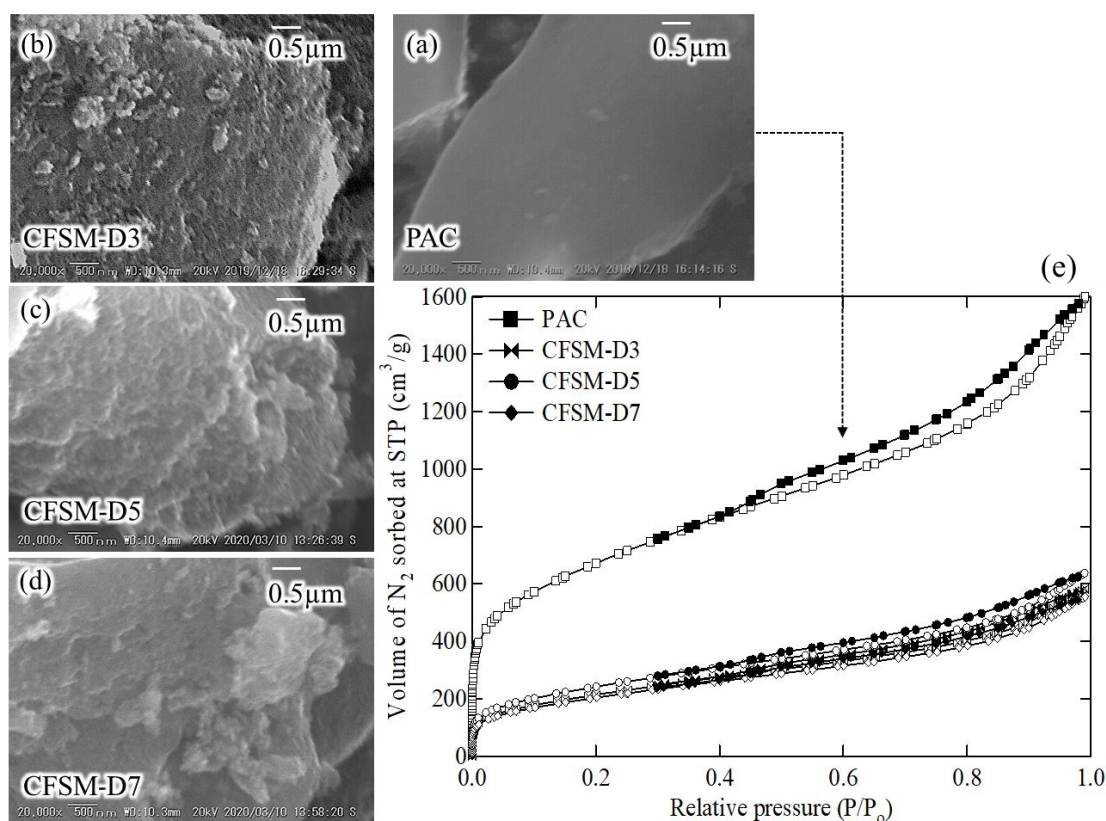


Fig. 4.3. SEM images of (a) the untreated and treated PAC using (b) 3 days harvested, (c) 5 days harvested (d) 7 days harvested CFSM. (e) Comparison of the  $N_2$  adsorption/desorption isotherms of the untreated and CFSM-treated PAC samples as detailed. CFSM treatment was conducted for 3 days.

#### 4.3.2. Chemical changes in PAC as a surrogate of carbonaceous matter in DRGO

FTIR transmission spectra for Lcc-treated and CFSM-treated PAC are displayed in Fig. 4.4 and Fig. 4.5. Pristine PAC shows a characteristic peak of aromatic bond ( $C=C$ ) between  $1515$  and  $1560\text{ cm}^{-1}$ . Lcc and CFSM series had in common the appearance of lactonic and carbonyl  $C=O$  stretching vibration mode at  $1740\text{ cm}^{-1}$  and  $1710\text{ cm}^{-1}$ , respectively, coming from enzymatic oxidation (Liu et al., 2016; Rivera-Hoyos et al., 2013).

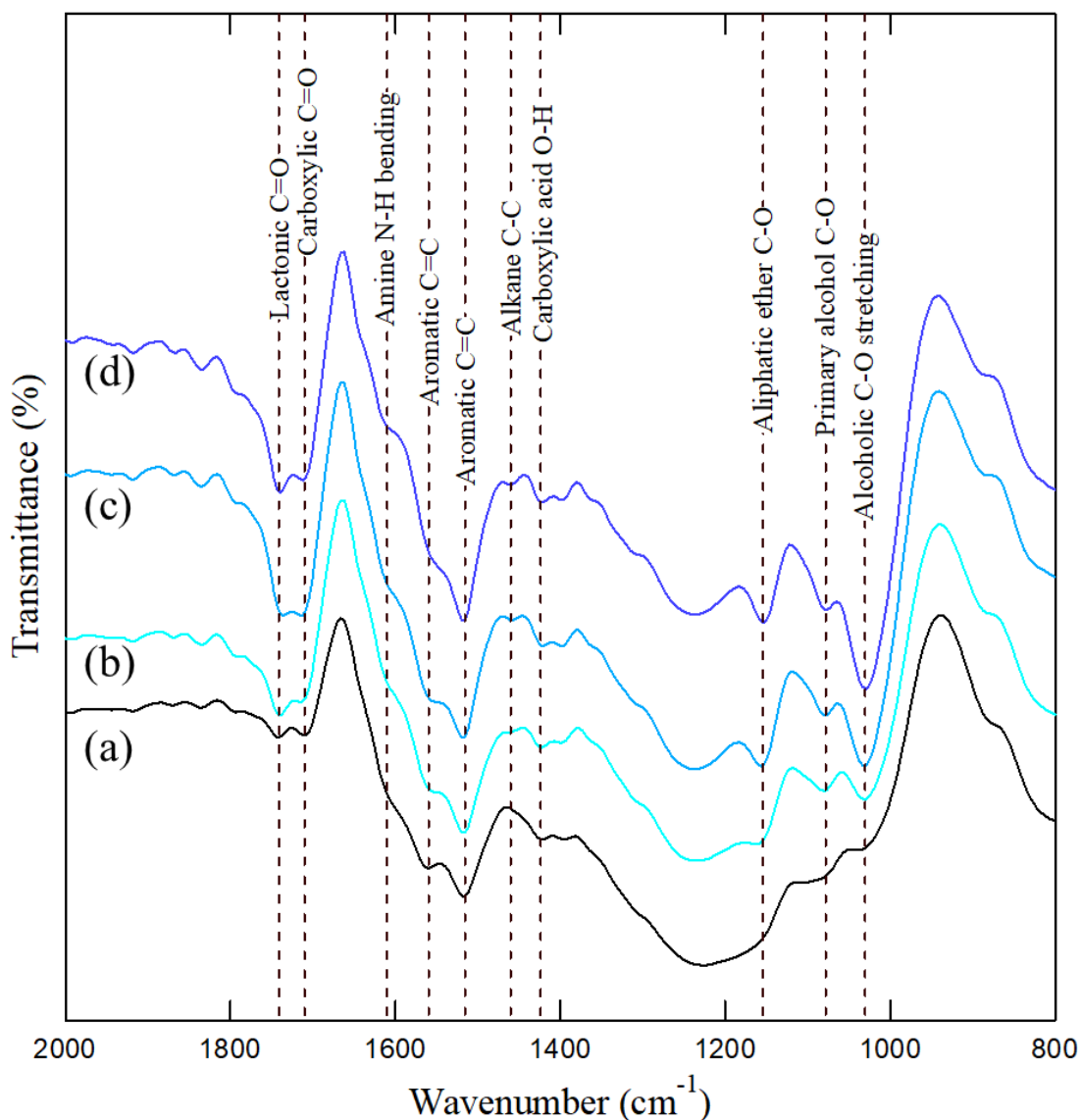


Fig. 4.4. FTIR spectra of (a) untreated and treated PAC using (b) Lcc 20, (c) Lcc 50, and (d) Lcc 100.

However, the formation of these peaks was prominent in CFSM-series, especially after 7 days of harvesting (Fig. 4.5). This is likely due to the higher production of carboxylic acids by the fungi under this growth time (Singh & Chen, 2008). Both enzymatic reactions seem to produce a variety of oxygen-containing functional groups in the region of the C-O stretching bond ( $1000\text{ cm}^{-1}$  to  $1300\text{ cm}^{-1}$ ).

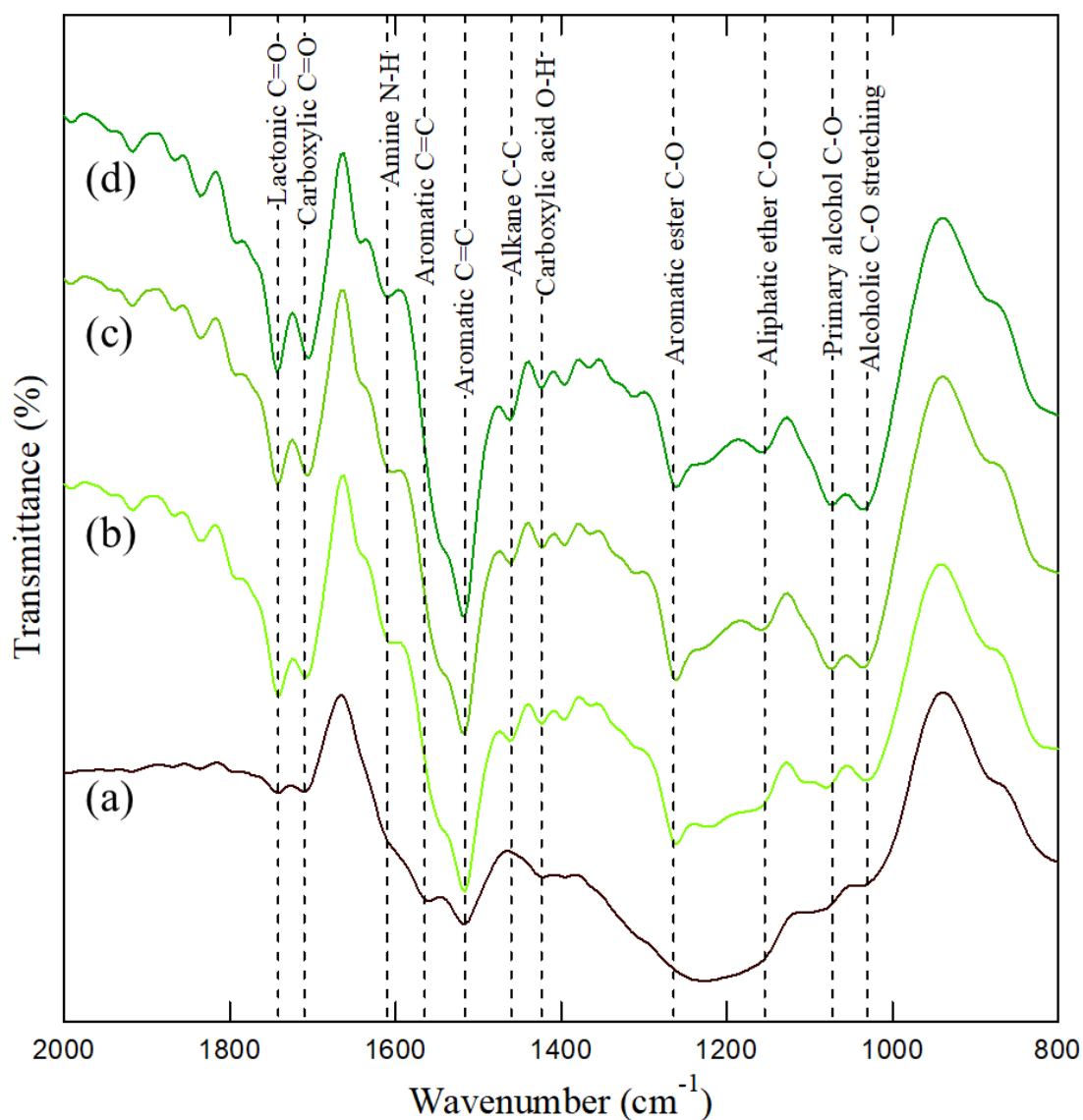


Fig. 4.5. FTIR spectra of (a) untreated and treated PAC using (b) 3 days, (c) 5 days, and (d) 7 days of CFSM harvesting.

Although the adsorption of laccase could have some impact on FTIR spectra for the Lcc series due to the presence of amino acids in the enzyme structure (Agrawal et al., 2018), the significant increase of the prominent peak at  $1030\text{ cm}^{-1}$  observed in Lcc 100, was not proportional to the carbonyl and hydroxyl assigned peaks. Inferring that oxidation takes place at much more parts than adsorption.

Besides that, the formation of several peaks attributed to alkyl group C-H between 1375  $\text{cm}^{-1}$  and 1465  $\text{cm}^{-1}$  (Ong et al., 2020) were more advantageous in CFSM-treated samples. Considering that the reaction pathways are different for both enzymatic conditions, some differences in the FTIR spectra were expected. However, it was clear that both enzyme conditions produced oxygen functional groups. Therefore, further reaction time in Lcc treatment could lead to the better observation of the C=C peak reduction, as observed by CFSM in Konadu et al. (2017).

#### 4.3.3. $\text{Au}(\text{CN})_2^-$ uptake

Fig. 4.6 illustrates  $\text{Au}(\text{CN})_2^-$  adsorption test on both enzymatic degradation series. After 24 hours, PAC adsorbed 0.053 mmol/g- $\text{Au}(\text{CN})_2^-$ , representing 100%.

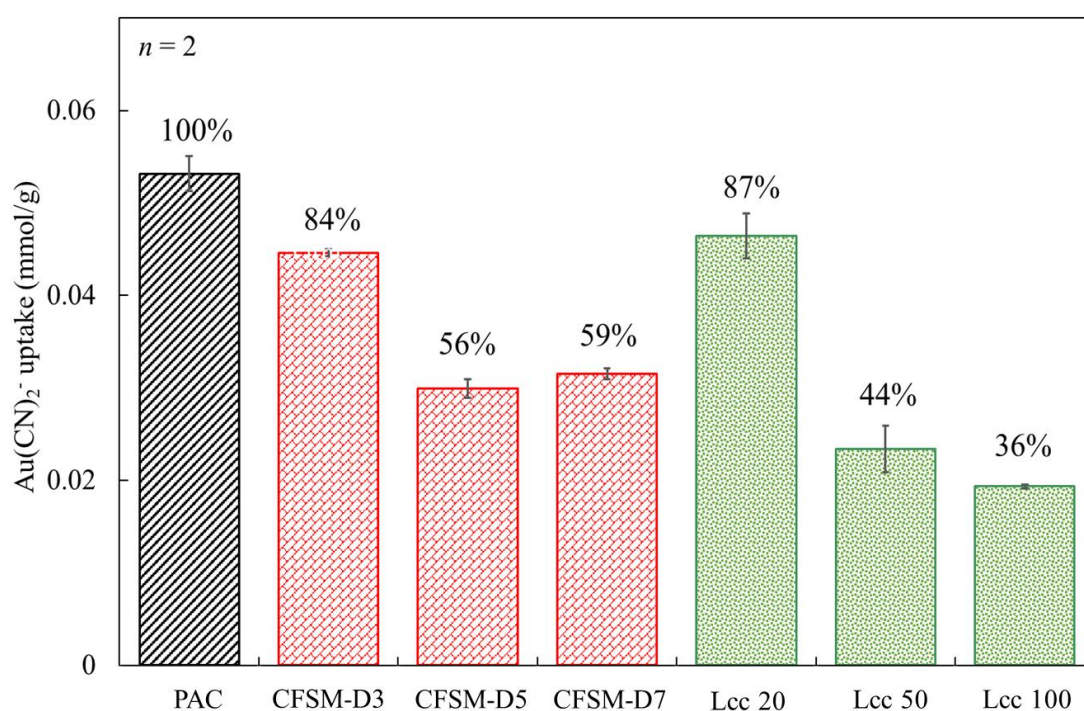


Fig. 4.6.  $\text{Au}(\text{CN})_2^-$  uptake on untreated PAC, CFSM-treated PAC, and Lcc-treated PAC after 24 hours. Initial  $[\text{Au}(\text{CN})_2^-]$  is 0.23 mM.

The gold uptake test revealed that the differences in the harvesting time in CFSM could be more critical for consideration. For example, CFSM-D7 shows a slight reduction of the specific surface area compared to CFSM-D3 (Table 4.1); however, it appears that the enzyme production was higher between 5-7 days of harvesting, leading to more significant degradation of the PAC surface and hence, less adsorption capacity. This premise was also supported by observing prominent peaks for C=O stretching vibration mode that appear due to oxidation under that condition.

As for the Lcc series, there was a big gap between Lcc 20 and Lcc 50, and this is likely due to the less amount of enzyme available to oxidize PAC and decreases the gold uptake. By increasing the Lcc activity to ~100 U/L, the adsorbed  $\text{Au}(\text{CN})_2^-$  was reduced to 0.019 mmol/g, representing a reduction of 64%. Since LiP and MnP peroxidase had lower reported activity in CFSM than those used in Lcc, the reduction of gold uptake in Lcc could also be influenced by the occupation of the enzyme on PAC pores. On the other hand, CFSM also possesses the advantage of including several organic substances secreted by *P. chrysosporium* that causes passivation, which is not included in Lcc because it is a crude powder enzyme. Overall, this preliminary study shows that Lcc has several benefits comparable to the one observed in CFSM.

#### **4.4. Conclusions**

Laccase (Lcc) is a copper oxidase that belongs to the family of lignin-degrading enzymes. This chapter discussed the viability of using Lcc to degrade carbonaceous matter in refractory gold ores. For this purpose, preliminary experiments using powder-activated carbon (PAC) as a surrogate were first explored. Then, the degradation



capacity of Lcc was compared with the well-studied cell-free spent medium (CFSM) from *P. chrysosporium*. As a result, Lcc shows similar oxidation characteristics as CFSM leading to the reduction of  $\text{Au}(\text{CN})_2^-$  adsorption after 3 days of treatment. Although the current findings are still indirect evidence, it provides a new approach for simplifying the enzyme treatment by using commercially purified laccase in hydrometallurgy. The improvement of the degradation conditions by using a laccase-mediator system (LMS) and the obtention of direct evidence to establish the method for natural carbonaceous matter degradation will be explored in the following chapter.

## References

- Abotsi, G. M. K., & Osseo-Asare, K. (1986) Surface chemistry of carbonaceous gold ores I. Characterization of the carbonaceous matter and adsorption behavior in aurocyanide solution. *International Journal of Mineral Processing*, 18(3–4), 217–236.
- Adams, M. D., & Fleming, C. A. (1989) The mechanism of adsorption of aurocyanide onto activated carbon. *Metallurgical and Materials Transactions B* 1989 20:3, 20(3), 315–325.
- Adams, M. D. (1990) The mechanism of adsorption of aurocyanide onto activated carbon, 1. Relation between the effects of oxygen and ionic strength. *Hydrometallurgy*, 25(2), 171–184.
- Agrawal, K., Chaturvedi, V., & Verma, P. (2018) Fungal laccase discovered but yet undiscovered. *Bioresources and Bioprocessing*, 5(1).

- Baldrian, P. (2003) Interactions of heavy metals with white-rot fungi. *Enzyme and Microbial Technology*, 32(1), 78–91.
- Claus, H. (2004) Laccases: Structure, reactions, distribution. *Micron*, 35(1–2), 93–96.
- Debnath, R., & Saha, T. (2020) An insight into the production strategies and applications of the ligninolytic enzyme laccase from bacteria and fungi. *Biocatalysis and Agricultural Biotechnology*, 26, 101645.
- Dittmer, J. K., Patel, N. J., Dhawale, S. W., & Dhawale, S. S. (1997) Production of multiple laccase isoforms by *Phanerochaete chrysosporium* grown under nutrient sufficiency. *FEMS Microbiology Letters*, 49(1), 65–70.
- Fakoussa, R. M., & Hofrichter, M. (1999) Biotechnology and microbiology of coal degradation. In *Applied Microbiology and Biotechnology*, 52 (1), 25–40.
- Fernández-Fernández, M., Sanromán, M. Á., & Moldes, D. (2013) Recent developments and applications of immobilized laccase. *Biotechnology Advances*, 31(8), 1808–1825.
- Gnanamani, A., Jayaprakashvel, M., Arulmani, M., & Sadulla, S. (2006) Effect of inducers and culturing processes on laccase synthesis in *Phanerochaete chrysosporium* NCIM 1197 and the constitutive expression of laccase isozymes. *Enzyme and Microbial Technology*, 38(7), 1017–1021.
- Ibrado, A. S., & Fuerstenau, D. W. (1992) Effect of the structure of carbon adsorbents on the adsorption of gold cyanide. *Hydrometallurgy*, 30(1–3), 243–256.

Ibrado, A. S., & Fuerstenau, D. W. (1995) Infrared and X-ray photoelectron spectroscopy studies on the adsorption of gold cyanide on activated carbon. *Minerals Engineering*, 8(4–5), 441–458.

Konadu, K. T., Sasaki, K., Kaneta, T., Ofori-Sarpong, G., & Osseo-Asare, K. (2017) Bio-modification of carbonaceous matter in gold ores: Model experiments using powdered activated carbon and cell-free spent medium of *Phanerochaete chrysosporium*. *Hydrometallurgy*, 168, 76–83.

Konadu, K. T., Huddy, R. J., Harrison, S. T. L., Osseo-Asare, K., & Sasaki, K. (2019a). Sequential pretreatment of double refractory gold ore (DRGO) with a thermophilic iron oxidizing archaeon and fungal crude enzymes. *Minerals Engineering*, 138, 86–94.

Konadu, K. T., Harrison, S. T. L., Osseo-asare, K., & Sasaki, K. (2019b). Transformation of the carbonaceous matter in double refractory gold ore by crude lignin peroxidase released from the white-rot fungus. *International Biodeterioration and Biodegradation*, 143, 104735.

Konadu, K. T., Mendoza, D. M., Huddy, R. J., Harrison, S. T. L., Kaneta, T., & Sasaki, K. (2020) Biological pretreatment of carbonaceous matter in double refractory gold ores: A review and some future considerations. *Hydrometallurgy*, 196, 105434.

Kudo, S., Harada, A., Kubota, H., Sasaki, K., & Kaneta, T. (2017) Simultaneous determination of manganese peroxidase and lignin peroxidase by capillary electrophoresis enzyme assays. *ACS Omega*, 2(10), 7329–7333.

- Lagerge, S., Zajac, J., Partyka, S., & Groszek, A. J. (1999) Comparative study on the adsorption of cyanide gold complexes onto different carbonaceous samples: Measurement of the reversibility of the process and assessment of the active surface inferred by flow microcalorimetry. *Langmuir*, 15(14), 4803–4811.
- Liu, Q., Yang, H., Tong, L., Jin, Z., & Sand, W. (2016) Fungal degradation of elemental carbon in Carbonaceous gold ore. *Hydrometallurgy*, 160, 90–97.
- McDougall, G. J., Adams, M. D., & Hancock, R. D. (1987) Models for the adsorption of aurocyanide onto activated carbon. Part I: Solvent extraction of aurocyanide ion pairs by 1-pentanol. *Hydrometallurgy*, 18(2), 125–138.
- Miki, T. (1983) Graphitization of carbonaceous matter in sedimentary rocks. *Journal of the Sedimentological Society of Japan*, 111–120.
- Miller, J. D., Wan, R.-Y., & Díaz, X. (2016) Preg-Robbing Gold Ores. *Gold Ore Processing*, 885–907.
- Ofori-Sarpong, G., Tien, M., & Osseo-Asare, K. (2010). Myco-hydrometallurgy: Coal model for potential reduction of preg-robbing capacity of carbonaceous gold ores using the fungus, *Phanerochaete chrysosporium*. *Hydrometallurgy*, 102(1–4), 66–72.
- Ofori-Sarpong, G., Amankwah, R. K., & Osseo-Asare, K. (2013a) Reduction of preg-robbing by biomodified carbonaceous matter-A proposed mechanism. *Minerals Engineering*, 42, 29–35.
- Ofori-Sarpong, G., Osseo-Asare, K., & Tien, M. (2013b) Mycohydrometallurgy: Biotransformation of double refractory gold ores by the fungus, *Phanerochaete chrysosporium*. *Hydrometallurgy*, 137, 38–44.

- Ong, H. C., Chen, W. H., Singh, Y., Gan, Y. Y., Chen, C. Y., & Show, P. L. (2020). A state-of-the-art review on thermochemical conversion of biomass for biofuel production: A TG-FTIR approach. *Energy Conversion and Management*, 209, 112634.
- Rivera-Hoyos, C. M., Morales-Álvarez, E. D., Poutou-Piñales, R. A., Pedroza-Rodríguez, A. M., Rodríguez-Vázquez, R., & Delgado-Boada, J. M. (2013) Fungal laccases. *Fungal Biology Reviews*, 27(3–4), 67–82.
- Shleev, S., Persson, P., Shumakovich, G., Mazhugo, Y., Yaropolov, A., Ruzgas, T., & Gorton, L. (2006) Interaction of fungal laccases and laccase-mediator systems with lignin. *Enzyme and Microbial Technology*, 39(4), 841–847.
- Sibrell, P. L., & Miller, J. D. (1992) Significance of graphitic structural features in gold adsorption by carbon. *Mining, Metallurgy & Exploration* 1992 9:4, 9(4), 189–195.
- Singh, D., & Chen, S. (2008) The white-rot fungus *Phanerochaete chrysosporium*: Conditions for the production of lignin-degrading enzymes. *Applied Microbiology and Biotechnology*, 81(3), 399–417.
- Tan, H., Feng, D., Lukey, G. C., & van Deventer, J. S. J. (2005) The behaviour of carbonaceous matter in cyanide leaching of gold. *Hydrometallurgy*, 78(3–4), 226–235.
- Van Vuuren, C. P. J., Snyman, C. P., & Boshoff, A. J. (2000) Gold losses from cyanide solutions. Part II: The influence of the carbonaceous materials present in the shale material. *Minerals Engineering*, 13(10), 1177–1181.
- Yang, H. Y., Liu, Q., Song, X. L., & Dong, J. K. (2013) Research status of carbonaceous matter in carbonaceous gold ores and bio-oxidation pretreatment. *Transactions of Nonferrous Metals Society of China*, 23(11), 3405–3411.

Zofair, S. F. F., Ahmad, S., Hashmi, M. A., Khan, S. H., Khan, M. A., & Younus, H. (2022) Catalytic roles, immobilization and management of recalcitrant environmental pollutants by laccases: Significance in sustainable green chemistry. *Journal of Environmental Management*, 309, 114676.

**Chapter 5:**

**Degradation of powder activated  
carbon by laccase-mediator  
system**

## 5.1.Introduction

In the gold mining industry, the extraction of gold from refractory carbonaceous ores is taking more attention since free native gold is rapidly exhausting worldwide (Dunne et al., 2012; Yang et al., 2013; Miller et al., 2016). Such refractoriness results from the encapsulation of gold in sulfide minerals and/or its association with gangue materials like carbonaceous matter (CM) (Afenya, 1991; Nanthakumar et al., 2007; Natarajan, 2018). Although gold grains could be liberated and/or not associated with sulfides, CM decreases the gold extraction during cyanidation through the adsorption of gold cyanide complex, a phenomenon named preg-robbing (Rees and van Deventer, 2000; Tan et al., 2005; Ofori-Sarpong & Osseo-Asare, 2013; Konadu et al., 2020).

Over the years, researchers have explored different ways to overcome gold losses in carbonaceous gold ores. Chemical pre-treatments like blanking, roasting, and chlorination for passivation and degradation of CM are well-described (Nanthakumar et al., 2007; Amankwah & Pickles, 2009; Wang et al., 2020; Owusu et al., 2021). Nevertheless, due to environmental and economic aspects, biological pre-treatments of CM are gaining interest in industrial applications. As introduced in the previous chapter, CM degradation was accomplished using the cell-free spent medium (CFSM) from the white-rot fungus *Phanerochaete chrysosporium* (Konadu et al., 2019; Mendoza et al., 2021) due to the presence of lignin peroxidase (LiP) and manganese peroxidase (MnP) (Kudo et al., 2017) and their ability to break the C-C bond in aromatic carbon (Hofrichter, 2002; Singh et al., 2021). However, the utilization of these enzymes seems complicated in a broad biotechnological application of mineral processing because their activities depend on hydrogen peroxide (H<sub>2</sub>O<sub>2</sub>) as an oxidant, high



purification cost, low stability, and limited production by specific fungal species (Fakoussa and Hofrichter, 1999). Besides the fungal peroxidases, a series of white-rot basidiomycetes produce laccase (Lcc), which would also be responsible for natural lignin degradation. Lcc belongs to a family of multi-copper oxidase and shows catalytic activities against a wide variety of compounds, including lignin-related materials. Lcc can oxidize various aromatic compounds by reducing molecular oxygen ( $O_2$ ) to water in which high-cost oxidants such as  $H_2O_2$  are not required (Rivera-Hoyos et al., 2013), being an attractive alternative biocatalyst for green and sustainable technologies. Lcc degradation ability on powder activated carbon (PAC) was also tested in Chapter 4, showing promising results comparable to CFSM. However, despite these advantages, it remains a practical matter to use Lcc in applications because it can oxidize mainly phenolic compounds due to its relatively low standard redox potential (0.5 – 0.8 V) (Christopher et al., 2014). This disadvantage can be overcome in the presence of several compounds which can act as mediators of electrons (Fig. 5.1), extending the catalytic application to a broader range of components (Longe et al., 2018). Laccase-mediator system (LMS) has been widely applied in the degradation of aromatic hydrocarbons (Vipotnik et al., 2021), pharmaceutical pollutants (Margot et al., 2015; Naghdi et al., 2018), herbicides (Torres-Duarte et al., 2009; Zeng et al., 2017), lignin (Elegir et al., 2005; Christopher et al., 2014), dyes decolorization (Du et al., 2020), pulp industry (Aracri et al., 2009; Valls et al., 2010; Andreu and Vidal, 2011) and in coal solubilization (Kwiatos et al., 2018). However, to the best of my knowledge, LMS has not yet been examined for bio-hydrometallurgical applications. Since the origin of CM in refractory gold ores derives from plant precursors, which involve the presence of phenolic and non-phenolic substrates, LMS degradation is expected to be possible.

For the LMS studies in the present chapter, PAC was continuously used as a CM surrogate due to the well-established similarities that this material has with the elemental carbon from CM (Yang et al., 2013; Miller et al., 2016). This study aims to obtain suitable conditions for LMS degradation before applying the method to natural ores. Compared to chapter 4, LMS was evaluated using a commercial Lcc from *Trametes sp.*, which shows higher enzyme activity than Lcc from Sigma-Aldrich and the synthetic mediator 1-hydroxybenzotriazole (HBT). These experimental conditions are first applied in model experiments to degrade PAC and reduce gold preg-robbing. In addition, gas chromatography-mass spectrometry (GC-MS) analysis is used to characterize the extracted by-products after LMS oxidation of PAC.

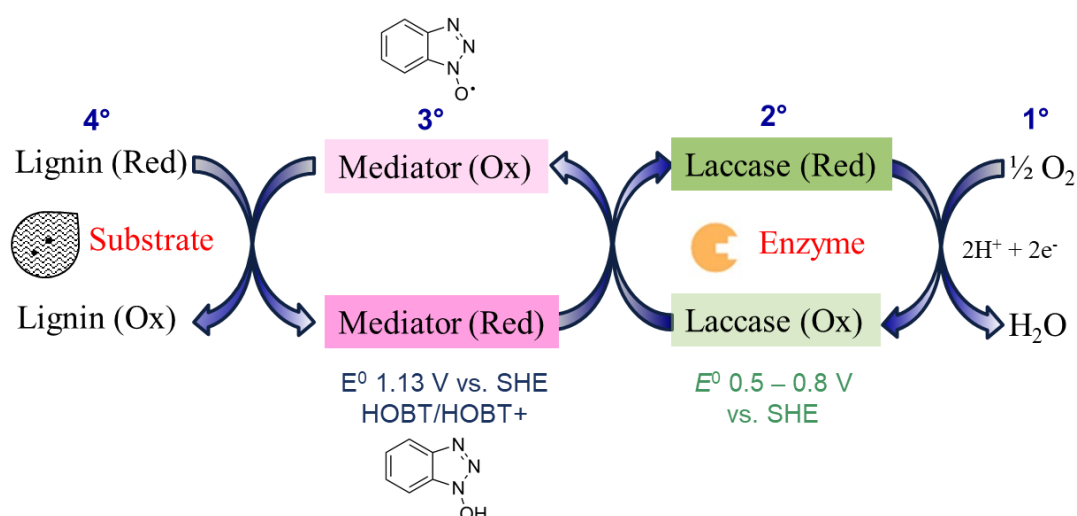


Fig. 5.1. Catalytic cycle of laccase and mechanism of laccase mediated biodegradation of carbon. Adapted from Longe et al. (2018).

## 5.2.Experimental

### 5.2.1. Materials

The following chemicals were used as received: sodium acetate anhydrous ( $\text{CH}_3\text{COONa}$ , 98.5%; Wako), HBT ( $\text{C}_6\text{H}_5\text{N}_3\text{O}\cdot x\text{H}_2\text{O}$ , 97%; Sigma-Aldrich), ABTS ( $\text{C}_{16}\text{H}_{16}\text{N}_4\text{O}_6\text{S}_4\cdot (\text{NH}_4)_2$ ; Wako), acetic acid ( $\text{CH}_3\text{COOH}$ , 99.7%; Wako), ethanol ( $\text{C}_2\text{H}_5\text{OH}$ , 99.5%, Wako), ethylene glycol ( $\text{HOCH}_2\text{CH}_2\text{OH}$ , 99.5%; Kishida), hexane ( $\text{CH}_3(\text{CH}_2)_4\text{CH}_3$ , 96%; Wako), and ethyl acetate ( $\text{CH}_3\text{COOC}_2\text{H}_5$ , 99%; Wako). In addition, PAC in a special grade was supplied by Wako Chemicals (Osaka, Japan). The measured average particle size was 36  $\mu\text{m}$  in diameter. Ultra-pure water produced by Millipore synergy unit was used throughout the experiments.

### 5.2.2. Laccase activity assay

The enzymatic activity of Lcc was evaluated by measuring the oxidation of ABTS as a substrate at 420 nm ( $\epsilon_{420} = 36,000 \text{ M}^{-1} \text{ cm}^{-1}$ ). The reaction mixture (3 mL) consisted of 0.2 mg of Lcc and 0.2 mM ABTS in 100 mM acetate buffer (pH 4.5). The reaction was initiated by adding Lcc, and the reaction velocity was determined by time-course data of ABTS oxidation between 0 and 5 min; the absorbance change was linear under the experimental conditions. The kinetic data were observed using an IMPLIN P300 spectrophotometer (Germany). One unit (U) is defined as the necessary amount of enzyme capable of oxidizing 1  $\mu\text{mol}$  of ABTS per minute. The enzyme activity is calculated according to the equation described in section 2.1.1. Initial laccase activity was  $\sim 150 \text{ U/L}$ .

#### 5.2.3. Laccase-mediator system using HBT for treating PAC

For this experiment, 100 mg of PAC was added to a 300 mL Erlenmeyer flask, followed by adding 90 mL of 100 mM acetate buffer (pH 4.5), 0.8 mL of 100 mM HBT dissolved in 99% ethanol, and finally 0.1 mg/mL Lcc Y-120 was added. The total volume was adjusted to 100 mL using the buffer. All the flasks were covered with a porous plug type C to permit oxygen to enter the system and activate the catalytic capacity of Lcc. The flasks were shaken at 37°C and 128 rpm using a TAITEC BR-40LF Bioshaker (Saitama, Japan). Through experimental data, the supplier provided the optimized pH and temperature where Lcc had the highest stability and activity. The experiments were performed in duplicate, considering a control test without adding Lcc Y-120. After the appropriate time intervals (1, 2, 5, and 7 days) of enzyme contact, the solid residues were separated from the supernatant by filtration, then dried-vacuum overnight for characterization and adsorption of  $\text{Au}(\text{CN})_2^-$ . The enzyme activity was measured for the supernatants over the reaction time as described in section 2.1.1. For HBT determination, the supernatant was subjected to high-performance liquid chromatography (HPLC) and quantified using calibration curves of standards as detailed in section 2.2.5.

#### 5.2.4. Sequential organic solvent extraction of LMS-degraded products for characterization by GC-MS

The washing was conducted in the following order: (i) ethylene glycol, (ii) methanol, (iii) ethyl acetate, and (iv) hexane, where the solvents were arranged from the most polar to non-polar. For this test, 100 mg of solid residues were separately washed and shaken in 2 mL of organic solvent at 25°C, 150 rpm for 1 h using an AS ONE SRR-2

shaker (Osaka, Japan) in a reciprocator mode. Afterward, centrifugation was applied at 4°C, 7600 rpm for 10 min using an Eppendorf 5430R centrifuge (Hamburg, Germany). The solid residue after the first washing with (i) ethylene glycol was provided for the second washing with (ii) and so on (iii) and (iv). The same procedure was applied to the untreated PAC for the baseline. The dissolved organic phases were supplied for gas chromatography-mass spectrometry (GC-MS) analysis, and the solid residues were for characterization and adsorption of  $\text{Au}(\text{CN})_2^-$ . The details of GC-MS analysis are described in section 2.2.4.

#### 5.2.5. Characterization of untreated and LMS-treated PAC

The chemical alterations in LMS-treated PAC were examined using Fourier-transformed infrared spectroscopy (FTIR), thermogravimetric-differential thermal analysis (TG-DTA), Raman spectroscopy, and gas chromatography-mass spectrometry (GC-MS). As for the physical changes in the solid, these were determined by  $\text{N}_2$  adsorption and scanning electron microscopy (SEM) and BET-specific surface area. Detailed information about these analytical techniques can be found in sections 2.2 and 2.3.

#### 5.2.6. Adsorption of $\text{Au}(\text{CN})_2^-$ on PAC before and after enzyme treatment

For this adsorption test, 36.6 mg of  $\text{KAu}(\text{CN})_2$  (Kanto Chemicals, Osaka, Japan) was completely dissolved in 500 mL of ultrapure water at pH 11.5 (adjusted by 1 M KOH). The untreated PAC, LMS-treated PAC, and washed PAC samples were provided as adsorbents for adsorption experiments. In addition, 10 mg of PAC powder samples

were suspended in 4.0 mL of 0.23 mM  $\text{Au}(\text{CN})_2^-$  at pH 11.5, and then the mixture was shaken at 120 rpm and room temperature using EYELA MMS5010 shaker (Tokyo, Japan) in duplicates. This experiment was completed in 24 h, and the remaining liquids were subsequently filtrated and supplied to determine the residual Au concentrations by Perkin Elmer Optima 8300 ICP-OES (Massachusetts, USA).

### **5.3.Results and Discussion**

#### **5.3.1. Laccase activity in the system**

Time-dependent change of Lcc activity was followed in the presence and the absence of PAC for evaluating the robustness of Lcc during PAC treatment. In Fig. 5.2, the Lcc activity gradually decreased in the reaction buffer medium even in the absence of PAC, leaving around 50% of activity remaining within 48 h. However, this reduction trend in Lcc activity was not the same when PAC was added to the system. In this case, after 1 h of contact, Lcc activity was observed in the PAC surface and the supernatant, even though the activity on the PAC surface was considerably higher than planktonic. As time passed, Lcc was still active on the PAC surface after 24 h (61%); nevertheless, with a slight activity loss compared to the results after 1 h. Several reports have demonstrated that Lcc could be immobilized in porous carries like activated carbon through physical (Fernández-Fernández et al., 2013; Alvarado-Ramírez et al., 2021) and chemical (Davis & Burns, 1992; Nguyen et al., 2016) adsorption. As for the results, it seemed the majority of Lcc was rapidly adsorbed and immobilized on PAC within 1 h.

For this reason, based on UV-Vis analysis, the remaining activity on the supernatant was likely lower than the detection limit after 24 h. Another important consideration is that PAC is composed of suspended particles that cannot be dissolved in an aqueous phase like other lignin-related materials. Thus, it was assumed that Lcc immobilization allowed prolonged PAC oxidation; nevertheless, we could assume the reaction proceeded in an early incubation stage because Lcc gradually became inactive after 48 h incubation.

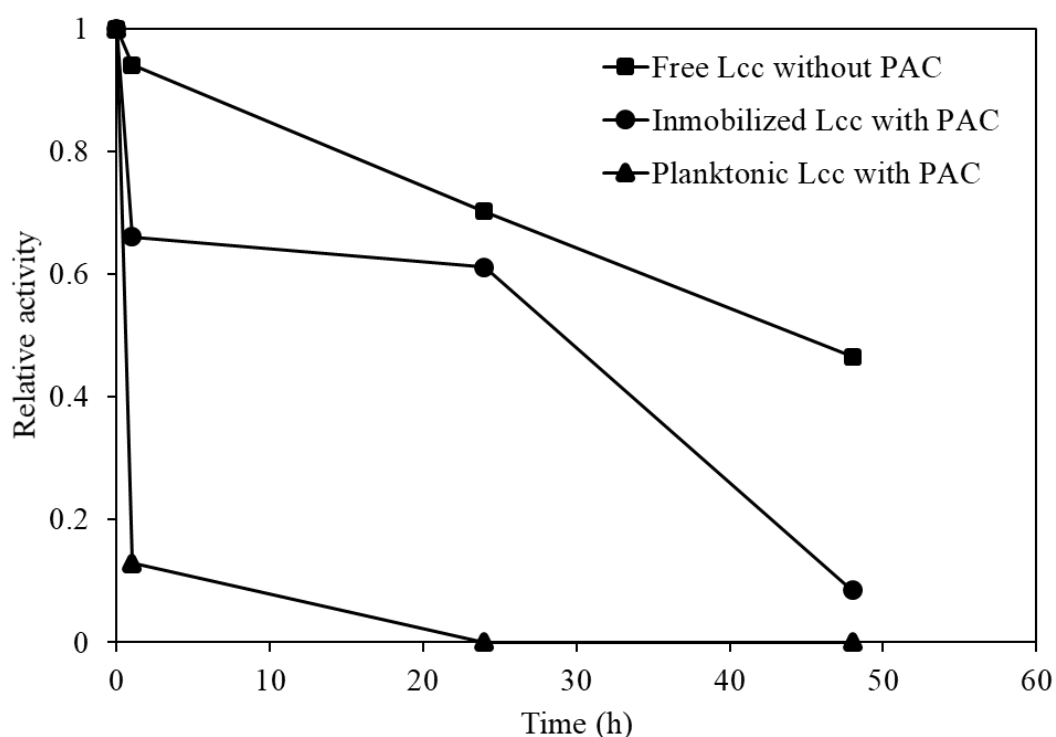


Fig. 5.2. Relative enzyme activity of free laccase (Lcc), immobilized Lcc and planktonic Lcc against time at 37°C, pH 4.5. Free (■) refers to the incubation of laccase without PAC. Immobilized (●) refers to the laccase relative activity detected after enzyme adsorption on the surface of PAC. Planktonic (▲) refers to the laccase relative activity in the supernatant over the contact time with PAC.

### 5.3.2. Changes in surface morphologies of PAC by LMS treatment

SEM observation helped to illustrate the alteration on the surface PAC particles after LMS treatment. As shown in Fig. 5.3(a), the untreated PAC shows a vast flat surface. However, activated carbon is a highly porous material (Mistar et al., 2020). The baseline characterization also shows that the untreated PAC was a typical microporous-mesoporous adsorbent (Fig. 5.4(a)-(b)) with a specific surface area of  $2342 \text{ m}^2/\text{g}$ , a pore volume of  $2.12 \text{ cm}^3/\text{g}$ , and an averaged pore diameter of  $4.2 \text{ nm}$ . Therefore, this indicates that under the current magnification, the very fine nanometer-sized pores in the PAC were not feasible to be observed (Gao et al., 2020; Jothi Ramalingam et al., 2020). Similar surface morphology was distinguished when HBT was present alone without Lcc (Fig. 5.3(b)). In fact, the mediator itself does not alter PAC; Lcc is necessary to start the catalytic oxidation of both the substrate and the mediator. This premise is confirmed as shown in Fig. 5.3(c)–(f), where the surface of PAC looks eroded and rough, already after 24 h of reaction. Moreover, during this 24 h period when Lcc is likely to be active in the surface of PAC (Fig. 5.2), significant changes in the reduction of the specific surface area ( $986 \text{ m}^2/\text{g}$ ) and the pore volume ( $0.93 \text{ cm}^3/\text{g}$ ) were detected (Table 5.1).

These values gradually decreased after 7 days of treatment to  $913 \text{ m}^2/\text{g}$  and  $0.86 \text{ cm}^3/\text{g}$ , respectively. Generally, reducing the specific surface area during the oxidation of activated carbon is associated with decreasing the pore volume (Fig. 5.4(b)) (Mangun et al., 1999; Konadu et al., 2017). This statement agrees with the current findings, and an explanation could be the blockage of the pores through the formation of oxygen-containing functional groups in the surface of PAC (Daud and Houshamnd, 2010).



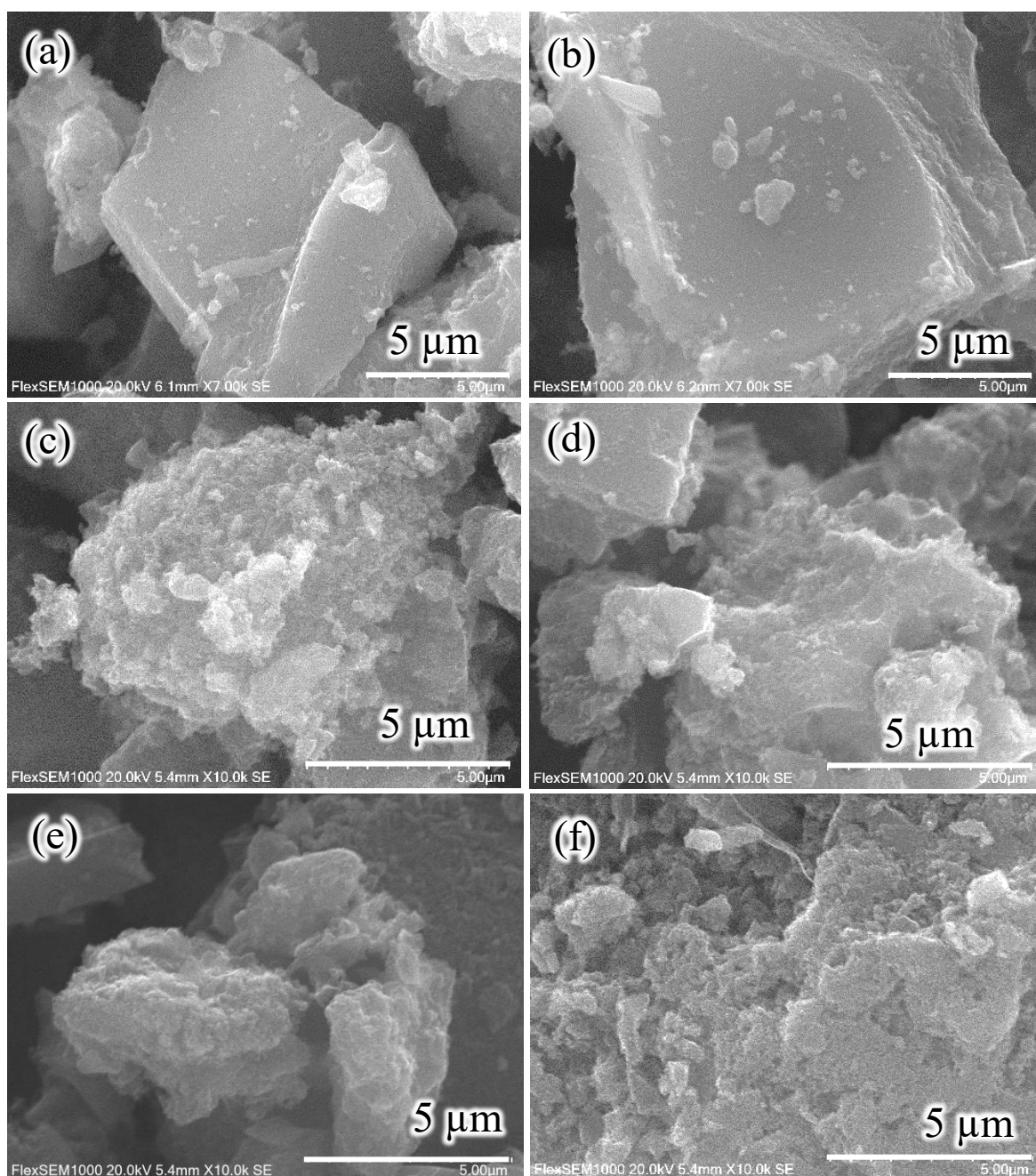


Fig. 5.3. SEM images of PAC (a) untreated, (b) mediator controlled in the absence of laccase after 2 days, and (c) LMS-HBT treated after 1 day, (d) 2 days, (e) 5 days and (f) 7 days.

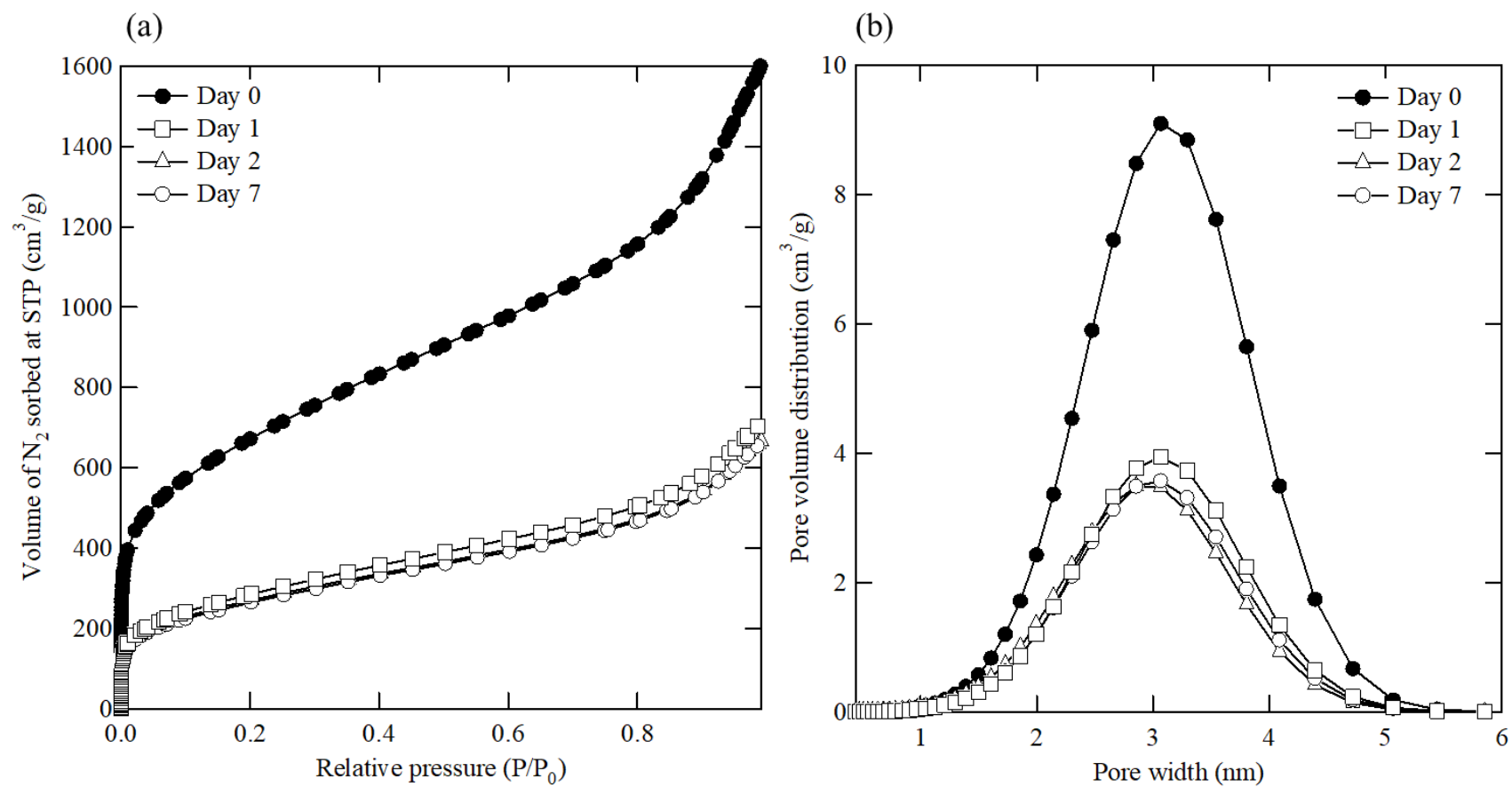


Fig. 5.4. Adsorption isotherms of  $N_2$  (a) and (b) NLDFT pore volume distribution of PAC before and after 1, 2 and 7 days of LMS treatment.

Table 5.1. Changes in specific surface area and pore volume of untreated and LMS-treated PAC

Treatment period (days)	BET-specific surface area (m <sup>2</sup> /g)	Pore volume (cm <sup>3</sup> /g)	Averaged pore diameter (nm)
0	2342	2.12	4.22
1	986	0.93	4.40
2	929	0.87	4.41
7	913	0.86	4.47

### 5.3.3. Chemical alterations of PAC by LMS treatment

#### 5.3.3.1. FTIR

FTIR spectra showed the changes in the functional groups in PAC during LMS treatment. The untreated PAC (Fig. 5.5(a)) shows two prominent peaks at 1150 cm<sup>-1</sup> and 1580 cm<sup>-1</sup>, assigned to the C-O and C=C stretching vibration modes in phenol and aromatic carbon (Shin et al., 1997; Bouchelta et al., 2008; Shafeeyan et al., 2010; Ong et al., 2020), respectively. They look relatively similar in the untreated PAC (Fig. 5.5(a)) and the mediator control (Fig. 5.5(b)), deducing that neither addition of HBT itself nor its adsorption on PAC altered the existing functional groups. Conversely, when the Lcc is added into the system (Fig. 5.5(c-f)), a disturbance between 1000 to 1400 cm<sup>-1</sup> is present. It was assigned to a C-O stretching bond in ether, phenol, ester, or alcohol (Biniak et al., 1997; Peng et al., 2015a; Doğan et al., 2020; Ong et al., 2020). Likewise, the carbonyl (-C=O) group formed gradually at 1700 cm<sup>-1</sup> (Ong et al., 2020; Peng et al., 2015b).

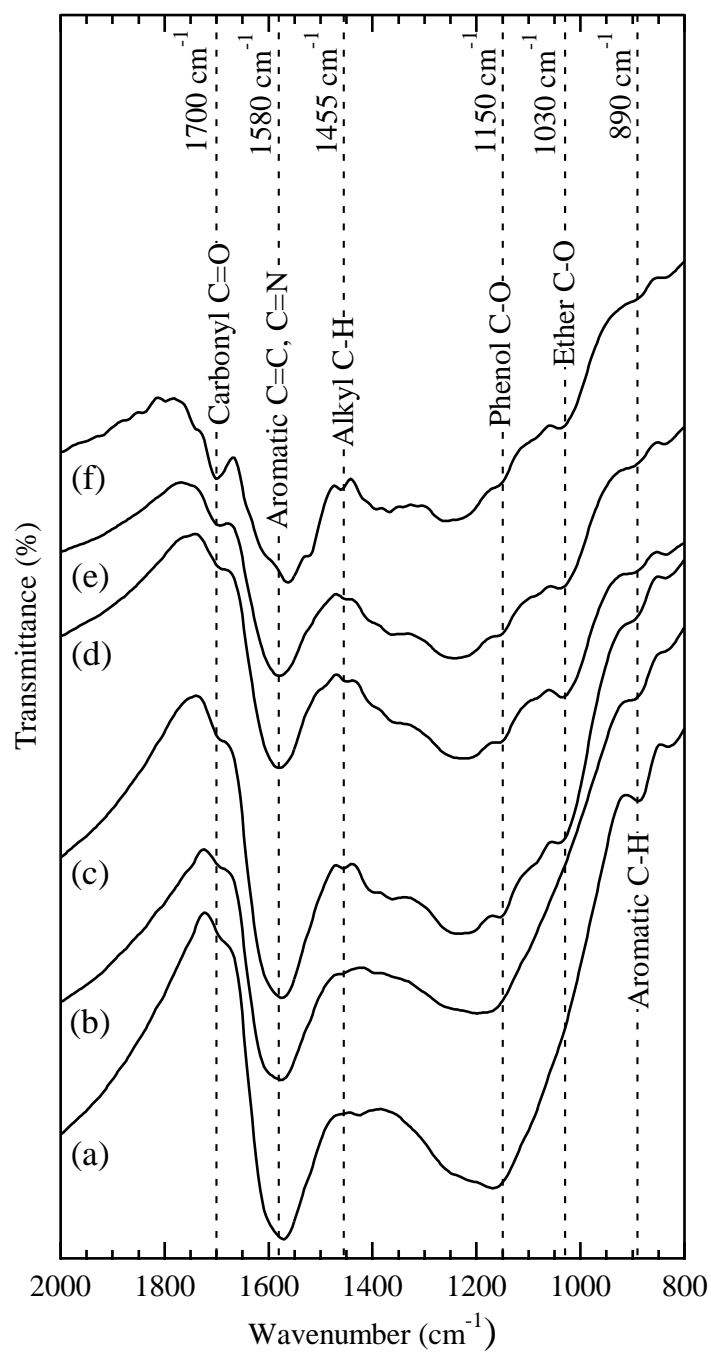


Fig. 5.5. FTIR spectra of PAC (a) untreated, (b) mediator controlled in the absence of laccase after 2 days, and (c) LMS treated after 1 day, (d) 2 days, (e) 5 days and (f) 7 days.

The carbonyl group formation could be attributed to the formation of C $\alpha$ -carbonyl product caused by the direct oxidation of phenolic substrates by Lcc (Rivera-Hoyos et al., 2013) and the indirect oxidation of non-phenolic substrates by HBT<sup>+</sup> (Galli and Gentili, 2004; Shiraishi et al., 2013). Additionally, the originally existing signal of C=C vibration mode apparently reduced in intensity over time for 5 days of LMS (Fig. 5.5(c-e)), with a slight shift to 1565 cm<sup>-1</sup> from the original position after 7 days (Fig. 5.5(f)). In the same way, a small shoulder peak attributed to the C-H vibration mode in the alkyl group was formed at 1455 cm<sup>-1</sup> (Biniak et al., 1997; Ong et al., 2020), and the peak 890 cm<sup>-1</sup> can be assigned to the aromatic C-H out-of-plane bending vibration mode (Bouchelta et al., 2008; Mistar et al., 2020) disappeared. It is visible that LMS oxidation decomposed aromatic moiety resulting in the formation of ether bonds, alkyl C-H bonds, and carboxyl C=O bonds on the surface of PAC.

#### 5.3.3.2. GC-MS

GC-MS performed the characterization of products generated through the LMS oxidation of PAC. However, the chemical compositions of activated carbon mainly depend on the characteristics of the precursor material and the activation process (Bouchelta et al., 2008; Shafeeyan et al., 2010), which are unknown in the case of commercial products. Thus, deep characterization of intermediate molecules was challenging compared to other substrates like lignin and lignin-model compounds, where the structure and by-products molecules by LMS are well-studied (Longe et al., 2018). Therefore, qualitative information rather than quantitative analysis was aimed to reveal by GC-MS analysis. The products extracted in the organic phases from the organic sequential washing were putatively identified by mass spectra using the MS

NIST library. A minimum similarity of 80% was applied to accept the characterization (Nahan et al., 2020). Since the ethylene glycol liquid phase was not applicable for GC-MS analysis, extracts in methanol, ethyl acetate, and hexane fractions were intensively analyzed. In the methanol phase, a unique peak at 7.46 min of the retention time (RT) was assigned to HBT (data not shown). As for the ethyl acetate fraction (Fig. 5.6(a)), the HBT peak was also observed simultaneously.

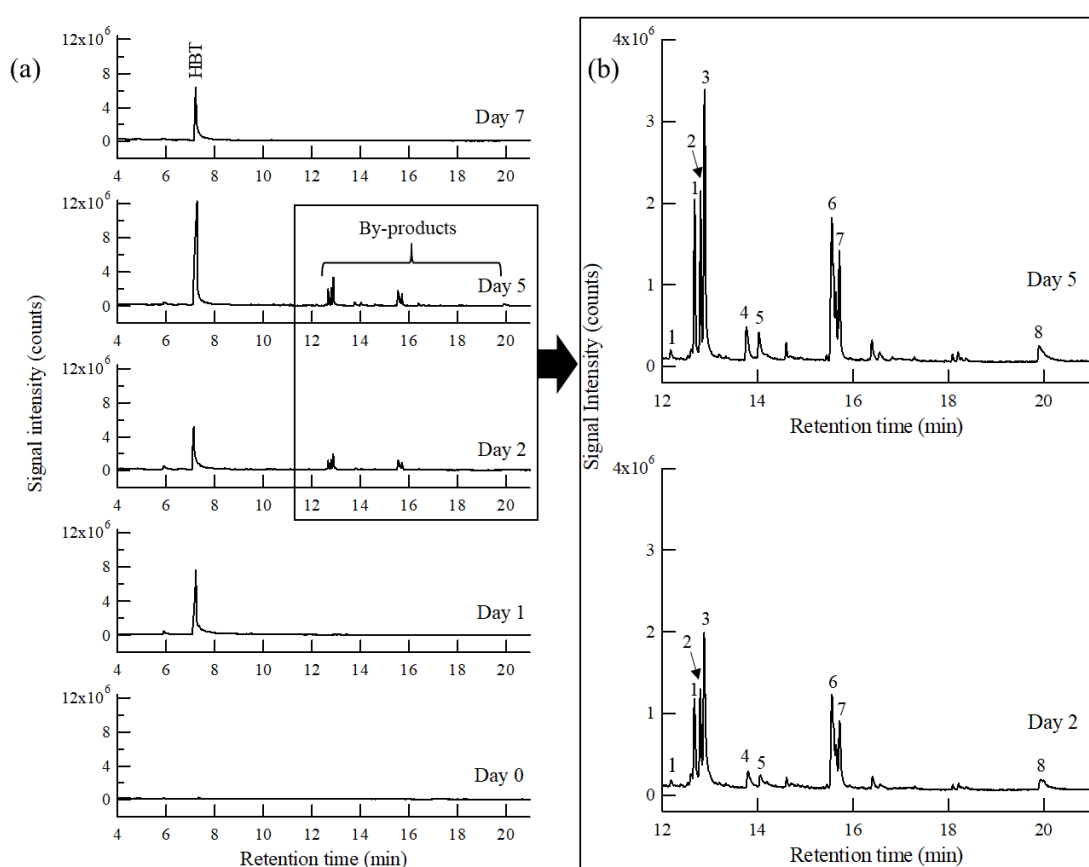


Fig. 5.6. GC-MS total ion chromatograms of extractants in ethyl acetate from the untreated and LMS-treated PAC using HBT for 1~7 days in (a). GC-MS spectra for 2 and 5 days in 12-20 min of retention time we expanded in (b). Peak assignments should be referred in Table 5.2.

After 2 and 5 days of incubation, peaks with aromatic moieties, mainly non-phenolic compounds (Table 5.2), appeared at RT 12.68 (peak 1), 12.79 (peak 2), 12.88 (peak 3), 13.80 (peak 4), 14.05 (peak 5), 15.56 (peak 6) and 15.70 min (peak 7) in Fig 5.6(b). The mass fragments of peaks 1, 2, 3, 4, and 5 were quite similar, suggesting their structural relationship, such as structural/stereoisomers. Lastly, a small peak at RT 19.94 min (peak 8) of aliphatic moiety was detected. The compounds mentioned above were not detected in the untreated and treated PAC after 1 and 7 days of LMS (Fig. 5.6(a)). Meanwhile, for the hexane extraction (Fig. 5.7), aromatic moieties from phenolic and non-phenolic compounds were predominant in the untreated PAC (Table 5.3). The chromatographic profile for 1 day of LMS was almost like that of untreated PAC. The most noticeable changes were perceived after 2 days of LMS treatment, where the formation of aliphatic moieties (Table 5.3) was distinguished. In addition, the aromatic moieties detected at RT 24.11 (peak 11) and 25.90 (peak 12) disappeared after 2 days. Although it remains challenging tasks to identify the chemical structure of the products, it was demonstrated that aromatic and aliphatic low-molecular weight compounds, at least in part, were released from PAC by LMS, being supporting data for SEM and FTIR analysis that provide clear evidence for morphological and chemical change of PAC.

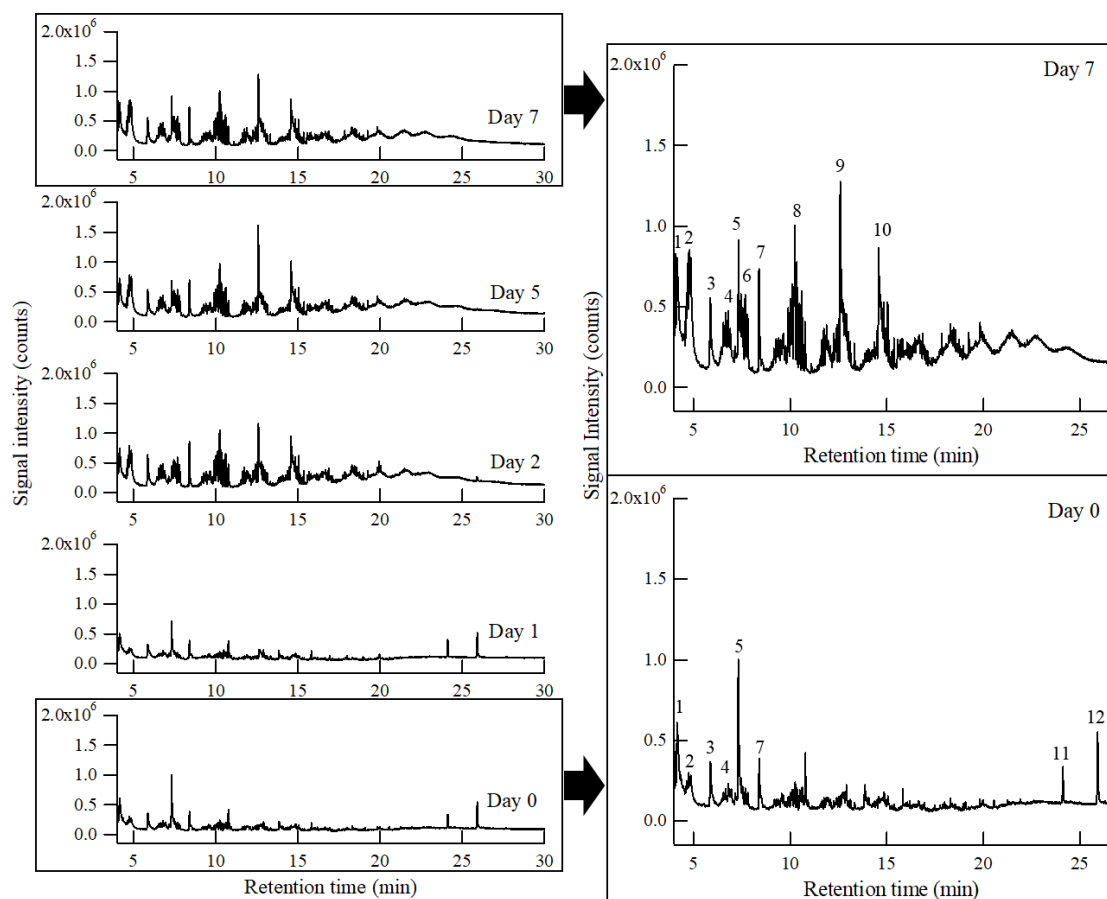
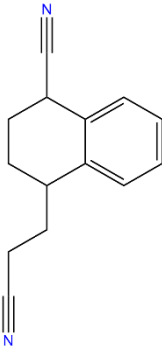


Fig. 5.7. GC-MS total ion chromatograms of extractants in hexane from the untreated and LMS-treated PAC using HBT for 1~7 days. Peak assignments should be referred in Table 5.3.



Table 5.2. Intermediates detected by GC-MS, peak No. 1~8 in Fig. 5.6 for extracted compounds in ethyl acetate on the LMS-treated PAC using HBT after 2 and 5 days

No.	Similarity (%)	Retention time (min)	<i>m/z</i> of major peaks (abundance)	Most similar compound suggest by NIST library	Chemical structure
1	82	12.68	43 (7), 77 (3), 102 (2), 129 (100), 156 (18), 210 (11)		
2	82	12.79	43 (6), 77 (3), 102 (2), 129 (100), 156 (30), 210 (2)		
3	82	12.88	43 (4), 77 (3), 102 (2), 129 (100), 156 (28), 210 (5)	3-[1-(4-Cyano-1,2,3,4-tetrahydronaphthyl)]propanenitrile	
4	86	13.80	43 (28), 77 (4), 102 (2), 115 (11), 129 (100), 156 (28), 210 (10)		
5	84	14.05	43 (49), 77 (4), 102 (2), 115 (13), 129 (100), 156 (15), 210 (19)		

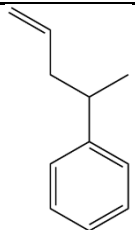
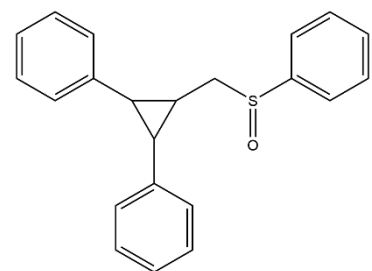
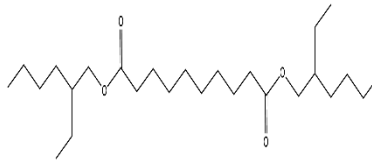
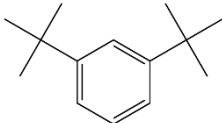
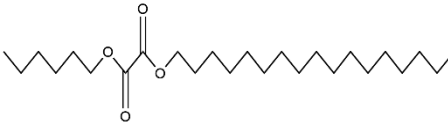


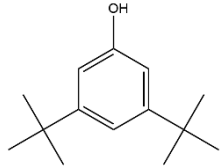
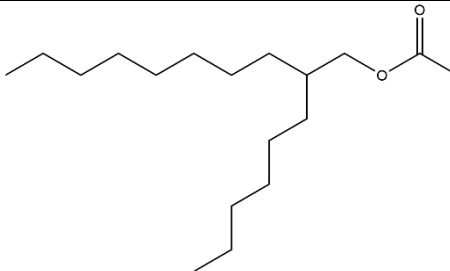

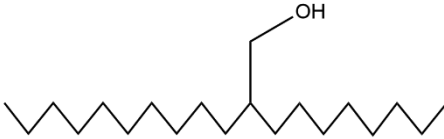

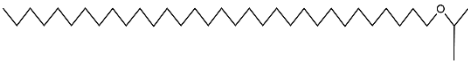
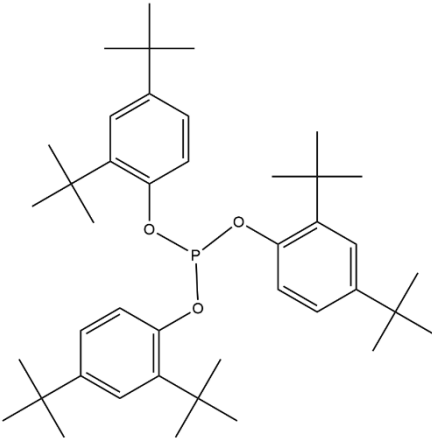
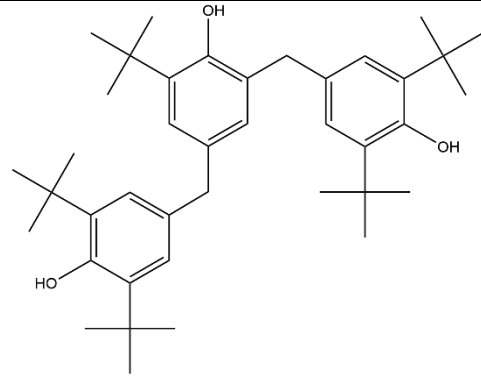
No.	Similarity (%)	Retention time (min)	<i>m/z</i> of major peaks (abundance)	Most similar compound suggest by NIST library	Chemical structure
6	85	15.56	43 (3), 79 (7), 105 (100), 129 (14), 155 (13), 156 (15), 210 (19)	2-methylbut-3-enylbenzene	
7	80	15.72	43 (9), 77 (8), 91 (100), 105 (49), 129 (78), 155 (7), 207 (35), 261 (20)	[2-(benzenesulfinylmethyl)-3-phenylcyclopropyl]benzene	
8	89	19.95	43 (66), 57 (82), 71 (53), 83 (30), 98 (18), 112 (42), 139 (10), 143 (12), 166 (7), 185 (100), 107 (23), 281 (11)	bis(2-ethylhexyl) dodecanedioate	

Table 5.3. Intermediates detected by GC-MS, peak No. 1~12 in Fig. 5.7 for extracted compounds in hexane on the untreated and LMS-treated PAC using HBT after 7 days

No.	Similarity (%)	Retention time (min)	<i>m/z</i> of major peaks (abundance)	Most similar compound suggest by NIST library	Chemical structure
1	88	4.16	41 (21), 43 (37), 57 (71), 71 (12), 91 (9), 117 (4), 147 (7), 175 (100), 190 (20),	1,3-bis(2-methyl-2-propanyl)benzene*	
2	88	4.79	43 (100), 57 (62), 69 (70), 85 (45), 97 (11), 111 (31), 154 (6)	2-O-hexadecyl 1-O-hexyl oxalate*	
3	95	5.86	43 (90), 57 (100), 71 (57), 85 (37), 99 (10), 113 (5), 141 (3)	Tetradecane*	
4	91	6.78	43 (100), 57 (91), 71 (83), 85 (48), 99 (17), 113 (15), 127 (5), 155 (9),	4-methyltridecane*	
5	91	7.32	43 (29), 57 (61), 69 (17), 69 (17), 83 (9), 111 (8), 191 (100), 206 (23)	3,5-ditert-butylphenol*	

No.	Similarity (%)	Retention time (min)	<i>m/z</i> of major peaks (abundance)	Most similar compound suggest by NIST library	Chemical structure
6	89	7.67	43 (100), 57 (86), 69 (88), 83 (48), 97 (19), 111 (42), 125 (16), 153 (9)	2-hexyldecyl acetate	
7	97	8.39	43 (76), 57 (100), 71 (65), 85 (40), 99 (13), 113 (7), 141 (3),	hexadecane*	
8	89	10.24	43 (8), 69 (100), 71 (63), 83 (53), 97 (27), 111 (51), 125 (25), 153 (14)	2-octyldodecan-1-ol	
9	95	12.59	43 (100), 57 (84), 73 (90), 85 (31), 97 (22), 115 (14), 129 (39), 143 (10), 157 (15), 171 (11), 185 (12), 213 (15), 256 (21)	hexadecanoic acid	

No.	Similarity (%)	Retention time (min)	<i>m/z</i> of major peaks (abundance)	Most similar compound suggest by NIST library	Chemical structure
10	86	14.61	43 (100), 57 (84), 69 (53), 85 (39), 97 (25), 111 (23), 129 (27), 147 (17), 153 (6), 185 (11), 241 (9), 284 (16)	1-propan-2-yloxydotriacontane	
11	83	24.11	41 (15), 57 (100), 91 (6), 119 (4), 147 (24), 159 (2), 191 (6), 308 (4), 441 (84), 442 (26)	tris(2,4- <i>di</i> <i>tert</i> -butylphenyl) phosphite*	

No.	Similarity (%)	Retention time (min)	<i>m/z</i> of major peaks (abundance)	Most similar compound suggest by NIST library	Chemical structure
12	67	25.90	41 (20), 57 (100), 73 (4), 91 (8), 119 (4), 147 (10), 175 (3), 191 (13), 207 (2), 316 (34)	2- <i>tert</i> -butyl-4,6-bis[(3,5-ditert-butyl-4-hydroxyphenyl)methyl]phenol*	

\* Indicates identification of the compound in the untreated PAC.

#### 5.3.3.3.TG-DTA

The thermal analysis supports the chemical alteration on the remaining surface of PAC over the 7 days of reaction time by LMS. TG-DTA results (Fig. 5.8) show two combustion stages for the untreated PAC, the first corresponding to moisture removal at a temperature below 50°C (Doğan et al., 2020) with 8.2% of weight loss (Fig. 5.8(a)). The second combustion range corresponds to the combustion of carbon, mainly aromatic compounds (Chen et al., 1995; Guo et al., 2021), between 250°C and 600°C, with an exothermic peak at 500°C with a complete mass loss (Fig. 5.8(a-b)). Conversely, for the solid residue after 2 days of reaction by LMS, an additional combustion stage was observed between 180°C and 330°C (Fig. 5.8(c)), with an exothermic peak at 280°C and 7.9% mass loss (Fig. 5.8(a-b)). This new stage could be attributed to the appearance of volatile organic matter (Chen et al., 1996) formed and adsorbed onto the surface of PAC caused by the LMS oxidative degradation. These compounds are likely to be from the dehydration of hydroxylated aliphatic compounds (Peuravuori et al., 1999; Francioso et al., 2005; Guo et al., 2021). It can be noticed that the combustion rate of aromatic carbon after 2 days of reaction by LMS was slightly higher than the untreated PAC. After 7 days of reaction by LMS, the reaction rate was even faster (Fig. 5.8(a)), showing a shift in the ignition temperature and the exothermic mass loss (Fig. 5.8(b-c)) for aromatic combustion (410°C), in comparison with the other samples (500°C). The decrease in the ignition temperature could indicate a decreasing aromatic compound content in PAC caused by the LMS oxidative degradation, like in the case of coal ranks (Chen et al., 1995; Umar et al., 2006). TG-DTA results are in accordance with the FTIR (Fig. 5.5) and GC-MS (Figs. 5.6 and 5.7) observations in the premise that after 7 days of reaction, the physicochemical characteristics of PAC are completely different compared with the pristine. TG-DTA supports the findings of

aliphatic carbon intermediates on the surface of PAC after 2 days of LMS treatment. However, until this point, it seems that the aromatic components were still prime and that a broad alteration of the surface of PAC was still ongoing. This was not the case after 7 days when the aromatic carbon intermediates were no less detected on GC-MS, which does not mean they were degraded entirely. Still, the aromaticity of PAC was clearly reduced.

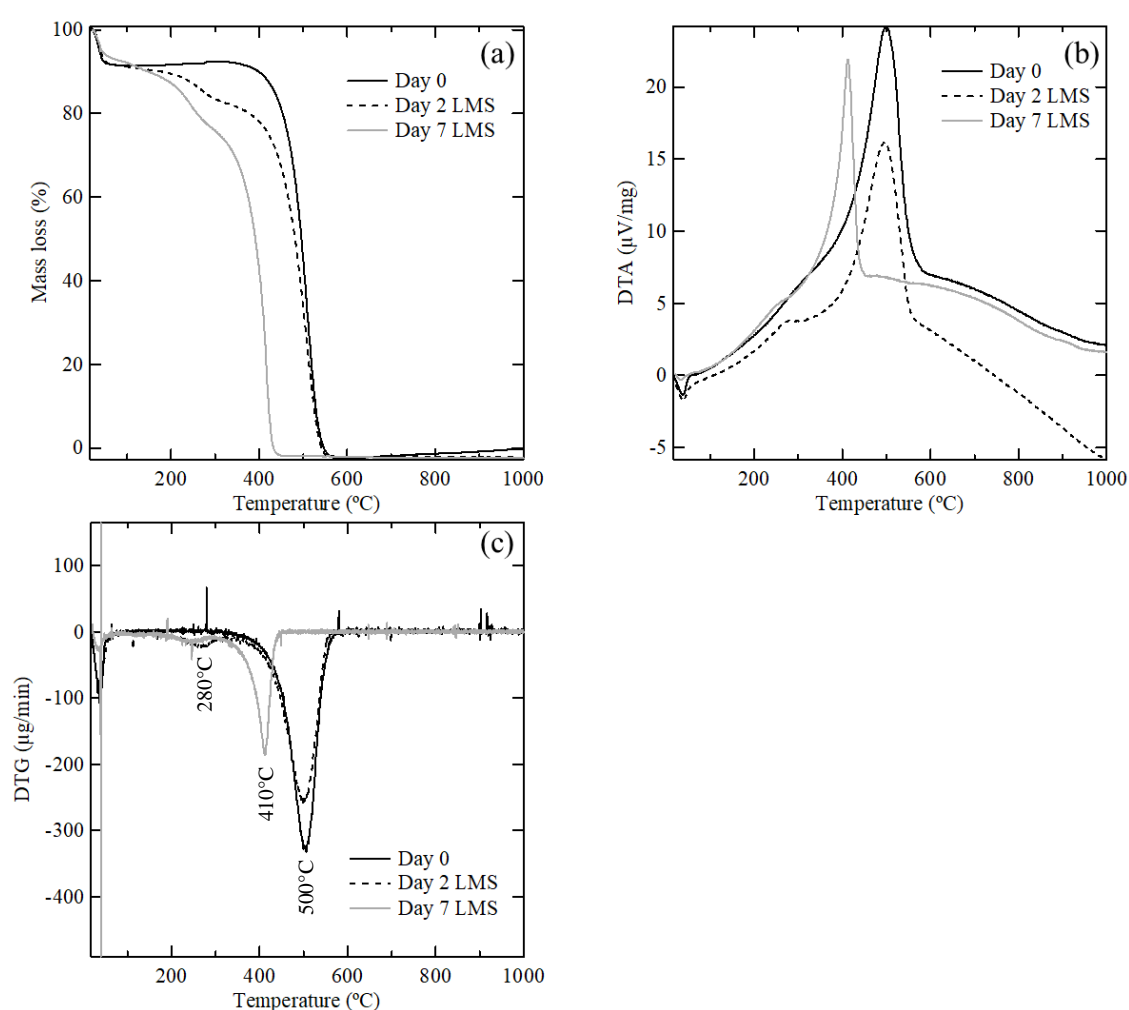


Fig. 5.8. Thermal decomposition characteristics of the untreated PAC and LMS treated PAC after 2 and 7 days, showing (a) mass loss, (b) differential thermal analysis (DTA), and (c) differential thermogravimetry (DTG).



#### 5.3.3.4. Raman spectra

The Raman spectra were obtained to observe the chemical alterations on the  $sp^2$  orbital of aromatic carbon in high graphitic compounds (Fig. 5.9). To evaluate the graphitic degree in CM, the relative intensity ( $I_D/I_G$ ) of the defect band around  $1360\text{ cm}^{-1}$  to graphitic band around  $1580\text{ cm}^{-1}$  can be often useful (Shimodaira & Masui, 2002). The untreated PAC showed 1.67 of  $I_D/I_G$ , and this value slightly increased in HBT control (data not shown). When Lcc was added to the system in the presence of HBT, the  $I_D/I_G$  decreased to 1.27 after 24 h, inferring that existing defected carbon was oxidatively dissolved by LMS treatment. This is understandable since the graphitic band is very stable for enzymatic degradation. Thus easily degraded substrates might be the first target for oxidation, which are probably located at the edges of PAC (Daud & Houshamnd, 2010). Then, the  $I_D/I_G$  increased to 1.74 after 2 days when the LMS converted graphitic carbon into defective carbon. After 5 days, the newly defected carbon was gradually dissolved, the premise reflected in the decrease of  $I_D/I_G$  to 1.24. The last asseveration was confirmed after detecting aliphatic compounds after two days of LMS oxidation by GC-MS (Figs. 5.6 and 5.7).

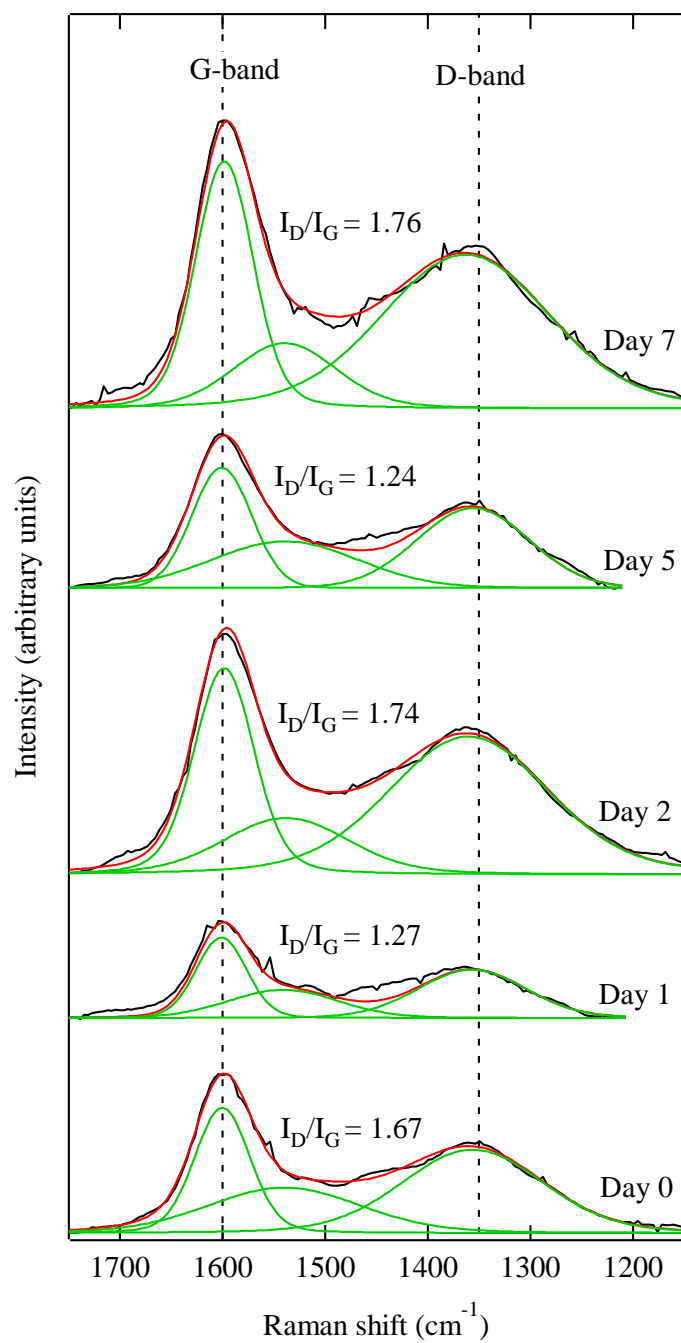


Fig. 5.9. Raman spectra for untreated and LMS treated PAC after 1-7 days. Relative intensity of D-band to G-band are included.

#### 5.3.3.5. Effect of LMS treatment on adsorption of $\text{Au}(\text{CN})_2^-$ onto PAC

$\text{Au}(\text{CN})_2^-$  adsorption was applied on the untreated and LMS-treated PAC after 1-7 days, before and after washing with ultra-pure water and organic solvents to extract by-products. Pristine PAC adsorbed 0.046 mmol- $\text{Au}(\text{CN})_2^-/\text{g}$  representing 100% of adsorption. The Au uptake was significantly reduced to 26% after 1 day of LMS, and this could be attributed to the physical changes in the specific surface area and pore characteristics of PAC (Fig. 5.4). Additionally, the immobilization of Lcc (Fig. 5.2), partial adsorption of  $\text{HBT}^+$  (Fig. 5.10) on the surface of PAC, and a preliminary oxidation state contributed to reducing the available sorption sites for  $\text{Au}(\text{CN})_2^-$  as illustrated in Fig. 5.10.

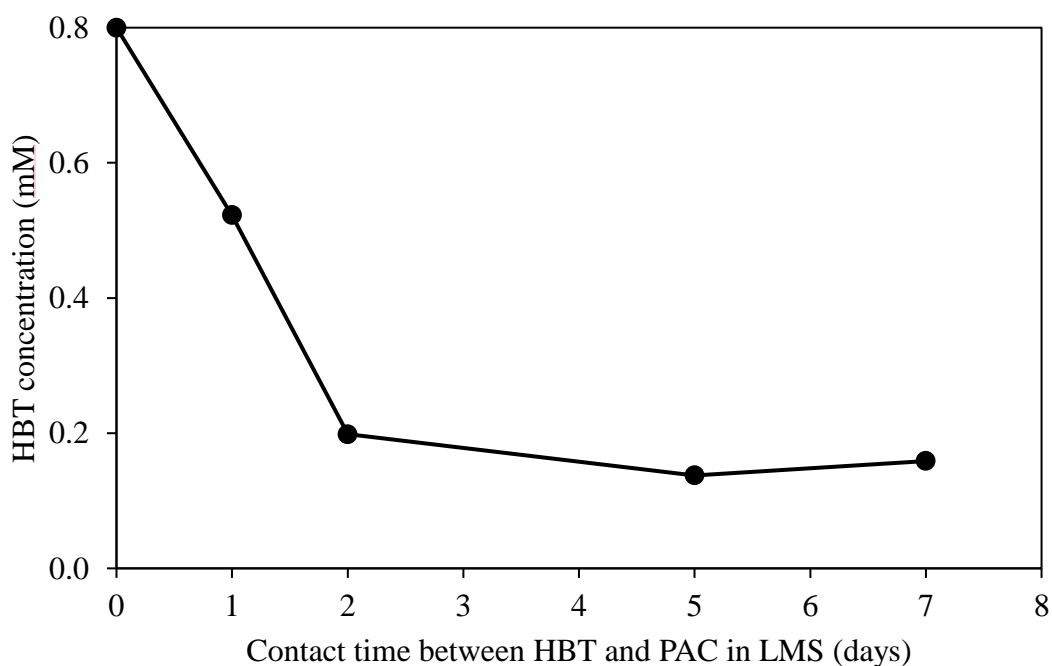


Fig. 5.10. Changes in HBT concentrations in the LMS over time.

A number of non-specific reactions causing the transformation of PAC will be possible in progress since Lcc was still active on the PAC surface for bio-oxidation (Fig. 5.2). Despite that, the adsorption  $\text{Au}(\text{CN})_2^-$  in 2-5 days decreased slightly due to oxidation but did not reflect a significant change comparing the values before and after water washing. This could mean that during this interval, a negligible number of water-soluble by-products was formed on the surface of PAC; therefore, water washing did not show any benefit. As previously shown on GC-MS spectra (Figs. 5.5 and 5.6), there is a transition in the surface bio-modification of PAC from 2 to 7 days of LMS treatment. Although Lcc was not active after 2 days (Fig. 5.2), the following reactions to cause PAC alteration could be attributed to  $\text{HBT}^+$  and by-products intermediates that continuously attached to the reactive surface of PAC by radical coupling, a phenomenon similar to the grafting of lignin (Kwiatos et al., 2018). The presence of aromatic and aliphatic moieties by-products was observed after 2 days, but it is clear there was rather an accumulation of aromatic intermediates on the PAC surface supported by TG-DTA (Fig. 5.8 (a-c)). After extracting the easily soluble aromatic carbons by organic sequential washing and leaving a less attracted surface to  $\text{Au}(\text{CN})_2^-$ , the uptake was reduced to 19% and 13% after 2 and 5 days of LMS.

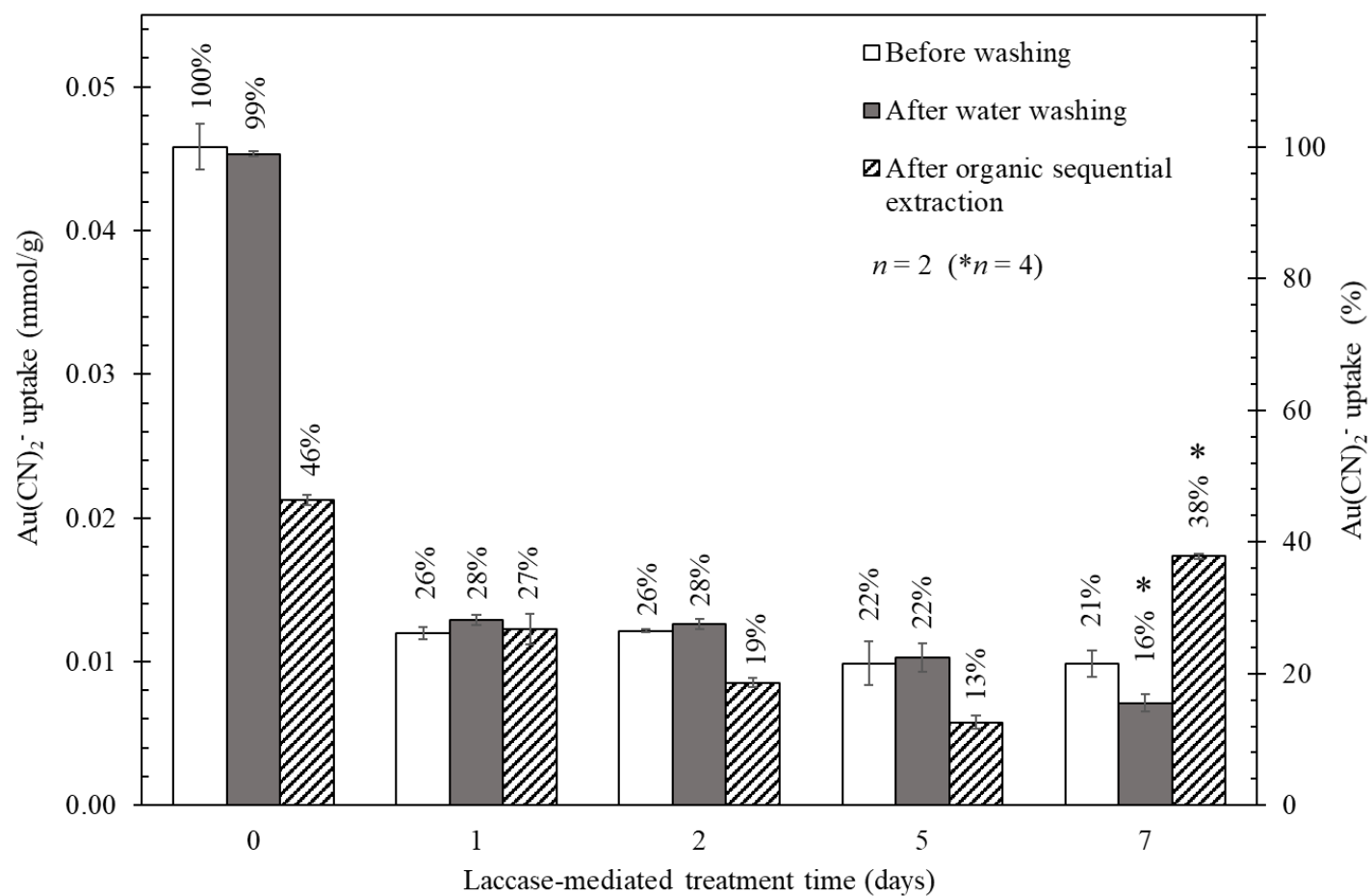


Fig. 5.11.  $\text{Au}(\text{CN})_2^-$  uptake on untreated and LMS-treated PAC using HBT for 0~7 days, before and after washing. LMS treatment was performed at 37°C and pH 4.5.

However, this trend was not observed after 7 days, where removal of the by-products negatively affected the  $\text{Au(CN)}_2^-$  adsorption. This change could result from a significant removal of the aliphatic by-products accumulated on the surface of PAC since aromatic moieties were not detected after 7 days (Figs. 5.6-5.7), leading the surface of PAC like the pristine one and thus increasing the  $\text{Au(CN)}_2^-$  uptake by 38% ( $n = 4$ ). The highest reduction of  $\text{Au(CN)}_2^-$  adsorption was observed after removing water-soluble compounds, reaching 16% of uptake after 7 days of LMS. This could also be associated with removing hydrophilic small carbonyl-containing-group compounds accumulated in the PAC surface (Fig. 5.4(f)) and the prevalence of aliphatic carbons (Fig. 5.6), which has lower affinity against  $\text{Au(CN)}_2^-$  adsorption. The above interpretations are schematically visualized in Fig. 5.12. In fact, LMS using Lcc Y-120 with HBT as a mediator reduced  $\text{Au(CN)}_2^-$  uptake (Fig. 5.11) by adding oxidized functional groups, surface passivation, and aromatic carbon disturbance on PAC. Similar findings were described by Ofori-Sarpong et al. (2013), Liu et al. (2014), Liu et al. (2016), and Konadu et al. (2017) with comparable carbon surrogates and CFMS of *Phanerochaete chrysosporium*, in which Lcc is not included.

#### **5.4. Conclusions**

Laccase-mediator system (LMS) using laccase Y-120 from *Trametes sp.* and HBT was examined for the first time to degrade powder-activated carbon (PAC) as a CM surrogate in carbonaceous gold ores. The LMS treatment significantly altered the surface morphologies of PAC to decrease the specific surface area and pore volumes.

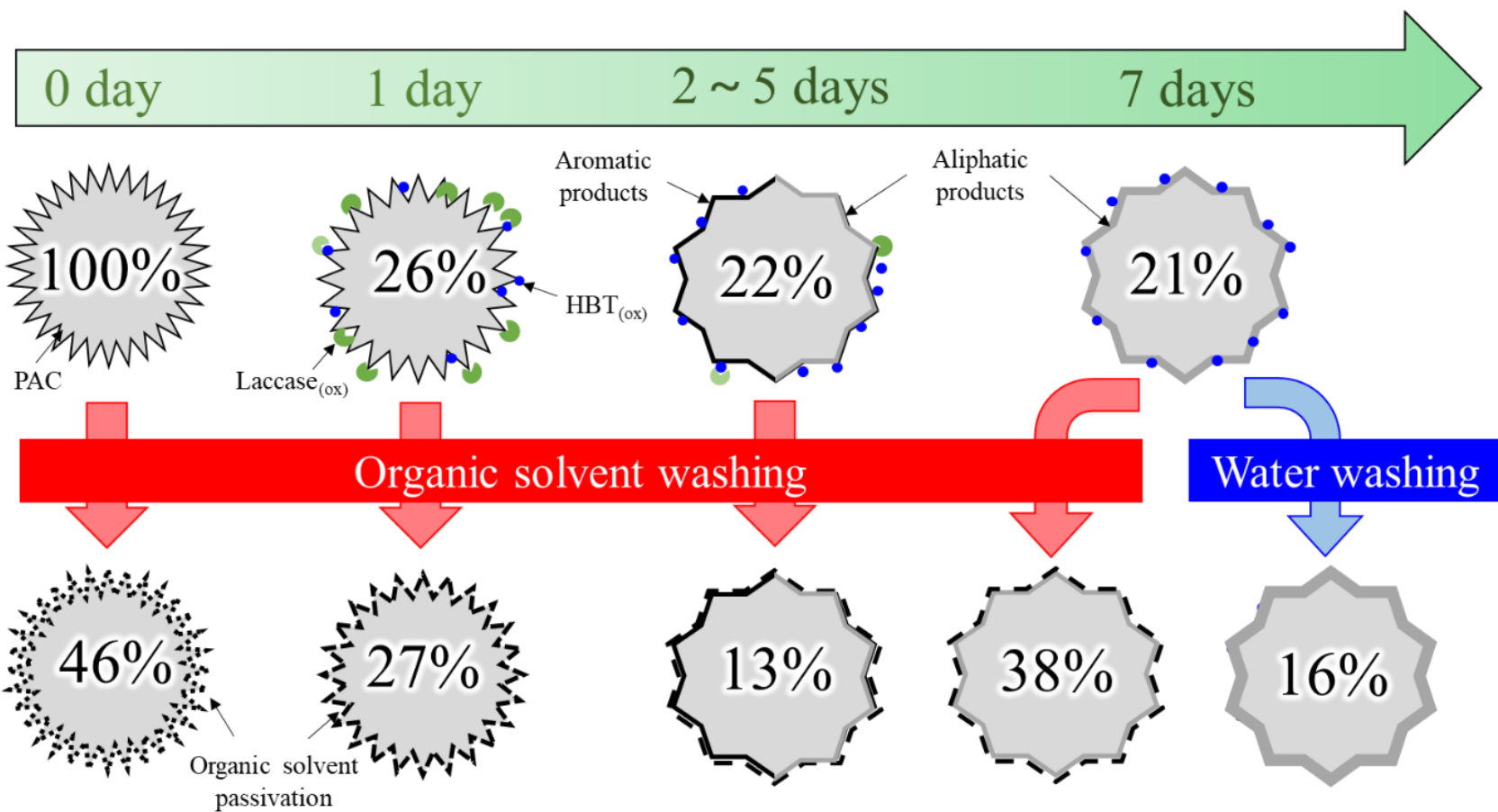


Fig. 5.12. Schematic illustration of changes in  $\text{Au(CN)}_2^-$  uptake (%) on PAC after LMS treatment, showing biodegradation and washing effects.

FTIR, TG-DTA, and Raman spectroscopy also confirmed chemical alteration by forming several oxidized functional groups, mostly C=O type, and graphiticity reduction, leading to the passivation of the active adsorption sites. Additionally, the GC-MS study for extracted intermediates of degradation products provided direct evidence of the chemical alteration of the surface by LMS treatment for 2~7 days, where monocyclic/polycyclic hydrocarbons were transformed to aliphatic hydrocarbons. The studied condition of LMS treatment of PAC followed by water washing revealed the decrease of  $\text{Au}(\text{CN})_2^-$  adsorption density from 46  $\mu\text{mol/g}$  to 7.36  $\mu\text{mol/g}$ . However, the application of the present LMS condition should be optimized depending on the specific characteristics of the carbonaceous gold ore. Future work will evaluate the quantitative decomposition rate since it is meant to scale up for industrial applications. Furthermore, to improve the ecological approach of LMS treatment, natural mediators (i.e., violuric acid and syringaldehyde) instead of synthetic ones (i.e., 1-hydroxybenzotriazole) could also be considered to reduce the environmental concerns of wastewater discharge. The above findings and considerations can contribute to the potential application of LMS in the mineral processing of carbonaceous gold ores and its future implementation.



## References

- Adams, M. D. (2016) Gold Ore Processing. In M. D. Adams, *Developments in Mineral Processing* (2nd ed.). Chapter 50, 909-918.
- Afenya, P. M. (1991) Treatment of carbonaceous refractory gold ores. *Minerals Engineering*, 4(7–11), 1043–1055.
- Alvarado-Ramírez, L., Rostro-Alanis, M., Rodríguez-Rodríguez, J., Castillo-Zacarías, C., Sosa-Hernández, J. E., Barceló, D., Iqbal, H. M. N., & Parra-Saldívar, R. (2021) Exploring current tendencies in techniques and materials for immobilization of laccases – A review. *International Journal of Biological Macromolecules*, 181, 683–696.
- Amankwah, R. K., & Pickles, C. A. (2009) Microwave roasting of a carbonaceous sulphidic gold concentrate. *Minerals Engineering*, 22(13), 1095–1101.
- Andreu, G., & Vidal, T. (2011) Effects of laccase-natural mediator systems on kenaf pulp. *Bioresource Technology*, 102(10), 5932–5937.
- Aracri, E., Colom, J. F., & Vidal, T. (2009) Application of laccase-natural mediator systems to sisal pulp: An effective approach to biobleaching or functionalizing pulp fibres? *Bioresource Technology*, 100(23), 5911–5916.
- Biniak, S., Szymański, G., Siedlewski, J., & Świątkoski, A. (1997) The characterization of activated carbons with oxygen and nitrogen surface groups. *Carbon*, 35(12), 1799–1810.
- Bouchelta, C., Medjram, M. S., Bertrand, O., & Bellat, J. P. (2008) Preparation and characterization of activated carbon from date stones by physical activation with steam. *Journal of Analytical and Applied Pyrolysis*, 82(1), 70–77.

- Chen, Y., Mori, S., & Pan, W. P. (1995) Estimating the Combustibility of Various Coals by TG-DTA. *Energy and Fuels*, 9(1), 71–74.
- Chen, Y., Mori, S., & Pan, W. P. (1996) Studying the mechanisms of ignition of coal particles by TG-DTA. *Thermochimica Acta*, 275(1), 149–158.
- Christopher, L. P., Yao, B., & Ji, Y. (2014) Lignin biodegradation with laccase-mediator systems. *Frontiers in Energy Research*, 2, 1-13.
- Daud, W. M. A. W., & Houshamnd, A. H. (2010) Textural characteristics, surface chemistry and oxidation of activated carbon. *Journal of Natural Gas Chemistry*, 19(3), 267–279.
- Davis, S., & Burns, R. G. (1992) Covalent immobilization of laccase on activated carbon for phenolic effluent treatment. *Applied Microbiology and Biotechnology*, 37(4), 474–479.
- Doğan, M., Sabaz, P., Bicil, Z., Koçer Kizilduman, B., & Turhan, Y. (2020) Activated carbon synthesis from tangerine peel and its use in hydrogen storage. *Journal of the Energy Institute*, 93(6), 2176–2185.
- Du, Y., Ma, H., Huang, L., Pan, Y., Huang, J., & Liu, Y. (2020) Electrochemical characteristics of the decolorization of three dyes by laccase mediator system (LMS) with synthetic and natural mediators. *Chemosphere*, 239, 124779.
- Dunne, R., Buda, K., Hill, M., Staunton, W., Wardell-Johnson, G., & Tjandrawan, V. (2012) Assessment of options for economic processing of preg-robbing gold ores. *Transactions of the Institutions of Mining and Metallurgy, Section C: Mineral Processing and Extractive Metallurgy*, 121(4), 217–223.

- Elegir, G., Daina, S., Zoia, L., Bestetti, G., & Orlandi, M. (2005) Laccase mediator system: Oxidation of recalcitrant lignin model structures present in residual kraft lignin. *Enzyme and Microbial Technology*, 37(3), 340–346.
- Fakoussa, R. M., & Hofrichter, M. (1999). Biotechnology and microbiology of coal degradation. In *Applied Microbiology and Biotechnology*. 52 (1), 25–40.
- Fernández-Fernández, M., Sanromán, M. Á., & Moldes, D. (2013) Recent developments and applications of immobilized laccase. *Biotechnology Advances*, 31(8), 1808–1825.
- Francioso, O., Montecchio, D., Gioacchini, P., & Ciavatta, C. (2005) Thermal analysis (TG-DTA) and isotopic characterization ( $^{13}\text{C}$ - $^{15}\text{N}$ ) of humic acids from different origins. *Applied Geochemistry*, 20(3), 537–544.
- Galli, C., & Gentili, P. (2004) Chemical messengers: Mediated oxidations with the enzyme laccase. *Journal of Physical Organic Chemistry*, 17(11), 973–977.
- Gao, Y., Yue, Q., Gao, B., & Li, A. (2020) Insight into activated carbon from different kinds of chemical activating agents: A review. *Science of the Total Environment*, 746, 141094.
- Guo, X., Xiao, Y., Zhao, L., Shi, L., Xue, X., Li, X., & Liu, Z. (2021) Combustion behaviors of various coals and chars: From covalent bonds' and radicals' perspective. *Fuel*, 297
- Hofrichter, M. (2002) Review: Lignin conversion by manganese peroxidase (MnP). In *Enzyme and Microbial Technology*. 30 (4), 454–466.

Ibrado, A. S., & Fuerstenau, D. W. (1992) Effect of the structure of carbon adsorbents on the adsorption of gold cyanide. *Hydrometallurgy*, 30(1–3), 243–256.

Jothi Ramalingam, R., Sivachidambaram, M., Vijaya, J. J., Al-Lohedan, H. A., & Muthumareeswaran, M. R. (2020) Synthesis of porous activated carbon powder formation from fruit peel and cow dung waste for modified electrode fabrication and application. *Biomass and Bioenergy*, 142, 105800.

Konadu, K. T., Sasaki, K., Kaneta, T., Ofori-Sarpong, G., & Osseo-Asare, K. (2017) Bio-modification of carbonaceous matter in gold ores: Model experiments using powdered activated carbon and cell-free spent medium of *Phanerochaete chrysosporium*. *Hydrometallurgy*, 168, 76–83.

Konadu, K. T., Harrison, S. T. L., Osseo-Asare, K., & Sasaki, K. (2019) Transformation of the carbonaceous matter in double refractory gold ore by crude lignin peroxidase released from the white-rot fungus. *International Biodeterioration and Biodegradation*, 143, 104735.

Konadu, K. T., Mendoza, D. M., Huddy, R. J., Harrison, S. T. L., Kaneta, T., & Sasaki, K. (2020) Biological pretreatment of carbonaceous matter in double refractory gold ores: A review and some future considerations. *Hydrometallurgy*, 196, 105434.

Kudo, S., Harada, A., Kubota, H., Sasaki, K., & Kaneta, T. (2017) Simultaneous determination of manganese peroxidase and lignin peroxidase by capillary electrophoresis enzyme assays. *ACS Omega*, 2(10), 7329–7333.

Kwiatos, N., Jędrzejczak-Krzepkowska, M., Strzelecki, B., & Bielecki, S. (2018) Improvement of efficiency of brown coal biosolubilization by novel recombinant *Fusarium oxysporum* laccase. *AMB Express*, 8(1), 1–9.

- Liu, Q., Yang, H., Tong, L., Jin, Z., & Sand, W. (2016) Fungal degradation of elemental carbon in Carbonaceous gold ore. *Hydrometallurgy*, 160, 90–97.
- Liu, Q., Yang, H. Y., & Tong, L. L. (2014) Influence of *Phanerochaete chrysosporium* on degradation and preg-robbing capacity of activated carbon. *Transactions of Nonferrous Metals Society of China*, 24(6), 1905–1911.
- Longe, L. F., Couvreur, J., Leriche Grandchamp, M., Garnier, G., Allais, F., & Saito, K. (2018) Importance of mediators for lignin degradation by fungal laccase. *ACS Sustainable Chemistry and Engineering*, 6(8), 10097–10107.
- Mangun, C. L., Benak, K. R., Daley, M. A., & Economy, J. (1999) Oxidation of activated carbon fibers: Effect on pore size, surface chemistry, and adsorption properties. *Chemistry of Materials*, 11(12), 3476–3483.
- Margot, J., Copin, P. J., von Gunten, U., Barry, D. A., & Holliger, C. (2015) Sulfamethoxazole and isoproturon degradation and detoxification by a laccase-mediator system: Influence of treatment conditions and mechanistic aspects. *Biochemical Engineering Journal*, 103, 47–59.
- Mendoza, D. M., Konadu, K. T., Aoki, Y., Kameya, M., & Sasaki, K. (2021). Carbonaceous matter degradation by fungal enzyme treatment to improve Ag recovery from an Au-Ag-bearing concentrate. *Minerals Engineering*, 163(January), 106768.
- Miller, J. D., Wan, R.-Y., & Díaz, X. (2016) Preg-Robbing Gold Ores. *Gold Ore Processing*, 885–907.

- Mistar, E. M., Alfatah, T., & Supardan, M. D. (2020) Synthesis and characterization of activated carbon from *Bambusa vulgaris* striata using two-step KOH activation. *Journal of Materials Research and Technology*, 9(3), 6278–6286.
- Naghdi, M., Taheran, M., Brar, S. K., Kermanshahi-pour, A., Verma, M., & Surampalli, R. Y. (2018) Biotransformation of carbamazepine by laccase-mediator system: Kinetics, by-products and toxicity assessment. *Process Biochemistry*, 67, 147–154.
- Nahan, K., Sussman, E. M., Oktem, B., Schultheis, L., & Wickramasekara, S. (2020) Screening for extractables in additive-manufactured acrylonitrile butadiene styrene orthopedic cast. *Talanta*, 212(June 2019), 120464.
- Nanthakumar, B., Pickles, C. A., & Kelebek, S. (2007) Microwave pretreatment of a double refractory gold ore. *Minerals Engineering*, 20(11), 1109–1119.
- Natarajan, K. A. (2018) Biotechnology for Gold Mining, Extraction, and Waste Control. In *Biotechnology of Metals*, 179–210.
- Nguyen, L. N., Hai, F. I., Dosseto, A., Richardson, C., Price, W. E., & Nghiem, L. D. (2016) Continuous adsorption and biotransformation of micropollutants by granular activated carbon-bound laccase in a packed-bed enzyme reactor. *Bioresource Technology*, 210, 108–116.
- Ofori-Sarpong, G., Amankwah, R. K., & Osseo-Asare, K. (2013) Reduction of preg-robbing by biomodified carbonaceous matter-A proposed mechanism. *Minerals Engineering*, 42, 29–35.

- Ofori-Sarpong, G., & Osseo-Asare, K. (2013) Preg-robbing of gold from cyanide and non-cyanide complexes: Effect of fungi pretreatment of carbonaceous matter. *International Journal of Mineral Processing*, 119, 27–33.
- Ong, H. C., Chen, W. H., Singh, Y., Gan, Y. Y., Chen, C. Y., & Show, P. L. (2020) A state-of-the-art review on thermochemical conversion of biomass for biofuel production: A TG-FTIR approach. *Energy Conversion and Management*, 209, 112634.
- Owusu, C., Mensah, S., Ackah, K., & Amankwah, R. K. (2021) Reducing preg-robbing in carbonaceous gold ores using passivative or blanking agents. *Minerals Engineering*, 170, 106990.
- Peng, X., Ma, X., Lin, Y., Guo, Z., Hu, S., Ning, X., Cao, Y., & Zhang, Y. (2015) Co-pyrolysis between microalgae and textile dyeing sludge by TG-FTIR: Kinetics and products. *Energy Conversion and Management*, 100, 391–402.
- Peuravuori, J., Paaso, N., & Pihlaja, K. (1999) Kinetic study of the thermal degradation of lake aquatic humic matter by thermogravimetric analysis. *Thermochimica Acta*, 325(2), 181–193.
- Rees, K. L., & van Deventer, J. S. J. (2000) Preg-robbing phenomena in the cyanidation of sulphide gold ores. *Hydrometallurgy*, 58(1), 61–80.
- Rivera-Hoyos, C. M., Morales-Álvarez, E. D., Poutou-Piñales, R. A., Pedroza-Rodríguez, A. M., Rodríguez-Vázquez, R., & Delgado-Boada, J. M. (2013) Fungal laccases. *Fungal Biology Reviews*, 27(3–4), 67–82.

- Shafeeyan, M. S., Daud, W. M. A. W., Houshmand, A., & Shamiri, A. (2010) A review on surface modification of activated carbon for carbon dioxide adsorption. *Journal of Analytical and Applied Pyrolysis*, 89(2), 143–151.
- Shimodaira, N., & Masui, A. (2002) Raman spectroscopic investigations of activated carbon materials. *Journal of Applied Physics*, 92(2), 902–909.
- Shin, S., Jang, J., Yoon, S. H., & Mochida, I. (1997) A study on the effect of heat treatment on functional groups of pitch based activated carbon fiber using FTIR. *Carbon*, 35(12), 1739–1743.
- Shiraishi, T., Sannami, Y., Kamitakahara, H., & Takano, T. (2013) Comparison of a series of laccase mediators in the electro-oxidation reactions of non-phenolic lignin model compounds. *Electrochimica Acta*, 106, 440–446.
- Singh, A. K., Bilal, M., Iqbal, H. M. N., & Raj, A. (2021) Lignin peroxidase in focus for catalytic elimination of contaminants — A critical review on recent progress and perspectives. In *International Journal of Biological Macromolecules*, 177, 58–82.
- Tan, H., Feng, D., Lukey, G. C., & van Deventer, J. S. J. (2005) The behaviour of carbonaceous matter in cyanide leaching of gold. *Hydrometallurgy*, 78(3–4), 226–235.
- Torres-Duarte, C., Roman, R., Tinoco, R., & Vazquez-Duhalt, R. (2009) Halogenated pesticide transformation by a laccase-mediator system. *Chemosphere*, 77(5), 687–692.
- Umar, D. F., Usui, H., & Daulay, B. (2006) Change of combustion characteristics of Indonesian low rank coal due to upgraded brown coal process. *Fuel Processing Technology*, 87(11), 1007–1011.



Valls, C., Vidal, T., & Roncero, M. B. (2010) Boosting the effect of a laccase-mediator system by using a xylanase stage in pulp bleaching. *Journal of Hazardous Materials*, 177(1–3), 586–592.

Vipotnik, Z., Michelin, M., & Tavares, T. (2021) Development of a packed bed reactor for the removal of aromatic hydrocarbons from soil using laccase/mediator feeding system. *Microbiological Research*, 245, 126687.

Wang, H. Jun, Feng, Y. li, Li, H. Ran, & Kang, J. Xing. (2020) Simultaneous extraction of gold and zinc from refractory carbonaceous gold ore by chlorination roasting process. *Transactions of Nonferrous Metals Society of China*, 30(4), 1111–1123.

Yang, H. Y., Liu, Q., Song, X. L., & Dong, J. K. (2013) Research status of carbonaceous matter in carbonaceous gold ores and bio-oxidation pretreatment. *Transactions of Nonferrous Metals Society of China*, 23(11), 3405–3411.

Zeng, S., Qin, X., & Xia, L. (2017) Degradation of the herbicide isoproturon by laccase-mediator systems. *Biochemical Engineering Journal*, 119, 92–100.

## **Chapter 6:**

### **Characterization of organic compounds in carbonaceous gold ores before and after laccase- mediator system treatment**

## 6.1.Introduction

The application of a sequential bio-treatment of double refractory gold ores (DRGO) was first reported by Ofori-Sarpong et al. (2013) in a new attempt to replace costly chemical pre-treatments in gold mineral processing. This idea was further demonstrated by Konadu et al. (2019), who showed the benefits of arranging a specific order and separating the bio-treatment into two stages. The arrangement consisted of using bio-oxidation as a first step to liberate gold from sulfide decomposition and enzymatic oxidation of carbonaceous matter (CM) by a fungal harvested cell-free spent medium (CFSM) as a second step to deactivate CM preg-robbing ability. This last step evidenced the importance of lignin-degrading enzymes like lignin peroxidase (LiP) and manganese peroxidase (MnP) in CM degradation. Sulfide bio-oxidation has been successfully applied in mines in operation over the world (Arrascue & van Niekerk, 2006); however, the use of peroxidases is still under research and optimization for further upgrade. Hence, alternative lignin-degrading enzymes were pointed out in the radar to facilitate their use at an industrial scale. In Chapters 4 and 5, the feasibility of using laccase (Lcc) over peroxidases from CFSM was demonstrated by the degradation of powder-activated carbon (PAC) as a CM surrogate. Lcc has been extensively used in pharmaceutical, food, biosensor, forest product, textile, cosmetic, pulp, and paper industries (Minussi et al., 2002; Widsten & Kandelbauer, 2008; Alessandra et al., 2010; Imran et al., 2012; Senthivelan et al., 2016; Pandi et al., 2019; Singh & Arya, 2019; Bhardwaj et al., 2022; Hussain et al., 2022; Han et al., 2023). In some cases, a laccase-mediator system was necessary because some organic compounds have higher standard redox potential than laccase alone (0.5- 0.8 V) (Ibarra et al., 2006). Despite this, it is clear that Lcc application in gold mineral processing seems promising, especially by

the company of mediator, because CM is a complex substrate and big enough to hardly enter into the Lcc catalytic site like in lignin (Christopher et al., 2014).

On the other hand, the physicochemical and, most notably, the graphitic characteristics of CM in natural ores can differ worldwide depending on environmental factors such as pressure and temperature over long-term time (Miki, 1983). The graphitic/amorphous structure plays a fundamental role in gold adsorption, especially the defect sites where gold seems to be adsorbed (Sibrell & Miller, 1992). The functional groups from the defective site in the carbon surface are also involved to some extent, like in activated carbon. Although CM properties have been studied and characterized by numerous methods, few studies consider CM characterization by gas chromatography-mass spectrometry (GC-MS) and encounter the relationship with CM preg-robbing ability. Moreover, characterization of the changes of CM after laccase-mediator system (LMS) degradation has not been reported. Therefore, in the present chapter, a sequential organic extraction followed by GC-MS analysis was used to qualitative characterize the surface functional groups in three different preg-robbing carbonaceous gold ores (PXX, BOG, and SYM) and support these findings with conventional CM characterization techniques (preg-robbing test, Raman spectroscopy, 3D-fluorescence and TG-DTA). Additionally, sequential pre-treatments were applied in the three carbonaceous gold ores including lignin-degrading enzymes treatment and further characterization by GC-MS of the by-products.

## 6.2.Experimental

### 6.2.1. Materials and CM characterization

The carbonaceous gold ores used in this chapter were the same as in Chapter 3 (PXX, BOG, and SYM). The gold ores were flotation concentrate provided by anonymous mines from Mali, Ghana, and the USA. The samples are named as follows: SYM (Mali), BOG (Ghana), and PXX (USA). SYM is a double refractory gold ore (DRGO), PXX is a carbonaceous refractory Au-Ag ore, and BOG is a pre-treated ore that went through an unrevealed bio-oxidation process. CM was characterized by CHN, Raman spectroscopy, TG-DTA, and three-dimensional fluorescence spectroscopy using the conditions described in section 2.3. Preg-robbing test was conducted using 5 g of the ore suspended in 12.5 mL of an alkaline solution containing  $80\ \mu\text{M}\ \text{Au}(\text{CN})_2^-$ . The flasks were shaken at 125 rpm for 24 h under room temperature. The supernatant after filtration was subjected to ICP-OES analysis to determine the remaining concentration of Au.

### 6.2.2. Soxhlet extraction and GC-MS characterization

The organic matter was characterized by gas chromatography-mass spectrometry (GC-MS) measuring for the extractants after a sequential extraction on the surface of the carbonaceous gold ores. The extraction was conducted in a Soxhlet apparatus in the following order: (i) hexane, (ii) ethyl acetate, and (iii) acetone, where the solvents were arranged from the most non-polar to polar (Fig. 6.1).

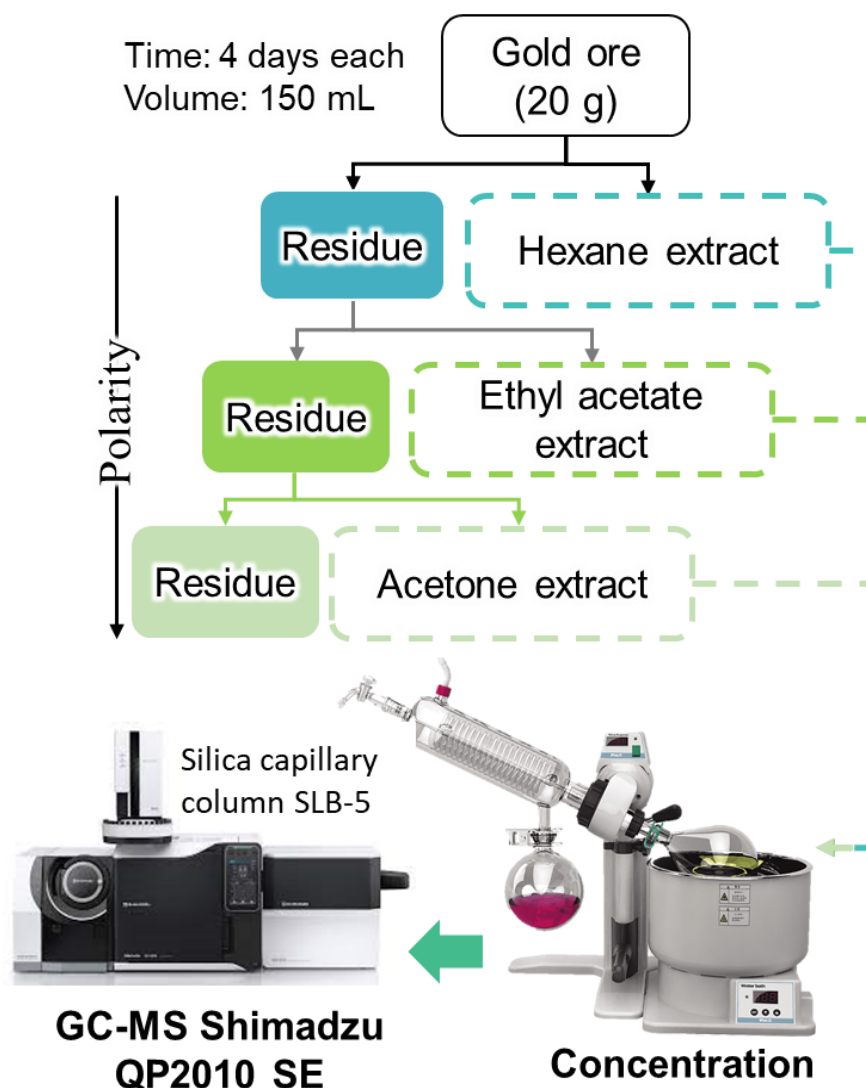


Fig. 6.1. Steps of sequential extraction and GC-MS characterization on carbonaceous gold ores.

Each extraction was conducted for at least 4 days. A parallel test was conducted using a reverse order of the solvents under the same conditions. SYM and PXX are flotation concentrate samples; therefore, a pre-washed step with ethanol,  $\text{HNO}_3$ , and an excess of ultra-pure water to remove the flotation concentrates and chemicals was necessary before the extraction. As for BOG, the sample was used as received. Solid residues after

enzymatic degradation were rinsed only with ultra-pure water. After freeze-drying, 20 g of each sample was separately introduced to an extraction thimble and proceeded with the extraction using 150 mL of solvent (Fig. 6.2). The solid residue after the first extraction with (i) hexane was provided for the second extraction with (ii) and so on (iii).

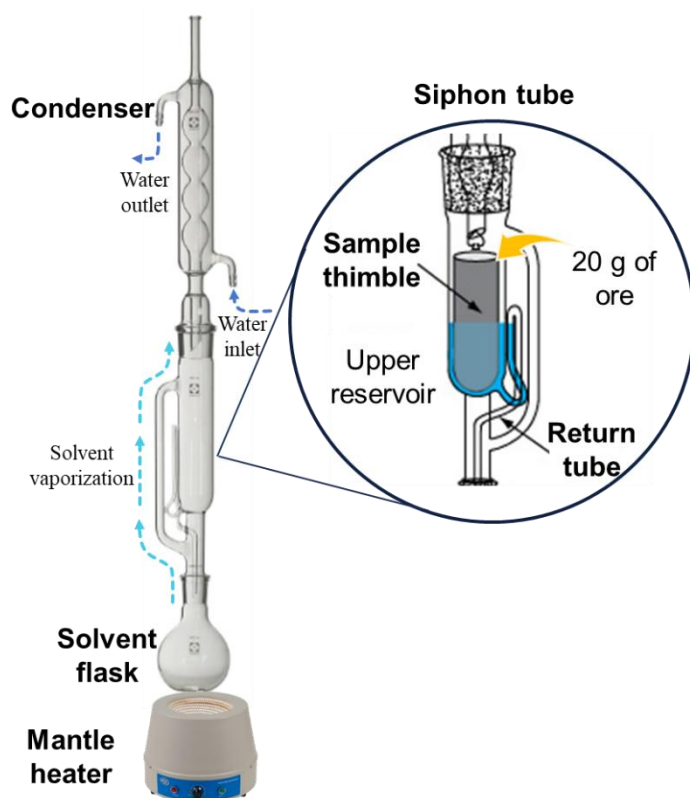


Fig. 6.2. Soxhlet apparatus parts and sample thimble location.

Each extract was concentrated by a rotary evaporator Eyela NVC-2100 (Tokyo, Japan) before supplying to GC-MS as illustrated in Fig. 6.1. Then, all the extractants were analyzed using a GC-MS Shimadzu QP2010 SE system (Kyoto, Japan). The separation of organic matter from the ores was performed using a 30 m fused silica capillary

column (SLB-5 ms, Supelco, Bellefonte, PA, USA) with an injection port temperature of 250°C and He as the carrier gas (constant pressure mode: 100 kPa). Mass spectra were observed by electron impact ionization at 70 eV. Before injection, the concentrated extracts were dissolved in 5mL acetone and injected in the splitless mode. The oven temperature was programmed from 120°C (with an initial hold for 2 min) to 320°C (with a final hold for 10 min) with a thermal gradient of 10°C/min. The products extracted in the organic phases from the sequential extraction were putatively identified using the MS NIST library by mass spectra. A minimum similarity of 80% was used for the characterization.

#### 6.2.3. Sequential bio-treatment and carbonaceous matter degradation by lignin-degrading enzymes

Based on the mineral, elemental and carbonaceous matter characterization of the three ores, sequential pre-treatments were designed and applied to maximize the gold recovery. PXX bio-treatment conditions are given in the supplemental section (Chapter 6S).

As for BOG (after BIOX), it was necessary to remove jarosite to prevent gold losses due to re-encapsulation (Asamoah, 2021) before going through enzymatic degradation. Then, the removal of jarosite was attempted using two washing conditions: (a) 0.1 M HCl, adopting Cindy et al. (2021) conditions, and (b) 0.4 M oxalic acid (20% pulp density; 24h; RT; 130 rpm). After the washing, ultra-pure water was used to rinse the solid residue several times and remove the remaining reagent until the pH reached 4.5. After 0.1 M HCl and 0.4 M oxalic acid washing, the samples were named DAW and DAO, respectively.



After jarosite removal, DAO went through various laccase treatment conditions (Table 6.1) with and without the addition of mediator 1-hydroxybenzotriazole (HBT). In this case, 5 g of DAO was suspended in the mixture of 90 mL of 0.1M sodium-acetate buffer (pH 4.5), 2 mM of HBT mediator, and 0.25 - 0.50 mg/mL of purified laccase Y-120 as shown in table 6.1. The total volume was adjusted to 100 mL using 0.1 M sodium-acetate buffer (pH 4.5). A porous plug type C that permits constant oxygen flow and an Erlenmeyer flask was used in all the experiments. The flasks were shaken at 37°C and 128 rpm using a TAITEC BR-40LF Bioshaker (Saitama, Japan). After 7 days of enzymatic treatment, the solid residues were separated from the supernatant by filtration (0.20  $\mu\text{m}\phi$ ), then freeze-dried for further characterization and gold extraction test.

On the other hand, SYM sequential bio-treatment followed a different path to avoid jarosite formation since 13.4% Fe and 2% K existed in the ore. Therefore, 0.5 M ferric chloride leaching ( $\text{FeCl}_3$ ) was used instead of bio-oxidation. After sulfide decomposition, the sample passed through an acidic washing (1 M HCl) to remove the remaining  $\text{Fe}^{3+}$  that could be detrimental to cyanidation and enzyme treatment. The final step was applying a laccase-mediator system using HBT as a mediator. Detailed information on the experimental conditions is described by Sakai et al. (2022).

#### 6.2.3.1. Solid residue characterization

Additional characterization of solid residues was performed using thermogravimetric-differential thermal analysis (TG-DTA), particle size analysis, and Raman spectroscopy. Elemental compositions were determined by X-ray fluorescence, and the relative intensity (RI) was expressed as the elemental content ((w/w)%) normalized for

Si content ((w/w)%). As for the supernatant after enzymatic treatment, total organic carbon (TOC) analysis was used to calculate dissolved organic carbon after buffer subtraction. Extraction of humic-like substances from the solid residues was carried out using 0.2 M NaOH under 60°C, shaken at 150 rpm for 24h. The obtained solutions were supplied for three-dimensional (3D) fluorescence spectrometry.

#### 6.2.4. Gold extraction

The gold extraction was carried out at a laboratory scale and calculated using Eq. (6.1). At first, 0.4 g of the sample was suspended in 8 mL of 2.5 mM KCN at pH 10.5 under room temperature. After 48 h of leaching, the supernatant and the solids were separated by filtration (0.20  $\mu\text{m}\phi$ ). Then, the extracted solution was supplied for ICP-MS Agilent 7900 to determine the gold concentration (A). As for the solid residue, 0.2 g was roasted at 800°C for 4 h and subsequently digested using aqua regia and the conditions developed in Chapter 3. After the aqua regia digestion, the liquid was collected, filtered, and filled up to 50 mL using ultra-pure water before supply to ICP-MS to calculate the remaining gold concentration in the solid after cyanidation (B). Finally, the gold recovery was calculated as follows:

$$\text{Gold extraction (\%)} = (A) / ((A) + (B)) \times 100 \quad (6.1)$$

Concerning ICP-MS analysis, the calibration standards and the supplied samples were diluted in a solution containing L-cysteine (1% w/v) and HCl (1% v/v) to avoid memory effect (Chen et al., 2000). All the cyanidation and acid digestion experiments were conducted in triplicates.

Table 6.1. Experimental conditions of LMS treatment for BOG

Characteristics	DAOY-1	DAOY-2	DAOY-3	DAOY-4	DAOY-5	DAOY-6	DAOY-7	DAOY-8	DAOY-9	DAOY-10	DAOY-11	DAOY-12
Final enzyme concentration	25 mg/ 100mL						50 mg/ 100mL					
Final HBT concentration	-	2 mM	-	2 mM	-	2 mM	-	2 mM	-	2 mM	-	2 mM
Addition time	day 0		day 0, day 2, day 4, day 6		day 0, day 1, day 2, day 3, day 4, day 5, day 6		day 0		day 0, day 2, day 4, day 6		day 0, day 1, day 2, day 3, day 4, day 5, day 6	
Enzyme stock addition	25 mg/mL (1 time)		6.25 mg/mL (4 times)		3.6mg/mL (7 times)		50 mg/mL (1 time)		12.5 mg/mL (4 times)		7.2 mg/mL (7 times)	
Mediator HBT addition	-	2mL of 100 mM (1 time)	-	0.50 mL of 100 mM (4 times)	-	0.28 mL of 100 mM (7 times)	-	2mL of 100 mM (1 time)	-	0.50 mL of 100 mM (4 times)	-	0.28 mL of 100 mM (7 times)

### 6.3.Results and discussion

#### 6.3.1. Carbon content, Raman spectra and preg-robbing test

Table 6.2 shows that the three carbonaceous gold ores have different preg-robbing abilities and gold recoveries. SYM is the most preg-robbing (95.9% of  $\text{Au}(\text{CN})_2^-$  adsorption) and, as such, shows less gold recovery (%) by cyanidation. Considering that 85 % of gold is liberated and exposed, it can be seen that  $\text{Au}(\text{CN})_2^-$  adsorption was highly influenced by CM and regardless gold encapsulation on pyrite, which corresponds to only 6.6% of gold. On the other hand, PXX shows the lowest preg-robbing (15.1%  $\text{Au}(\text{CN})_2^-$  adsorption) and better gold recovery despite having less liberated gold (79.5%) and higher organic carbon (5.8 wt%) than SYM, inferring that CM is less refractory in PXX. As for BOG shows 77% of gold recovery despite possessing moderate preg-robbing capacity, and this is because gold was liberated after the bio-oxidation. Therefore, during cyanidation, more gold could be recovered.

Table 6.2. Carbon and preg-robbing characterization of three carbonaceous gold ores

Characteristics	SYM	BOG	PXX
C (%)	5.3	3.9	5.8
Organic carbon(%)	4.1	3.9	5.1
Gold recovery by cyanidation (%)	44	77	67
Gold robbed (%)	95.9	55.6	15.1
Preg-robbing classification	Highly	Moderately	Mildly

The differences in the preg-robbing abilities were also reflected in the Raman spectra from the three carbonaceous gold ores. Fig. 6.3 shows there are two notorious peaks in the spectra. The peak position at  $1350\text{ cm}^{-1}$ , assigned to the defective carbon (D-band) (Bokobza et al., 2015), is common in the three ores. However, the peak position assigned to the graphitic carbon (G-band) has a different Raman shift in each ore, and they are located as follows:  $1580\text{ cm}^{-1}$  for PXX,  $1590\text{ cm}^{-1}$  for BOG, and  $1600\text{ cm}^{-1}$  for SYM. The relative intensity was calculated using the peak areas after the peak separation of each spectrum.

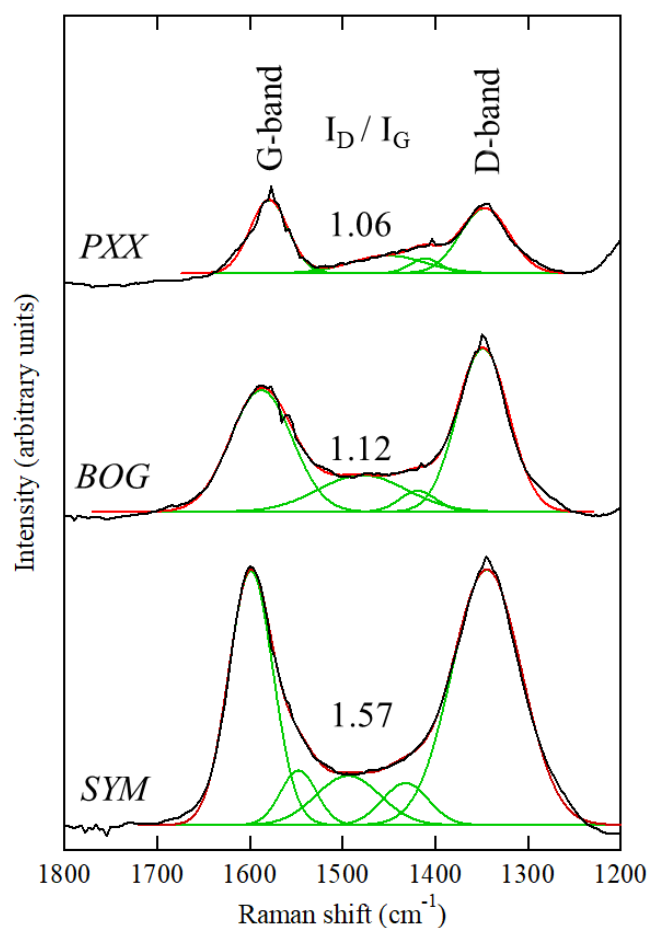


Fig. 6.3. Raman spectra for PXX, BOG, and SYM in a region from  $1800\text{ cm}^{-1}$  to  $1200\text{ cm}^{-1}$  with relative intensities of  $I_D/I_G$ .

Similar to the preg-robbing test, there are two extremes: SYM showing the highest value of  $I_D/I_G$  (1.57) and PXX the lowest (1.06). The relative intensity trend is similar to the preg-robbing ability discussed in the above paragraph. These findings also agreed with Ng et al. (2022), who demonstrated that Raman spectra could predict the preg-robbing ability. That said, a higher value of  $I_D/I_G$  reflects higher preg-robbing behavior of CM (Fig. 6.4). This could be attributed to the more extensive area encountered in the defective carbon, which has been suggested to be more responsible for  $\text{Au}(\text{CN})_2^-$  adsorption through the carbon edges (Adams, 1990).

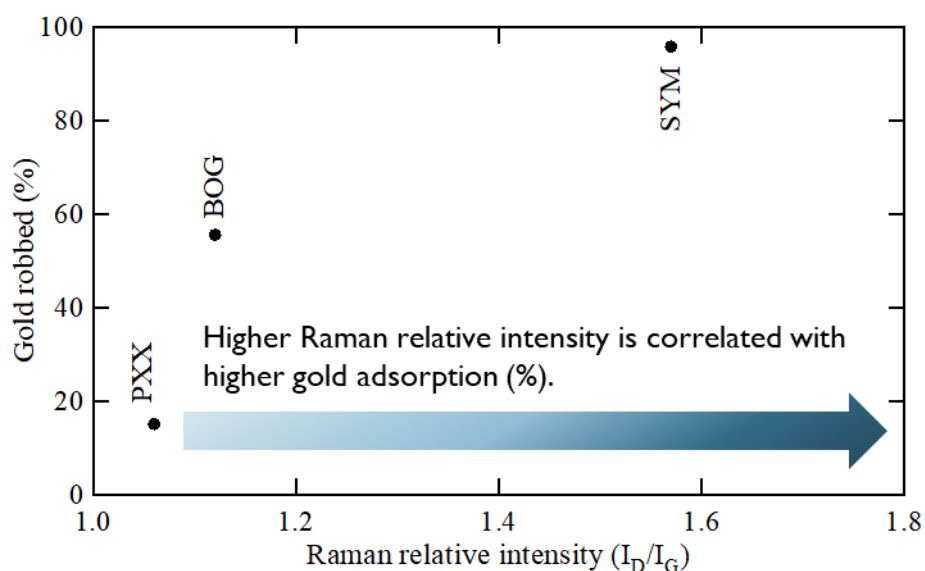


Fig. 6.4. Relation between Raman relative intensities ( $I_D/I_G$ ) and  $\text{Au}(\text{CN})_2^-$  adsorption abilities on PXX, BOG, and SYM.

### 6.3.2. TG-DTA

Two main ranges of mass loss were observed in DTG (Fig. 6.5): (I) 420–465°C, assigned to the release of  $\text{SO}_2$  from pyrite combustion, and (II) 465–650°C (Liu et al.,

2022), assigned to the release of CO<sub>2</sub> due to thermal oxidation of CM (Konadu et al., 2019). These assignments apply for PXX and SYM because BOG does not contain pyrite; instead, SO<sub>2</sub> might be released from jarosite that is combusted at a slightly lower temperature. However, based on Table 6.2, organic carbon content (wt%) in PXX, BOG, and SYM is 5.1, 3.9, and 4.1, respectively, less than the mass loss (%) observed between 465–650°C (Table 6.3). This difference may be caused by the pyrite's second peak combustion, as reported by Liu et al. (2022). Therefore, CM and pyrite combustion overlapped.

Table 6.3. Mass loss (%) separated in temperature combustion ranges

Sample	0-200°C	200-420°C	420-465°C	465-650°C	650-1000°C	Total
SYM	1.2	0.5	5.9	11.6	1.4	20.6
PXX	0.2	0.0	1.6	8.5	6.5	16.8
BOG	8.8	1.9	0.4	9.5	0.0	20.6

Due to overlapping, it was difficult to differentiate the exact temperature range of CM combustion using TG-DTA. Nevertheless, the most important difference in the carbon combustion between the three samples was observed in PXX, in which combustion in the (II) temperature range finishes at a lower temperature (560°C), suggesting that aromaticity might be less than in BOG and SYM as in coal ranks (Chen et al., 1995, 1996).

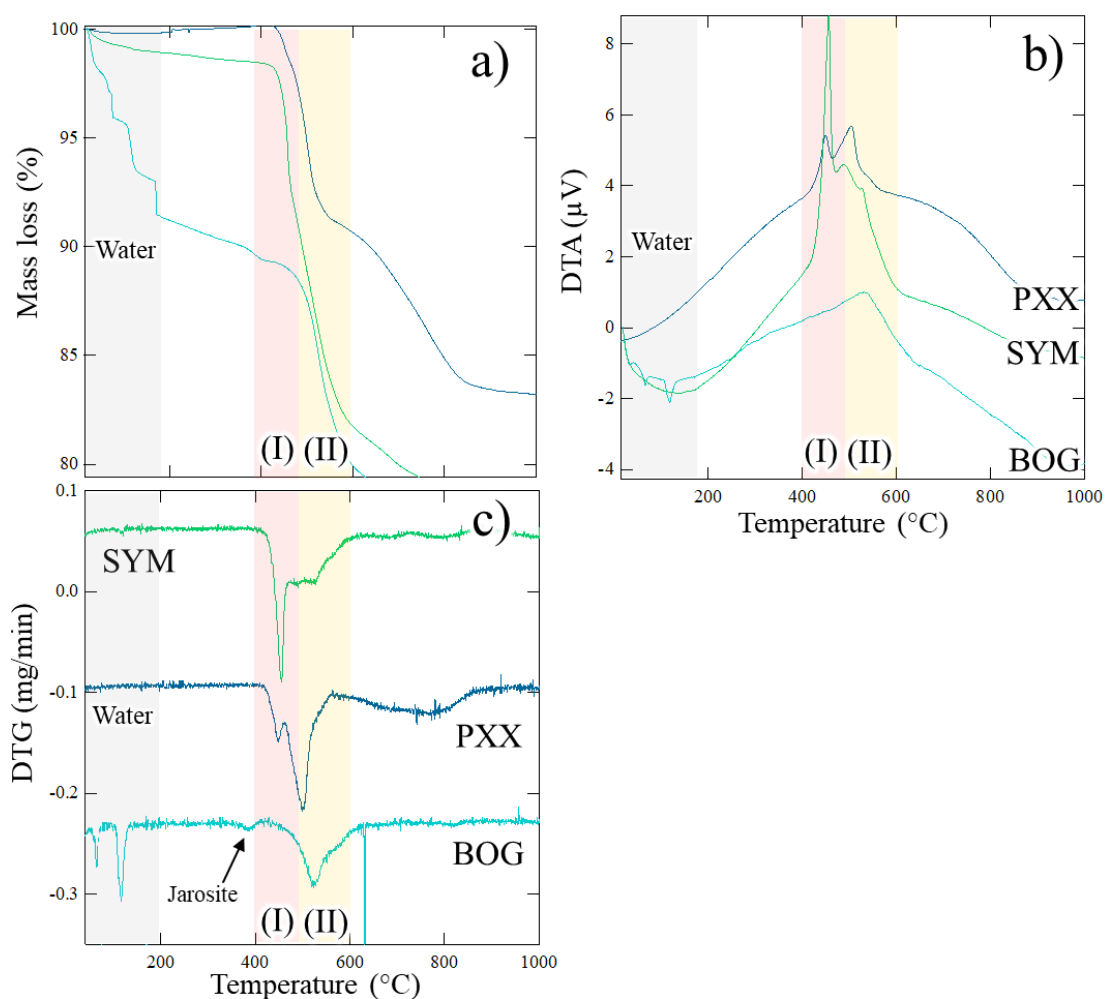


Fig. 6.5. Thermogravimetric analysis (TG-DTA) for PXX, BOG, and SYM, (a) mass loss (%), (b) DTA ( $\mu\text{V}$ ), (c) DTG ( $\text{mg/min}$ ).

### 6.3.3. GC-MS characterization of PXX, BOG, and SYM

The total ion chromatograms for each extractant in the three ores are shown in Fig. 6.6(a)-6.8(a). The dissolved organic matter in the hexane extraction was mainly alkanes and fatty acids in the three carbonaceous gold ores, which are generally dissolved in non-polar solvents (Hu et al., 2022). The prominent peaks 9 and 16 in PXX (Fig. 6.6(a)) are assigned to organic contaminants from the plastic clamp during Soxhlet extraction.



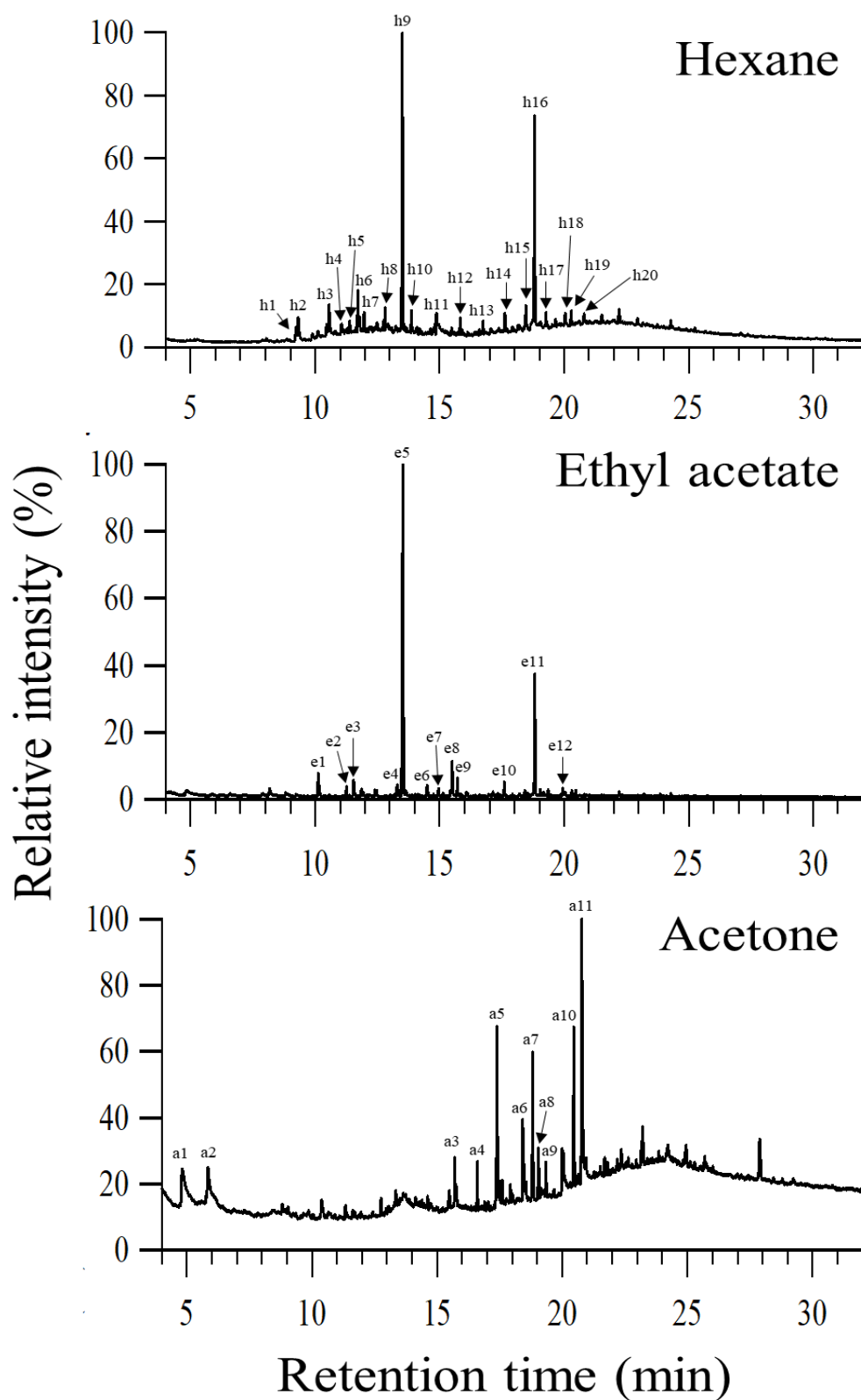
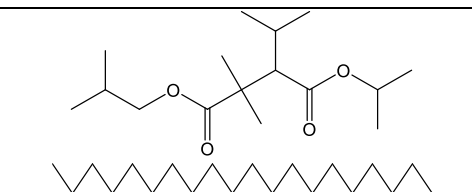
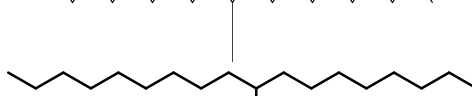
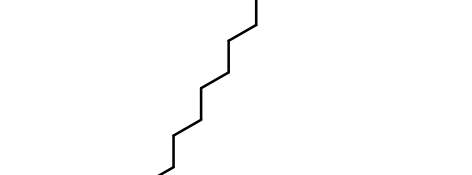
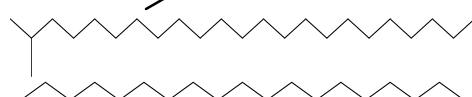
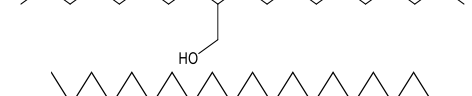
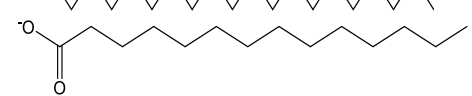
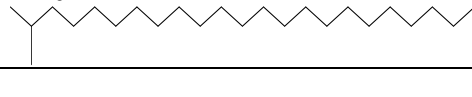

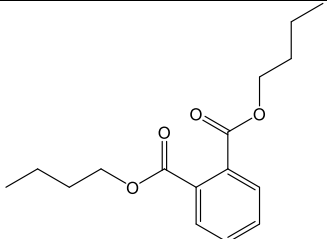
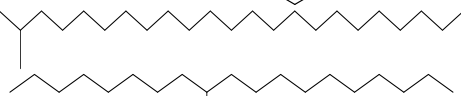
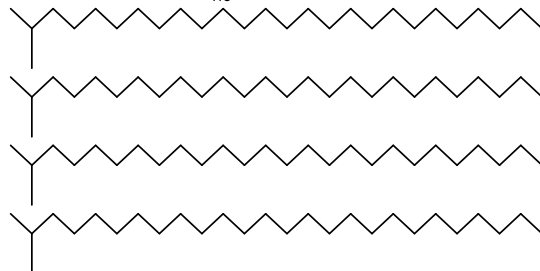
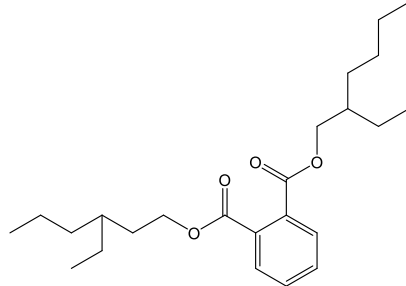


Fig. 6.6. GC-MS total ion chromatograms of (a) hexane, (b) ethyl acetate, and (c) acetone extracts from PXX after sequential extraction.

Table 6.4. Organic moieties detected by GC-MS in Fig. 6.6(a) for extracted compounds in hexane phase from PXX

Peak No.	Similarity (%)	Retention time (min)	Most similar compound suggest by NIST library	Type of compound	Chemical structure
h1	90	9.21	pentanoic acid, 2,2,4-trimethyl-3-carboxyisopropyl, isobutyl ester	contaminant from plastic clamp	
h2	94	9.32	eicosane, 10-methyl-	alkane	
h3	93	10.54	heptadecane, 9-octyl-	alkane	
h4	90	11.06	2-methyltetracosane	alkane	
h5	90	11.39	1-decanol, 2-octyl-	branched-chain primary alcohol	
h6	94	11.70	eicosane	alkane	
h7	90	11.97	tetradecanoate	fatty acid	
h8	93	12.81	2-methyltetracosane	alkane	

Peak No.	Similarity (%)	Retention time (min)	Most similar compound suggest by NIST library	Type of compound	Chemical structure
h9	97	13.50	dibutyl phthalate	contaminant from plastic clamp	
h10	92	13.86	2-methyltetracosane	alkane	
h11	94	14.87	1-decanol, 2-octyl-	branched-chain primary alcohol	
h12	92	15.81	2-methylhexacosane	alkane	
h13	92	16.72	2-methylhexacosane	alkane	
h14	92	17.61	2-methylhexacosane	alkane	
h15	91	18.45	2-methylhexacosane	alkane	
h16	97	18.80	phthalic acid, bis(2-ethylhexyl) ester	contaminant from plastic clamp	





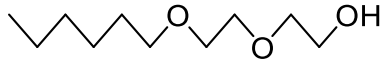
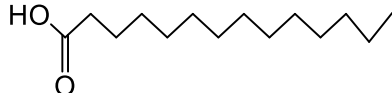
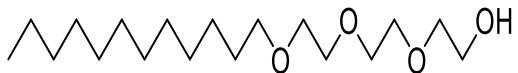

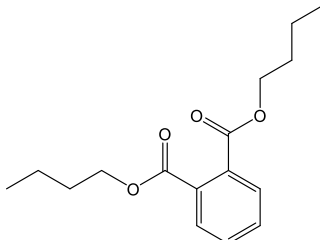
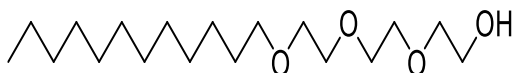
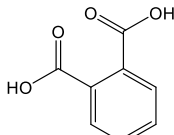
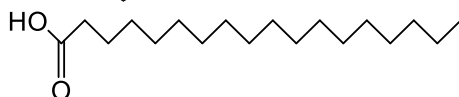
Peak No.	Similarity (%)	Retention time (min)	Most similar compound suggest by NIST library	Type of compound	Chemical structure
h17	92	19.27	tetrapentacontane, 1,54-dibromo-	alkane	
h18	92	20.03	tetrapentacontane, 1,54-dibromo-	alkane	
h19	92	20.27	tetrapentacontane, 1,54-dibromo-	alkane	
h20	92	20.78	tetrapentacontane, 1,54-dibromo-	alkane	

Table 6.5. Organic moieties detected by GC-MS in Fig. 6.6(b) for extracted compounds in ethyl acetate phase from PXX

Peak No.	Similarity (%)	Retention time (min)	Most similar compound suggest by NIST library	Type of compound	Chemical structure
e1	88	10.13	diethylene glycol hexyl ether	ether	
e2	93	11.25	tetradecanoic acid	fatty acid	
e3	86	11.53	triethylene glycol monododecyl ether	ether	
e4	86	11.30	hexaethylene glycol monododecyl ether	ether	
e5	97	13.52	dibutyl phthalate	contaminant from plastic clamp	
e6	86	14.49	triethylene glycol monododecyl ether	ether	
e7	84	14.96	phthalic acid	contaminant	
e8	97	15.50	octadecanoic acid	fatty acid	

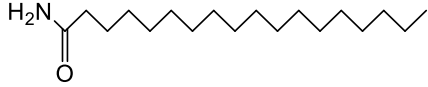
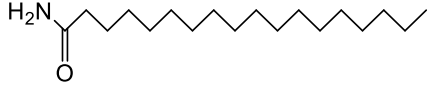
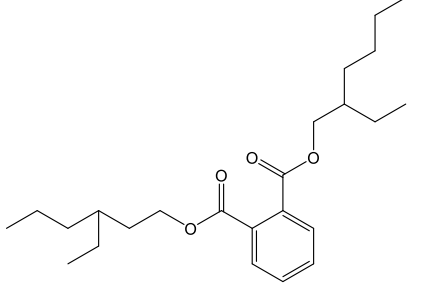
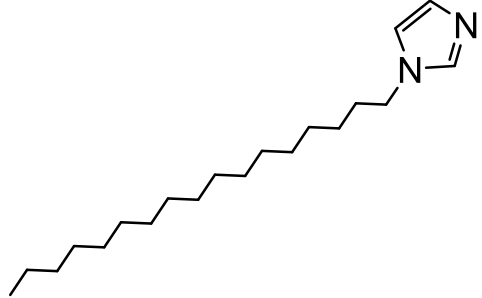
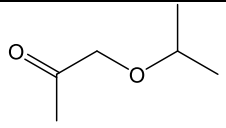
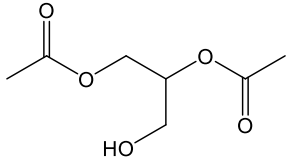
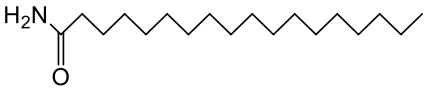
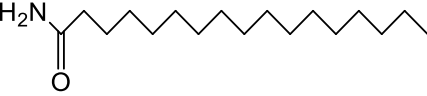
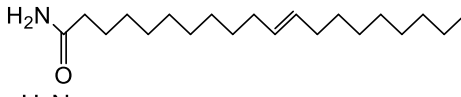
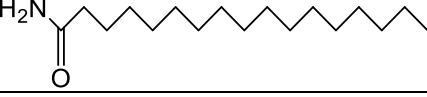
Peak No.	Similarity (%)	Retention time (min)	Most similar compound suggest by NIST library	Type of compound	Chemical structure
e9	95	15.72	octadecanamide	amide of fatty acid	
e10	96	17.60	octadecanamide	amide of fatty acid	
e11	98	18.82	phthalic acid, bis(2-ethylhexyl) ester	contaminant from plastic clamp	
e12	81	19.94	1h-imidazole, 1-octadecyl-	alkyl aromatic	

Table 6.6. Organic moieties detected by GC-MS in Fig. 6.6(c) for extracted compounds in acetone phase from PXX

Peak No.	Similarity (%)	Retention time (min)	Most similar compound suggest by NIST library	Type of compound	Chemical structure
a1	78	4.82	2-propanone, 1-(1-methylethoxy)	methyl ketone	
a2	82	5.84	1,2,3-propanetriol, diacetate	diester of glycerol	
a3	82	15.69	octadecanamide	amide of fatty acid	
a4	87	16.60	hexadecyl formamide	amide of fatty acid	
a5	88	17.39	9-octadecenamide	amide of fatty acid	
a6	87	18.42	hexadecyl formamide	amide of fatty acid	

Peak No.	Similarity (%)	Retention time (min)	Most similar compound suggest by NIST library	Type of compound	Chemical structure
a7	94	18.81	phthalic acid, bis(2-ethylhexyl) ester	contaminant from plastic clamp	
a8	82	19.03	10-octadecenal	fatty aldehydes	
a9	83	19.34	propyl triacontyl ether	alkyl ether	
a10	84	20.47	terephthalic acid	contaminant from plastic clamp	
a11	89	20.77	13-docosenamide	amide of fatty acid	



Peaks 4, 8, 10, 12, 13, 14, and 15, with similarities higher than 90%, are assigned to the mass fractions of 2-methyltetracosane. Other detected alkanes (peaks 2, 3, 6, and 16) were also saturated aliphatic hydrocarbons. Only peak 7 was assigned to the fatty acid tetranodecanoate. On the other hand, peaks 5 and 11 were mass fractions of primary branched-chain alcohol.

BOG (Fig. 6.7(a)) has three prominent peaks (2, 3, and 10) assigned to fatty acids. However, ether (peak 6) and aldehyde (peak 7) with long aliphatic chains were also identified in a very minor proportion. The other peaks, except peak 5, were also saturated aliphatic hydrocarbons like in PXX. The hexane phase in SYM (Fig. 6.8(a)) showed several prominent peaks in the chromatogram assigned to saturated aliphatic hydrocarbons and their structural isomers. Only peaks 3, 11, and 19 were assigned to the contaminant described above, fatty acid and an aromatic compound, respectively. Unsaturated aliphatic hydrocarbons were not found in the three hexane extracts.

The ethyl acetate extract in PXX (Fig. 6.6(b)) also showed the same prominent peaks (5 and 11) assigned to the contaminant as in the hexane extract. The new components in this phase were ethers (peaks 1, 3, 4, and 6) like diethylene glycol hexyl ether, triethylene glycol monododecyl ether, and hexaethylene glycol monododecyl ether, which are known to be nonionic surfactants (Tucker et al., 2022). In addition, fatty acids (peaks 2 and 8) and fatty amides (peaks 9 and 10) were also found in this phase. Lastly, peak 12 corresponded to an alkyl aromatic; however, this was unrelated to the benzene aromatic family. BOG (Fig. 6.7(b)) shows two predominant peaks (6 and 7) coming from the fatty acid hexadecanoic acid. Other fatty acids with 17, 18, 25, and 32 carbon chains were also observed in peaks 8, 10, 11, 13, and 14.

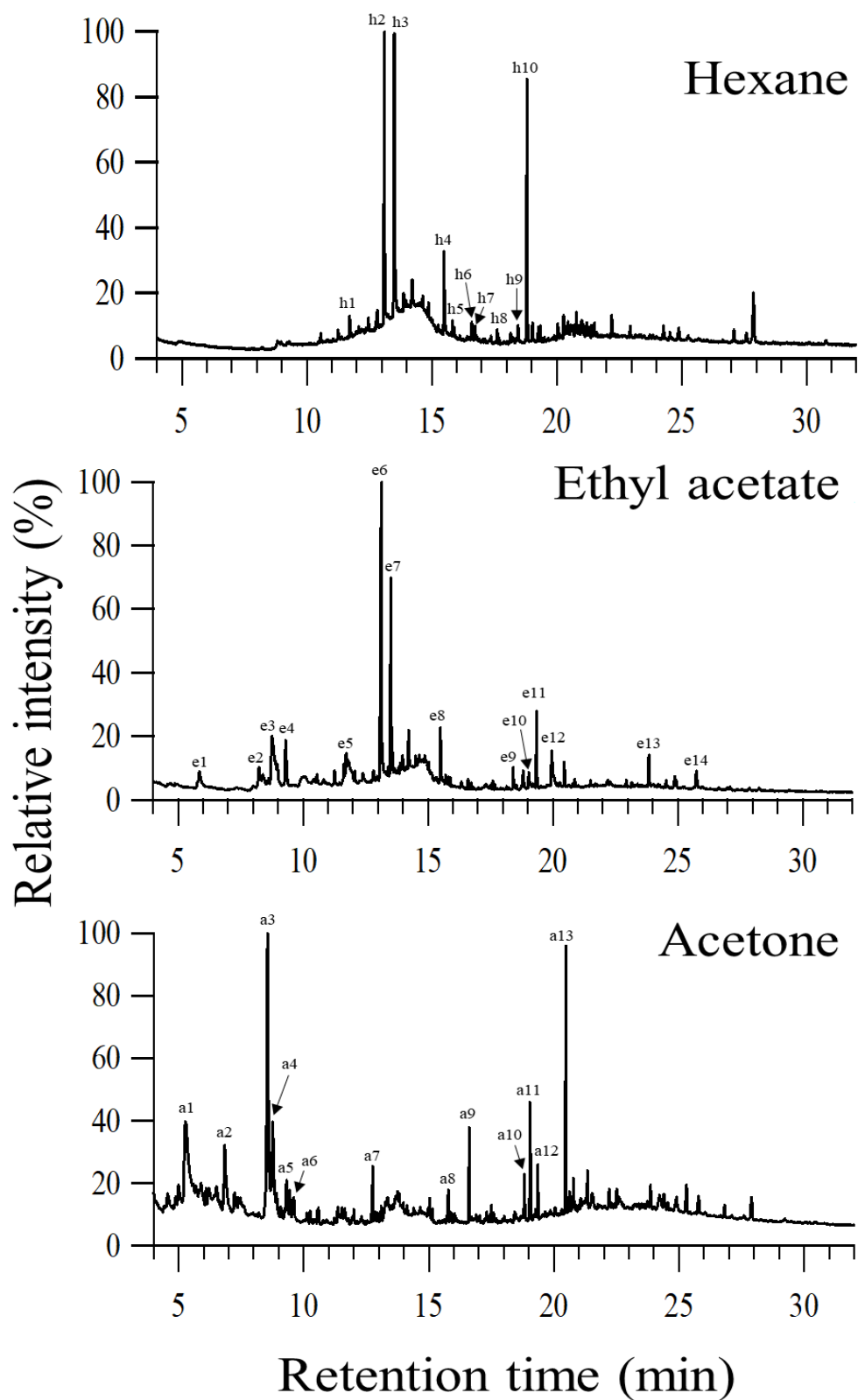


Fig. 6.7. GC-MS total ion chromatograms of (a) hexane, (b) ethyl acetate, and (c) acetone extracts from BOG after sequential extraction.

Table 6.7. Organic moieties detected by GC-MS in Fig. 6.7(a) for extracted compounds in hexane phase from BOG

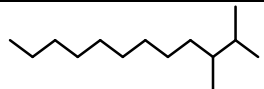
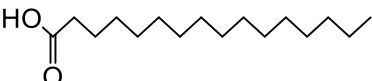
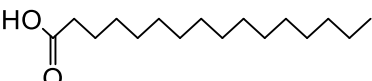




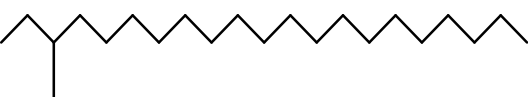
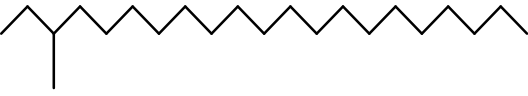

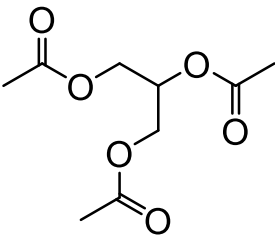
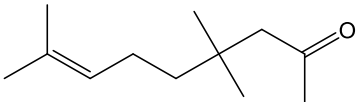
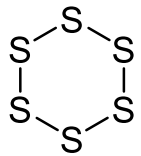
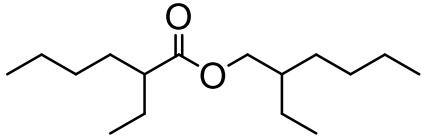

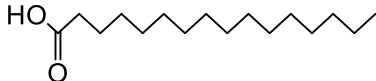
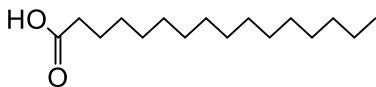
Peak No.	Similarity (%)	Retention time (min)	Most similar compound suggest by NIST library	Type of compound	Chemical structure
h1	82	11.72	2,3-dimethyldodecane	alkane	
h2	91	13.10	hexadecanoic acid	fatty acid	
h3	90	13.48	hexadecanoic acid	fatty acid	
h4	92	15.48	octadecanoic acid	fatty acid	
h5	81	15.81	sulfurous acid, octadecyl 2-propyl ester	unknown	
h6	80	15.89	propyl triacontyl ether	alkyl ether	
h7	83	16.59	4-octadecenal	stearyl aldehyde	
h8	88	16.73	2-methyltetracosane	alkane	
h9	90	17.61	2-methylhexacosane	alkane	
h10	90	18.81	2-methylhexacosane	alkane	

Table 6.8. Organic moieties detected by GC-MS in Fig. 6.7(b) for extracted compounds in ethyl acetate phase from BOG

Peak No.	Similarity (%)	Retention time (min)	Most similar compound suggest by NIST library	Type of compound	Chemical structure
e1	86	5.82	1,2,3-propanetriol, triacetate	triglyceride	
e2	80	8.23	4,4,8-trimethyl-non-7en-2-one	acyclic monoterpenes	
e3	92	8.76	cyclohexasulfide	sulfur hexamer	
e4	90	9.28	2-ethylhexyl 2-ethylhexanoate	fatty acid alkyl esters	
e5	80	11.72	4,8,12,16-tetraoxaeicosan-1-ol		
e6	93	13.14	hexadecanoic acid	fatty acid	
e7	93	13.51	hexadecanoic acid	fatty acid	

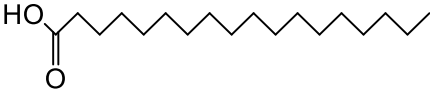

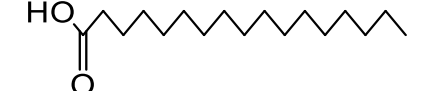
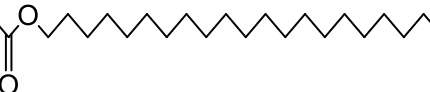
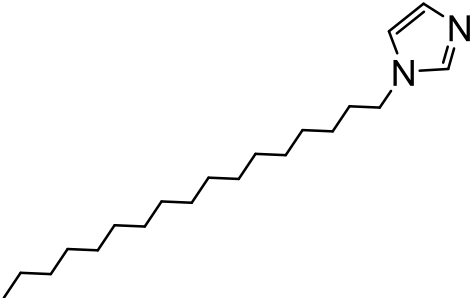
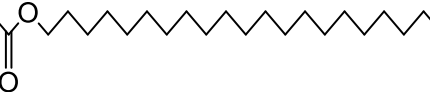
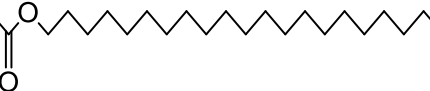
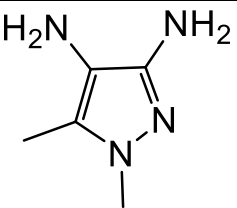
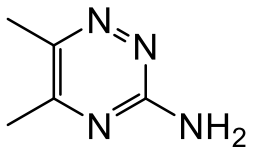
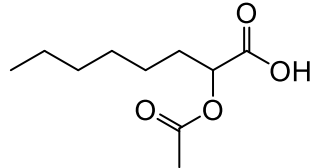
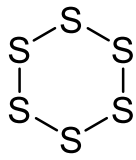
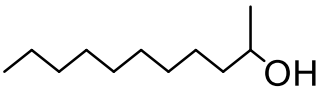
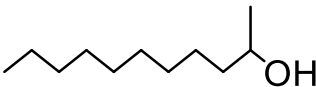



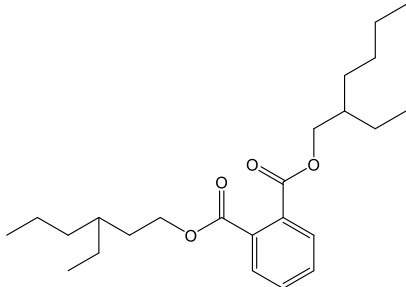

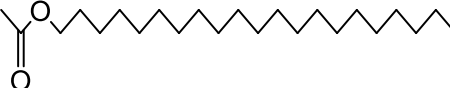
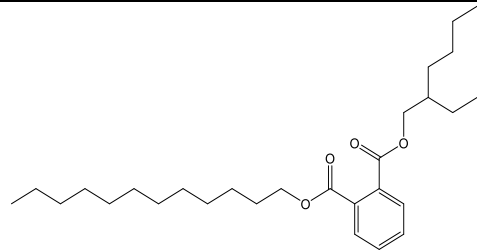
Peak No.	Similarity (%)	Retention time (min)	Most similar compound suggest by NIST library	Type of compound	Chemical structure
e8	93	15.48	octadecanoic acid	fatty acid	
e9	86	18.41	hexadecyl formamide	amide of fatty acid	
e10	87	19.05	heptadecanoic acid	fatty acid	
e11	97	19.34	tricosyl acetate	fatty acid	
e12	83	19.95	1h-imidazole, 1-octadecyl-	alkyl aromatic	
e13	94	23.85	tricosyl acetate	fatty acid	
e14	90	25.75	tricosyl acetate	fatty acid	

Table 6.9. Organic moieties detected by GC-MS in Fig. 6.7(c) for extracted compounds in acetone phase from BOG

Peak No.	Similarity (%)	Retention time (min)	Most similar compound suggest by NIST library	Type of compound	Chemical structure
a1	74	5.28	1H-pyrazole-3,4-diamine, 1,5-dimethyl-	aromatic	
a2	83	6.84	1,2,4-triazin-3-amine, 5,6-dimethyl-	aromatic	
a3	82	8.54	(+/-)-2-hydroxyoctanoic acid, acetate	fatty acid	
a4	81	8.76	cyclohexasulfide	sulfur hexamer	
a5	89	9.31	2-methyl-1-undecanol	branched-chain primary alcohol	

Peak No.	Similarity (%)	Retention time (min)	Most similar compound suggest by NIST library	Type of compound	Chemical structure
a6	84	9.61	2-methyl-1-undecanol	branched-chain primary alcohol	
a7	90	12.76	heptadecanal	aldehyde	
a8	90	15.78	pentacos-1-ene	alkene	
a9	92	16.61	hexadecyl formamide	amide of fatty acid	
a10	91	18.80	phthalic acid, bis(2-ethylhexyl) ester	contaminant from plastic clamp	
a11	91	19.05	hexadecanol act-16-one	fatty alcohol	
a12	95	19.34	tricosyl acetate	fatty acid	

Peak No.	Similarity (%)	Retention time (min)	Most similar compound suggest by NIST library	Type of compound	Chemical structure
a13	86	20.47	terephthalic acid, 2-ethylhexyl undecyl ester	contaminant from plastic clamp	



The presence of triglyceride (peak 1), sugar (peak 2), and sulfur-containing compounds like cyclohexasulfide (peak 3) were also observed. The abundance of fatty acids in BOG could be strongly related to the lipid fraction from the passivation layer of the extracellular polymeric substances (EPS) (Conrad et al., 2003; Gehrke et al., 1998b). GC-MS results support the statement that the carbon surface in this sample could be affected by the coating of EPS from the microorganisms after bio-oxidation (Wingender et al., 1999).

In the case of SYM (Fig. 6.8(b)), large peaks coming from ethers (peaks 1, 2, 4, 7, 9, 15, 18, 19, and 20), fatty acids (peaks 3 and 5), esters (peak 10), and fractions of 2-methylhexacosane, which is a branched alkane (peak 8, 11, 13, and 17) were observed. Nevertheless, one noticeable difference compared to the other TICs in PXX and BOG was the presence of various aromatic moieties (peaks 14, 16, 21, and 22) relevant for the preg-robbing ability as SYM shows to be a highly-preg-robbing ore (Table 6.2).

As for the most polar phase, PXX (Fig. 6.6(c)) shows a large proportion of fatty acid amides (peaks 3, 4, 5, 6, and 11), which could be associated with low carbon maturity (Dembitsky et al., 2000). Regarding BOG, heterocyclic compounds containing nitrogen atoms (peaks 1 and 2) are possibly related to biomass. Since fatty acids (peaks 4 and 12), fatty alcohol (peak 11), fatty amide (peak 9), and hexasulfur (peak 4) were also detected in this phase, it was clear the organic substances coming from EPS were considerably extracted by all the fractions, interfering with the surface functional groups coming from carbonaceous matter characterization. Lastly, SYM (Fig. 6.8(c)) does not show prominent peaks in the acetone phase compared to the non-polar phases, indicating the carbonaceous matter surface was covered to some extent by hydrophobic organic matter. However, quantitative data is required to appoint this asseveration.

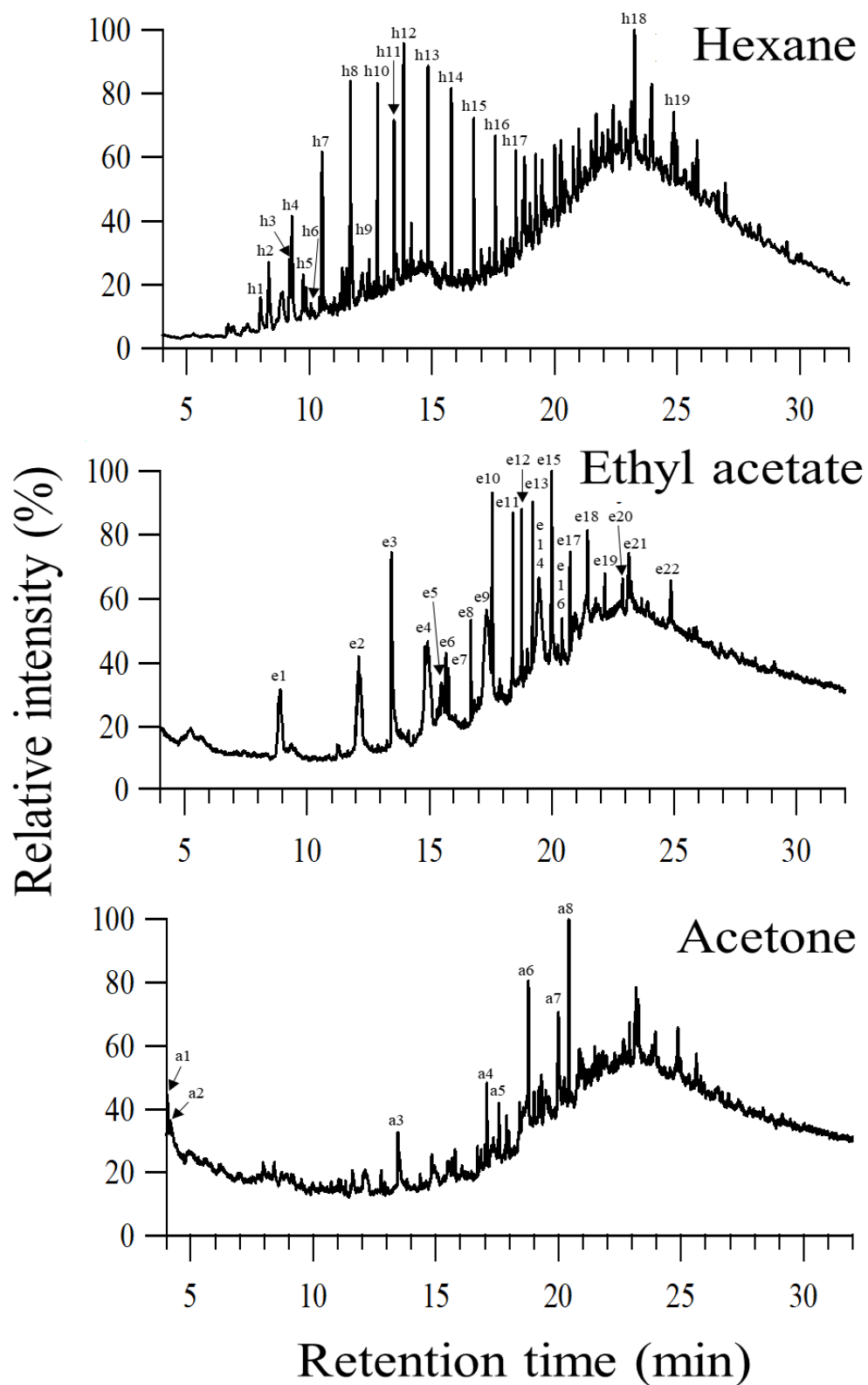
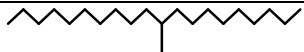
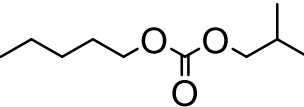
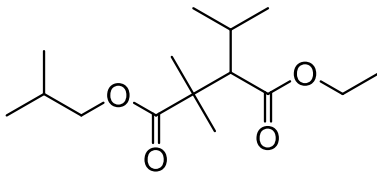
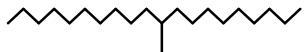
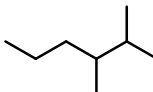
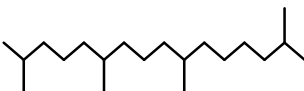


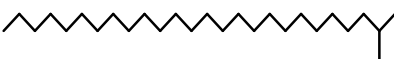

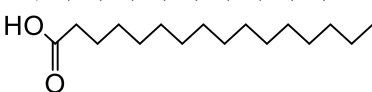


Fig. 6.8. GC-MS total ion chromatograms of (a) hexane, (b) ethyl acetate, and (c) acetone extracts from SYM after sequential extraction.

Table 6.10. Organic moieties detected by GC-MS in Fig. 6.8(a) for extracted compounds in hexane phase from SYM

Peak No.	Similarity (%)	Retention time (min)	Most similar compound suggest by NIST library	Type of compound	Chemical structure
h1	94	8.00	eicosane, 10-methyl-	alkane	
h2	80	8.32	carbonic acid, isobutyl pentyl ester	ester	
h3	89	9.16	pentanoic acid, 2,2,4-trimethyl-3-carboxyisopropyl, isobutyl ester	contaminant from plastic clamp	
h4	93	9.26	eicosane, 10-methyl-	alkane	
h5	82	9.73	hexane, 2,3-dimethyl-	alkane	
h6	89	9.84	hexadecane, 2,6,10,14-tetramethyl-	alkane	
h7	93	10.51	heptadecane	alkane	
h8	94	11.67	octadecane	alkane	
h9	89	11.74	2-methylhexacosane	alkane	
h10	92	12.78	eicosane	alkane	
h11	80	13.44	hexadecanoic acid	fatty acid	








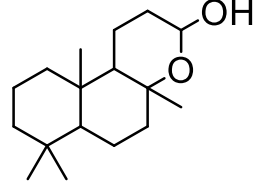
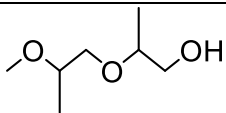
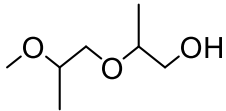
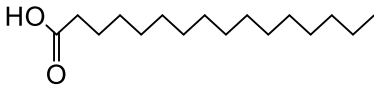
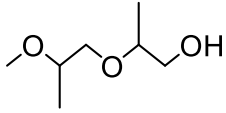
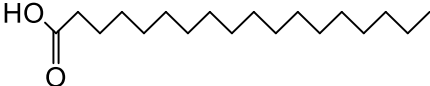
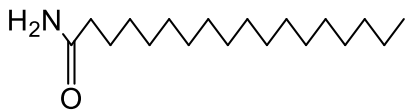


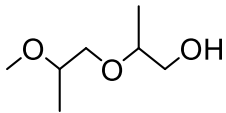

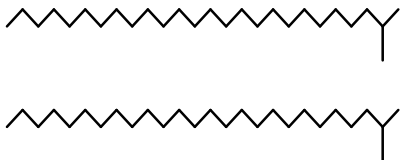
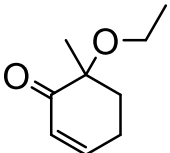
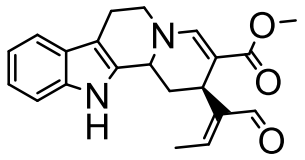
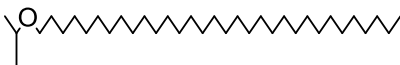
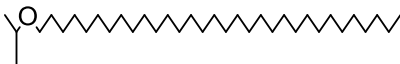
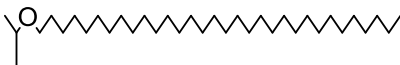
Peak No.	Similarity (%)	Retention time (min)	Most similar compound suggest by NIST library	Type of compound	Chemical structure
h12	90	13.83	eicosane	alkane	
h13	88	14.82	2-methylhexacosane	alkane	
h14	93	15.77	2-methylhexacosane	alkane	
h15	94	16.71	2-methylhexacosane	alkane	
h16	95	17.57	2-methylhexacosane	alkane	
h17	94	18.41	2-methylhexacosane	alkane	
h18	91	23.26	tetrapentacontane, 1,54-dibromo-	alkane	
h19	81	24.87	4a,7,7,10a-tetramethyldodecahydrobenzo[f]chromen-3-ol	aromatic	

Table 6.11. Organic moieties detected by GC-MS in Fig. 6.8(b) for extracted compounds in ethyl acetate phase from SYM

Peak No.	Similarity (%)	Retention time (min)	Most similar compound suggest by NIST library	Type of compound	Chemical structure
e1	85	8.87	2-(2-methoxypropoxy)-1-propanol	ether	
e2	84	12.12	2-(2-methoxypropoxy)-1-propanol	ether	
e3	94	13.44	hexadecanoic acid	fatty acid	
e4	80	14.92	2-(2-methoxypropoxy)-1-propanol	ether	
e5	86	15.50	octadecanoic acid	fatty acid	
e6	83	15.65	octadecanamide	amide	
e7	87	15.78	dotriacontyl isopropyl ether	ether	
e8	92	16.67	2-methylhexacosane	branched alkane	
e9	78	17.36	2-(2-methoxypropoxy)-1-propanol	ether	

Peak No.	Similarity (%)	Retention time (min)	Most similar compound suggest by NIST library	Type of compound	Chemical structure
e10	86	17.56	carbonic acid, eicosyl prop-1-en-2-yl ester	ester	
e11	93	18.42	2-methylhexacosane	branched alkane	
e12	90	18.75	diisooctyl phthalate	contaminant	
e13	90	19.20	2-methylhexacosane	branched alkane	
e14	74	19.47	6-ethoxy-6-methylcyclohex-2-en-1-one	cycloalkene	
e15	81	19.98	eicosyl isopropyl ether	ether	
e16	74	20.41	8,19-secoyohimban-19-oic acid, 16,17,20,21-tetradehydro-16-(hydroxymethyl)-, methyl ester, (15.beta.,16E)	aromatic	
e17	89	20.71	2-methylhexacosane	branched alkane	
e18	83	21.45	dotriacontyl isopropyl ether	ether	
e19	80	22.16	dotriacontyl isopropyl ether	ether	
e20	75	22.86	dotriacontyl isopropyl ether	ether	

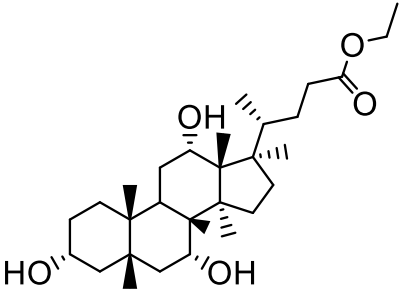
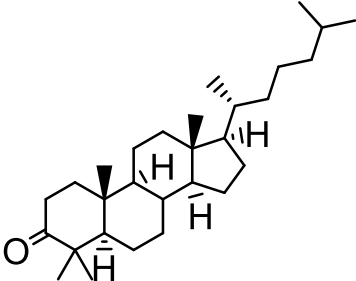
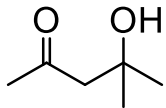
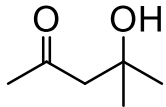
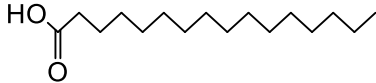
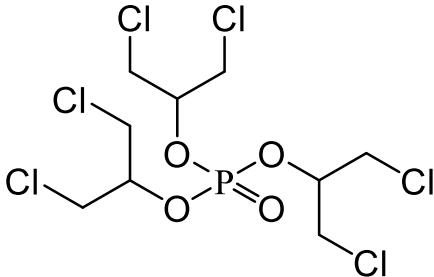
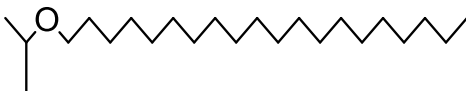
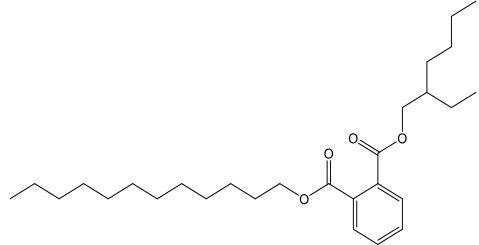
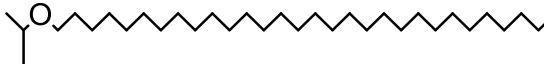
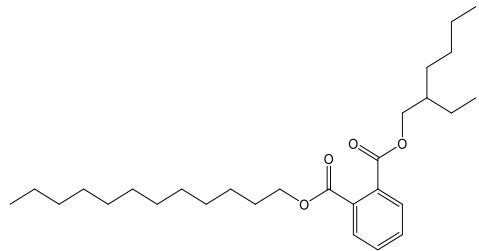
Peak No.	Similarity (%)	Retention time (min)	Most similar compound suggest by NIST library	Type of compound	Chemical structure
e21	72	23.17	ethyl iso-allocholate	steroid	
e22	69	24.88	cholest-7-en-3-one, 4,4-dimethyl-, (5.alpha.)-	steroid	

Table 6.12. Organic moieties detected by GC-MS in Fig. 6.8(c) for extracted compounds in acetone phase from SYM

Peak No.	Similarity (%)	Retention time (min)	Most similar compound suggest by NIST library	Type of compound	Chemical structure
a1	92	4.04	2-pentanone, 4-hydroxy-4-methyl-	diacetone alcohol	
a2	91	4.17	2-pentanone, 4-hydroxy-4-methyl-	diacetone alcohol	
a3	86	13.45	hexadecanoic acid	fatty acid	
a4	81	17.06	tris(1,3-dichloroisopropyl)phosphate	contaminant	
a5	86	17.58	eicosyl isopropyl ether	ether	



Peak No.	Similarity (%)	Retention time (min)	Most similar compound suggest by NIST library	Type of compound	Chemical structure
a6	88	18.77	terephthalic acid, 2-ethylhexyl undecyl ester	contaminant from plastic clamp	
a7	73	20.00	dotriacontyl isopropyl ether	ether	
a8	82	20.42	terephthalic acid, 2-ethylhexyl undecyl ester	contaminant from plastic clamp	

#### 6.3.4. EPS interference on Au recovery in laccase treatment of BOG

##### 6.3.4.1. Pre-washing optimization and characterization of BOG after BIOX treatment

The removal of jarosite from the bio-oxidation process that could prevent the improvement of gold recovery in a sequential treatment was evaluated under two washing conditions. Particle size distribution (Fig. 6.9) confirmed agglomerates formation caused by the physically adsorbed  $\text{Fe}^{3+}$  on the surface of DA. As described by Konadu et al. (2019),  $\text{Fe}^{3+}$  produced during bio-oxidation may assist in the formation of large particles that can trap some of the liberated gold grains.

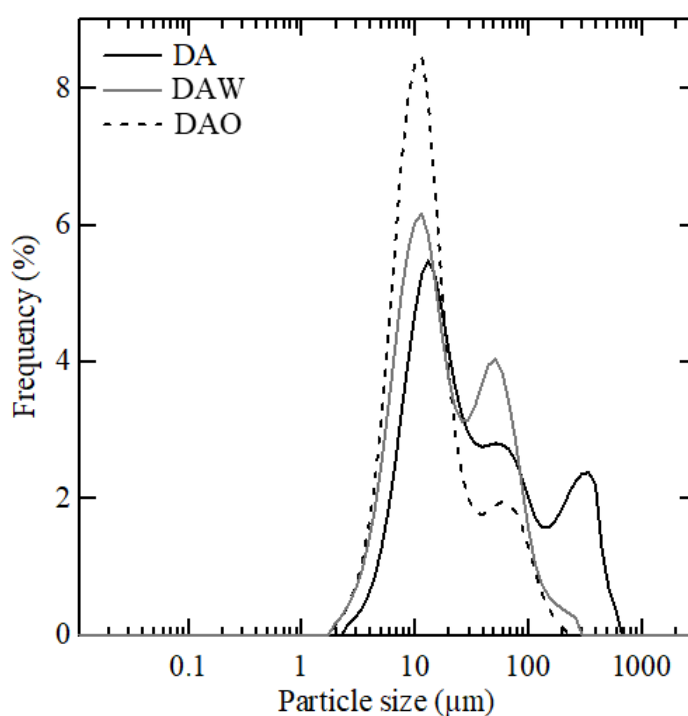


Fig. 6.9. Particle size distribution of untreated DA, DA after 0.1M HCl washing (DAW), and DA after 0.4 M oxalic acid washing (DAO).

Although this agglomeration may be mainly detrimental to the cyanidation process (Andrianandraina et al., 2022), it could also affect the laccase effectiveness because the enzyme preferentially attacks finer particles and small molecules (Setswalo et al., 2019). Additionally,  $\text{Fe}^{3+}$  has been reported to have an inhibitory effect on laccase activity (S. Li et al., 2022). Thus, based on this preliminary information, 0.1M HCl washing was applied before supplying DA for LMS treatment. Fig. 6.9 shows the agglomerates in the size fraction +100/-1000  $\mu\text{m}$  were efficiently removed after HCl washing. Elemental composition by XRF shows the partial reduction in RI of Fe, suggesting the removal of the physically adsorb  $\text{Fe}^{3+}$  from the surface of DA. XRD patterns show that the peaks assigned to jarosite were also partially reduced by the HCl washing (Fig. 6.10). This statement was supported by the decrease in RI of S and Fe from 0.20 to 0.07 and 0.25 to 0.17, respectively (Table 6.4), indicating jarosite was slightly dissolved. Moreover, Fig. 6.11 also shows the reduction of the thermal decomposition peak at 400°C from jarosite (Liu et al., 2007). As for the other mineral phases, as expected, gypsum was dissolved, and the silicates were not affected by the acid washing (Fig. 6.10(a)), as documented by Terry (1983).

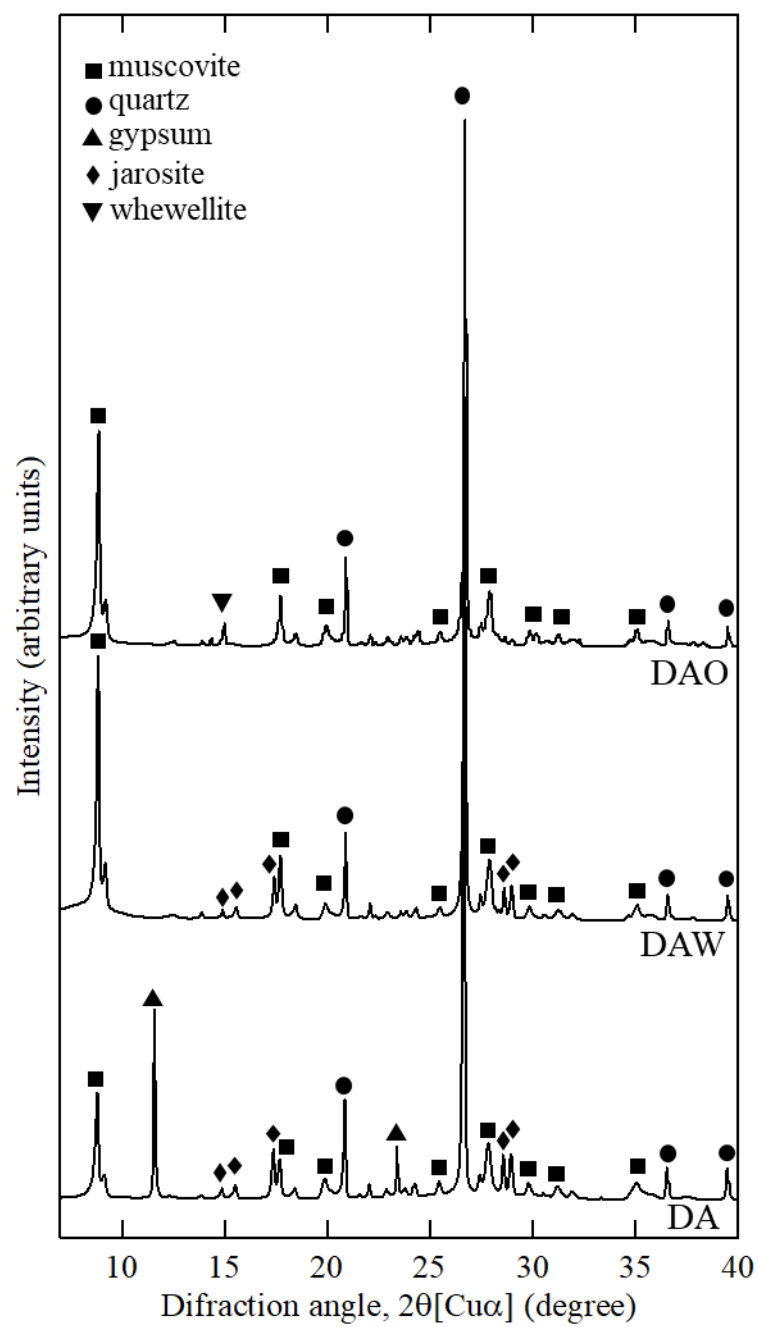


Fig. 6.10. Changes in XRD patterns of as-received BOG (DA), after 0.1M HCl washing (DAW), and after 0.4 M oxalic acid washing (DAO).

Table 6.13. Elemental compositions for DA before and after different washing conditions

Element	DA		DAW		DAO	
	% (w/w)	RI	% (w/w)	RI	% (w/w)	RI
C*	3.92	0.20	4.89	0.21	6.25	0.27
Fe	5.01	0.25	4.09	0.17	1.01	0.04
S	3.96	0.20	1.69	0.07	0.45	0.02
As	0.41	0.02	0.11	0.00	0.03	0.00
Si	20.10	1.00	23.40	1.00	22.93	1.00
Al	8.92	0.44	10.32	0.44	10.70	0.47
Na	1.05	0.05	1.19	0.05	1.33	0.06
Mg	0.39	0.02	0.14	0.01	0.15	0.01
K	2.23	0.11	2.62	0.11	2.43	0.11
Others	54.01	2.69	51.54	2.20	54.72	2.39

\*Determined by CHN analysis. RI: relative intensity

Despite the benefits of 0.1 M HCl washing, jarosite was still observed in XRD (Fig. 6.10), and increasing the concentration of HCl could not lead to further disappearance. Hence, a stronger washing condition for jarosite dissolution was conducted using oxalic acid. Welch et al. (2007) reported that oxalic acid has a high affinity through complexation with  $\text{Fe}^{3+}$ , either as a mono-or di-oxalate complex. The first condition used to remove jarosite from DA was 0.2 M oxalic acid, and the washing kinetics are displayed in Fig. 6.12. The results show that it was necessary to wash at least for 24 h to observe a general dissolution of Fe; however, jarosite did not disappear on XRD patterns (data not shown). For this reason, 0.4 M oxalic acid was used for further washing.

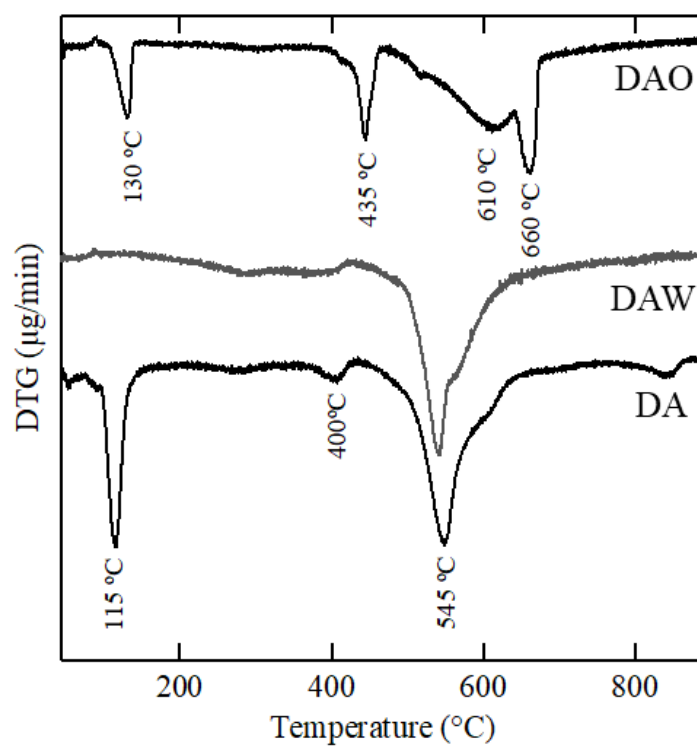


Fig. 6.11. Differential thermogravimetry (DTG) of as-received BOG (DA), after 0.1M HCl washing (DAW), and after 0.4 M oxalic acid washing (DAO).

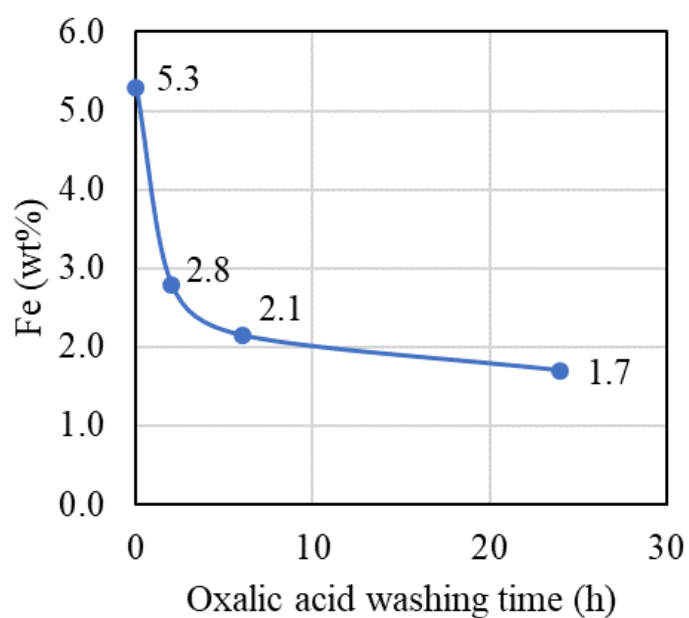


Fig. 6.12. Remaining Fe concentrations (wt%) on DA during 0.2 M oxalic acid washing.

After the optimized oxalic acid washing, jarosite removal was observed by the disappearance of the jarosite peaks in XRD (Fig. 6.10). This is also supported by the large reduction of Fe relative intensity by XRF (Table 6.13) and the frequency between the size fraction +40/-200  $\mu\text{m}$  (Fig. 6.9). Although TG-DTA (Fig. 6.11) also supports jarosite decomposition, the formation of a new phase after the washing was more pronounced. This new component corresponds to whewellite (Fig. 6.10), a hydrated calcium oxalate ( $\text{CaC}_2\text{O}_4 \cdot \text{H}_2\text{O}$ ) that is formed through the precipitation of oxalate and  $\text{Ca}^{2+}$  (Zeng et al., 2021). As reported by Kaloustian et al. (2003), whewellite has three characteristic mass-loss steps. The first (130°C) and the third (660°C) mass-loss correspond to endothermic effects caused by bound water and  $\text{CO}_2$  released after  $\text{CaCO}_3$  oxidation, respectively. Finally, the second mass loss (435°C) corresponds to the exothermic oxidation of  $\text{CaC}_2\text{O}_4$  (Perez-Rodriguez et al., 2011). Having allocated whewellite decomposition peaks, the mass loss observed at 610°C corresponded to the exothermal decomposition of carbonaceous matter. After efficiently removing jarosite and free  $\text{Fe}^{3+}$  from DA, DAO was subjected to LMS treatment.

#### 6.3.4.2. Gold recovery and EPS interference on Lcc/LMS treatment

The positive effect of oxalic acid washing was reflected in the improvement of gold recovery from DA ( $76.6 \pm 0.8\%$ ) to DAO ( $90.0 \pm 0.7\%$ ). The current extraction was already close to the extractable maximum (92.5%) described in section 6.2.1, suggesting that CM deleterious impact could have been hampered to some extent during bio-oxidation. As for the samples after Lcc only and LMS treatment, the gold recovery in all DAOY series (Fig. 6.13), except for DAOY-1, was less than DAO. This reduction had a specific trend in both treatments (Lcc only and LMS), which is related to the

enzyme activity and the addition of mediator. Precisely, when Lcc final concentration was divided and added 7 times, it showed the lowest recovery in each group.

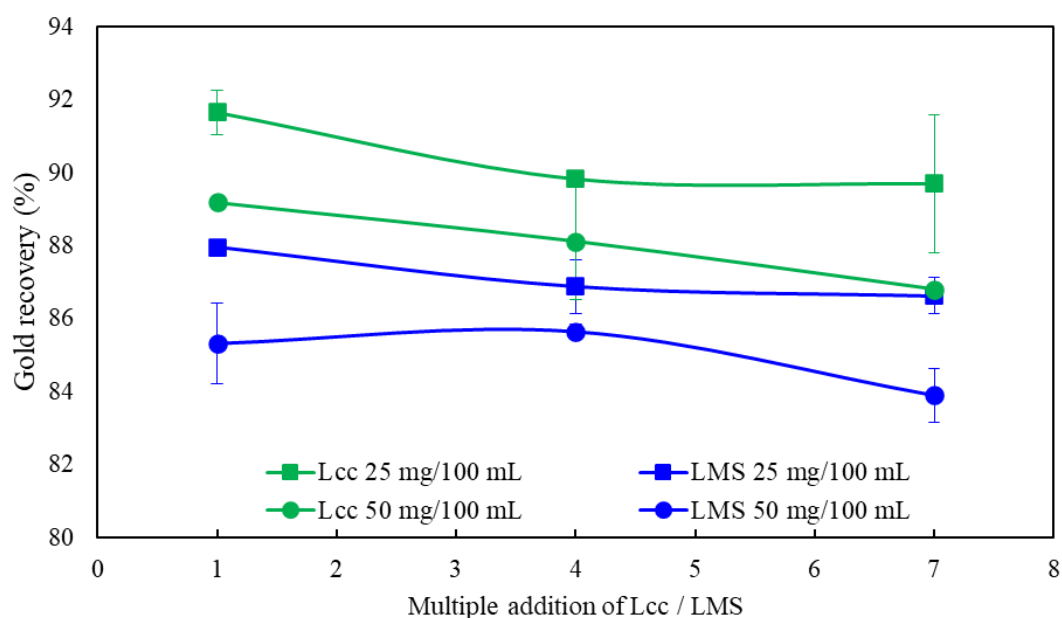


Fig. 6.13. Gold recovery depending on the multiple additions of Lcc with and without mediator.

Considering that Lcc is also spent in the mediator oxidation, it was desirable to maintain the activity by adding Lcc multiple times and evaluating its effect on the system. Part of this effect is observed in the gold recovery, although not as expected. The most likely cause is that enzymatic degradation proceeded on the passivation layer constituted by extracellular polymeric substances (EPS) that coated CM. Yang et al. (2013) reported that EPS secreted by microbes could coat CM during bio-oxidation causing passivation and decreasing its preg-robbing behavior. This inference agrees with DAO's already high gold recovery ( $90.0 \pm 0.7\%$ ). EPS composition varies depending on the microbial



species, environment, and leaching time, but it generally comprises proteins, lipids, sugars, humic and fulvic-like substances (Cao et al., 2011). These organic matters could have acted as a substrate for enzymatic oxidation, leading to the decrease of gold recovery by degrading the passivation layer on CM. This phenomenon was enhanced when Lcc concentration was doubled and by the presence of HBT (Fig. 6.13), inferring that LMS conducted more oxidation than Lcc only.

EPS in DA and DAO was partially characterized by 3D fluorescence after extraction on the DAOY solid residues under alkaline conditions (section 6.2.4) for further understanding. The results are displayed in Fig. 6.14. Based on Chen et al. (2003) method, the organic substances associated with EPS belonged to the humic acid-like ( $Ex/Em = 320/398$ ). This kind of EPS is formed in large batches with long retention times, where enriched bacterial growth predominates (Zhu et al., 2012).

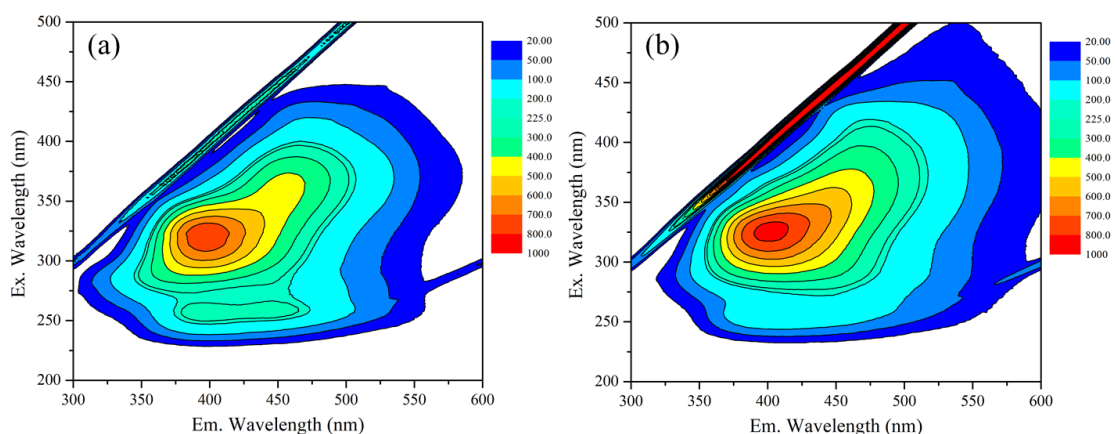


Fig. 6.14. Three-dimensional fluorescence spectrum for the supernatant after 0.2 M NaOH at 60°C washing of (a) DA and (b) DAO.

Sticky EPS was not removed by oxalic acid washing; on the contrary, the intensity slightly increased because EPS was more exposed after jarosite removal. The exposition of these humic acid-like substances made accessible more easily degradable substrates for Lcc and LMS compared to CM (Lisov et al., 2021); therefore, oxidation proceeded similarly in all the conditions, but the oxidation grade could have varied depending on the Lcc concentration, the activity maintenance (addition time), and the presence of mediator. Part of the EPS degradation on DAOY series was observed by TOC (Fig. 6.15) and 3D fluorescence (Fig. 6.16).

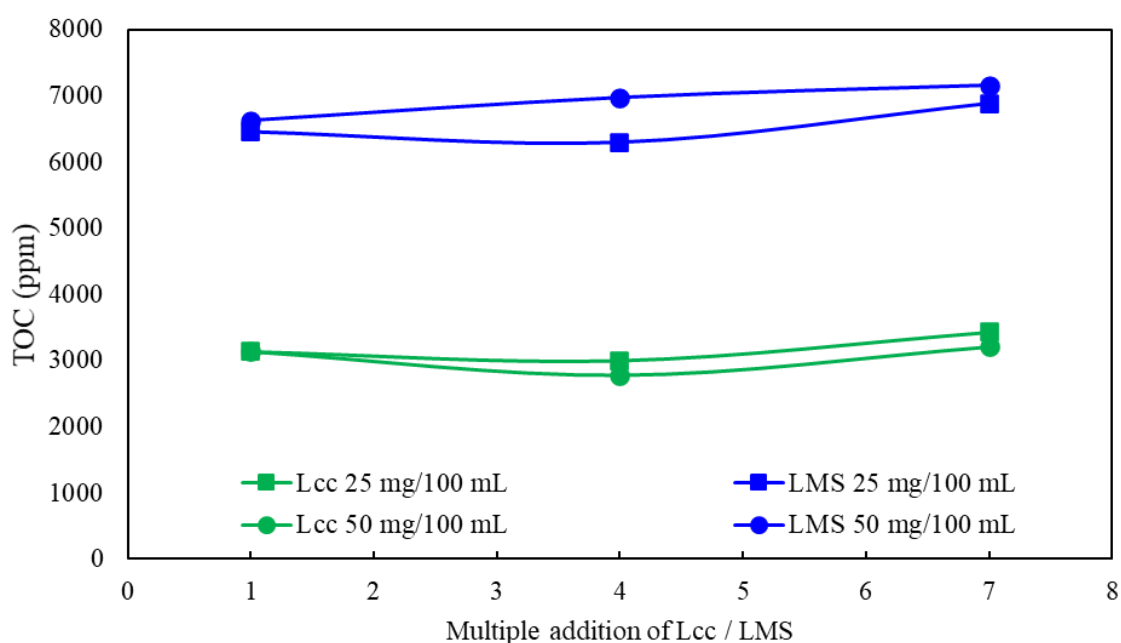


Fig. 6.15. Total organic carbon (TOC) after 7 days of Lcc/LMS reaction on DAO. 25mg/100 mL and 50 mg/100 mL indicates the final concentration of Lcc in the reaction.

TOC at day 0 varied between 2600-2800 mg/L in the DAOY series, and these values slightly increased for Lcc treatment (2772-3133 mg/L) and highly increased for LMS treatment (6451-7151 mg/L), inferring that as for Lcc treatment, a negligible number of EPS was solubilized in the water phase. This was also reflected in 3D fluorescence (Fig. 6.16) by the slight reduction of intensity compared to DAO (Fig. 6.14). The addition of mediator increased the TOC concentration in the supernatant, and the intensity of the humic-like substance fingerprint further reduced the intensity. However, it appears that there is a fraction of degraded EPS that these analytical techniques cannot see because the 3D-fluorescence of each DAOY sample does not have a trend like gold recovery reduction (Fig. 6.13). Table 6.14 summarizes the gold recovery (%) and gives additional information on the laccase and mediator roles in the system. Gold dissolution was observed during the 7 days treatment of Lcc/LMS. Anusaraporn et al., (2022) reported that Lcc could directly oxidize insoluble gold through unknown reaction mechanisms. Then, oxidized gold might be complex with solubilized humic-like substances from Lcc/LMS reaction at pH 4.5 (Baker, 1978; Yang et al., 2013). Under these pH, Zashikhin & Sviridova, (2020) described humic-acid-like substances has the most active fraction for gold chelation. In the DAOY series, the highest gold dissolution was observed on DAOY-12.

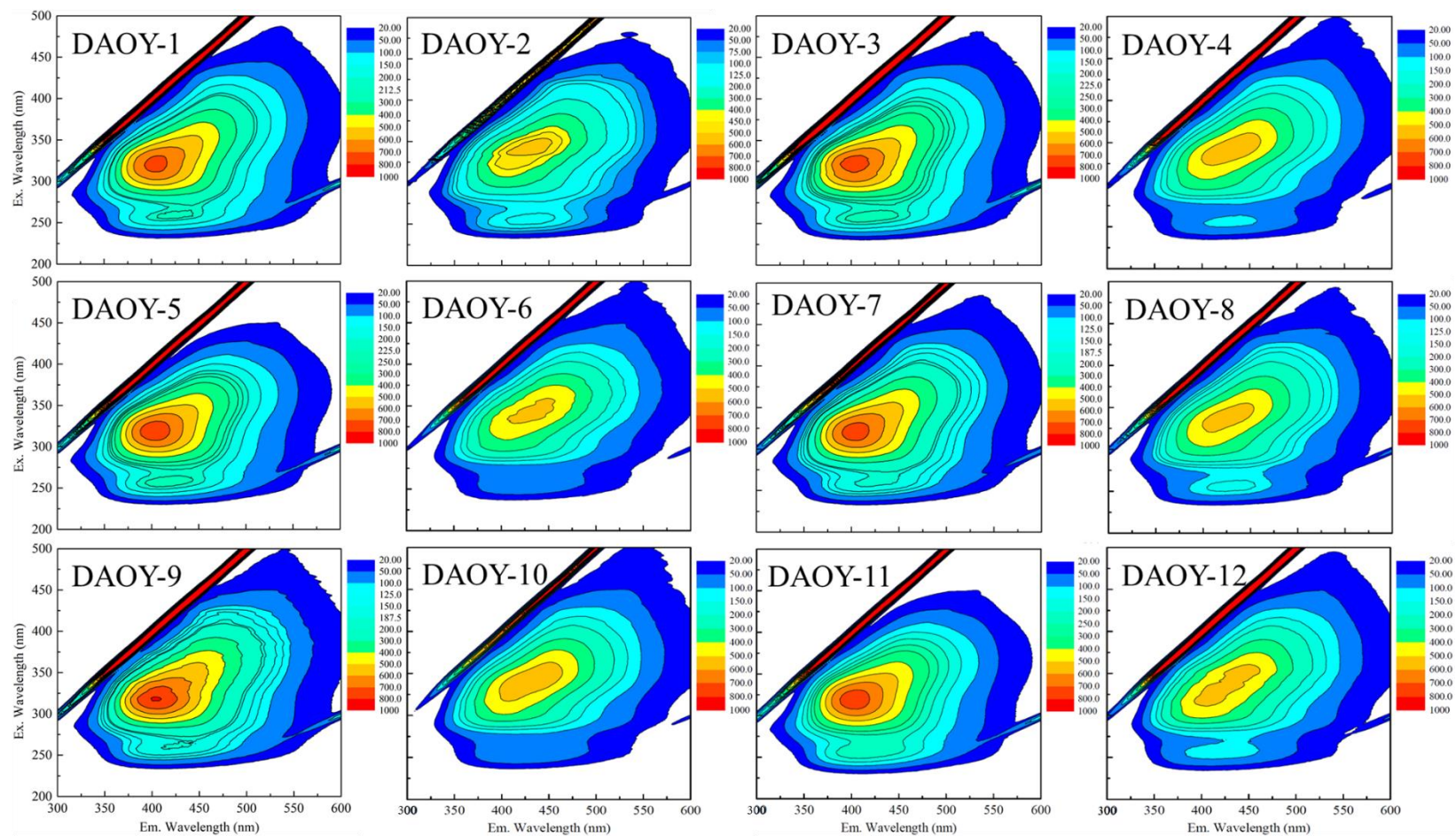


Fig. 6.16. Three-dimensional fluorescence spectrum for the supernatant after 0.2 M NaOH at 60°C washing of DAOY series .

Table 6.14. Summary of DAOY series gold recovery, C (wt%) and TOC (mg/L)

Sample	Supernatant (g/t)	Cyanidation (g/t)	Acid dig. (g/t)	Total (g/t)	Gold recovery (%)	C (wt%)	TOC (mg/L) in supernatant
DA	0.0	19.9	6.1	26.0	76.6 ± 0.8	3.9	-
DAO	0.0	26.7	3.0	29.7	89.9 ± 0.7	6.3	-
DAOY-1	0.0	23.9	2.2	26.1	91.7 ± 0.6	6.2	3133.0
DAOY-2	0.1	19.2	2.6	21.9	88.0 ± 0.1	6.3	6451.0
DAOY-3	0.0	23.7	2.7	26.3	89.8 ± 0.1	5.8	2999.0
DAOY-4	0.1	23.3	3.5	27.0	86.9 ± 0.7	6.0	6292.0
DAOY-5	0.0	25.7	3.0	28.7	89.7 ± 1.9	6.0	3243.0
DAOY-6	0.2	21.0	3.3	24.5	86.6 ± 0.5	6.5	6878.0
DAOY-7	0.0	24.6	3.0	27.6	89.2 ± 0.1	6.3	3138.0
DAOY-8	0.2	22.7	3.9	26.8	86.3 ± 1.1	6.1	6622.0
DAOY-9	0.0	25.2	3.4	28.6	88.1 ± 1.6	6.2	2772.0
DAOY-10	0.2	24.2	4.1	28.5	85.6 ± 0.2	6.2	6967.0
DAOY-11	0.0	26.3	4.0	30.3	86.8 ± 0.2	6.4	3211.0
DAOY-12	0.3	24.8	4.8	29.9	83.9 ± 0.7	6.4	7151.0

TOC: Total organic carbon.

Gold recovery is a technique that indirectly evaluates carbonaceous matter degradation; however, it depends on the cyanidation conditions and the components involved in that. In this case, an individual cyanidation test using stronger KCN concentrations was conducted using DAO and DAOY-12. Unfortunately, gold recovery did not improve and kept the same trend (Fig. 6.17), suggesting that EPS degradation by laccase was detrimental in this case because EPS acted as a passivation layer on CM.

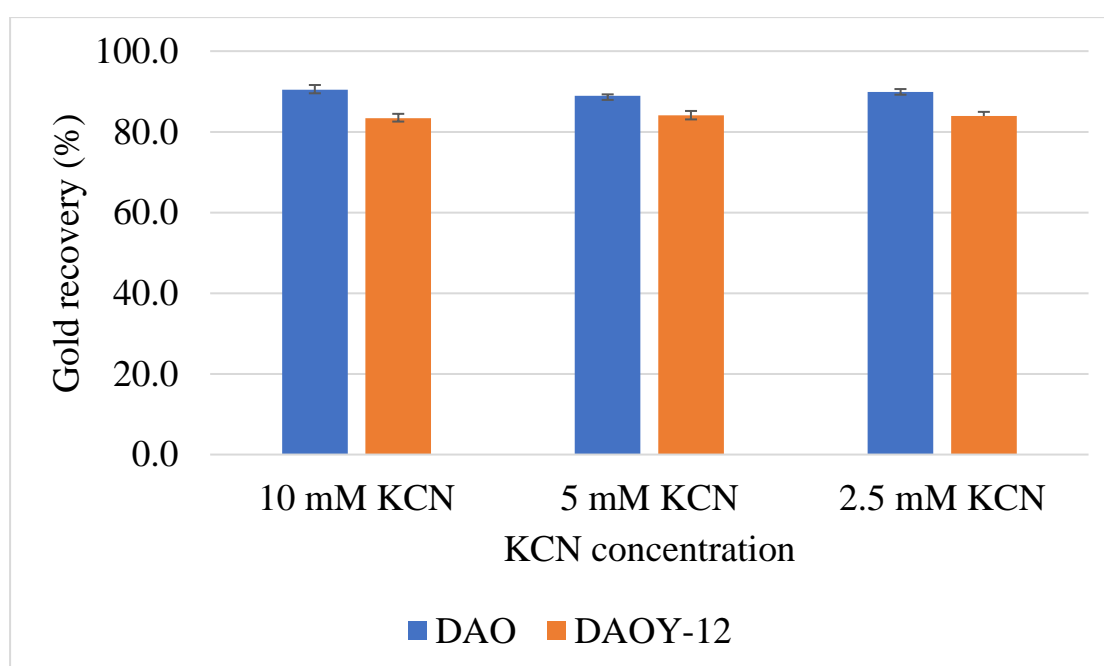


Fig. 6.17. Gold recovery on DAO and DAOY-12 under strong cyanide concentration.

#### 6.3.4.3. Preg-robbing test and Raman spectroscopy

The presence of EPS and their interference during cyanidation did not help to differentiate between EPS and CM degradation. Therefore, the preg-robbing test and Raman spectroscopy were used to observe if Lcc/LMS had a degradation effect on CM decomposition.

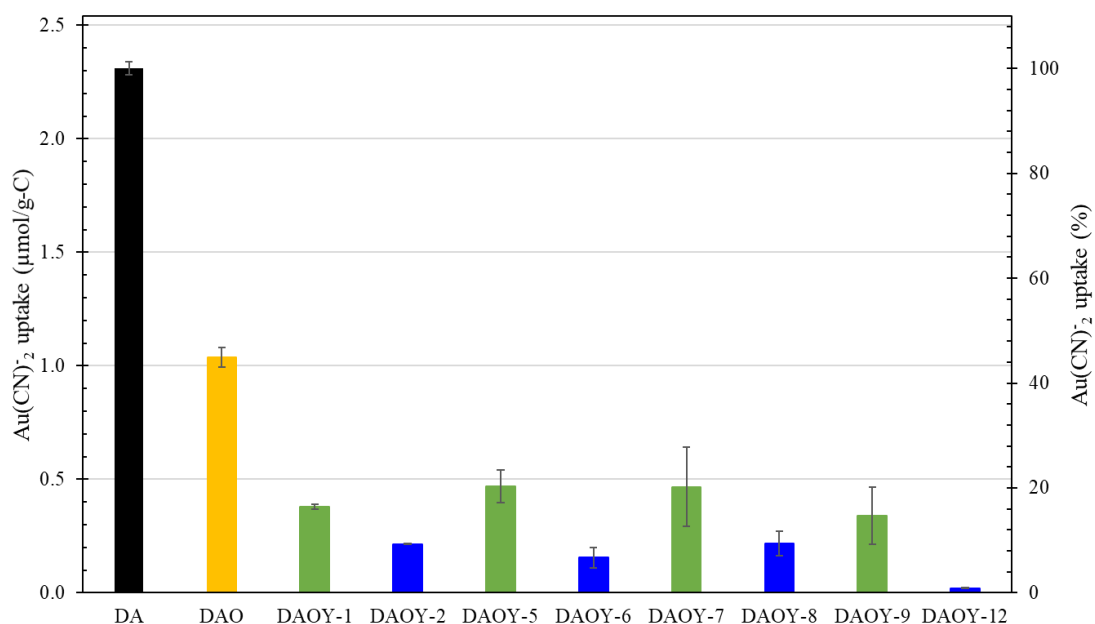


Fig. 6.18. Uptake of  $\text{Au(CN)}_2^-$  on DA, DAO and Lcc/LMS treated DAO ( $n=2$ ).

Fig. 6.18 shows DA adsorbed  $2.3 \mu\text{mol Au/g C}$ , representing 100%. Oxalic washing decreased 65% of the gold-robbing ability of CM, and this might be due to the removal of jarosite and the exposition of acid-soluble CM present in DA, causing the reduction of the  $I_D/I_G$  from 1.12 to 0.98. DAOY-1, which improved ~2% the gold recovery decreased the preg-robbing ability of CM, suggesting that under this condition Lcc reached CM without affecting EPS. However, a further decrease was observed in the strongest condition of LMS (DAOY-12), where the gold robbing decreased to 1%, inferring that LMS treatment under this condition could attack the not passivated CM after bio-oxidation. Moreover, LMS preferentially oxidized defective carbon (D-band) because the  $I_D/I_G$  on DAOY-12 decreased from 0.98 to 0.90 (Fig. 6.19).

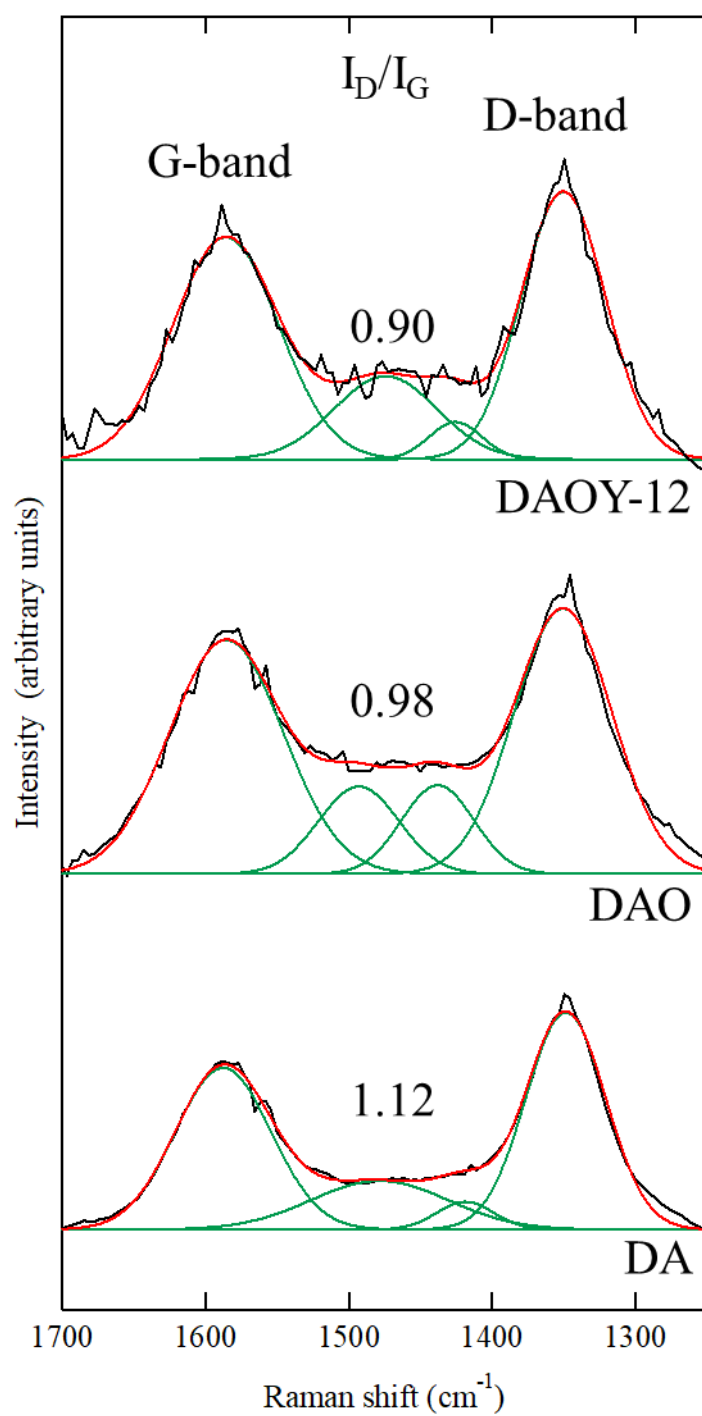


Fig. 6.19. Changes in Raman spectra for solid residues before and after LMS treatment for CM degradation in a region from  $1200\text{ cm}^{-1}$  to  $1700\text{ cm}^{-1}$  with relative intensities of  $I_D/I_G$ .



#### 6.3.4.4. Interpretation of EPS interference and LMS treatment

Microorganisms involved in pyrite oxidation secrete EPS for attachment on the mineral surface (Natarajan, 2018). Under strong acidic conditions (pH 1.5), pyrite and CM are negatively charged; therefore, cell attachment occurs through electrochemical interactions mediated by exopolymer-complexed iron (III) ions (Gehrke et al., 1998; Kinzler et al., 2003). Strong biooxidation leads to EPS growth, creating a passivation layer on CM (Yang et al., 2013). Then, constantly produced  $\text{Fe}^{3+}$  through bio-oxidation is adsorbed on EPS and facilitates jarosite formation on this layer. As a result, the formation of a second layer on CM is expected (Li et al., 2020), as illustrated in Fig. 6.20. Oxalic acid washing efficiently removed jarosite, leaving sticky EPS exposed during Lcc/LMS treatment. In this stage, Lcc participates in a series of reactions involving EPS degradation, CM degradation, and gold oxidation. The current findings infer that keeping the enzyme activity by enzyme doses promotes the above-described reactions.

These effects were further enhanced when HBT participated in the system because HBT has a higher redox potential than Lcc and a small size, enabling LMS to promote the oxidation of different organic substrates, including non-phenolic molecules, through hydrogen atom transfer mechanisms and radical formation (Galli & Gentili, 2004; Hilgers et al., 2020).

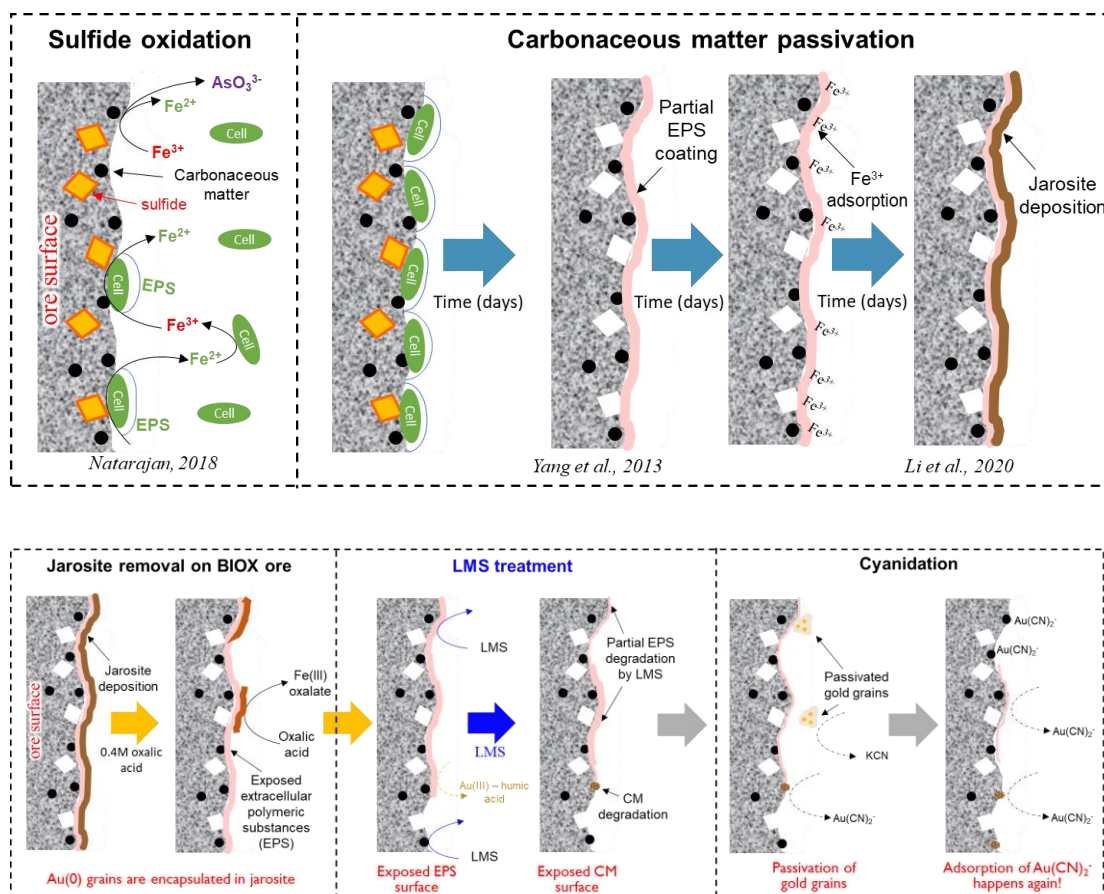


Fig. 6.20. Graphical interpretation of extracellular polymeric substances (EPS) formation during bio-oxidation and its interference on LMS reaction on BOG.

### 6.3.5. GC-MS characterization after LMS treatment on SYM

The bio-oxidation step was replaced with ferric chloride leaching to avoid the formation of jarosite, especially EPS. Fig. 6.21 illustrates the sequential pre-treatment of SYM, including LMS treatment. In this way, the carbonaceous matter is aimed to be the primary carbon source for LMS degradation. In addition, by-products after LMS were characterized by GC-MS for further understanding.

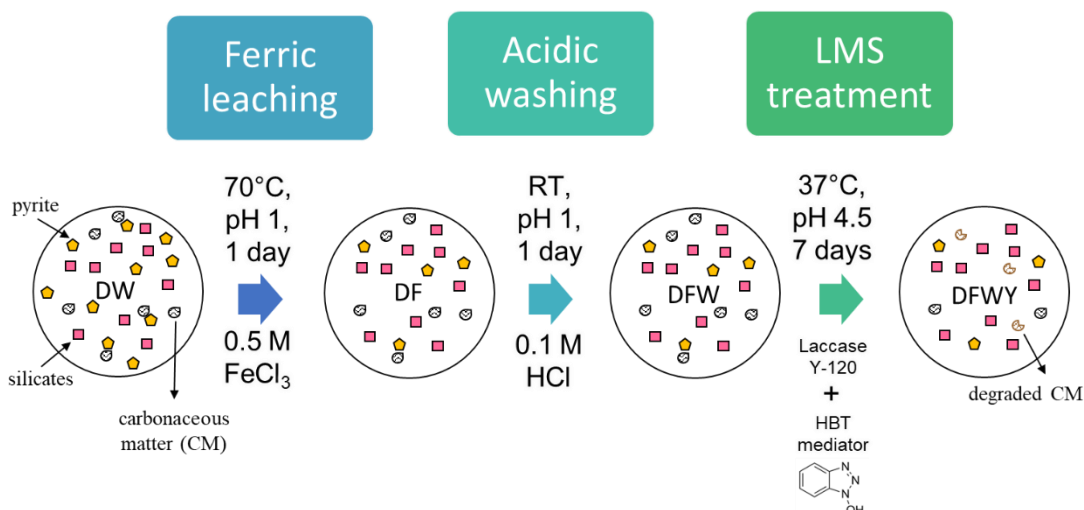


Fig. 6.21. Sequential pre-treatment of SYM including laccase-mediator system.

GC-MS results showed the non-polar fraction of LMS-treated SYM has negligible changes in the total ion chromatogram (TIC), as no particular new peaks appeared after hexane extraction (Fig. 6.22(b)). On the contrary, the TIC on the ethyl acetate phase displayed an increase in absolute intensity due to the appearance of several new peaks. The mediator 1-hydroxybenzotriazole (HBT) possesses a unique peak at 7.92 min retention time (RT), also detected in the acetone phase. Table 6.15 lists the peak assignment on ethyl acetate fraction, revealing the presence of new aliphatic moieties and an increase in the intensity of the oxygen-containing functional groups, including fatty acids, ether, ester, and ketones. The second prominent peak (RT = 13.47 min) on this fraction is assigned to the fatty acid hexadecenoic acid.

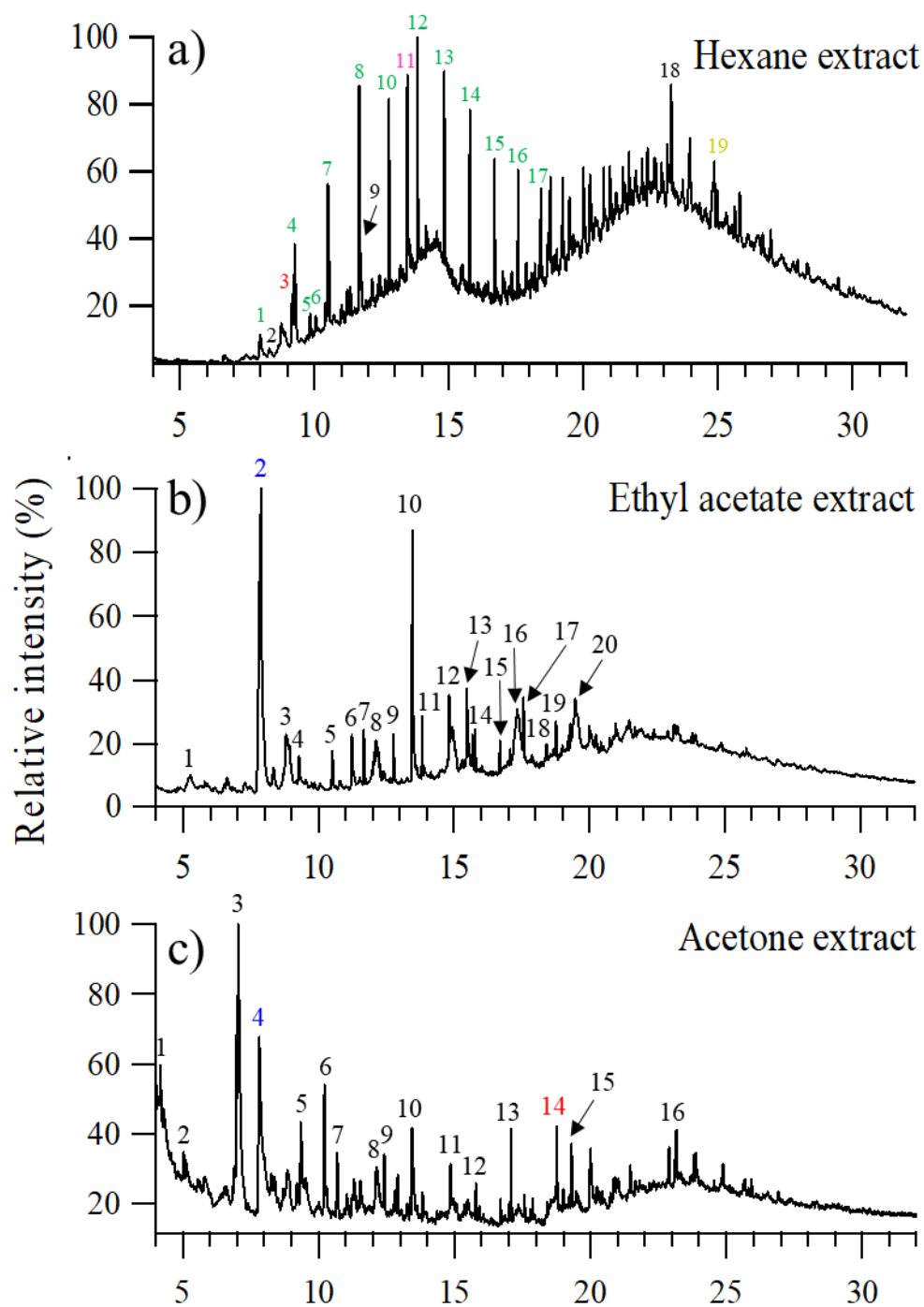
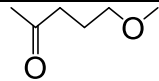
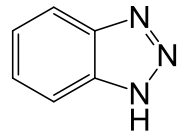
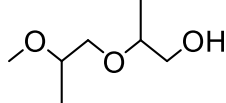
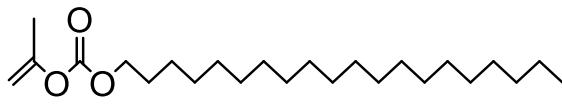

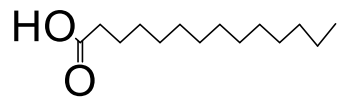

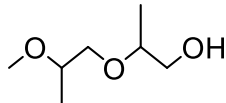

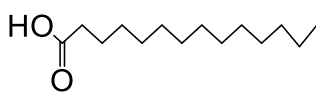

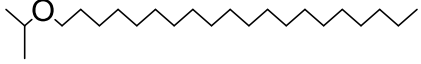
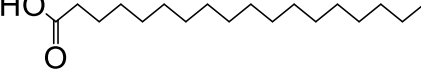
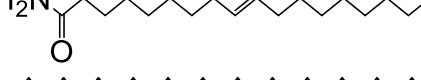
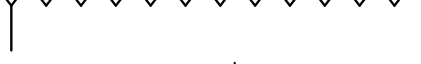
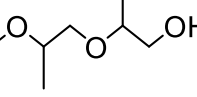
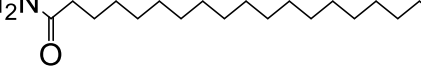

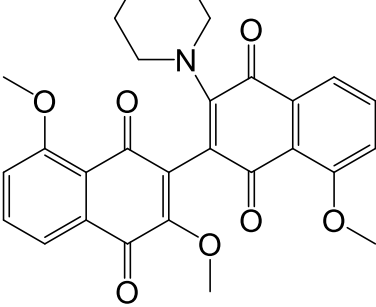


Fig. 6.22. GC-MS total ion chromatograms of (a) hexane, (b) ethyl acetate, and (c) acetone extracts from SYM after sequential extraction.

Table 6.15. Intermediates detected by GC-MS in Fig. 6.22(b) for extracted compounds in ethyl acetate on the LMS-treated SYM

Peak No.	Similarity (%)	Retention time (min)	Most similar compound suggest by NIST library	Type of compound	Chemical structure
1	82	5.25	2-pentanone, 5-methoxy-	ketone	
2	93	7.92	1H-benzotriazole	aromatic (mediator)	
3	87	8.88	2-(2-methoxypropoxy)-1-propanol	ether	
4	86	9.25	carbonic acid, decyl prop-1-en-2-yl ester	ester	
5	91	10.51	eicosane, 10-methyl-	alkane	
6	93	11.17	tetradecanoic acid	fatty acid	
7	92	11.68	eicosane	alkane	
8	86	12.14	2-(2-methoxypropoxy)-1-propanol	ether	
9	89	12.73	eicosane	alkane	
10	94	13.47	hexadecanoic acid	fatty acid	

Peak No.	Similarity (%)	Retention time (min)	Most similar compound suggest by NIST library	Type of compound	Chemical structure
11	92	13.84	eicosane	alkane	
12	81	14.81	eicosyl isopropyl ether	ether	
13	93	15.54	stearic acid	fatty acid	
14	83	15.69	9-octadecenamide	fatty amide	
15	91	16.66	2-methylhexacosane	alkane	
16	79	17.32	2-(2-methoxypropoxy)-1-propanol	ether	
17	82	17.54	nonadecanamide	fatty amide	
18	87	18.43	dotriacontyl isopropyl ether	ether	
19	82	18.73	3',8,8'-Trimethoxy-3-piperidyl-2,2'-binaphthalene-1,1',4,4'-tetrone	polyaromatic	

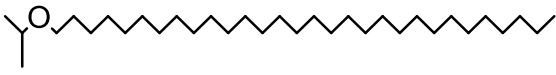
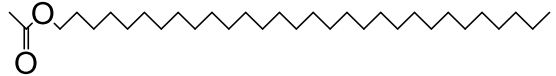
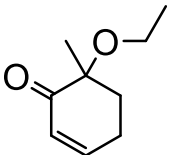
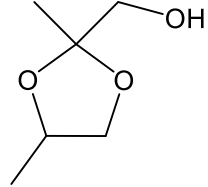
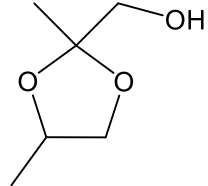
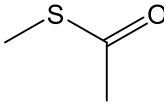
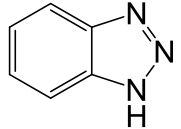
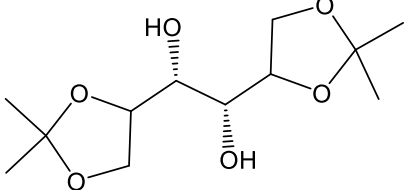
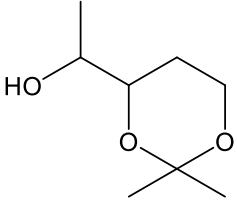
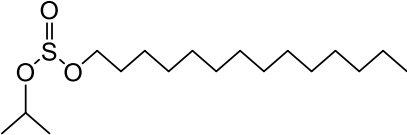
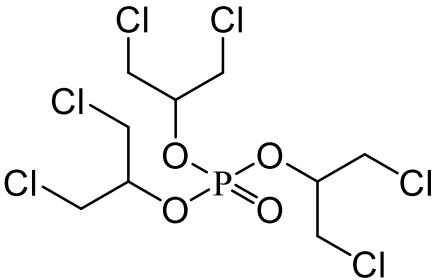
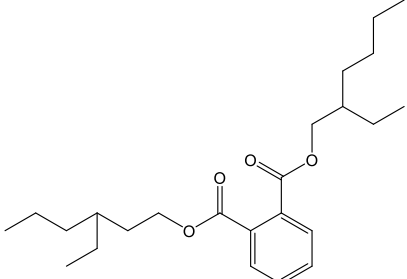
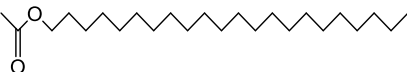
Peak No.	Similarity (%)	Retention time (min)	Most similar compound suggest by NIST library	Type of compound	Chemical structure
20	84	19.17	dotriacontyl isopropyl ether	ether	
21	81	19.47	triacontyl acetate	acetate	
22	75	19.99	6-ethoxy-6-methylcyclohex-2-en-1-one	aromatic	

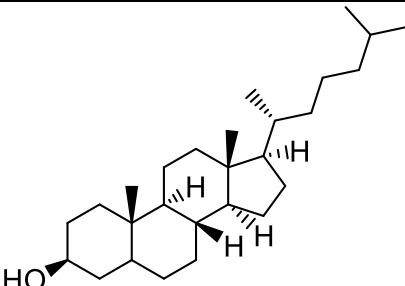
Table 6.16. Intermediates detected by GC-MS in Fig. 6.22(c) for extracted compounds in acetone on the LMS-treated SYM

Peak No.	Similarity (%)	Retention time (min)	Identified/suggested compound	Type of compound	Chemical structure
1	86	4.17	1,3-dioxolane-2-methanol, 2,4-dimethyl-	dioxalane	
2	86	5.01	1,3-dioxolane-2-methanol, 2,4-dimethyl-	dioxalane	
3	81	7.03	S-methyl ethanethioate	thioester	
4	89	7.92	1H-benzotriazole	aromatic (mediator)	
5	81	9.36	(1S,2S)-1,2-bis[(4R)-2,2-dimethyl-1,3-dioxolan-4-yl]ethane-1,2-diol	dioxalane	



Peak No.	Similarity (%)	Retention time (min)	Identified/suggested compound	Type of compound	Chemical structure
6	81	10.20	acetic acid, thio-, S,S'-thiodimethylene ester	methylthioester	
7	79	10.69	1,4-dioxane-2,3-diol, diacetate	dioxalane	
8	79	12.13	methyl 3,4-O-isopropylidene-L-threonate	dioxalane	
9	69	12.42	3-acetyl-1-phenyl-4,5-dihydro-1H-[1,2,4]triazin-6-one	aromatic	
10	88	13.44	hexadecanoic acid	fatty acid	

Peak No.	Similarity (%)	Retention time (min)	Identified/suggested compound	Type of compound	Chemical structure
11	73	14.83	1-(2,2-Dimethyl[1,3]dioxan-4-yl)ethanol	dioxalane	
12	87	15.78	sulfurous acid, 2-propyl tetradecyl ester	ester	
13	85	17.10	tris(1,3-dichloroisopropyl)phosphate	contaminant	
14	87	18.75	phthalic acid, bis(2-ethylhexyl) ester	contaminant from plastic clamp	
15	90	19.32	1-docosanol, acetate	carboxylic ester	

Peak No.	Similarity (%)	Retention time (min)	Identified/suggested compound	Type of compound	Chemical structure
16	70	23.15	cholesta-4,6-dien-3-ol, (3.β.)-	steroid	 <p>The chemical structure is a steroid molecule with four fused rings (A, B, C, D). It features a hydroxyl group (HO-) at the 3-position of the A ring. There are double bonds at the 4 and 6 positions of the B ring. The D ring has a side chain consisting of a methyl group at C-13, a methylene group at C-14, and a branched alkyl chain at C-15. Stereochemistry is indicated with wedges and dashes at various chiral centers.</p>

The presence and increment of the fatty acids and aliphatic carbon indicate that LMS degradation went through the disruption of aromatic moieties present in CM, similarly described in Zhang et al. (2022). The current findings are in accordance with the GC-MS results of powder-activated carbon (PAC) degradation in chapter 5. Moreover, the most notable changes and increments in the LMS intermediates come from the polar phase. This premise infers that the presence of more hydrophilic intermediate compounds on the surface of CM coming from LMS treatment might have helped to decrease the preg-robbing ability in SYM because  $\text{Au}(\text{CN})_2^-$  has less affinity with hydrophilic surfaces. As a result, the final gold recovery after LMS treatment increased to  $86.3 \pm 4.1 \%$  (Fig. 6.23).

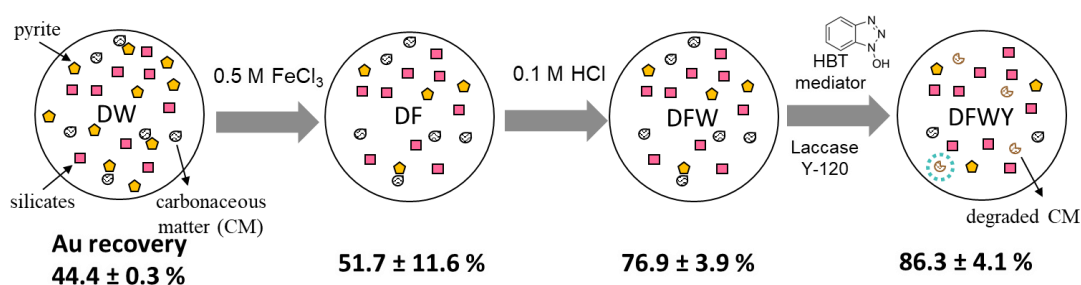


Fig. 6.23. Gold recoveries from the solid residues in SYM sequential pre-treatment, including laccase-mediator system (LMS).

## 6.4. Conclusions

Sequential extraction of organic compounds was carried out in three carbonaceous gold ores. Raman spectroscopy helped to predict the preg-robbing ability of the CM through the  $I_D/I_G$ , indicating that the increasing in this value reflects more preg-robbing

behaviors, as shown by SYM. TG-DTA could not help to differentiate the combustion range for CM because carbon is combusted under a similar temperature range, where CO<sub>2</sub> and SO<sub>2</sub> coming from pyrite thermal oxidation are released. Most of the compounds extracted by hexane were saturated aliphatic hydrocarbons in the three ores. Ethyl acetate dissolved overall non-polar and polar organic compounds like alkanes, ethers, fatty acids, and aromatic moieties containing oxygen-functional groups (SYM). Acetone extracted several fatty acid amides (PXX), hydroxyl and carbonyl groups. PXX appears to be the less mature of the three ores, resulting in a low preg-robbing ability. As for SYM, the presence of several aromatic moieties could be related to its highly preg-robbing capacity. The presence of EPS in BOG interfered with the extraction, not allowing accurate characterization. The EPS passivation layer appears to be an obstacle to enzymatic degradation due to its nature as an easily degradable carbon substrate. However, keeping Lcc activity through daily dose addition maintains the oxidation conditions to the extent of degrading CM despite EPS interference. However, gold recoveries still are affected by the degradation of the EPS layer and gold particles passivation. Lcc also participates in reactions involving gold oxidation and further complexation through humic-acid-like substances from EPS. CM degradation was observed by the reduction of preg-robbing and Raman relative intensity. Removal of EPS could be beneficial to lead laccase treatment target CM degradation to a complete extent.

Besides, GC-MS characterization on LMS-treated SYM, where biooxidation was not included as part of the sequential bio-treatment, revealed the abundance of hydrophilic compounds on the surface of CM, suggesting the beneficial effect of LMS treatment to degrade carbonaceous matter, without focusing on other substrates like EPS, leading to

the reduction of  $\text{Au}(\text{CN})_2^-$  adsorption. Further quantitative studies are necessary to correlate these findings with other carbon characterization techniques.

## References

Adams, M. D. (1990) The mechanism of adsorption of aurocyanide onto activated carbon, 1. Relation between the effects of oxygen and ionic strength. *Hydrometallurgy*, 25(2), 171–184.

Alessandra, P., Cinzia, P., Paola, G., Vincenza, F., & Sannia, G. (2010) Heterologous laccase production and its role in industrial applications. *Bioengineered Bugs*, 1(4), 252–262.

Andrianandraina, S. H., Dionne, J., Darvishi-Alamdari, H., & Blais, J. F. (2022) Effect of grain size on the bacterial oxidation of a refractory gold sulfide concentrate and its dissolution by cyanidation. *Minerals Engineering*, 176, 107360.

Anusaraporn, S., Dolphen, R., & Thiravetyan, P. (2022) Importance of laccase enzyme and triiodide for gold leaching from silicate ore by marine bacterium *Acinetobacter* sp. *Process Safety and Environmental Protection*, 161, 788–800.

Arrascue, M. E. L., & van Niekerk, J. (2006) Biooxidation of arsenopyrite concentrate using BIOX® process: Industrial experience in Tamboraque, Peru. *Hydrometallurgy*, 83(1–4), 90–96.

Asamoah, R. K. (2021) Specific refractory gold flotation and bio-oxidation products: Research overview. In *Minerals*, 11(1), 1–14.

- Baker, W. E. (1978) The role of humic acid in the transport of gold. *Geochimica et Cosmochimica Acta*, 42(6), 645–649.
- Bhardwaj, P., Kaur, N., Selvaraj, M., Ghramh, H. A., Al-Shehri, B. M., Singh, G., Arya, S. K., Bhatt, K., Ghotekar, S., Mani, R., Chang, S. W., Ravindran, B., & Awasthi, M. K. (2022) Laccase-assisted degradation of emerging recalcitrant compounds – A review. *Bioresource Technology*, 364, 128031.
- Bokobza, L., Bruneel, J.-L., & Couzi, M. (2015) Raman Spectra of Carbon-Based Materials (from Graphite to Carbon Black) and of Some Silicone Composites. *C*, 1(1), 77–94.
- Cao, B., Shi, L., Brown, R. N., Xiong, Y., Fredrickson, J. K., Romine, M. F., Marshall, M. J., Lipton, M. S., & Beyenal, H. (2011) Extracellular polymeric substances from *Shewanella sp.* HRCR-1 biofilms: Characterization by infrared spectroscopy and proteomics. *Environmental Microbiology*, 13(4), 1018–1031.
- Chen, W., Wee, P., & Brindle, I. D. (2000) Elimination of the memory effects of gold, mercury and silver in inductively coupled plasma atomic emission spectroscopy. *Journal of Analytical Atomic Spectrometry*, 15(4), 409–413.
- Chen, W., Westerhoff, P., Leenheer, J. A., & Booksh, K. (2003) Fluorescence excitation-emission matrix regional integration to quantify spectra for dissolved organic matter. *Environmental Science and Technology*, 37(24), 5701–5710.
- Chen, Y., Mori, S., & Pan, W. P. (1995) Estimating the combustibility of various coals by TG-DTA. *Energy and Fuels*, 9(1), 71–74.

- Chen, Y., Mori, S., & Pan, W. P. (1996) Studying the mechanisms of ignition of coal particles by tg-dta. *Thermochimica Acta*, 275(1), 149–158.
- Christopher, L. P., Yao, B., & Ji, Y. (2014) Lignin biodegradation with laccase-mediator systems. *Frontiers in Energy Research*, 2, 1-13.
- Cindy, Sakai, R., Mendoza, D. M., Konadu, K. T., & Sasaki, K. (2021) Significance of acid washing after biooxidation of sulfides in sequential biotreatment of double refractory gold ore from the syama mine, Mali. *Minerals*, 11(12).
- Conrad, A., Kontro, M., Keinänen, M. M., Cadoret, A., Faure, P., Mansuy-Huault, L., & Block, J. C. (2003) Fatty acids of lipid fractions in extracellular polymeric substances of activated sludge flocs. *Lipids*, 38(10), 1093–1105.
- Dembitsky, V. M., Shkrob, I., & Rozentsvet, O. A. (2000) Fatty acid amides from freshwater green alga *Rhizoclonium hieroglyphicum*. *Phytochemistry*, 54(8), 965–967.
- Galli, C., & Gentili, P. (2004) Chemical messengers: Mediated oxidations with the enzyme laccase. *Journal of Physical Organic Chemistry*, 17(11), 973–977.
- Gehrke, T., Telegdi, J., Thierry, D., & Sand, W. (1998) Importance of extracellular polymeric substances from *Thiobacillus ferrooxidans* for bioleaching. *Applied and Environmental Microbiology*, 64(7), 2743–2747.
- Han, Z., Wang, H., Zheng, J., Wang, S., Yu, S., & Lu, L. (2023) Ultrafast synthesis of laccase-copper phosphate hybrid nanoflowers for efficient degradation of tetracycline antibiotics. *Environmental Research*, 216, 114690.



Hilgers, R., Van Erven, G., Boerkamp, V., Sulaeva, I., Potthast, A., Kabel, M. A., & Vincken, J. P. (2020) Understanding laccase/HBT-catalyzed grass delignification at the molecular level. *Green Chemistry*, 22(5), 1735–1746.

Hu, Y., Chen, X., Mu, S., & Li, Q. (2022) Extraction and separation of petroleum pollutants from oil-based drilling cuttings using methanol/n-hexane solvent. *Process Safety and Environmental Protection*, 168, 760–767.

Hussain, A., Bilal, M., Rafeeq, H., Jabeen, Z., Afsheen, N., Sher, F., Kumar, V., Bharagava, R. N., Ferreira, L. F. R., & Iqbal, H. M. N. (2022) Role of laccase in the pulp and paper industry. *Nanotechnology in Paper and Wood Engineering: Fundamentals, Challenges and Applications*, 35–60.

Ibarra, D., Romero, J., Martínez, M. J., Martínez, A. T., & Camarero, S. (2006) Exploring the enzymatic parameters for optimal delignification of eucalypt pulp by laccase-mediator. *Enzyme and Microbial Technology*, 39(6), 1319–1327.

Imran, M., Asad, M. J., Hadri, S. H., & Mehmood, S. (2012) Production and industrial applications of laccase enzyme. *Journal of Cell and Molecular Biology*, 10(1), 1–11.

Kaloustian, J., El-Moselhy, T. F., & Portugal, H. (2003) Determination of calcium oxalate (mono- and dihydrate) in mixtures with magnesium ammonium phosphate or uric acid: The use of simultaneous thermal analysis in urinary calculi. *Clinica Chimica Acta*, 334(1–2), 117–129.

Kinzler, K., Gehrke, T., Telegdi, J., & Sand, W. (2003) Bioleaching - A result of interfacial processes caused by extracellular polymeric substances (EPS). *Hydrometallurgy*, 71(1–2), 83–88.

- Konadu, K. T., Huddy, R. J., Harrison, S. T. L., Osseo-Asare, K., & Sasaki, K. (2019a) Sequential pretreatment of double refractory gold ore (DRGO) with a thermophilic iron oxidizing archaeon and fungal crude enzymes. *Minerals Engineering*, 138, 86–94.
- Konadu, K. T., Harrison, S. T. L., Osseo-asare, K., & Sasaki, K. (2019b) Transformation of the carbonaceous matter in double refractory gold ore by crude lignin peroxidase released from the white-rot fungus. *International Biodeterioration and Biodegradation*, 143, 104735.
- Li, Q., Shen, H., Xu, R., Zhang, Y., Yang, Y., Xu, B., Jiang, T., & Yin, H. (2020) Effect of *Acidithiobacillus ferrooxidans* and *Leptospirillum ferrooxidans* on preg-robbing of gold by graphite from thiourea leaching solution. *Journal of Cleaner Production*, 261, 121122.
- Li, S., Liu, Q., Liu, J., Sun, K., Yang, W., Si, Y., & Li, Y. (2022) Chemosphere Inhibition mechanisms of  $\text{Fe}^{2+}/\text{Fe}^{3+}$  and  $\text{Mn}^{2+}$  on fungal laccase-enabled bisphenol a polyreaction. *Chemosphere*, 307(P1), 135685.
- Lisov, A., Belova, O., Zavarzina, A., Konstantinov, A., & Leontievsky, A. (2021) The role of laccase from Zygomycetous fungus *Mortierella elasson* in humic acids degradation. *Agronomy*, 11(11), 2169.
- Liu, J., Li, B., Zhong, D., Le-xian, X., & Qiu, G. (2007) Preparation of jarosite by *Acidithiobacillus ferrooxidans* oxidation. 4, 1139–1143.
- Liu, L., Liu, Q., Zhang, S., Li, Y., & Yang, L. (2022) The thermal transformation behavior and products of pyrite during coal gangue combustion. *Fuel*, 324, 124803.

- Miki, T. (1983) Graphitization of carbonaceous matter in sedimentary rocks. *Journal of the Sedimentological Society of Japan*, 111–120.
- Minussi, R. C., Pastore, G. M., & Durán, N. (2002) Potential applications of laccase in the food industry. *Trends in Food Science & Technology*, 13(6–7), 205–216.
- Natarajan, K. A. (2018) Microbiological Aspects of Leaching Microorganisms. In *Biotechnology of Metals*, 29–47.
- Ng, W. S., Yang, Y., Su, X., Zhong, S., & Chen, M. (2022) Characterization of preg-robbing carbonaceous minerals from the Shuiyindong carlin-type gold deposit via spectroscopic techniques. *Mining, Metallurgy and Exploration*, 39(1), 169–188.
- Ofori-Sarpong, G., Osseo-Asare, K., & Tien, M. (2013) Mycohydrometallurgy: Biotransformation of double refractory gold ores by the fungus, *Phanerochaete chrysosporium*. *Hydrometallurgy*, 137, 38–44.
- Pandi, A., Marichetti Kuppuswami, G., Numbi Ramudu, K., & Palanivel, S. (2019) A sustainable approach for degradation of leather dyes by a new fungal laccase. *Journal of Cleaner Production*, 211, 590–597.
- Perez-Rodriguez, J. L., Duran, A., Centeno, M. A., Martinez-Blanes, J. M., & Robador, M. D. (2011) Thermal analysis of monument patina containing hydrated calcium oxalates. *Thermochimica Acta*, 512(1–2), 5–12.
- Sakai, R., Mendoza, D. M., Konadu, K. T., Cindy, Aoki, Y., Hirajima, T., Ichinose, H., & Sasaki, K. (2022) Laccase-mediator system for enzymatic degradation of carbonaceous matter in the sequential pretreatment of double refractory gold ore from Syama mine, Mali. *Hydrometallurgy*, 212, 105894.

- Senthivelan, T., Kanagaraj, J., & Panda, R. C. (2016) Recent trends in fungal laccase for various industrial applications: An eco-friendly approach - A review. *Biotechnology and Bioprocess Engineering*, 21(1), 19–38.
- Setswalo, K., Oladijo, O. P., Namoshe, M., Akinlabi, E. T., & Mokoba, M. (2019) Effect of particle size and alkali-laccase on the properties of *pterocarpus angolensis* (Mukwa) wood flour. *Procedia Manufacturing*, 35, 465–470.
- Sibrell, P. L., & Miller, J. D. (1992) Significance of graphitic structural features in gold adsorption by carbon. *Mining, Metallurgy & Exploration*, 9(4), 189–195.
- Singh, G., & Arya, S. K. (2019) Utility of laccase in pulp and paper industry: A progressive step towards the green technology. *International Journal of Biological Macromolecules*, 134, 1070–1084.
- Terry, B. (1983) The acid decomposition of silicate minerals. Part I. Reactivities and modes of dissolution of silicates. *Hydrometallurgy*, 10(2), 135–150.
- Tucker, I. M., Burley, A., Petkova, R. E., Hosking, S. L., R P Webster, J., X Li, P., Ma, K., Douth, J., Penfold, J., & Thomas, R. K. (2022) Self-assembly in escin-nonionic surfactant mixtures: From micelles to vesicles. *Journal of Colloid and Interface Science*, 626, 305–313.
- Welch, S. A., Christy, A. G., Kirste, D., Beavis, S. G., & Beavis, F. (2007) Jarosite dissolution I - Trace cation flux in acid sulfate soils. *Chemical Geology*, 245(3–4), 183–197.
- Widsten, P., & Kandelbauer, A. (2008) Laccase applications in the forest products industry: A review. *Enzyme and Microbial Technology*, 42(4), 293–307.

Wingender, J., Neu, T. R., & Flemming, H.-C. (1999) What are Bacterial Extracellular Polymeric Substances? Microbial Extracellular Polymeric Substances, 1–19.

Yang, H. Y., Liu, Q., Song, X. L., & Dong, J. K. (2013) Research status of carbonaceous matter in carbonaceous gold ores and bio-oxidation pretreatment. Transactions of Nonferrous Metals Society of China (English Edition), 23(11), 3405–3411.

Zashikhin, A. V., & Sviridova, M. L. (2020) Gold Leaching with Humic Substances. Journal of Mining Science 2019 55:4, 55(4), 652–657.

Zeng, Q., Wang, S., Hu, L., Zhong, H., He, Z., Sun, W., & Xiong, D. (2021) Oxalic acid modified copper tailings as an efficient adsorbent with super high capacities for the removal of  $Pb^{2+}$ . Chemosphere, 263, 127833.

Zhang, S., Dong, Z., Shi, J., Yang, C., Fang, Y., Chen, G., Chen, H., & Tian, C. (2022) Enzymatic hydrolysis of corn stover lignin by laccase, lignin peroxidase, and manganese peroxidase. Bioresource Technology, 361, 127699.

Zhu, L., Qi, H. ying, Lv, M. Le, Kong, Y., Yu, Y. W., & Xu, X. Y. (2012) Component analysis of extracellular polymeric substances (EPS) during aerobic sludge granulation using FTIR and 3D-EEM technologies. Bioresource Technology, 124, 455–459.

# **Chapter 7:**

# **Conclusions**

The use of more environmentally friendly pre-treatments of carbonaceous matter (CM) in double refractory gold ores (DRGO) is encouraged due to the rapid exhaust of easily extractable gold deposits. As such, enzymatic pre-treatments are leading researchers' preferences to study their application capabilities for carbonaceous gold ores in operating mines in the future. Previously, attempts were made to find the profit of using the cell-free spent medium (CFSM) of *P. chrysosporium*, which contains lignin peroxidase (LiP) and manganese peroxidase (MnP) at an industrial scale. However, several disadvantages were found while looking for the best conditions for scaling up the process. Therefore, attention was moved to an adequate alternative that could solve the downsides of CFSM and conserve their beneficial effects on CM degradation. In this premise, laccase, which is also a lignin-degrading enzyme shows promising applications on a mining scale due to its well-developed background in other profitable activities.

Moreover, commercially purified laccases are produced from several fungal sources due to their wider availability, solving the problems in large quantities for continuous processing. Furthermore, laccase in the presence of mediators is capable of equaling LiP and MnP effectiveness among substrates with high standard redox potential. Considering such advantages on laccase utilization, it is considered a possible alternative for carbonaceous matter degradation. Thus, deep understanding from a hydrometallurgical aspect is necessary.

**Chapter 3** delivers the optimal condition for trace gold determination using DRGO. Au contents determined by ICP-OES were in good agreement with the fire assay results, especially in the acid matrix with the molar ratio of HCl: HNO<sub>3</sub> =1:5 (highly reverse aqua regia). Under this condition, the detection limit of Au was 20 ppb. Oppositely, for

ICP-MS determination, the memory effect was completely solved when 1% HCl, including 1% L-cysteine is used to prepare the dilution matrix.

Before applying laccase to natural carbonaceous gold ores, it was necessary to compare the use of purified laccase against CFSM on a carbonaceous matter surrogate. **Chapter 4** elucidated that purified laccase from *Trametes versicolor* decreased the adsorption of  $\text{Au}(\text{CN})_2^-$  on powder-activated carbon (PAC) in a similar way to CFSM from *P. chrysosporium*. Relatively similar activities of laccase (19.5 U/L) to LiP and MnP in CFSM (1.1 U/L and 20.6 U/L, respectively) decreased around 15% of adsorption capacity of  $\text{Au}(\text{CN})_2^-$  after 3 days of enzymatic treatment, and this reduction was further improved to ~55% by increasing the enzyme activity in the case of Lcc. Additional understanding and the application of the laccase-mediator treatment on PAC degradation were supported by GC-MS characterization of the degraded intermediates in **Chapter 5**. Laccase-mediator system (LMS) using laccase Y-120 from *Trametes sp.* and HBT significantly altered the surface morphologies of PAC to decrease the specific surface area (from 2342 to 913  $\text{m}^2/\text{g}$ ) and pore volumes (from 2.12 to 0.86  $\text{cm}^3/\text{g}$ ) after 7 days of treatment. The benefits of increasing the enzymatic treatment compared to the conditions used in **Chapter 4** relies on the chemical alterations provided by GC-MS and TG-DTA, which were also supported by FTIR and Raman spectra. GC-MS study for extracted intermediates of degradation products provided a direct evidence of the chemical alteration of the surface by LMS treatment for 2~7 days, where monocyclic/polycyclic hydrocarbons were transformed to aliphatic hydrocarbons. Furthermore, the formation of oxidized functional groups, mostly ketones ( $\text{C}=\text{O}$ ) type, and graphiticity reduction led to the passivation of the active adsorption sites and thus decreased the  $\text{Au}(\text{CN})_2^-$  adsorption density on PAC from 46.0  $\mu\text{mol/g}$  to 7.36  $\mu\text{mol/g}$ .



In **Chapter 6**, sequential extraction by non-polar and polar solvents (in that order) of three CM that contain different pre-robbing degrees were evaluated, and the extractants were subjected to GC-MS characterization. The total ion chromatogram of compounds extracted by hexane was saturated aliphatic hydrocarbons in the three ores. Ethyl acetate dissolved overall non-polar and polar organic compounds like alkanes, ethers, fatty acids, and aromatic moieties containing oxygen-functional groups (SYM). Acetone extracted several fatty acid amides (PXX), hydroxyl and carbonyl groups. PXX appears to be the less mature of the three ores, resulting in a low pre-robbing ability. As for SYM, the presence of several aromatic moieties could be related to its highly pre-robbing capacity. The presence of EPS in BOG interfered with the extraction, not allowing accurate characterization. The interference of EPS was also elucidated when BOG was subjected to laccase treatment. In this case, gold recoveries of BOG were already high (90%) after the removal of jarosite and free  $\text{Fe}^{3+}$  attached to the surface of the ore by using 0.4 M oxalic acid. Laccase treatment slightly improved ~2% of the gold recovery. However, for stronger oxidation conditions using LMS, the EPS passivation layer on CM appears to be an obstacle to enzymatic degradation due to its nature as an easily degradable carbon substrate. Despite this, laccase also participates in reactions involving gold oxidation and further complexation through humic-acid-like substances from EPS. This phenomenon was also enhanced in the presence of HBT by dissolving 0.3 g/t of gold compared to negligible amounts detected in the solution when laccase was applied alone. Although gold recoveries did not increase as expected, the current findings allow the understanding of LMS applications in DRGO that have passed through bio-oxidation. In this case, removing EPS or applying another sulfide treatment instead of bio-oxidation is beneficial for the following laccase treatment.

As such, bio-oxidation was replaced with ferric chloride leaching in the sequential bio-treatment of SYM to avoid the issues above-described for LMS treatment. Sequential extraction on LMS-treated SYM revealed the abundance of hydrophilic compounds on the surface of CM, suggesting the beneficial effect of LMS treatment to degrade carbonaceous matter and reduce  $\text{Au}(\text{CN})_2^-$  adsorption (Fig. 7.1).

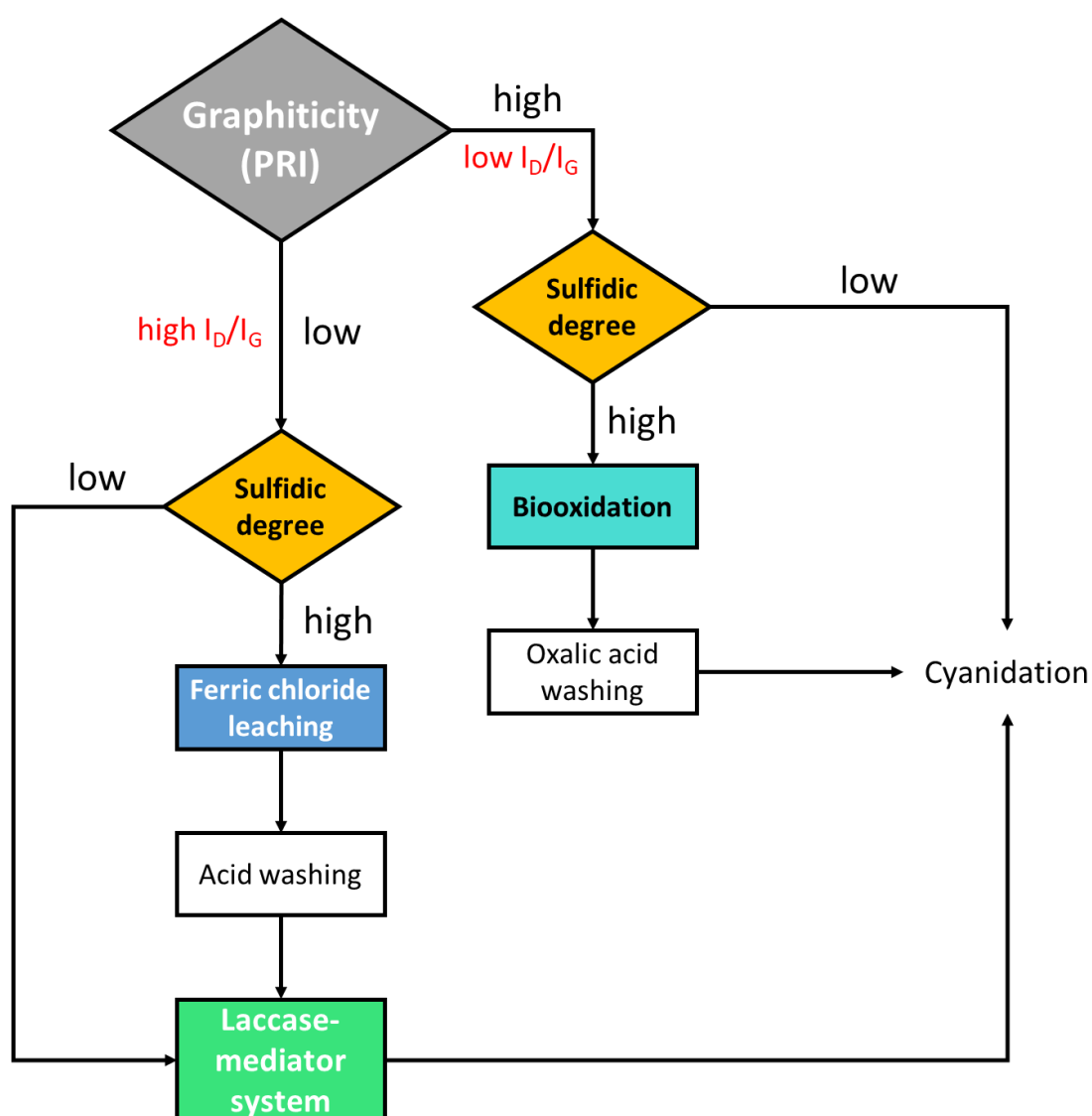


Fig. 7.1. Flowchart of carbonaceous gold ore treatment to maximize gold recovery.

## **Chapter 6S:**

**Carbonaceous matter degradation  
by fungal enzyme treatment to  
improve Ag recovery from Au-Ag  
bearing concentrate, PXX**

## 6S.1. Introduction

In recent years, the mining industry gradually trends to be interested in refractory ores due to the rapid expenditure of free milling Au-Ag-bearing ores. Such refractory behavior is mainly caused by two factors: the interlocking of Au/Ag grains in sulfides and the preg-robbing behavior of carbonaceous matter (CM). During the Au and Ag extraction in the cyanidation step, CM tends to act as an activated carbon to adsorb  $\text{Au}(\text{CN})_2^-$  and  $\text{Ag}(\text{CN})_2^-$  complexes, making the refractory ores inaccessible and usually abandoned (Afenya, 1991; Pyke et al., 1999; Schmitz et al. 2001; Ofori-Sarpong et al., 2010; Konadu et al., 2019a). Carbonaceous ores require some pretreatments before cyanidation to avoid high recovery losses of gold and silver. Roasting seems to be accessible but not acceptable because of emission of pollutant gasses like  $\text{SO}_x$  and  $\text{As}_2\text{O}_3$  (Nanthakumar et al., 2007; Amankwah and Pickles, 2009; Yang et al., 2013). Biological pretreatment of carbonaceous refractory ores has been gaining attentiveness due to not only the economic and environmental aspects but also the contribution to sustainable development goals (Amankwah et al., 2005; Ofori-Sarpong et al., 2013; Liu et al., 2016; Konadu et al., 2019a). The application of a sequential biotreatment for treating carbonaceous gold ore using *Acidianus brierleyi* and cell free-spent medium (CFSM) from a white-rot fungus *Phanerochaete chrysosporium* achieved 92% of Au recovery after alkaline washing, in comparison with the initial 24% recovery from the as-received sample (Konadu et al., 2019a). It has been quantitatively confirmed by capillary electrophoresis enzyme assays that the cell free spent medium of *P. chrysosporium* contains lignin peroxidase (LiP) and manganese peroxidase (MnP) (Kudo et al., 2017). These lignin-degrading enzymes possess high standard redox potentials (LiP: 1.2 – 1.5 V and MnP: 1.1. V) (Fakoussa and Hofrichter, 1999) and the

capacity to split the C-C bond in aromatic compounds presented in CM (Ofori-Sarpong et al., 2013). The physicochemical and, most notably, the graphitic characteristics of CM in natural ores can differ worldwide depending on environmental factors (Miki, 1983). Therefore, it is imperative to use this bio-sequential technique in another analogical sample for a better understanding of the degradation of CM.

In the present supplemental section, the mentioned sequence was applied to a carbonaceous Au-Ag concentrate where Au(0) grains were mainly liberated and non-refractory, focusing on improvement in Ag recovery.

## **6S.2. Experimental**

### **6S.2.1. Sample preparation and characterization**

The present sample is a carbonaceous Au-Ag-bearing flotation concentrate supplied by an anonymous mine. This sample is named PXX and to remove flotation reagents, 100 g of the untreated concentrate was washed using 400 mL of 70% ethanol in an ultrasonic bath for 30 sec followed by 1 L of ultra-pure water. To dissolve the soluble salts on the surface of sulfides, the solid residues were washed with 400 mL of 1 M HNO<sub>3</sub> in an ultrasonic bath for 1 min followed by a final washing of 1 L of ultra-pure water. Finally, ultra-pure water washing was thoroughly repeated three times to remove the remaining reagents.

The elemental and mineralogical compositions of PXX and the sample after acid treatment were determined by FEI Mineral Liberation Analysis (MLA), details of the observation are given in section 2.3.9.

In a process of sequential treatment, each solid residue was provided for the following characterizations. The main mineral phases were also collected by X-ray diffraction analysis (XRD). The carbonaceous compounds were characterized by thermogravimetric-differential thermal analysis (TG-DTA 2000SA) with airflow and heating rate of 100 mL/min and 5°C/min, respectively. The samples were heated until 800°C using  $\alpha$ -Al<sub>2</sub>O<sub>3</sub> as a reference. The particle size distribution was determined by a laser scattering particle size distribution analyzer (HORIBA Partica LA-950, Kyoto, Japan).

The total Au and Ag contents were determined by induced coupled plasma-mass spectrometry (ICP-MS, Agilent 7500c, USA) after acid digestion as follows: by roasting 0.4 g of the ore in air conditions at 800°C for 3 h; followed by microwave digestion of about 0.1 g of sample in a solution of 0.5 mL 60% HClO<sub>4</sub>, 5 mL 99.9% HF and 2 mL H<sub>2</sub>O for 2 h at 140°C, the digested solutions were heated up to 150°C for 4 h for the complete evaporation of HF. Afterward, the solutions were mixed with 2 mL of aqua regia and left for 12 h at room temperature. Microwave digestion was conducted for a second time at 150°C for 2 h.

Au and Ag recoveries for the original concentrate were determined by cyanidation using 10.75 mM KCN at pH 10.5 for 48 hrs. It was revealed that extracted Au and Ag were 100% and 33.3%, respectively, indicating that the present carbonaceous sample is not refractory gold ore, but refractory silver ore. So, for the purpose of the sequential bio-treatment, the sample was named as carbonaceous silver ore (CSC).

### 6S.2.2. Sequential bio-treatment of carbonaceous silver concentrate (CSC)

For improving the silver recovery, CSC was treated by a sequential bio-treatment using a mixed thermophilic culture of *Acidianus brierleyi*, *Acidianus manzaensis*, and *Metallosphaera sedula*, for oxidative dissolution of sulfides, followed by cell-free spent medium (CFSM) from *Phanerochaete chrysosporium* for the decomposition of carbonaceous matter.

#### 6S.2.2.1. Biooxidation of sulfides in CSC by mixed thermophilic archaea

Three iron- and sulfur-oxidizing thermophilic archaea strains, *Acidianus brierleyi* (DSM 1651), *Acidianus manzaensis* (NA-1T), and *Metallosphaera sedula* (JCM 9064), were employed in the biooxidation of sulfides (Olson & Clark, 2004; Auernik et al., 2008). Each microorganism was regularly cultivated in a sterile 500 mL Erlenmeyer flask with 200 mL solution containing 4 mL of acidophile basal (ABS) medium (22.5 g NH<sub>4</sub>SO<sub>4</sub>; 2.5 g KCl; 2.5 g KH<sub>2</sub>PO<sub>4</sub>; 25 g MgSO<sub>4</sub>·7H<sub>2</sub>O; 0.7 g Ca(NO<sub>3</sub>)<sub>2</sub>·4H<sub>2</sub>O; and 7.1 g NaSO<sub>4</sub> per liter at pH 1.5 with 1M H<sub>2</sub>SO<sub>4</sub>), 0.2 mL of trace elements (10 g ZnSO<sub>4</sub>·7H<sub>2</sub>O; 1 g CuSO<sub>4</sub>·5H<sub>2</sub>O; 1.09 g MnSO<sub>4</sub>·5H<sub>2</sub>O; 1 g CoSO<sub>4</sub>·7H<sub>2</sub>O; 0.39 g Cr<sub>2</sub>(SO<sub>4</sub>)<sub>3</sub>·7H<sub>2</sub>O; 0.6 g H<sub>3</sub>BO<sub>3</sub>; 0.5 g Na<sub>2</sub>MoO<sub>4</sub>·2H<sub>2</sub>O; 0.1 g NaVO<sub>3</sub>; 1 g NiSO<sub>4</sub>·6H<sub>2</sub>O; 0.51 g Na<sub>2</sub>SeO<sub>4</sub> and 0.1 g Na<sub>2</sub>WO<sub>4</sub>·6H<sub>2</sub>O per liter, pH 2), 0.04% yeast extract and 20 mM FeSO<sub>4</sub>·7H<sub>2</sub>O as an initial energy source. Yeast extract was added to enhance As(III) oxidation (Okibe et al., 2014) since CSC contained 18.6 wt% of arsenopyrite. The flasks were shaken using a Bio-shaker G•BR-200 at 70°C and 120 rpm, covered with silicon plug type T for permitting constant aeration. Before running the biooxidation experiments, the cells were adapted to 2 g of the untreated CSC in a 200 mL solution containing the above chemicals including 5 mM FeSO<sub>4</sub>·7H<sub>2</sub>O for 7 days.

Then, each grown strain was collected by two steps of centrifugation ( $630 \times G$  for 10 min and  $15660 \times G$  for 15 min) and re-suspended in sterilized acidic water (pH 1.2) for inoculation.

The biooxidation was conducted using 20 g of CSC in a sterile 2 L Erlenmeyer flask containing 1 L ABS medium (pH 1.2), including 1 mL of trace elements, 0.04% yeast extract, and 5 mM  $\text{FeSO}_4 \cdot 7\text{H}_2\text{O}$ . The collected cells were inoculated, setting an initial cell density of each strain at  $1.0 \times 10^7$  cells/mL (i.e.,  $3.0 \times 10^7$  cells/mL in total). The biooxidation was run in triplicate with one sterilized control at  $70^\circ\text{C}$ , shaking at 120 rpm for 15 days using a Bio-shaker G•BR-200. For daily control in the supernatant, the pH and Eh, cell density, dissolved Fe and As, and dissolved Cd, and Ag concentrations were determined by electrodes, direct observation under the microscope, inductively coupled plasma-optical emission spectrometry (ICP-OES, Perkin Elmer Optima 8300, USA) and inductively coupled plasma-mass spectrometry (ICP-MS, Agilent 7500c, USA), respectively. The solid residue after biooxidation was dried vacuum with silica gel overnight. The solid residue after this process was named DA.

#### 6S.2.2.2. Degradation of carbonaceous matter by cell-free spent medium (CFSM)

from *Phanerochaete chrysosporium*

The CM degradation was performed by CFSM of *P. chrysosporium*, where the presence of manganese peroxidase (MnP) and lignin peroxidase (LiP) was confirmed previously using in-capillary enzymatic reaction followed by separation via capillary electrophoresis (Kudo et al., 2017). For this work, the spent medium harvesting conditions, where the enzymes are constantly active, followed the procedure described in Konadu et al. (2019a; 2019b). *P. chrysosporium* was cultured in a sterile 2 L



Erlenmeyer flask containing 500 mL liquid medium at pH 4 adjusted with 1 M NaOH, composed by 10 g glucose, 1.18 g succinic acid, 0.2 g ammonium tartrate, 10 mg thiamine hydrochloride, 25.6 mg 2,6-dimethoxyphenol, 2 g  $\text{KH}_2\text{PO}_4$ , 0.5 g  $\text{MgSO}_4 \cdot 7\text{H}_2\text{O}$  and 0.1 g  $\text{CaCl}_2 \cdot 2\text{H}_2\text{O}$  per liter in addition to 70 mL trace element solution (3 g  $\text{MgSO}_4 \cdot 7\text{H}_2\text{O}$ , 1 g NaCl, 0.5 g  $\text{MnSO}_4 \cdot 5\text{H}_2\text{O}$ , 0.1 g  $\text{FeSO}_4 \cdot 7\text{H}_2\text{O}$  and 0.1 g  $\text{CuSO}_4 \cdot 5\text{H}_2\text{O}$ , 10 mg boric acid per liter). The flasks were shaken at 37°C and 60 rpm using a Bio-shaker BR-40LF, a silicone plug type C was used to cover the flasks for permitting constant aeration. After three day-growth, the fungal tissue was harvested using a sterilized 0.22  $\mu\text{m}$  stericup® filter to separate the cell-free spent medium (CFSM) to transfer into the flasks for sequential treatment. LiP and MnP activities in CFSM after three day-growth were previously determined by UV spectrometry to be  $1.1 \pm 0.2$  U/L and  $20.6 \pm 1.2$  U/L, respectively (Konadu et al., 2019b), where one unit of enzyme activity (U) was defined as the amount of enzyme required to oxidize 1 mM of substrate per minute, and expressed as a specific activity using U/L.

10 g of DA was added to 250 mL of freshly harvested CFSM in a sterile 500 mL Erlenmeyer flask. A porous plug was used to cover the flasks to allow aeration. The experiment was run in triplicate shaken at 30°C and 128 rpm, covered with silicone plug type C. Then, the solid was collected by centrifugation at  $15660 \times G$  for 5 min and suspended in new fresh CFSM. This process was repeated five times, for which the primary purpose was to provide high enzyme activities continuously into the system (Konadu et al., 2019a). After 15 days of treatment, the solid residues were collected and washed with ultra-pure water before being dried vacuum with silica gel overnight. The solid residue after this process was named DAC.

Direct CFSM treatment of CSC was singly tested to evaluate if the biooxidation of DA process is essential in the sequential biotreatment of the present sample. 10 g of DA was added to 250 mL of freshly harvested CFSM in a sterile 500 mL Erlenmeyer flask. The treatment was run in duplicate with one sterilized control shaken at 30°C and 128 rpm, covered with silicon plug type C to allow aeration. The same evaluation time and the experimental process were followed in this test. The solid residue after this process was named DC.

The extraction of silver by cyanidation was conducted for DA, DAC, and DC samples in the same manner as mentioned in the section 6S.2.1.

#### 6S.2.3. Characterization of the bio-treated residues

The obtained solid residues DA, DAC, and DC were supplied for XRD, TG-DTA, particle size, and Raman spectroscopy characterization, in the same manner as CSC. Carbonaceous matter was not possible to differentiate from the epoxy resin used in MLA observation; therefore, after biotreatment, only DA was possible to characterize by MLA.

### 6S.3. Results and discussion

#### 6S.3.1. Mineralogical and elemental characterization of CSC

Based on the XRD pattern for the original sample (CSC), it includes pyrite ( $\text{FeS}_2$ , PDF 01-042-1340) and arsenopyrite ( $\text{FeAsS}$ , PDF 00-060-0322) in addition of quartz ( $\text{SiO}_2$ , PDF 00-014-0218), muscovite ( $\text{KAl}_2(\text{AlSi}_3\text{O}_{10})(\text{OH})_2$ , PDF 01-076-0929) and chlorite

(Mg, Al)<sub>6</sub> (Si, Al)<sub>4</sub>O<sub>10</sub> (OH)<sub>8</sub>, PDF 00-060-0322) (Fig. 6S.1). MLA result was consistent with the above and suggests other minor minerals like apatite and dolomite might possibly increase the alkalinity in DA process (Table 6S.1). Fire assay revealed the Au and Ag contents are similar, 27.5 g/t and 26.0 g/t, respectively (Table 6S.2). CHN analysis resulted in 5.0 % of C contents, which includes inorganic and organic carbons. However, according to the mineralogical analysis showing 1.5% dolomite in Table 6S.1, the C contents is mainly derived from organic carbon. There are characteristic peaks of organic matters in TG-DTA around 455 and 510°C in Fig. 6S.2(c). The total mass loss at 545°C was recorded around 8%, but it is overlapped with mass loss through the decomposition of sulfides.

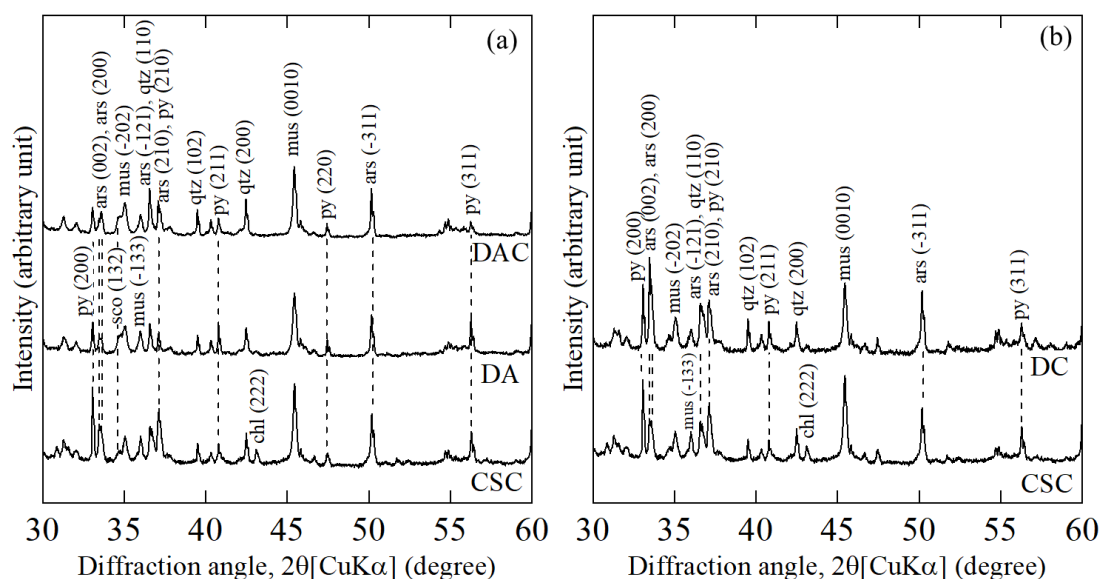


Fig. 6S.1. Changes in XRD patterns of solid residues after sequential bio-treatment. (a) DA: CSC after bio-oxidation of mixed culture; DAC: treated DA by cell-free spent medium of *P. chrysosporium* and (b) DC: treated CSC by cell-free spent medium of *P. chrysosporium* Symbols: py (pyrite, PDF 01-042-1340); ars (arsenopyrite, PDF 00-

060-0322); sco (scorodite, PDF 00-018-0654); mus (muscovite, PDF 01-076-0929); qtz (quartz, PDF 00-014-0218); chl (chlorite, PDF 00-060-0322).

Table 6S.1. Mineral compositions (wt%) of CSC and DA determined by MLA

Mineral	CSC	DA
electrum	<0.1	<0.1
hessite	<0.1	<0.1
other silver minerals	<0.1	<0.1
arsenopyrite	18.6	9.6
bismuth telluride	<0.1	<0.1
loellingite	<0.1	<0.1
pyrite	10.1	13.4
other sulfides	0.7	0.1
quartz	23.5	30.9
feldspar	<0.1	<0.1
muscovite	34.4	44.7
chlorite	10.0	<0.1
other silicates	0.1	0.1
other oxides	0.8	0.8
dolomite	1.5	<0.1
apatite	0.2	<0.1
others	0.1	0.1

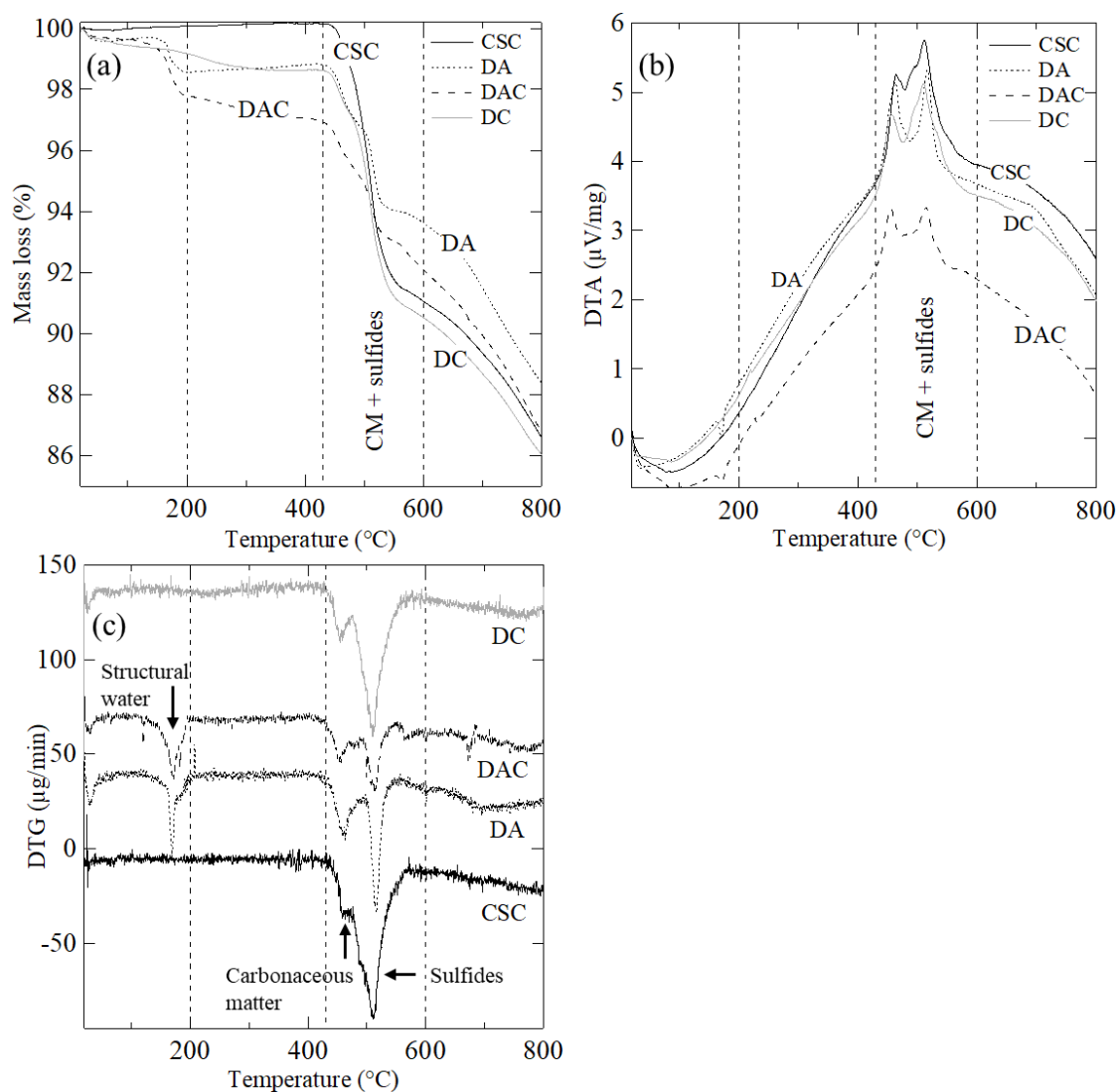


Fig. 6S.2. Thermal decomposition characteristics of the as-received sample (CSC) and the bio-treated residues (DA, DAC and DC), showing (a) mass loss, differential thermal analysis (b) DTA, and (c) differential thermogravimetry DTG. CM means carbonaceous matter.

Table 6S.2. Elemental compositions of CSC and DA

Element	CSC	DA
Au(g/t)	27.5	19.9
Ag (g/t)	26.0	22.0
C (%)	5.0	5.5
As (%)	6.7	4.1
Fe (%)	12.0	8.2
S (%)	7.3	7.5
Si (%)	19.0	22.0
Al (%)	7.6	8.2
others (%)	41.4	43.5

Detailed characterization of Ag in CSC was explored by MLA observation (Fig. 6S.3). They are classified into three types of Ag-bearing minerals: (a) electrum (Au-Ag solid solution), (b) hessite ( $\text{Ag}_2\text{Te}$ ), (c) Ag-bearing other minerals, which are mainly associated with CdO. It is clear that hessite is mostly liberated in CSC, while the other two types of Ag minerals are primarily associated with arsenopyrite, pyrite, other sulfides, and gangue minerals, which could be attributed to silicates, carbonates, and carbonaceous matter (Qiu et al., 2014; Celep and Serbest 2015; Li et al., 2016). Based on MLA analytical results, the distribution of Au and Ag liberation and association with other minerals against the particle sizes can be depicted in Fig. 6S.4 (a), (b). The identification of electrum here is the mass ratio of Au: Ag = 9:1. There is a clear difference between Au and Ag; that is, Au is well liberated and/or exposed, while a non-negligible fraction of Ag is enclosed by gangue minerals. MLA also revealed that some Ag-bearing grains are associated with Cd oxides (Fig. 6S.4(b)).

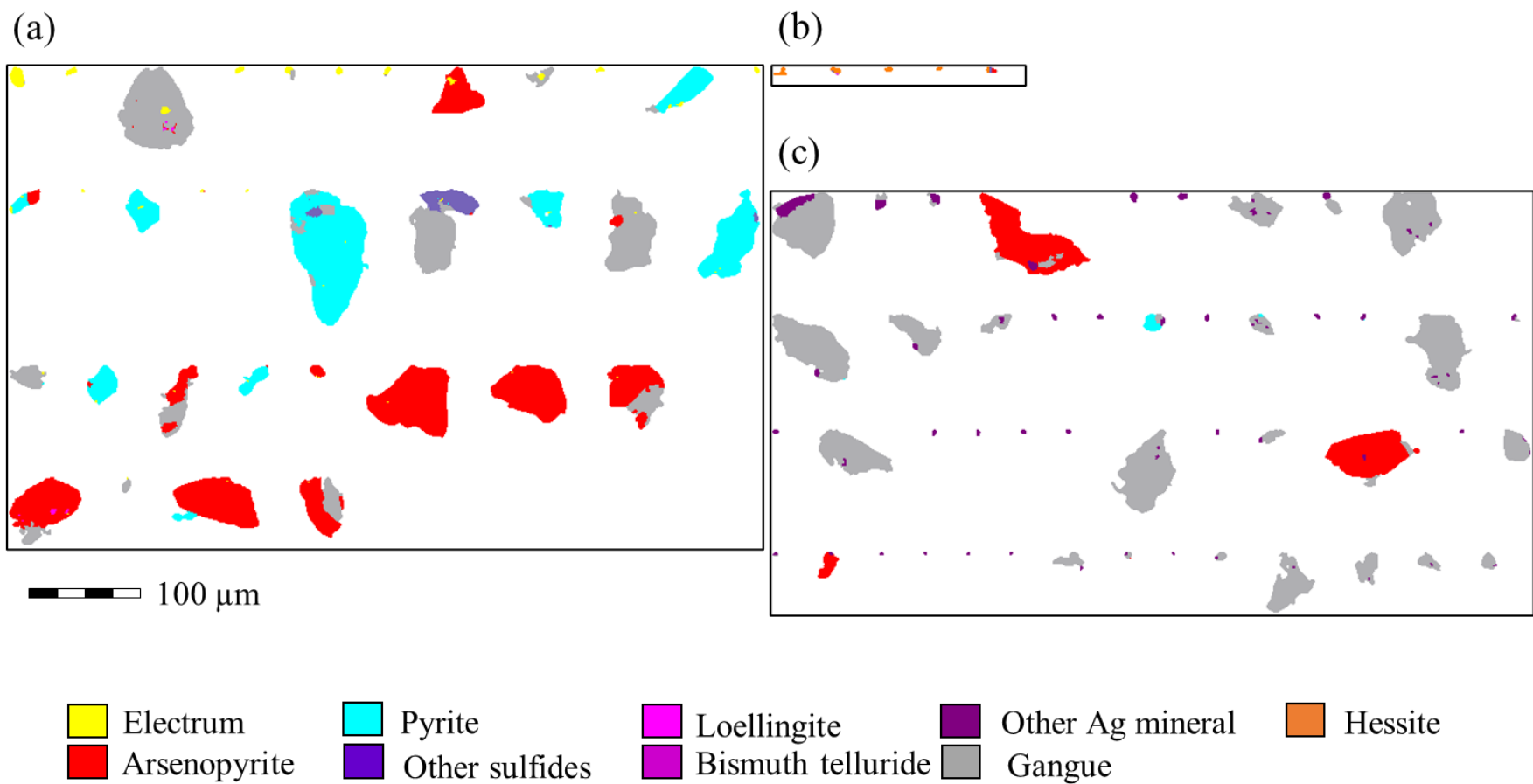


Fig. 6S.3. MLA classified images showing (a) electrum, (b) hessite particles, and (c) silver-containing other minerals in CSC.

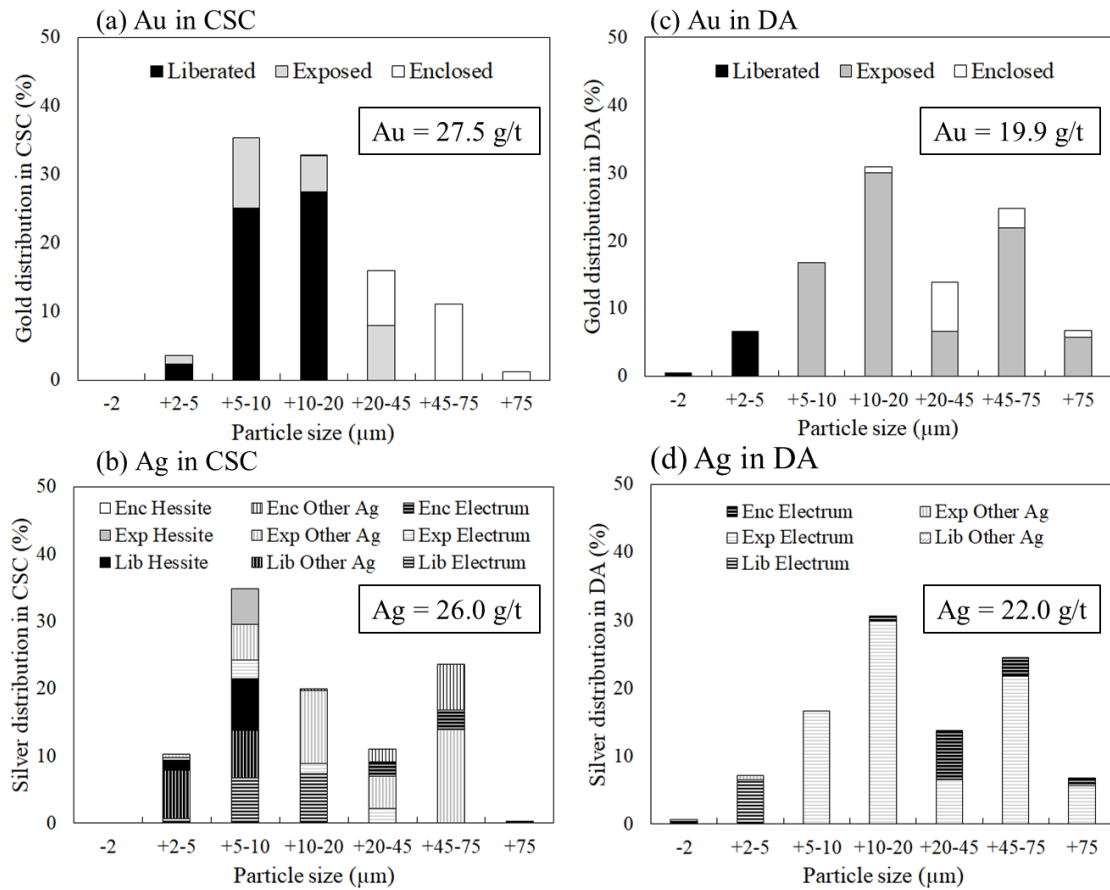


Fig. 6S.4. Gold and silver distribution in accordance with the particle size in carbonaceous silver ore concentrate before and after bio-oxidation of mixed culture. Lib: liberated, Exp: exposed and Enc: enclosed.

This observation makes sense because the cyanidation test yielded ~100 % of gold recovery in the untreated CSC; considering how gold grains were distributed in the ore, it seems like cyanide could access gold and form the complex of  $\text{Au}(\text{CN})_2^-$ . Conversely, only 33% of silver was recovered after cyanidation. Concerning MLA observation (Fig. 6S.3), this finding can infer that the present sample is refractory in silver due to its association with gangue and partially interlocking in sulfides.



### 6S.3.2. Sequential bio-treatment of carbonaceous silver concentrate (CSC)

The biooxidation of sulfides in DA process was monitored by dissolution of Fe, As concentrations as well as pH, Eh and cell densities in triplicate (Fig. 6S.5). Although cell growth of archaea was observed (Fig. 6S.5(b)), the redox potential did not increase (Fig. 6S.5(e)) and dissolution behaviors of metals were not accelerated by cell inoculation (Fig. 6S.5(c, d)). Around 23 mM total Fe including around 8 mM  $\text{Fe}^{2+}$  and 7 mM arsenate were dissolved within 14 days, mainly from pyrite and arsenopyrite independently of the cell inoculation. The dissolved fractions were partial, leaving some pyrite and arsenopyrite in the solid residues (Fig. 6S.6 (a)). Thus, the biological oxidation of sulfides was clearly inhibited, meaning that DA process is mainly chemical process by acid dissolution instead of biological one. Although thermoacidophilic archaea possess two resistant mechanisms against heavy metals: (i) Metal complexation by enzyme-segregated inorganic polyphosphates (polyP) (Remonsellez et al., 2006) and (ii) Efflux pump mechanism by transporting proteins (Ettema et al., 2006), the minimal inhibitory concentration (MIC) for several archaea, are unknown. In DA process, dissolution of around 80  $\mu\text{M}$   $\text{Cd}^{2+}$  and 7  $\mu\text{M}$   $\text{Ag}^+$  (Fig. 6S.5(f)) were observed within 14 days independently of ion oxidizers inoculation, in which Ag dissolution is directly associated with dissolution of hessite ( $\text{Ag}_2\text{Te}$ ) and partially associated with chemical dissolution of Cd oxide minerals under strongly acidic condition (Fig. 6S.5(a, f)). Orell et al., (2013) reported that some archaeon could not tolerate cadmium up to 10  $\mu\text{M}$ , and Fig 6S.5(f) shows that after 2 days of biooxidation, more than 10  $\mu\text{M}$   $\text{Cd}^{2+}$  was dissolved in the system.

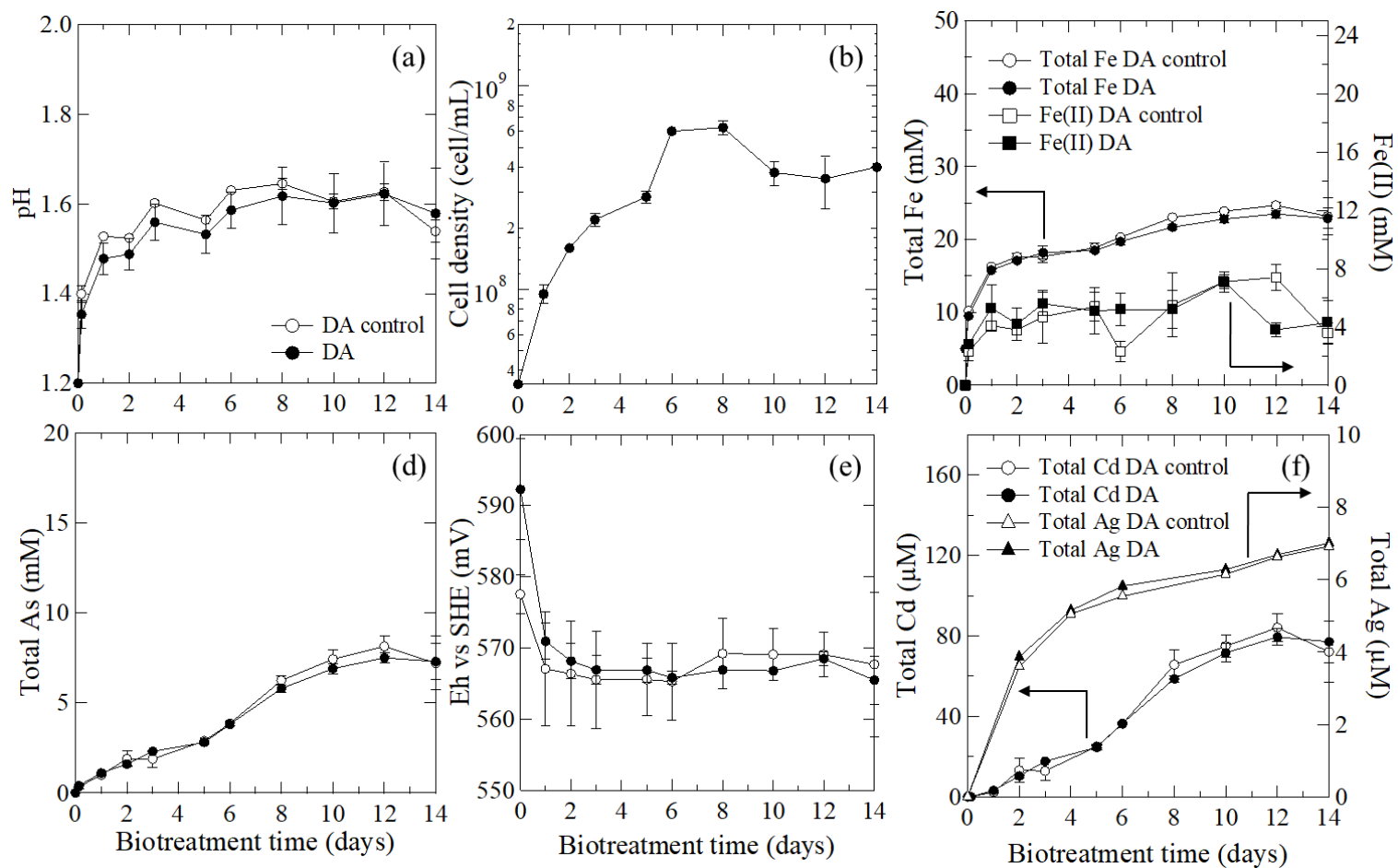


Fig. 6S.5. Changes in (a) pH, (b) cell density, (c) total Fe, (d) As concentrations, and (e) Eh vs SHE, (f) total Cd and total Ag concentrations with time of biooxidation by mix culture ( $n=3$ ).

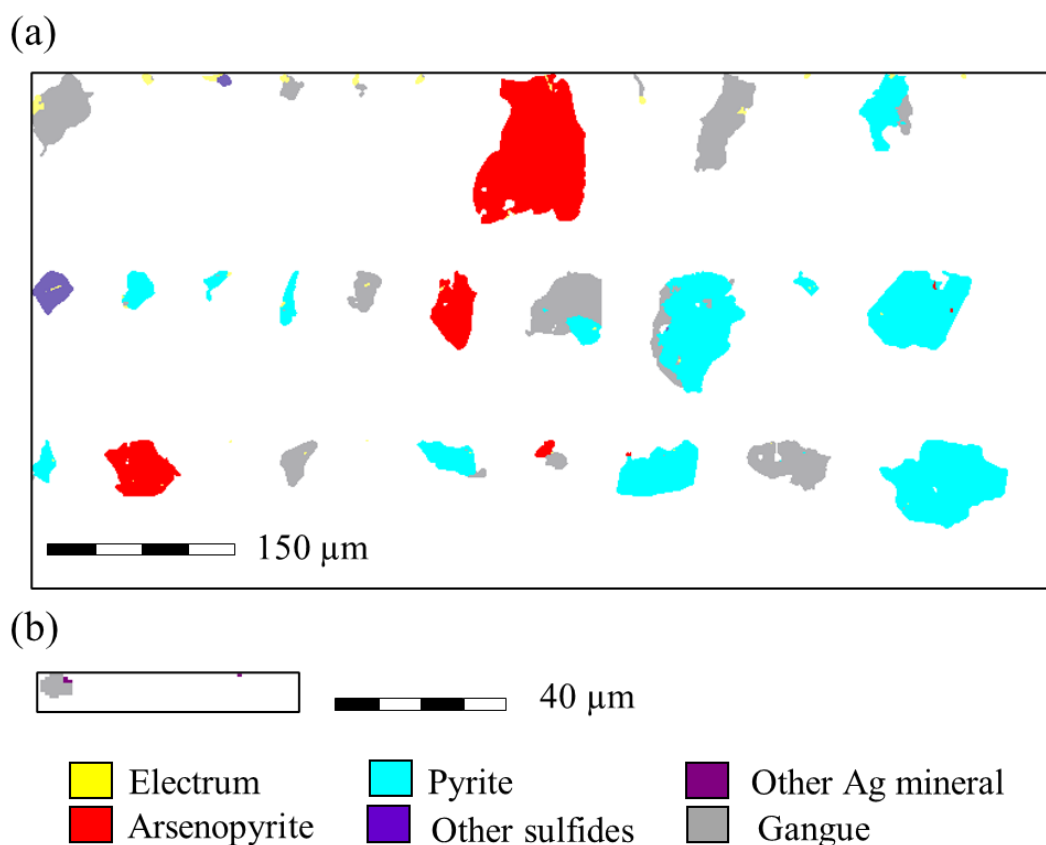


Fig. 6S.6. MLA classified images showing (a) electrum, (b) silver-containing other minerals in carbonaceous silver ore concentrate after bio-oxidation using mixed culture of *Acidianus brierleyi*, *Acidianus manzaensis* and *Metallosphaera sedula* (DA).

Considering that total content of Cd in CSC was 10.7 g/t, in which 84% was dissolved in DA treatment, this high accumulation of  $\text{Cd}^{2+}$  had a deleterious effect on the archaea. Regarding silver toxicity, acidophiles are reported to be sensitive to the presence of dissolved  $\text{Ag}^+$  since it is capable of inactivating enzymes (De et al., 1996) and contributes to the inhibition of  $\text{Fe}^{2+}$  oxidation (Dopson et al., 2003). It was reported elsewhere that *Metallosphaera sedula* seems to be the most tolerant archaeon against cadmium and silver, but not to arsenic (Dopson et al., 2003; Auernik et al., 2008; Orell

et al., 2013). On the other hand, *Acidianus brierleyi* in the presence of yeast extract can tolerate arsenic (Okibe et al., 2013; Okibe et al., 2017), but information about cadmium and silver tolerance is still unknown. Therefore, it is believed that the dissolution of these heavy metals during the biooxidation may affect the mixed culture performance to oxidize sulfides.

However, it is clear in the solid residue after DA treatment, that hessite was not presented and other Ag-containing minerals were mostly reduced (Fig. 6S.6(b)). Dissolved  $\text{Ag}^+$  concentration ( $7\text{ }\mu\text{M}$ ) corresponds to ~16% of total Ag contents, which would be derived from hessite and Ag-bearing minerals associated with oxides, detected by MLA map for CSC (Fig. 6S.3(b), (c)).

XRD pattern for DA shows the relative peak intensities of pyrite and arsenopyrite to quartz always decreased (Fig. 6S.1, Table 6S.3). It is reasonable because archaea attack sulfides and quartz is not affected in DA process. In TG-DTA, the characteristic peaks of sulfides at  $510^\circ\text{C}$  decreased (Fig. 6S.2(c)), in good agreement with XRD.

Detailed mineralogical changes can be seen in MLA results for DA (Fig. 6S.6). Hessite was not detected, indicating it was entirely dissolved by under strongly acidic conditions. Pyrite and arsenopyrite grains remain, where electrum is associated. Ag-bearing other minerals much decreased, probably because they are mainly  $\text{CdO}$ , soluble under strongly acidic conditions. The results are exemplified to be consistent with the solution data (Fig. 6S.5).

Table 6S.3. XRD peak intensity ratio of sulfides against quartz in as-received sample (CSC), after biooxidation (DA), DA treated by CFSM (DAC) and CSC treated by CFSM (DC)

Mineral	Miller indices	XRD relative intensity to $I_{\text{qtz}(011)}$ (%)			
		CSC	DA	DAC	DC
py	(200)	13.2	5.9	5.6	12.0
	(210)	8.7	4.4	5.8	9.5
	(211)	5.6	5.4	4.1	6.6
	(311)	7.4	6.3	3.4	7.3
ars	(002)	8.0	4.2	4.1	12.0
	(200)	8.1	4.2	5.0	11.4
	(012)	8.7	4.4	5.8	9.5
	(-311)	9.7	7.0	7.0	11.3

More detailed MLA results for DA are depicted in Fig. 6S.4 (c), (d), where Au and Ag distribution are shown for each particle size fraction. Liberated Au, mainly in an electrum form, was changed to exposed type, and enclosed Au was also converted into exposed type (Fig. 6S.4(a), (c)). Au(0) grains should not be dissolved in DA process. The most probable interpretation is that originally existing liberated electrum grains and generating liberated electrum grains from the enclosed type are adsorbed on other minerals like gangue and remaining sulfides to be exposed type. Alternatively, the changes in Ag association showed that DA process dissolved  $\text{Ag}^+$  in hessite mainly with 5-10  $\mu\text{m}$  and Ag-bearing minerals in all size fractions, while Ag in an electrum form remained mainly as an exposed type. This type of Ag is associated with the remaining sulfides and partially with gangue minerals in a large variety of particle sizes from 5  $\mu\text{m}$  to larger than 100  $\mu\text{m}$  (Fig. 6S.4(b), (d)).

DC process did not significantly affect XRD pattern, since lignin-degrading enzymes attack carbonaceous matters in ore (Fig. 6S.1(a)). TG-DTA for DAC shows a more considerable mass loss at 455°C than DA (Fig. 6S.2(a)) and decrease in a peak intensity at the same temperature, which is assigned to carbonaceous matter (Fig. 6S.2(c)). Changes in particle size distribution happened at DA process with the peak top around 60  $\mu\text{m}$ , which is mainly responsible for sulfide minerals (Fig. 6S.7). It is also notable that a small peak around 200-300  $\mu\text{m}$  appeared after DAC and DC processes, indicating agglomeration of smaller grains that happened through by-products after biodegradation of carbonaceous matter (Konadu et al., 2019b). They are very similar to humic substances in three-dimensional fluorescence spectroscopy, which make agglomerates by linkages with heavy metal ion adsorbed silicate gangues through their carboxylic groups.

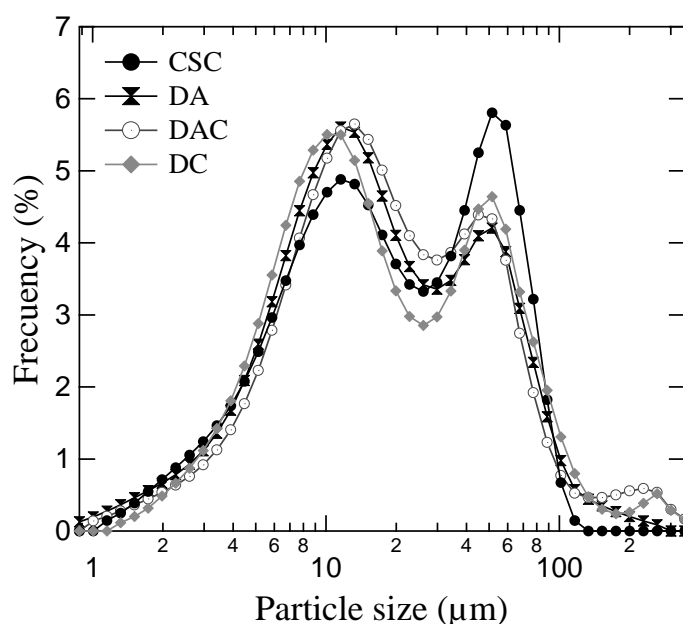


Fig. 6S.7. Particle size distribution of the as-received sample (CSC) and the bio-treated solid residues (DA, DAC and DC).

### 6S.3.3. Direct CFSM treatment of CSC (DC)

Considering there are only chemical reactions in DA process, direct CFSM treatment of CSC was explored (DC). XRD results revealed that the lignin-degrading enzyme reaction did not remarkably decompose sulfides (Fig. 6S.1(b)). Relative XRD peak intensities of arsenopyrite normalized for quartz (011) increased in the process of DC, while the relative peak intensities of pyrite to quartz did not show apparent changes (Table 6S.3). However, the process affected particle size distribution around 200-300  $\mu\text{m}$  range, suggesting the formation of the agglomerates similarly to DAC (Fig. 6S.7).

### 6S.3.4. Extraction of Au and Ag by cyanidation

The Ag recovery was evaluated in each process (DA, DAC and DC) by cyanidation in the same manner as applied to CSC as schematically shown in Fig. 6S.8, where the results were obtained in duplicate. As previously mentioned, 16%  $\text{Ag}^+$  was dissolved in DA process, where acid dissolution of hessite and Ag-bearing other minerals (mainly oxides) is responsible at pH 1.2, inferring that the microbiological contribution is negligibly small. The Ag recovery from the solid residues of DA seems to reveal a meaningless improvement, evidencing the small contribution of the mixed culture to alter the physicochemical characteristics of the carbonaceous matter.

As opposed to the DA sample, the Ag recovery of DAC in cyanidation increased to  $83.7 \pm 11.8 \%$ , inferring that carbonaceous matter might have been biodegraded into smaller molecular weight components, resulting in the formation of agglomerated particles coming from the by-products (Fig. 6S.7) (Konadu et al., 2019b).

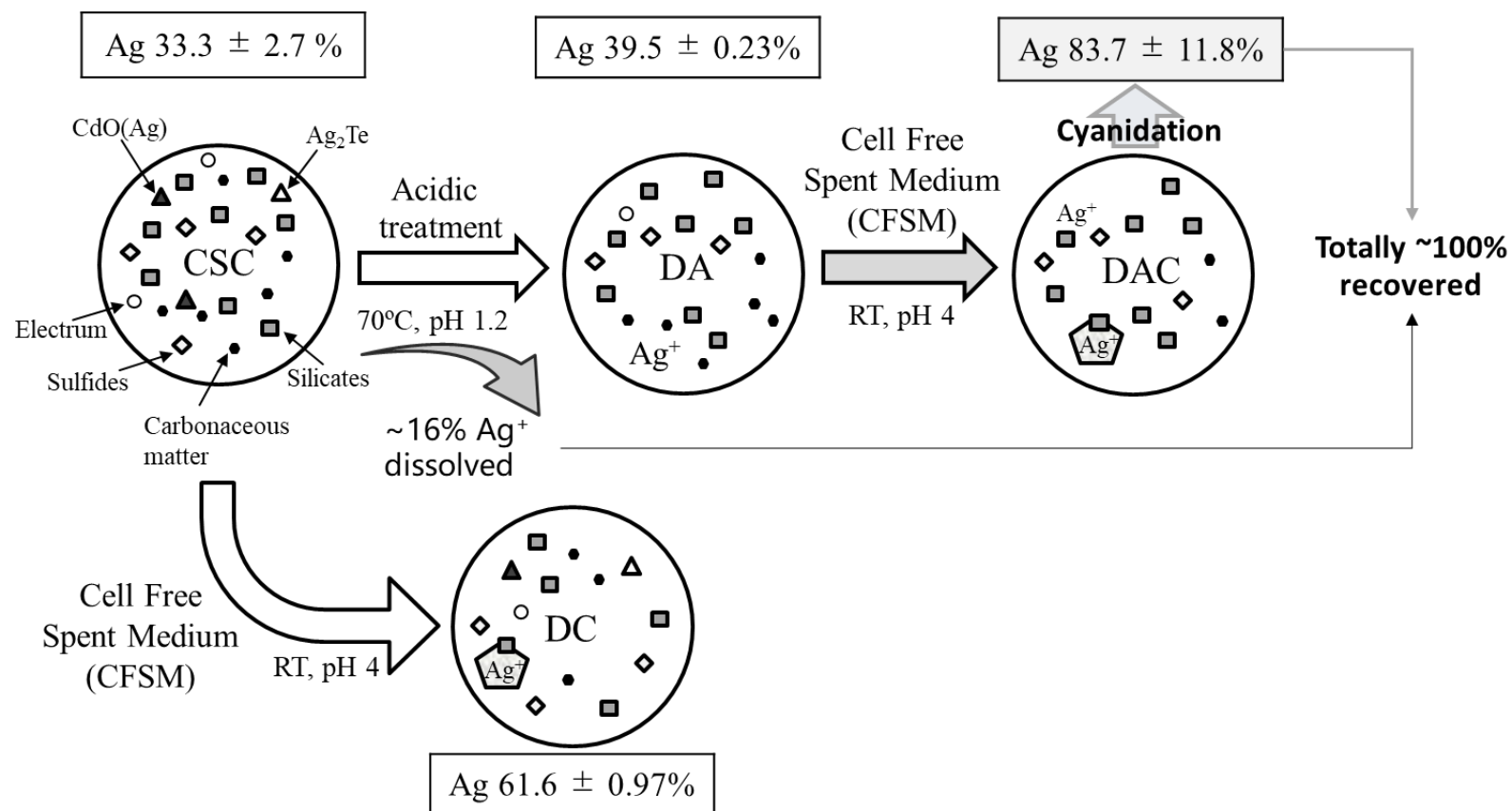


Fig. 6S.8. Schematic illustration of Ag recovery in sequential biomineral processing of carbonaceous silver concentrate (CSC). DA: treated CSC by iron- and sulfur-oxidizing mixed archaea culture, *Acidianus brierleyi*, *Acidianus manzaensis* and *Metallosphaera sedula*; DAC: treated DA by CFSM of *Phanerochaete chrysosporium*; DC: treated CSC by CFSM of *P. chrysosporium*.



However, it appears that the chemical characteristics of the carbonaceous matter presented in CSC produced easily dissolved smaller biomolecules after enzymatic degradation, making them unchallenging for breaking down during cyanidation at pH 10.5. Therefore, the release of adsorbed  $\text{Ag}^+$  species was quantitatively complexed with  $\text{CN}^-$  to form  $[\text{Ag}(\text{CN})_2]^-$  permitting an upper recovery in this step. In this case, a final alkaline washing with 1 M NaOH, like in the previous study (Konadu et al., 2019a), should not be carried out with DAC, because the adsorbed  $\text{Ag}^+$  ions under high alkaline conditions must be converted into  $\text{Ag}_2\text{O}$  (dominant species in pH-Eh diagram), through dehydration of  $\text{AgOH}$  ( $2 \text{AgOH} = 2 \text{AgO} + \text{H}_2\text{O}$ ). This causes the recovery loss again.

In the sequential treatment, the location of the remaining Ag (16%) from the supernatant of DA sequence should be considered to add in the whole recovery. As a result, the Ag recovery from CSC was totally achieved to ~100%. Compared with Ag recovery after DC process without strongly acidic treatment ( $61.6 \pm 0.97\%$ ), DAC process showed much better performance. Pretreatment under strongly acidic condition is meaningful to dissolve acid soluble Ag species in CSC and to remove toxic ions like  $\text{Cd}^{2+}$ ,  $\text{Ag}^+$  and  $\text{AsO}_4^{3-}$ , which can inhibit the peroxidase enzymes, prior to carbonaceous matter treatment (Baldrian, 2003).

#### 6S.4. Conclusions

The present carbonaceous ore included mainly three types of Ag presented as electrum, hessite ( $\text{Ag}_2\text{Te}$ ) and other Ag-bearing other minerals. The electrum grains were mostly liberated, since Au was easily extracted from the present ore by cyanidation. Two steps of the sequential treatment using *Acidianus brierleyi*, *Acidianus manzaensis*, and

*Metallosphaera sedula* followed by the cell-free spent medium (CFSM) from *Phanerochaete chrysosporium* in a carbonaceous silver concentrate, greatly improved the silver recovery from 33 % to ~100 %, including the dissolved  $\text{Ag}^+$  concentration in acid treatment. Although, in the first step (DA), the acidophilic iron-oxidizing microorganisms were inhibited by the dissolution of toxic heavy metals presented in CSC, the strong acidic conditions helped in the dissolution of  $\text{Ag}_2\text{Te}$  (hessite) and Ag-bearing other minerals, which are mainly associated with  $\text{CdO}$ , to solubilize  $\text{Ag}^+$ . This step cannot be cut out to maximize the Ag recovery. However, carbonaceous matter acted to sorb  $\text{Ag}(\text{CN})_2^-$  in cyanidation, causing the recovery loss. So, in the next step the lignin-degrading enzymes degraded carbonaceous matter in the ore. This step is necessary to avoid the adsorption of  $\text{Ag}(\text{CN})_2^-$  on graphitic carbonaceous matter, leading a very high recovery of the remaining Ag in the solid residues. The sequential treatment also has an additional advantage to avoid the emission of air pollutants.

## References

- Afenya, P. M. (1991) Treatment of carbonaceous refractory gold ores. *Minerals Engineering*, 4(7–11), 1043–1055.
- Amankwah, R. K., & Pickles, C. A. (2009) Microwave roasting of a carbonaceous sulphidic gold concentrate. *Minerals Engineering*, 22(13), 1095–1101.
- Amankwah, R. K., Yen, W-T., & Ramsay, J. A. (2005) A two-stage bacterial pretreatment process for double refractory gold ores. *Minerals Engineering*, 18(1),
- Aoki, Y. (2016) Application of mineralogical analysis with MLA in metallurgical testing for copper-molybdenum ore. *Copper*, 298–309.

- Auernik, K. S., Maezato, Y., Blum, P. H., & Kelly, R. M. (2008). The genome sequence of the metal-mobilizing, extremely thermoacidophilic archaeon *Metallosphaera sedula* provides insights into bioleaching-associated metabolism. *Applied and Environmental Microbiology*, 74(3), 682–692.
- Baldrian, P. (2003) Interactions of heavy metals with white-rot fungi. *Enzyme and Microbial Technology*, 32(1), 78–91.
- Celep, O., & Serbest, V. (2015) Characterization of an iron oxy/hydroxide (gossan type) bearing refractory gold and silver ore by diagnostic leaching. *Transactions of Nonferrous Metals Society of China*, 25(4), 1286–1297.
- De, G. C., Oliver, D. J., & Pesic, B. M. (1996) Effect of silver on the ferrous iron oxidizing ability of *Thiobacillus ferrooxidans*. *Hydrometallurgy*, 41(2–3), 211–229.
- Dopson, M., Baker-Austin, C., Koppineedi, P. R., & Bond, P. L. (2003) Growth in sulfidic mineral environments: Metal resistance mechanisms in acidophilic micro-organisms. *Microbiology*, 149(8), 1959–1970.
- Ettema, T. J. G., Brinkman, A. B., Lamers, P. P., Kornet, N. G., de Vos, W. M., & van der Oost, J. (2006) Molecular characterization of a conserved archaeal copper resistance (cop) gene cluster and its copper-responsive regulator in *Sulfolobus solfataricus* P2. *Microbiology*, 152(7), 1969–1979.
- Fakoussa, R. M., & Hofrichter, M. (1999) Biotechnology and microbiology of coal degradation. In *Applied Microbiology and Biotechnology* (Vol. 52, Issue 1, pp. 25–40).
- Fandrich, R., Gu, Y., Burrows, D., & Moeller, K. (2007) Modern SEM-based mineral liberation analysis. *International Journal of Mineral Processing*, 84(1–4), 310–320.

Goodall, W. R., & Scales, P. J. (2007) An overview of the advantages and disadvantages of the determination of gold mineralogy by automated mineralogy. *Minerals Engineering*, 20(5), 506–517.

Konadu, K. T., Harrison, S. T. L., Osseo-asare, K., & Sasaki, K. (2019). Transformation of the carbonaceous matter in double refractory gold ore by crude lignin peroxidase released from the white-rot fungus. *International Biodeterioration and Biodegradation*, 143, 104735.

Konadu, K. T., Harrison, S. T. L., Osseo-Asare, K., & Sasaki, K. (2019) Transformation of the carbonaceous matter in double refractory gold ore by crude lignin peroxidase released from the white-rot fungus. *International Biodeterioration and Biodegradation*, 143, 104735.

Konadu, K. T., Huddy, R. J., Harrison, S. T. L., Osseo-Asare, K., & Sasaki, K. (2019) Sequential pretreatment of double refractory gold ore (DRGO) with a thermophilic iron oxidizing archaeon and fungal crude enzymes. *Minerals Engineering*, 138, 86–94.

Kudo, S., Harada, A., Kubota, H., Sasaki, K., & Kaneta, T. (2017) Simultaneous Determination of Manganese Peroxidase and Lignin Peroxidase by Capillary Electrophoresis Enzyme Assays. *ACS Omega*, 2(10), 7329–7333.

Li, W., Liu, Z., Huang, Q., Tang, Y., & Qiu, X. (2016) Extraction of low-grade silver from a refractory Au-Ag ore in cyanidation by pretreatment with reductive alkaline leaching. *Hydrometallurgy*, 164, 257–264.

Liu, Q., Yang, H., Tong, L., Jin, Z., & Sand, W. (2016) Fungal degradation of elemental carbon in carbonaceous gold ore. *Hydrometallurgy*, 160, 90–97.

- Miki, T. (1983) Graphitization of carbonaceous matter in sedimentary rocks. *Journal of the Sedimentological Society of Japan*, 17to19(17–19), 111–120.
- Nanthakumar, B., Pickles, C. A., & Kelebek, S. (2007) Microwave pretreatment of a double refractory gold ore. *Minerals Engineering*, 20(11), 1109–1119.
- Ofori-Sarpong, G., Amankwah, R. K., & Osseo-Asare, K. (2013) Reduction of preg-robbing by biomodified carbonaceous matter-A proposed mechanism. *Minerals Engineering*, 42, 29–35.
- Ofori-Sarpong, G., Tien, M., & Osseo-Asare, K. (2010) Myco-hydrometallurgy: Coal model for potential reduction of preg-robbing capacity of carbonaceous gold ores using the fungus, *Phanerochaete chrysosporium*. *Hydrometallurgy*, 102(1–4), 66–72.
- Okibe, N., Koga, M., Morishita, S., Tanaka, M., Heguri, S., Asano, S., Sasaki, K., & Hirajima, T. (2014) Microbial formation of crystalline scorodite for treatment of As(III)-bearing copper refinery process solution using *Acidianus brierleyi*. *Hydrometallurgy*, 143, 34–41.
- Okibe, N., Koga, M., Sasaki, K., Hirajima, T., Heguri, S., & Asano, S. (2013) Simultaneous oxidation and immobilization of arsenite from refinery wastewater by thermoacidophilic iron-oxidizing archaeon, *Acidianus brierleyi*. *Minerals Engineering*, 48, 126–134.
- Okibe, N., Morishita, S., Tanaka, M., Sasaki, K., Hirajima, T., Hatano, K., & Ohata, A. (2017) Bioscorodite crystallization using *Acidianus brierleyi*: Effects caused by Cu(II) present in As(III)-bearing copper refinery wastewaters. *Hydrometallurgy*, 168, 121–126.

- Olson, G. J., & Clark, T. R. (2004) Fundamentals of metal sulfide biooxidation. *Mining Engineering*, 56(8), 40–46.
- Orell, A., Remonsellez, F., Arancibia, R., & Jerez, C. A. (2013) Molecular characterization of copper and cadmium resistance determinants in the biomining thermoacidophilic archaeon *Sulfolobus metallicus*. *Archaea*, 2013.
- Pyke, B. L., Johnston, R. F., & Brooks, P. (1999) The characterisation and behaviour of carbonaceous material in a refractory gold bearing ore. *Minerals Engineering*, 12(8), 851–862.
- Qiu, X., Hu, Z., Song, B., Li, H., & Zou, J. (2014) A novel process for silver recovery from a refractory Au–Ag ore in cyanidation by pretreatment with sulfating leaching using pyrite as reductant. *Hydrometallurgy*, 144–145, 34–38.
- Remonsellez, F., Orell, A., & Jerez, C. A. (2006) Copper tolerance of the thermoacidophilic archaeon *Sulfolobus metallicus*: Possible role of polyphosphate metabolism. *Microbiology*, 152(1), 59–66.
- Schmitz, P. A., Duyvesteyn, S., Johnson, W. P., Enloe, L., & McMullen, J. (2001) Adsorption of aurocyanide complexes onto carbonaceous matter from preg-robbing Goldstrike ore. *Hydrometallurgy*, 61(2), 121–135.
- Yang, H. Y., Liu, Q., Song, X. L., & Dong, J. K. (2013) Research status of carbonaceous matter in carbonaceous gold ores and bio-oxidation pretreatment. *Transactions of Nonferrous Metals Society of China (English Edition)*, 23(11), 3405–3411.

## Acknowledgments

Firstly, I am expressing my most profound and honest gratitude to my supervisor, Prof. Keiko Sasaki, for her guidance, patience, constant support, kindness, constructive criticism, essential lessons, and encouragement throughout this work. Also, thank you for cheering me on to learn and speak the Japanese language and culture, which was very decisive for my future as the bridge between Peru and Japan. During my Ph.D., Prof. Sasaki spent her precious time and energy on my research, presentation rehearsals, discussions, and manuscript. I could only finish this research work with her supervision and support. It is my honor and privilege to be her student. Working with Prof. Sasaki during these four years has been an unforgettable experience with many learned lessons that I can apply in my life. Thank you for making me a better researcher and, most importantly, a better person that can contribute to this complex society. Once again, thank you for believing in me and always encouraging me not to give up. All the challenges Prof. Sasaki have put me through made me a stronger human being.

My Sincere gratitude also goes to the committee members that evaluated this work, Assoc. Prof. Hirofumi Ichinose from the Department of Agro-environmental Sciences, Kyushu University; Assoc. Prof. Naoko Okibe, and Assoc. Prof. Hajime Miki from the Department of Earth Resources Engineering, Kyushu University. Their precious advice, constructive comments, and different points of view during this research journey helped me to improve this work.

During my Ph.D. journey, I visited the University of Cape Town and accumulated several academic and life experiences in South Africa. Therefore, I would like to thank

the Core-to-Core Program “Advanced Research Network for Biohydrometallurgy of Double Refractory Gold ores” and the team of the Center for Bioprocess Engineering Research (CEBER) for their support, hospitality, assistance, and cares during my stay.

Furthermore, I would like to thank Ms. Makiko Semba and Ms. Yasura Oiwa for their constant help regarding my University life and their thoughtful conversations and encouragement.

I have great pleasure in acknowledging the DRGO group members: Dr. Kojo Twum Konadu, Mr. Ryotaro Sakai, Ms. Cindy, and Ms. Ikumi Suyama because during our seminars, we could discuss, collaborate, and grow each other. Your friendship and support were significant to me. I believe even aqua regia cannot break the golden bond we have created together.

In the Mineral Processing, Recycling and Environmental Remediation laboratory, I spent precious experiences and valuable moments. I will never forget the friendship and kindness I have received here. Thus, I would like to thanks to all the members I have met during my Ph.D. Journey: Dr. Chitiphon Chuaicham, Dr. Gde Pandhe Wisnu Suyantara, Dr. Radheshyam Pawar, Dr. Binglin Guo, Dr. Karthikeyan Sekar, Dr. Balakumar Vellaichamy, Dr. Santisak Kitjanukit, Dr. Keishi Oyama, Dr. Quanzhi Tian, Dr, Mengmeng Wang, Dr. Zhang Li, Dr. Shlakshana Shenoy, Dr. Kasun Godigamuwa, Dr. Assadawoot Srikhaow, Dr. Jirawat Trakulmututa, Shu Kaiqian, Liu Tia You, Liu Pei Yu, Brian Nzuki, Shunsuke Imamura, Shingou Nakama, Ryohei Nishi, Haruki Noguchi, Tsubasa Oji, Yu Tanaka, Yuta Orii, Kohei Nonaka, Kaito Hayashi, Zenta Shirozu, Yuki Semoto, Takumi Inoue, Taiki Kondo, Daniyarov Berdakh, Efendi Rihan, Idol Phann, Ulmaszoda Akbarshokh, Yuika Kawazoe, Ryoji Ogi, Yuto Noguchi, Kazuma Kimura, Sae Yamamoto, Shota Kondo, Ryota Nakao, and Kazuto Satomura.



I would like to acknowledge Sumitomo Metal Mining Corporation for their collaboration and for kindly providing us a carbonaceous refractory gold-silver ore, Mineral Liberation Analysis data for my research, and valuable academic and economic support on the DRGO group.

There were many important people from Peru who gave me several opportunities and lessons in my academic and work life. Just to mention some: Dr. Rubén Rodríguez Flores, Dr. Máximo Baca Neglia, and Ms.C. Teresa Valderrama Rojas from the National University of Callao, Peru; Mr. Luis Vera Barandiaran from Vera y Moreno S.A. and Ms. Lexsy Vidal Atanacio from SCG VIVAL S.A.C. To all of you, I also say thank you. The experiences and lessons I have gained from you also helped me to mold my knowledge and character.

My appreciation also goes to Mr. Shojiro Irie, Mr. Ryo Nakano, Mr. Koichiro Takatsugi, and the collaborators from Mitsubishi Materials Corporation for their support during my job hunting, for believing in me and for giving me the opportunity to work in Japan. I am looking forward to my future at Mitsubishi Materials Corporation.

Nothing would have been possible without my scholarship sponsor. Hence, I would like to give my deep appreciation to the Japanese government for the scholarship provided through the Ministry of Education, Culture, Sports, Science and Technology, Japan (MEXT). Without this prestigious scholarship, my dream to come to Japan and achieve the highest academic degree will not be possible. In addition, I want to thank the Embassy of Japan in Peru and their collaborators for their assistance and cheering from the very beginning.

Finally, the two persons that gave me life, raised, educated, encouraged, supported, and let me follow my dreams far from you, my parents: Felipe Hernán Mendoza Tasayco and Ana Luisa Flores Quezada. You are the engine and the motivation for my constant self-improvement and hunger to achieve everything. Thank you for being not only my parents but also my best friends. Thanks to my family and friends for their spiritual support; to my four siblings, I hope to serve you as an inspiration for your bright future. I am also very thankful to my girlfriend, Haruka Kakigi, who gave color to my gray days; with your company and warm care, the most difficult days in my Ph.D. were appeased, and I could keep smiling regardless of the stress and tough times. Thank you for being my rainbow.

Gracias Totales!

March 2023, Diego Moizes Mendoza Flores

Kyushu University

Fukuoka, Japan